

TECHNISCHE UNIVERSITÄT MÜNCHEN
TUM School of Engineering and Design

Knee Injuries in Alpine Skiing

-

Why and How Mechatronic Ski Bindings Can Help

Aljoscha Hermann

Vollständiger Abdruck der von der
TUM School of Engineering and Design
der Technischen Universität München zur Erlangung des akademischen Grades
eines Doktors der Ingenieurwissenschaften (Dr.-Ing.)
genehmigten Dissertation.

Vorsitzender:

Prof. Dr. ir. Daniel J. Rixen

Prüfende der Dissertation:

1. Prof. Dr.-Ing. Veit St. Senner
2. Prof. Tron Krosshaug, Ph.D., The Norwegian School of Sport Sciences, Oslo
3. Priv.-Doz. Dr. med. Peter U. Brucker

Die Dissertation wurde am 19. Oktober 2021 bei der Technischen Universität München eingereicht und durch die TUM School of Engineering and Design am 23. August 2022 angenommen.

To all the curious

who like to know
who keep on trying, even though

in their way stand tall and wide
frustration and failure with all their might.

the curious will try and say:
there will be more than just one way

and afterward one might so say:
an easy thing!

but this is true just for the one
who after the curious will come

Note of Thanks

I thank Prof. Veit Senner for giving me the freedom to do this research and for supervising my dissertation. I also thank Prof. Daniel Rixen who acted as a mentor for me. Thank you PD Peter Brucker for the support concerning all medical topics.

I thank my wife and my family, who supported me over all the years. I thank my daughter who made me finish this work by being born. Many thanks to my colleagues from SpGM and LfE for all the good times we spent.

This manuscript is also a result of all the students who worked with me and who's bachelor and master thesis I had the privilege to supervise:

Foremost, I thank Johannes Mayer, Florian Franz, Maximilian Irlinger, Michael Hirschmann, Alexander Hofer, Nicole Bauer, Janina Fritzenschaft, Thomas Urban, Larissa Isele, Christian Laimer, Mara Brandl, Dirk Baumeister, Ann-Kathrin Stadler, Patrick Boscher, Sophia Hornbacher, Yakira Mafterwardelanie Baldinger, Alexandra Grün, Julia Stulpe, Eric Zipse, Alexander Jung, Julius Ostarhild, Luis Hermann and Patrick Carqueville (who will proceed my work) for all our discussions the shared frustration and glorious moments, and the small and large inputs you contributed to this work.

Acknowledgments

I thank the companies Smith and Nephew and LARS Ligaments for providing materials for the surrogate, as well as Herbert and Renate Jehl (HJM Messtechnik) for the sensors of the surrogate.

I also thank Philipp Staub and Matthias Kauffmann (Klüber Lubrication) for the performance of the lubrication tests and the company for providing the lubricants for our surrogate. Moreover, my thanks go to Melanie Feist and the team of the Clinic for Ruminants with Ambulatory and Herd Health Services at the Centre for Clinical Veterinary Medicine, Ludwig Maximilian University of Munich for the harvesting of bovine synovial fluid.

I thank Prof. Klaus Meier and the team from the University of Reutlingen and Peter Müller GmbH for manufacturing the textile prototypes of the sensor pants.

Table of Contents

NOTE OF THANKS	I
ACKNOWLEDGMENTS	I
TABLE OF CONTENTS	II
ABBREVIATIONS	VII
ABSTRACT	XI
ZUSAMMENFASSUNG	XII
1 INTRODUCTION	1-1
1.1 Aim of this Work	1-2
1.2 Structure of this Manuscript	1-3
2 BACKGROUND - INJURY MECHANISMS OF THE KNEE	2-5
2.1 The Knee Joint	2-6
2.1.1 Anatomy of the Knee	2-6
2.1.2 Kinematics of the Knee Joint	2-9
2.2 General Methods of Injury Research	2-13
2.2.1 In-Vivo – Test with Humans	2-15
2.2.2 Cadaver Tests	2-18
2.2.3 Surrogate Tests	2-20
2.2.4 Digital Modelling	2-23
2.3 Currently Described Knee Injury Mechanisms in Alpine Ski Sports	2-25
2.4 Parameters Influencing ACL Loads	2-29
2.4.1 Influence of the Quadriceps-Hamstring-Ratio on the ACL	2-29
2.4.2 Influence of Anterior – Posterior Translation, Tibia Rotation, and Varus-Valgus Stress on the ACL	2-31
2.5 Summary and Derivation of Research Questions	2-36
3 TOWARDS A COMPREHENSIVE UNDERSTANDING OF KNEE INJURY MECHANISMS	3-37

3.1	Study with a Leg Surrogate to Test the Influence of Muscle Activation on the ACL	3-39
3.1.1	Introduction	3-39
3.1.2	Method	3-39
3.1.2.1	The Surrogate	3-39
3.1.2.2	Test Scenarios	3-43
3.1.3	Results	3-46
3.1.4	Discussion of the Surrogate Study	3-50
3.2	Studies with a Multi-Body-Simulation-Model	3-53
3.2.1	Introduction	3-53
3.2.2	Method	3-53
3.2.2.1	Infrastructure and Simulation Environment	3-53
3.2.2.2	Model	3-54
3.2.3	Model Validation	3-59
3.2.3.1	Test Scenarios	3-59
3.2.3.2	Results	3-60
3.2.3.3	Discussion	3-63
3.2.4	Testing Ski Typical External Loads	3-67
3.2.4.1	Test Scenarios	3-67
3.2.4.2	Results	3-68
3.2.4.3	Discussion	3-80
3.3	Discussion of the Performed Studies with Respect to Knee Injury Prevention	3-82
4	TOWARDS A KNEE INJURY PREVENTIVE SKI BINDING	4-85
4.1	Overview of Existing Binding Concepts	4-87
4.2	Biomechanical Design Concept of a Mechatronic Ski Binding	4-91
4.2.1	System for Tracking the Knee Flexion Angle	4-93
4.2.1.1	Prototypes	4-94
4.2.1.2	Validation Study: Methodology	4-96
4.2.1.3	Validation Study: Results	4-99

TABLE OF CONTENTS

4.2.1.4	Discussion	4-101
4.2.1.5	Conclusion with respect to a mechatronic ski binding	4-106
4.2.2	System for Tracking the Muscle Activity of the Thighs	4-107
4.2.2.1	Prototype	4-109
4.2.2.2	Validation Study: Methodology	4-110
4.2.2.3	Validation Study: Results	4-114
4.2.2.4	Discussion	4-114
4.2.2.5	Conclusion with respect to a mechatronic ski binding	4-118
4.2.3	System for Tracking the Loads on the Feet	4-119
4.2.3.1	Prototypes	4-124
4.2.3.2	Validation Study: Methodology	4-129
4.2.3.3	Validation Study: Results	4-131
4.2.3.4	Discussion	4-134
4.2.3.5	Conclusion with respect to a mechatronic ski binding	4-137
4.2.4	System for Tracking the Skiing Speed	4-138
4.2.4.1	State of the Art	4-138
4.2.4.2	Validation Study: Methodology	4-140
4.2.4.3	Results	4-146
4.2.4.4	Discussion	4-153
4.2.4.5	Conclusion with Respect to a Mechatronic Ski Binding	4-155
4.3	Design Concept of an Algorithm	4-156
4.3.1	Basics of Fuzzy Controllers	4-157
4.3.2	Exemplary Fuzzy Controller for a Mechatronic Ski Binding	4-160
4.3.2.1	Structure	4-160
4.3.2.2	Membership Functions and Fuzzy Rules	4-162
4.3.3	Example of Application	4-166
4.3.4	Discussion of the Proposed Algorithm	4-169
5	DISCUSSION	5-173

6	CONCLUSION	6-177
	LIST OF FIGURES	179
	LIST OF TABLES	198
	LITERATURE	203
7	APPENDIX	7-238
7.1	The Human Knee	7-238
7.1.1	Axes of the Leg	7-238
7.1.2	Knee Joint	7-239
7.1.3	Musculature	7-240
7.1.4	Kinematics	7-243
7.1.4.1	Flexion und Extension	7-243
7.1.4.2	Rotation	7-244
7.2	Review of Studies Investigating Internal and External Rotation of the Tibia	7-248
7.3	Measuring ACL loads – An overview of methodologies	7-254
7.4	RMSE and NRMSE	7-258
7.5	Surrogate Study – Complete Measurement Results	7-259
7.5.1	Results of Each Individual Measurement	7-259
7.5.2	Further Results and Statistics of the Investigation	7-263
7.5.2.1	Setting: Hip Angle -20°; Preload ACL 50 N; Preload MCL 45 N	7-263
7.5.2.2	Setting: Hip Angle +20°; Preload ACL 50 N; Preload MCL 45 N	7-267
7.5.2.3	Setting: Hip Angle -20°; Preload ACL 85 N; Preload MCL 75 N	7-271
7.5.2.4	Setting: Hip Angle +20°; Preload ACL 85 N; Preload MCL 75 N	7-275
7.6	Study with the Digital Model	7-278
7.6.1	Mathematical Description of the Visco-Elastic Behaviour of the Ligaments	7-278
7.6.2	Determination of the Stiffness k and Parameter ϵl	7-280
7.6.3	Determination of the Initial Length l_0	7-281
7.6.4	Parameter Sensitivity Study	7-283
7.6.4.1	Test Scenarios	7-283

TABLE OF CONTENTS

7.6.4.2	Results	7-283
7.6.4.3	Discussion	7-288
7.7	Basics of Pressure Sensors and Pressure Sensor Measurements	7-290
7.8	Pressure Sensors Measuring Loads on the Feet	7-297
7.9	Speed of the Skier	7-298
7.9.1	Map Visualisation of Runs – Scenario D	7-298
7.9.2	Kalman Filter	7-302
7.10	Algorithm of the Mechatronic Ski Binding	7-307
7.10.1	Definition of Risk Values	7-307
7.10.2	Definition Membership Functions for the Knee Flexion Angle	7-315
7.10.3	Definition Membership Function High Internal/External Torque	7-316
7.10.4	Definition Membership Function High Varus/Valgus Moment	7-317

Abbreviations

Abbreviation	Meaning	Unit
ACL	Anterior cruciate ligament	
bar	Bar	Unit for pressure
°C	Degree Celcius	degree of temperature
CS	Silicon-based capacitive sensor	
deg	Degree of arc (geometrics)	degrees of arc
DGNSS	Differential global navigation satellite system	
DGPS	Differential global positioning system	
DoF	Degrees of freedom	
ϵ_1	Parameter defining the linear stress characteristics of a ligament	[-]
EMG	Electromyography	
f	Female	
F	Force	Newton [N]
F _x	Force acting in x / y / z direction.	Newton [N]
F _y	x: axis longitudinal to the ski	
F _z	y: axis perpendicular to the ski axis. z: vertical axis	
FEM	Finite element model	
GGA	Global Positioning System Fix Data; GPS data format	
GNSS	Global navigation satellite system	
GPS	Global positioning system	

ABBREVIATIONS

HDOP	Horizontal dilution of position	
Hz kHz	Herz / kilo-herz	Unit of frequency
IMU	Inertial measurement units	
k	Ligament stiffness	Newton [N]
k_0 / k_1	Calibration coefficients	
km/h	Kilometres per hour	Unit for speed and velocity
KFA	Knee flexion angle	
l	Length of ligament	
l_0	Initial length of ligament	
LCL	Lateral collateral ligament	
Lig.	Ligamentum (Ligament)	
M.	Musculus (Muscle)	
m	Male	
m mm cm km	Metre millimetre centimetre kilometer	Unit of distance
m/s	Meters per second	Unit for speed and velocity
M_x M_y M_z	Torque acting around an x y z x: axis longitudinal to the ski y: axis perpendicular to the ski axis. z: vertical axis	Newton metres [Nm]
MBS	Multi-body-simulation	
MCL	Medial collateral ligament	
ME	Mean Error	
MPa	Mega Pascal	Unit of pressure
MUX	Multiplexer	

ABBREVIATIONS

μ	Friction coefficient	
N	Newton	Unit of force
Nm	Newton metre	Unit of moment or torque
NMEA	National Marine Electronics Association Standard for GPS codes	
NRMSE	Normalised root mean square error	
Ω	Ohm	Unit for electrical resistance
PCL	Posterior cruciate ligament	
PTBoot PTSock PTFoot	Prototypes of pressure sensing systems	
φ_i	Knee flexion angle	Degree [°]
Q5H0 Q0H5 Q5H5 Q15H5 Q5H15 Q15H15	Muscle setup in the surrogate and simulation studies: quadriceps (Q) / hamstring (H) ratio numeric value: % of maximum forces for the respective muscle group reported by Arnold et al. (2010)	
R	Resistance (electrical)	Ohm [Ω]
R ²	Coefficient of determination	
RMC	Recommended Minimum Sentence; GPS data format	
RMSE	Root mean square error	
RS	Silicon-based piezo-resistive sensor	
RTK	Real-time-kinematics	
s ms	Seconds / milliseconds	Unit of time
S_i	Sensor value at measurement i	

ABBREVIATIONS

SD	Standard deviation	
U	Electrical potential	Volt [V]
v v_{abs}	Speed absolute of velocity	Metres per second [m/s] or kilometers per hour [km/h]
V	Volt	Unit for electric potential
°	Degree	degrees of arc (geometrics)
°/s	Degree per seconds	Unit of angular velocity
%	Percent	Fraction of 100

Abstract

It is estimated that annually almost half a million knee injuries, including 128.000 ACL injuries, occur in recreational alpine skiing. A suitable prevention system has not been developed for two main reasons: the incomplete understanding of knee injury mechanisms and technological limitations with respect to sensor systems allowing the supervision of kinetic and kinematical parameters of the skier in the skiing equipment. When these sensor systems are integrated into a mechatronic ski binding a more targeted reaction to the different loading situations the skier is exposed to is possible. Recent advancements in the field of sensors and microelectronic technologies make a mechatronic ski binding a feasible concept.

This thesis first aims to expand the understanding of knee injuries by quantifying the relationship between external loads acting on the ski, internally acting muscle forces, the flexion angles of the knee, and the resulting ACL loads. A combination of a surrogate study and a multi-body simulation is used for this purpose.

A set of input parameters for a mechatronic ski binding are derived from investigations detailed in this thesis and from the state of knowledge reported in the literature. These recommended parameters are the knee flexion angle, the muscle activity of the thigh, the loads acting on the feet, the skiing velocity, and individual information about the skier.

The second aim of this thesis is to give proof of the feasibility of a mechatronic ski binding. To achieve this, a sensor system prototype is presented for each of the four input parameters measurable with sensors, proving the concept and stating challenges that must be overcome for a successful product. In addition, a fuzzy logic algorithm is presented that combines the sensor values with an estimated risk level and resulting in a decision to adjust the retention settings of the binding.

This thesis also hopes to encourage the industry, as well as research institutions, standard committees, and other stakeholders in the alpine ski sports, to combine efforts to make skiing safer. It outlines a possible way to achieve this goal and acts as starting point for the development of a mechatronic ski binding that prevents knee injuries.

Zusammenfassung

Weltweit treten im alpinen Freizeitskisport circa eine halbe Millionen Knieverletzungen pro Jahr auf, darunter 128.000 Kreuzbandverletzungen. Ein Präventionssystem zur Reduzierung dieser Verletzungen wurde bisher aus zwei Gründen nicht entwickelt: Zum einen existierte nur ein unvollständiges Verständnis in Bezug auf Knieverletzungsmechanismen, zum anderen bestanden technologische Einschränkungen in Bezug auf Sensorsysteme, welche eine Überwachung kinetischer und kinematischer Parameter des/der Skifahrers/-in ermöglichen. Werden derartige Sensorsysteme in eine mechatronische Skibindung integriert, kann gezielt auf die unterschiedlichen Belastungssituationen, denen der/die Skifahrer/in ausgesetzt ist, reagiert werden. Neue Entwicklungen im Bereich Mikroelektronik machen eine mechatronische Skibindung inzwischen zu einem umsetzbaren Konzept.

Diese Arbeit zielt darauf ab, das Verständnis von Knieverletzungsmechanismen zu erweitern, indem die Zusammenhänge zwischen den auf den Ski wirkenden Belastungen, den Muskelkräften, dem Flexionswinkel des Knies und den Belastungen des vorderen Kreuzbandes quantifiziert werden. Hierzu werden Surrogatstudien und Mehrkörpersimulationen durchgeführt. Aus den durchgeführten Untersuchungen und dem in der Literatur berichteten Kenntnisstand leiten sich fünf Eingangsparmeter für eine mechatronische Skibindung ab: Der Kniewinkel, die Muskelaktivität des Oberschenkels, die Reaktionslasten an der Bindung, die Fahrgeschwindigkeit und individuelle Informationen zum Skifahrer.

Das zweite Ziel dieser Arbeit ist ein Machbarkeitsnachweis für eine mechatronische Skibindung. Für die vier sensorisch messbaren Eingangsparmeter werden jeweils ein Prototyp eines Sensorsystems vorgestellt, welcher als proof-of-concept dient und Herausforderungen für ein erfolgreiches Produkt aufzeigt. Zudem wird eine Fuzzy-Logik-Algorithmus präsentiert, der anhand der Sensorwerte ein Verletzungsrisiko bestimmt und eine Anpassung des Sicherheitswertes der Skibindung herbeiführt.

Diese Dissertation soll die Industrie, sowie Forschungseinrichtungen, Normungsgremien und andere Akteure des alpinen Skisports dazu anregen, gemeinsame Anstrengungen zu unternehmen, das Skifahren sicherer zu machen. Sie skizziert einen möglichen Weg, dieses Ziel zu erreichen und dient als Ausgangspunkt für die Entwicklung einer mechatronischen Skibindung, die Knieverletzungen verhindern kann.

1 Introduction

Ski bindings are used to separate the ski boot from the ski if there is a high risk of injury to the lower leg. Modern ski bindings and the setting parameters are developed on the assumption that the forces and moments that act on the leg during injury-free skiing are always smaller than the forces and moments that lead to an injury. (Scher and Mote Jr. 2001)

However, the knee joint is the most often injured part of the body when skiing (Ruedl et al. 2011). More than a third of all injuries involve the knee joint (Brucker et al. 2014). According to the annual report of the ASU (statistical evaluation centre for ski accidents in Germany), around 44,000 to 46,000 German skiers alone required medical treatment in 2018/2019 (Schulz 2019). 400 million skiing days worldwide (Vanat 2019) and an incidence of injury between 1.9 and 3.5 per 1000 skiing days for recreational skiers (Bianchi and Brügger 2016) result in a total of 760,000 to 1.4 million injuries annually, meaning 250,000 to 467,000 knee injuries. The anterior cruciate ligament (ACL) is involved in most of these injuries. Laporte et al. (2000) report an incidence of ACL-injuries of 3125 mean days between injuries, which results in about 128.000 ACL injuries worldwide.

In the short-term, ACL treatments and reconstruction promise a restoration of the knee function, but in the long-term, about 65 to 90% of patients develop early onset osteoarthritis and knee degeneration within 20 years post-surgery (Lohmander et al. 2007).

One reason for the prevalence of knee injuries may be that ski bindings primarily aim to reduce the risk of fracturing the tibia. Between 1980 and 1995, improved or new equipment resulted in a decrease of 90% for tibia and ankle injuries. At the same time, knee injuries tripled. (Ettlenger et al. 1995)

Even though the introduction of the carving ski in the mid-90s led to a decrease in knee injuries (Johnson et al. 2009), the rate of injuries remains high up to today. No relevant development in equipment appeared in the last years so to date, there is still no ski binding or other technical system, which reacts appropriately to prevent knee injuries and ACL injuries in particular.

This is regrettable, as the aforementioned numbers emphasize that knee injuries lead to suffering and long-term impairments for those affected. In addition, considerable

costs for the individual and the society arise due to surgeries, rehabilitation, stay-away from work (about 43 days immediately after surgery (Schulz 2019)), secondary diseases, and long-term impairments. For professionals, a knee injury can be the end of their career.

Schulz (2019) associates 83% of all injuries with non-contact injuries, meaning that the injury occurred without contact with an obstacle or other person at the time of injury occurrence. A study from New Zealand reports that every third ACL surgery after skiing is associated with a non-contact situation (Gianotti et al. 2009). This clearly shows that, besides preventive training and teaching measures, equipment plays an important role, as such non-contact injuries may be partly preventable with equipment that can react in a situation of knee injury risk.

1.1 Aim of this Work

The motivation for this work is based on the fact that there has been no significant progress in the development of safety systems preventing knee injuries in skiing for decades. Hence, the question arises:

“Why, for so many years, was there no equipment presented on the market which prevents injuries of the knee?”

The fact that there exist at least two major scientific societies, which are concerned with skiing safety, the *International Society of Skiing Safety (ISSS)* and the *International Congress on Science and Skiing (ICSS)*, indicates that it is not due to a lack of trying. Various suggestions for preventive measures and equipment design can be found in the 23 proceedings of the biennial congress of the ISSS, first held in 1977.

Two main reasons can be found that none of the suggestions related to equipment reached the market:

The first and most critical reason is that understanding of the injury mechanisms in alpine skiing is still limited to a general description (Bere et al. 2011; Freudiger and Friedrich 2000). A full understanding of the complex kinematic and kinetic nature of the injury mechanisms is needed, including the great individuality of the human anatomy and physiology, but also the ever-changing influences of the environment, like snow conditions and slope angle. This understanding would allow deriving critical

parameters, as well as thresholds for these parameters, as a basis for a possible safety system.

The second reason concerns the conceptual design of the ski binding: Various reviews suggest that a successful knee-injury-preventing ski binding design must be “system based” (Senner et al. 2014; Natri et al. 1999). This means that the binding is not simply acting on forces at the binding itself, but includes parameters such as muscle activity, kinematics of the knee and ankle, and location of the skier’s centre of mass relative to the ski. As a result, the system includes sensors, actuators, a controller, and a power supply. Miniaturization, accuracy, and cost efficiency of such components are only recently reaching a state, which would allow the integration into the skier’s hardware.

In the meantime, the technology in the field of microsensors and actuators has developed significantly, and new, and better systems are now conceivable in alpine skiing.

The following work addresses both the mentioned reasons for the non-existence of a knee injury prevention safety system in alpine skiing with the hope that the presented results and concepts will help in the development of consumer-ready systems which make skiing safer. This work focuses on ACL injuries, as the ACL is the most often injured structure of the knee. Nevertheless, the proposed system of a mechatronic ski binding may also prevent injuries to other structures of the knee, like meniscus injuries.

An overview of the approach followed in this work was published in the article “Knee injury prevention in alpine skiing. A technological paradigm shift towards a mechatronic ski binding” (Hermann and Senner 2020b).

1.2 Structure of this Manuscript

A comprehensive quantitative description of influencing parameters on injury mechanisms of the ACL (and the knee in total) in alpine skiing continues to be the greatest challenge and is elaborated on in the first section of this manuscript. Using a leg surrogate and multi-body simulations, the influence of various internal forces (muscles) and external forces and moments (loads acting on the ski) at different body postures on the ACL is examined. A mechatronic solution represents the most

promising concept for reducing ACL injuries in alpine skiing. A concept for a mechatronic ski binding is discussed in the second section of this manuscript and prototypes of sensor systems providing input information to such binding are presented and validated regarding their feasibility. In the last section of this manuscript, a conceptual algorithm for a Fuzzy-controller is presented.

This work is structured in three blocks as shown in Figure 1-1.

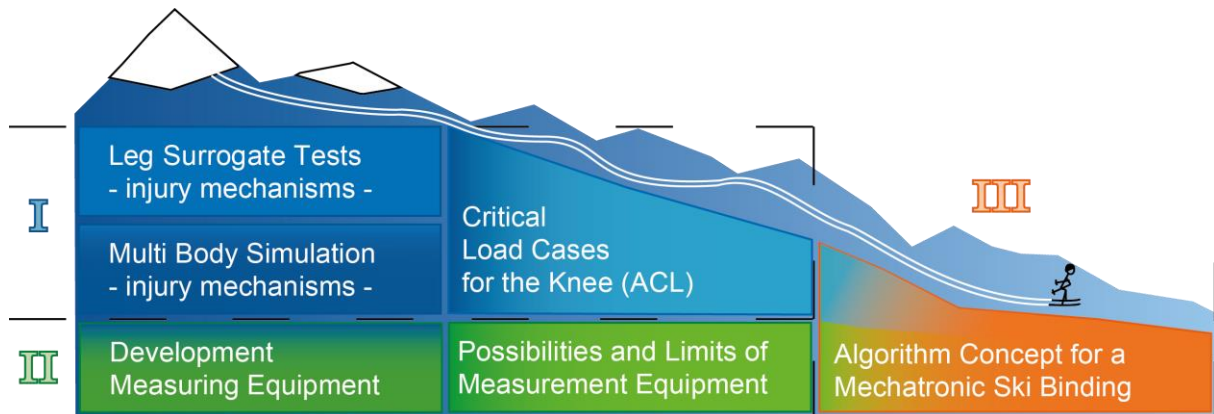


Figure 1-1 This manuscript is structured in three main blocks.

The respective blocks focus on:

<p>I Injury mechanisms in alpine skiing:</p>	<p>Understanding the mechanisms leading to ACL injuries. Defining critical parameters, which should be measured to enable a prediction of a risk of ACL injury. Quantifying the influence of these parameters with respect to critical loads for the knee and its ligaments using literature review, surrogate studies, and multi-body simulations (MBS) to determine critical load cases for the ACL.</p>	<p>Chapter 2 and 3</p>
<p>II Equipment for a mechatronic ski binding:</p>	<p>Development of measuring equipment for the use in a mechatronic ski binding and determining the limits of this equipment.</p>	<p>Chapter 4.1 to 4.4</p>
<p>III Algorithm concept for a mechatronic ski binding:</p>	<p>Proposal of a structure for an algorithm for a mechatronic ski binding based on the results of the previous two steps. This algorithm supervises the actual skiing situation and predicts the risk of injury.</p>	<p>Chapter 4.5</p>

2 Background - Injury Mechanisms of the Knee

Key points of this chapter

General Methods of Injury Research

The great complexity of the knee joint resulted in a great number of publications concerning the knee's biomechanics and the injury mechanisms in sports. Yet, we still have only a very limited understanding of both. Methodology to study injury mechanisms includes in-vivo studies, cadaver studies, dummy and surrogate studies, and digital modelling. As each method has advantages and drawbacks, a comprehensive understanding of the knee's biomechanics and knee injury mechanisms can only be achieved by combining all methods in a coordinated way. As this is expensive, resource intensive, time-consuming and in need of various expertise, a combined effort of research institutes, medical institutions, and industry is necessary.

Currently described Knee Injury Mechanisms in Alpine Skiing

Skiing is a highly complex activity, as the skier is interacting with the skiing equipment (boot, binding, ski, poles) and with the environment (snow, slope conditions, temperature). Hence, a multitude of variables influence the knee's safety, both extrinsic and intrinsic. In total 17 injury mechanisms are described for recreational skiing, of which three are the main consideration in literature: External rotation of the tibia + valgus, internal rotation in flexion (+varus), and a boot-induced anterior tibial translation. Three additional mechanisms are described for professional skiing: slip-catch, landing back weighted (similar to boot-induced anterior tibial translation), and dynamic snow plow (deep flexion of the knee + internal rotation of the tibia + valgus).

Parameters Influencing ACL Loads

A review of the literature results in a multitude of parameters associated with the risk of knee injuries, including activation ratios of the thigh, flexion angles of the body, external loads acting on the body, gender, age, training level, environmental influences, and more. The focus of the given review is on the thigh muscle activation, flexion angles of the lower extremities, and external loads acting on the ski, as these are of high impact to ACL loads and are measurable with sensors.

Symbols, like the following two examples, are used (throughout the whole manuscript) to improve readability and to enable information to be retrieved quickly:



Symbol indicates that the influence on ACL loads of a quadriceps dominant muscle activation is discussed in this section.



Symbol indicates that the influence of a load combination of an internal torque at the tibia and an anterior tibial translation on ACL loads is discussed in this section.

2.1 The Knee Joint

2.1.1 Anatomy of the Knee

Knowledge of the basics of anatomy and biomechanics of the human knee joint and leg is necessary when reading the present manuscript. As the knee is the biggest and one of the most complex joints of the human body, a comprehensive description is not possible without losing the focus of this work and the reader. In the following, a brief overview of relevant anatomy and kinetics of the knee joint is given. The focus is on the cruciate and collateral ligaments, as most injured structures in modern alpine skiing. In appendix 7.1 additional information about main aspects of the knee and its kinematics is given. For intensive and detailed information, the reader is referred to the standard literature, which is available in abundance (e.g. in German: Kohn (2005), Schünke et al. (2018) or in English: Prodromos (2018), Stoller (2017) or the Elsevier Journal “The Knee”).

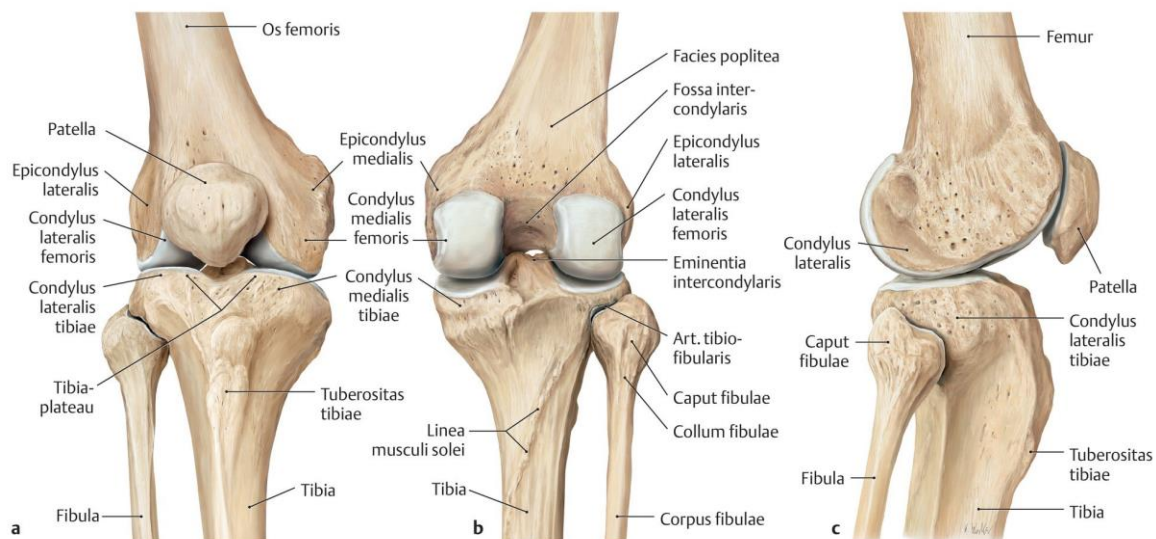


Figure 2-1 Bones and structures of the bones of the knee joint. Source: Wurzinger L. Kniegelenk (Articulatio genus). In: Aumüller et al. (2017). ©Thieme 2017, reprinted with permission.

Bones and joints

The bones forming the knee are the femur, tibia, fibula, and patella (Figure 2-1). These bones form complex joints:

- the patella-femoral joint, where the patella is gliding in the intercondylar gap (Facies articularis patellae). Proximal, the patella is attached to the quadriceps tendon and is increasing the acting lever arm of the extensor muscles. Distal, the patella is connected to the tibia head by the patella tendon.
- the tibia-femoral joint, where the two biconvex condyles of the femur and the tibia plateau interact. The gap between the articulating bones is filled by the menisci (see Figure 2-2).
- the fibula-tibial joint.

Ligaments

The knee is stabilized by multiple ligaments (Figure 2-2).

Collateral ligaments:

- LCL: Lateral collateral ligament (Lig. collaterale fibulare)
- MCL: Medial collateral ligament (Lig. collaterale tibiale). The MCL consists of various functional parts (Robinson et al. 2005).

In the extended leg, both ligaments are tensioned and stabilize the knee medial-lateral-wise and counteract varus and valgus moments. When the knee is flexed, the ligaments become slack, which increasingly enables rotational and lateral movements. (Schünke et al. 2018)

Cruciate ligaments are both considered of having two bundles:

- ACL: anterior cruciate ligament (Lig. cruciata anterior). The two bundles of the ACL are the anterior-medial and posterior-lateral bundles.
- PCL: posterior cruciate ligament (Lig. cruciata posterior): the two bundles of the PCL are the anterior-lateral and posterior-medial bundles.

The cruciate ligaments fulfill multiple roles. They limit the anterior-posterior translation and make a significant contribution to stabilising the joint in flexion. In internal rotation of the knee, they wind around each other, slowing down the rotation (Schünke et al. 2018). In addition to the muscles, they are responsible for the sliding movement between the tibia and femur. Not all fibre bundles of the cruciate ligaments have the same length and orientation so not all bundles are tense at the same time during the movement. The anterior cruciate ligament also prevents excessive hyperextension (Kapandji and Koebke 2006).

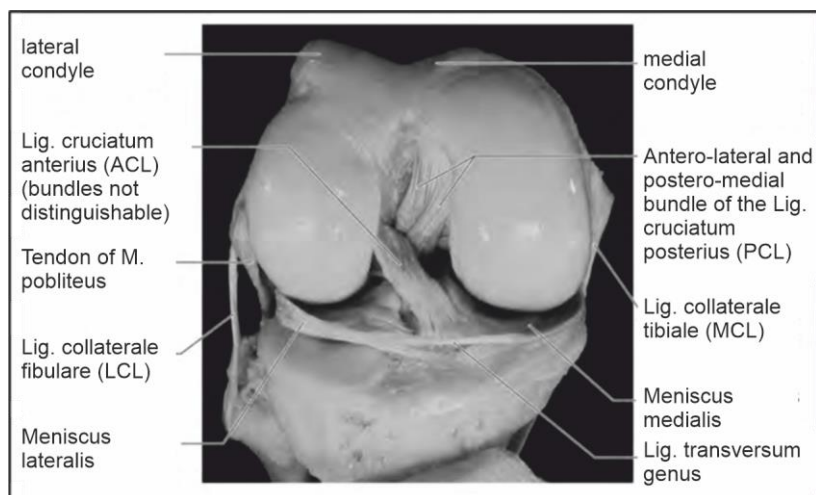


Figure 2-2 A frontal view in the knee joint (right leg). The cruciate, the collateral ligaments and the menisci are observable. Source: Kohn (2005), page 23. ©Thieme 2004, reprinted and modified with permission.

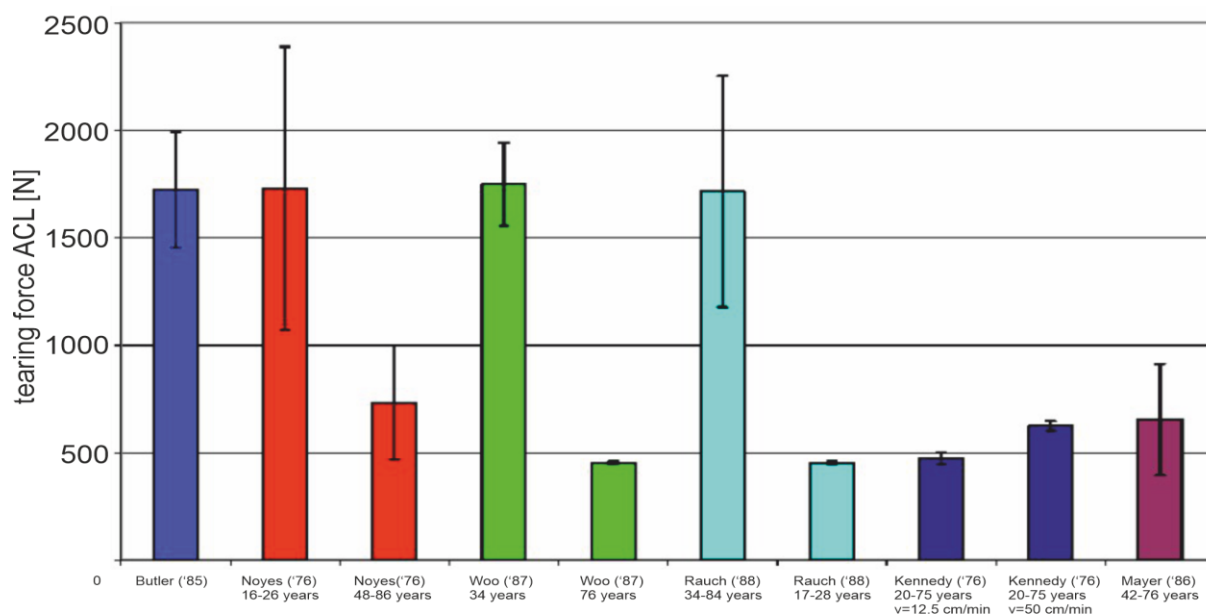


Figure 2-3 Tearing force of the human ACL as reported in different publications. Original graphic by Lehner (2007) p.30, modified and translated.

The tensional tearing force for the ACL varies strongly, depending on the measurement method used to determine it, the age of the used specimen, and the velocity of force application (Figure 2-3). Moreover, other factors influencing the tearing force are discussed in the literature. Therefore, quantification is difficult and values range from less than 500N to more than 2000 N tensional tearing force (Lehner 2007).

All ligaments are anisotropic, non-linear, non-compressible, hyperelastic, and show viscoelastic behaviour (Hirokawa and Tsuruno 2000), therefore, being stiffer, showing

a larger modulus of elasticity, an increasing tear resistance, and less extensibility for faster loadings (Siebels 1993).

Muscles spanning the knee

Several muscles are available to the body for knee joint movements. Those are mainly categorized as flexors and extensors. The major muscles listed in Table 2-1 are implemented in the knee surrogate and the multi-body simulations used for the studies presented in this manuscript. The reader is referred to chapter 3 and appendix 7.1.3 for more detailed information.

Table 2-1 Muscles and their main function regarding the knee joint used in the knee surrogate studies and the multi-body simulations.

Muscle	Function regarding the knee joint
Quadriceps	
M. vastus intermedius	extensor
M. vastus lateralis	extensor
M. vastus medialis (longus / obliquus)	extensor
M. rectus femoris	extensor / external rotator
Hamstrings	
M. biceps femoris	flexor
M. semitendinosus	flexor / internal rotator
M. semimembranosus	flexor / internal rotator
M. gastrocnemius (medialis / lateralis) *	(flexor) / joint stabilising
M. popliteus**	internal rotator

*Due to similar modes of action regarded as part of the hamstrings in this work.
 **Only passively implemented (ligamental structure) in the surrogate and multi-body model.

2.1.2 Kinematics of the Knee Joint

The kinematics of the knee joint are highly complex as all degrees of freedom, meaning translations, rotations, and pivots (flexion-extension / varus-valgus) are possible (Figure 2-4). These degrees of freedom are not independent. The motion is controlled by the articular geometry, ligaments, and muscular tension. In simulations or theoretical considerations, the knee joint is often simplified to a hinge joint. Strictly, this is not correct. Even if only the flexion-extension movement of the knee is considered, the centre of rotation is following a complex trajectory itself, often described as a roll-

glide movement. Moreover, this trajectory is different for the medial and the lateral side of the knee.

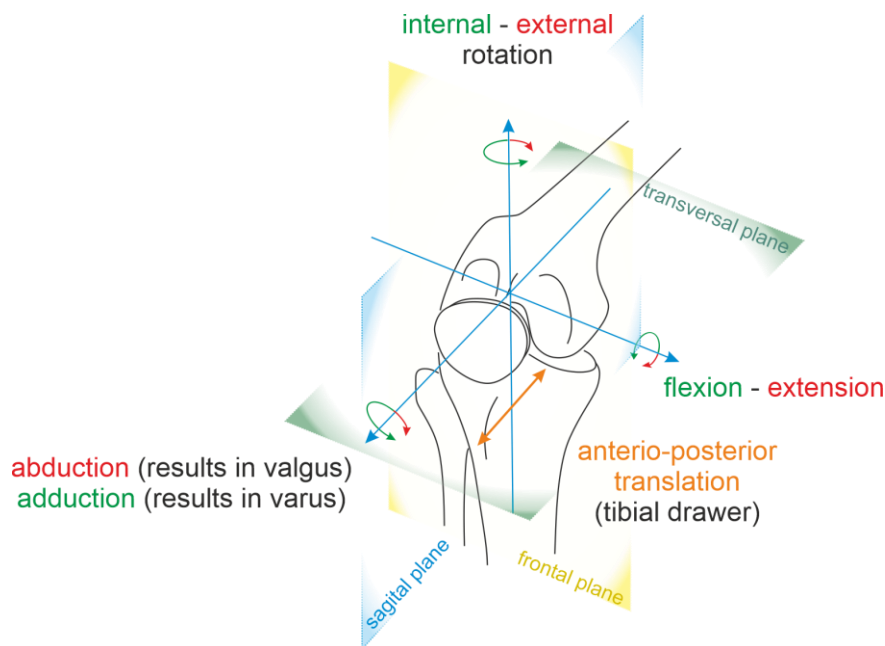


Figure 2-4 Main degrees of freedom of the knee (right leg | tibia is moved & femur is fix). To a small extent translations in the other directions are also possible.

Flexion and extension

The maximal possible flexion of the knee is 120° to 150° and is limited by soft tissue contact. The maximal extension is about 5° and results in a terminal rotation of the tibia. (Schünke 2014)

Tibial rotation

A rotation of the tibia can only occur in a flexed joint. The maximum possible rotation is increasing with the flexion angle. Most literature state largest rotations in 90° flexion (Kapandji and Koebke 2006; Almquist et al. 2002).

Maximal external rotation is larger than maximal internal rotation. At a 90° knee flexion angle, the maximal external rotation is 30 to 40° and the maximal internal rotation is 10 to 30° (Schünke 2014; Kapandji and Koebke 2006).

Woman can rotate the tibia 10 to 40% further than men (Mouton et al. 2012; Shultz et al. 2011; Shultz et al. 2007b; Park et al. 2008; Hsu et al. 2006; Branch et al. 2010; Almquist et al. 2013). A reason could be a lower torsional stiffness in the female leg (Schmitz et al. 2008) due to hormonal reasons (Branch et al. 2010).

According to Branch et al. (2010), maximal internal rotation increases by 9° and maximal external rotation decreases by 10° after an ACL injury.

The axis of rotation is not congruent with the central axis of the joint but shifted medially. This means that the lateral condyle has a trajectory that is almost twice as long as the medial condyle. As collateral and cruciate ligaments play an important role in restricting rotation, the rotation of the leg is one risk factor for knee injuries. During external tibia rotation, the collateral ligaments wind around the proximal end of the tibia and thus slow down the rotation. At the same time, the cruciate ligaments separate from each other. During internal rotation, the two cruciate ligaments become entangled and act against the movement. This results in an increased compressional load between the femur and tibia and increased rotational stiffness of the knee.

Muscle activation of individual thigh muscles can increase torsional stiffness (Louie and Mote 1987). The torsional stiffness of the knee increases with increasing rotation (which is commonly approximated by two linear stiffnesses for small rotations (primary stiffness) 0.1 to 0.7 Nm/° (Markolf et al. 1976), and large rotations (secondary stiffness) 2.2 to 2.8 Nm / ° (Louie and Mote 1987).

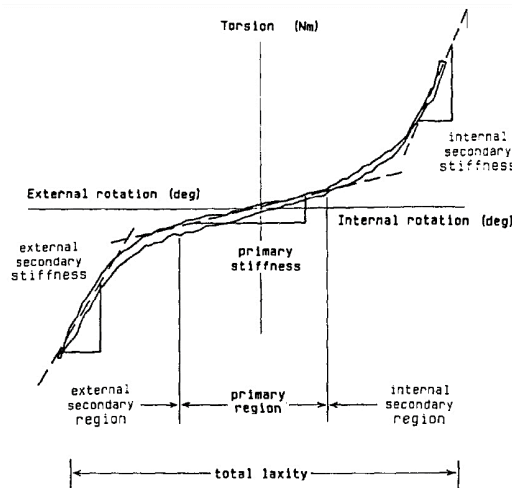


Figure 2-5 Torsional stiffness (rotational laxity) of the knee joint. The stiffness of the knee increases with increasing rotation and can be divided into two approximately linear areas (primary and secondary stiffness). The hysteresis that occurs when the leg is turned back can also be seen. Taken and adapted from (Louie and Mote 1987), p. 294.

Varus and Valgus

A varus describes an inward angulation (adduction) of the tibia versus the femur in the frontal plane. A valgus describes an outward angulation (abduction) of the tibia versus

the femur in the frontal plane. Varus and valgus angles resulting from biomechanical loadings are in general small. Both terms are also describing pathological deformations of the knee.

Anterior-posterior translation

The anterior-posterior translation is also called tibial drawer and describes the relative translation of the tibia and femur in the sagittal plane. A ruptured ACL can be diagnosed by testing the extent of a possible tibial drawer in the anterior direction.

Axial compression and body weight

With an increase in axial compression (meaning the femur is pressing on the tibia and thus compressing the menisci) the rotational and translational stiffness of the leg increases (Shultz et al. 2007b; Louie and Mote 1987; Markolf et al. 1981). Increased body weight thus may lessen the movement range of the knee (Mouton et al. 2012).

2.2 General Methods of Injury Research

The great complexity of the knee joint resulted in a great number of publications with respect to the knee's biomechanics, but also the injury mechanisms in sports. Yet, we still have only a very limited understanding of both. Figure 2-6 is an example of the confusing state of knowledge presently available. The graph shows the torsional stiffness of the knee (rotation of tibia with respect to the femur) as stated in different studies, which used different methodologies. A great variation of results is observable (for example at 5 Nm torsional load we see a 5° to 25° internal rotation and nearly 5° to 40° external rotation). This variation can be due to the individual properties of each tested (cadaver or living) knee. Also, the variation can be a result of the different test devices and methodologies used in the studies. Latter limits the transferability of these results for use in the development of safety systems for the knee.

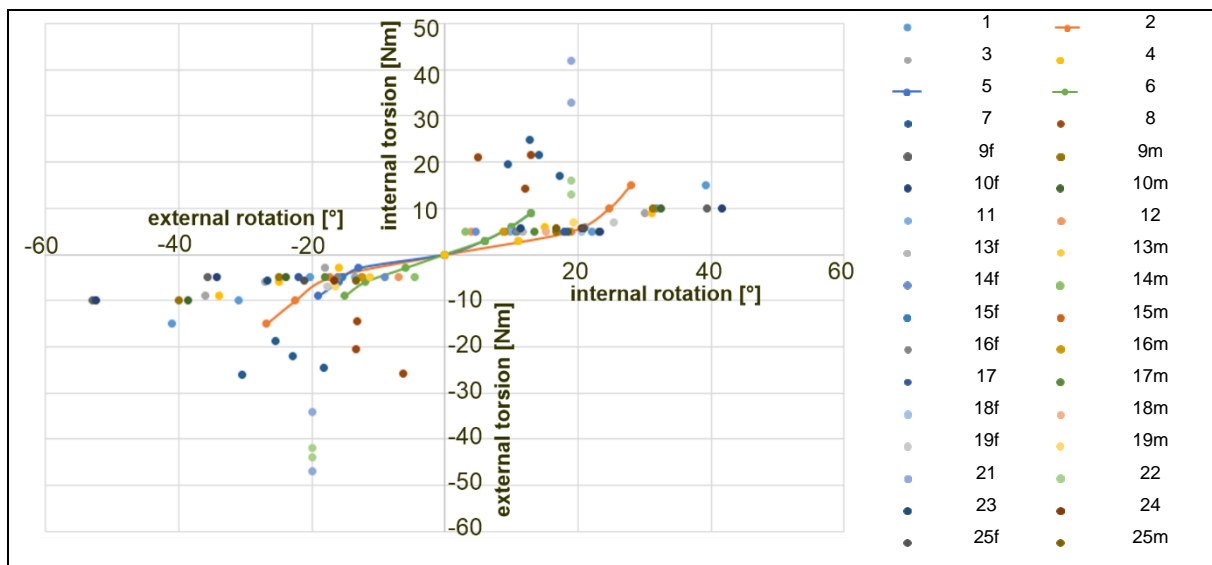


Figure 2-6 Results of various studies testing the torsional stiffness of the knee. The variation of the respective results shows the complexity of the knee's kinematics, but also the influence of the study's methodology on the results. Each number in the legend is associated with a study referenced in Table 7-1 in appendix 7.2. Studies 2, 5, and 6 are plotted with a line. Due to the used methodology, the results of these three studies are estimated to be very accurate, but they do only describe the torsional stiffness for specific tested conditions (knee flexion angle / external loads / muscle activations).

This chapter will give an overview¹ of different methodologies to test for the kinematic and kinetic relationship of the knee and its structures, as well as the interaction with other body structures and internal or/and external loads.

Each method has advantages and drawbacks. A comprehensive understanding can only be achieved by combining the results of all. Coordinated use of multiple methods is expensive, resource intensive, time-consuming, and needs various expertise. Therefore, only a few publications of this level can be found (Cassidy et al. 2013; Bates et al. 2015; Hangalur et al. 2016; Li et al. 2008).

Due to the lack of studies directly testing skiing, the focus of the given review is on general injury research.

¹ For a more comprehensive review of methodologies, the reader is referred to Krosshaug et al. (2005) and van Mechelen et al. (1992) as a starting point.

2.2.1 In-Vivo – Test with Humans

In-vivo tests on the knee are performed with living humans (animal tests are not considered in this chapter, as the focus is on kinematics and kinetics in skiing). Only in-vivo studies allow the testing of anatomical structures in a natural, undamaged state and environment. At the same time, the participant can give feedback on the experimental setup and his/her perceiving.

Study designs can be differentiated between clinical studies, laboratory studies, and in-sport studies. General characteristics of in-vivo studies are given in Table 2-2. A combination of study methodologies is essential to allow conclusions on the causes of injuries. For example, defining the pathology of injuries in a specific sport and using video data and interviews to describe the circumstances leading to an injury.

Table 2-2 Common characteristics of different in-vivo study designs

Type of study	Clinical and laboratory	In sport
Focus	<ul style="list-style-type: none"> • Pathology of injury • Treatment/Intervention methods • Basic research on human kinetics and kinematics 	<ul style="list-style-type: none"> • Sport specific interactions and injury mechanisms. • Training
Exemplary methodologies	Invasive and non-invasive <ul style="list-style-type: none"> • MRT, CT, radiography • Motion tracking • Force Plates • EMG • 	Non-invasive <ul style="list-style-type: none"> • Motion tracking (e.g. IMU, Video, GPS) • Surface EMG • Pressure insoles • Interviews • ...
Subjects	Healthy and injured	healthy

Especially image-based technologies are of high importance. MRT, CT, and X-Ray allow a view into the body without additional (physical) damage. Cameras allow the tracking of movements without influencing interactions and without changing the natural environment of athletes. Especially professional sport events with multiple cameras allow various viewing directions on interesting situations. Multiple useful information can be extracted from videos and images. For example, they can be interpreted by experts (Bere et al. 2014) or used for (automatic) tracking of kinematics and digital modelling of such (Krosshaug and Bahr 2005).

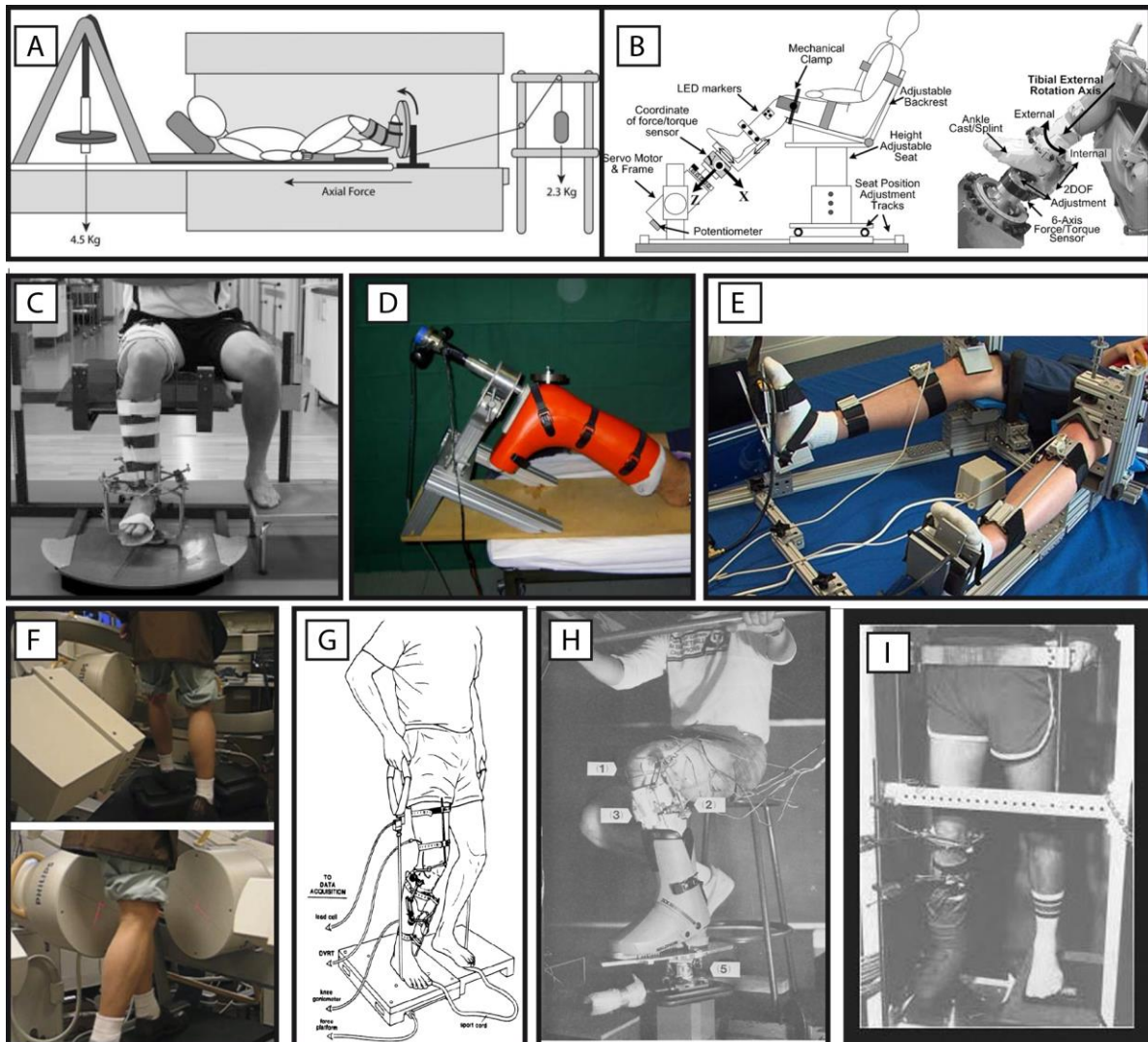


Figure 2-7 Exemplary test designs of different in-vivo studies with applications of external loads: A) Haughom et al. (2012)¹, B) Park et al. (2008), C) Rottometer by Almquist et al. (2013)², D) Lorbach et al. (2009b)¹, E) Branch et al. (2010)¹, F) Li et al. (2008)³, G) Beynnon et al. (1997)⁴, H) Louie and Mote (1987)³, I) Hull and Johnson (1989)⁵. ¹©Springer Nature, ²©John Wiley and Sons, ³©Elsevier, ⁴©SAGE Publications, ⁵©ASTM; all figures reprinted with permission of the respective copyright holder.

Implementing sensors in humans to test for internal loads, stress, deformation, elongation, or other variables is ethically and technically challenging. In rare cases, when such was done for scientific purposes (e.g. Cerulli et al. (2003), Beynnon et al. (1997) (see Figure 2-7 (G)) or Fleming et al. (2001)), results may have limited meaningfulness due to methodological limitations and sample size. Examples of methodological limitations are changed movement patterns due to impingements or only a limited spatial resolution of force or pressure sensors.

Ethical reasons forbid to replicate injuries in experimental in-vivo studies. Barone et al. (1999) unintentionally recorded an injury in alpine skiing during an experiment. Such cases are rare and allow valuable insights. Due to the singularity of such events, conclusions cannot be generalized and must be interpreted with respective prudence.

The quantification of the influence of axial rotation and anterior-posterior translation on knee laxity and loads are major questions in the last decades and multiple in-vivo test designs are published. Figure 2-7 gives an exemplary overview of clinical and laboratory test designs. The work of the group around Guoan Li can be highlighted (Figure 2-7 (F)). They made an approach to use a clinical tool, a fluoroscopic imaging system to study joint kinematics on probands walking on a treadmill (Li et al. 2008) or doing lounges (Hosseini et al. 2015; Papannagari et al. 2007). This allows the simultaneous observation of the movement from outside and inside the body.

2.2.2 Cadaver Tests

The principal advantage of cadaver studies is that pathological loads can be applied to anatomical structures. At the same time, this also limits the usage of cadaveric body parts to one time.

Common study designs are:

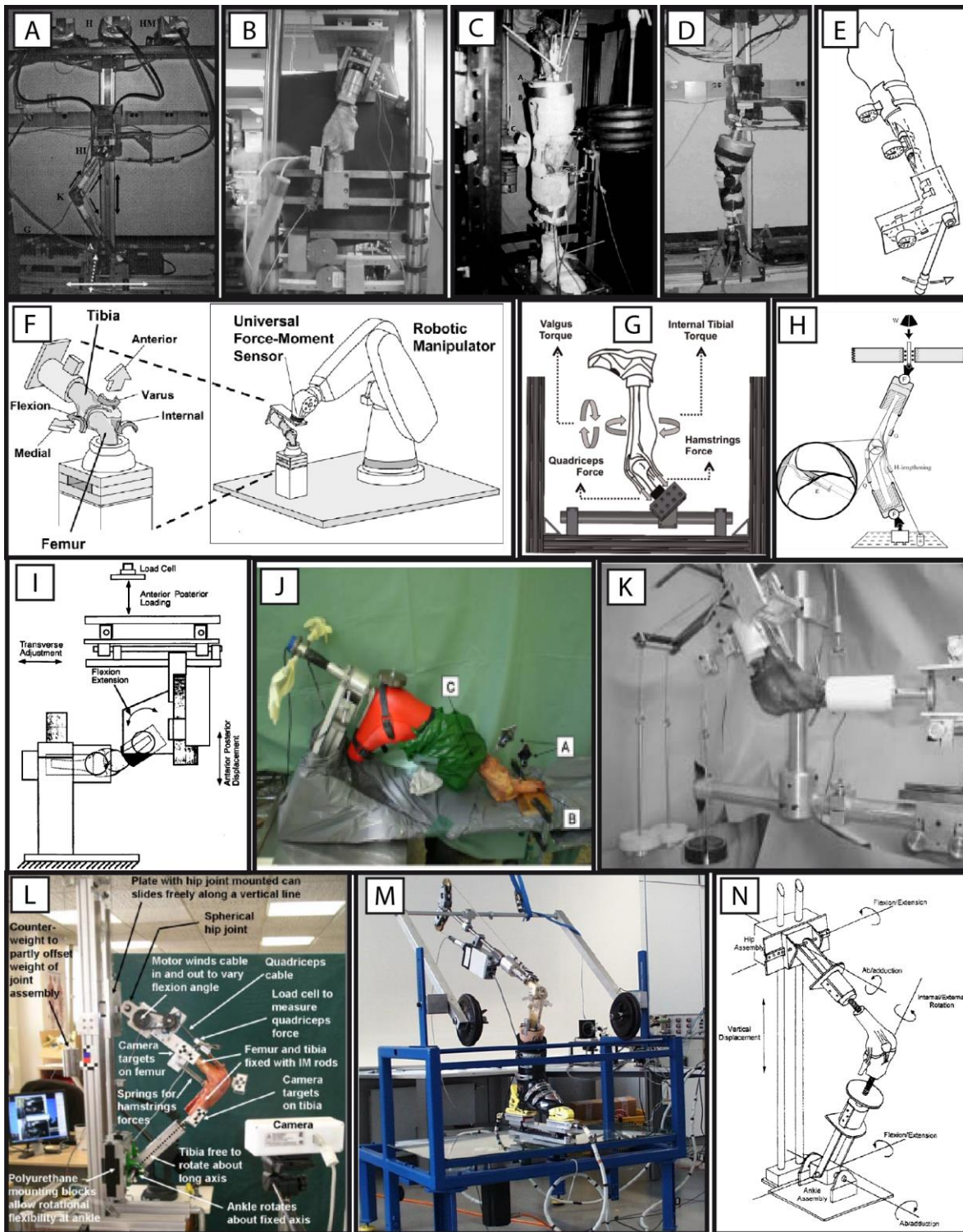
- kinematics is measured before and after dissecting a specific structure (for example a ligament or muscle).
- specific influencing parameters are tested on a sub-pathological level,
- or until a pathologic effect occurs (for example the effect of different levels of tendon/muscle forces or knee angle).

By implementing force, pressure, or elongation sensors into the knee, more sophisticated measurements can be achieved. The exact location of implementation can be extremely important. Load transmission in the ligaments is inhomogeneous (Hull et al. 1996) and could be influenced by the sensor itself.

The chosen test methodology impacts results and reported methodologies do differentiate fundamentally (Bates et al. 2015), ranging from an application of a single force (e.g. Withrow et al. (2008)) to robotic manipulators controlling limb position and force application (e.g. Hsu et al. (2006)). Examples of different methodologies of cadaver studies are shown in Figure 2-8.

Further limitations of cadaver studies are:

- missing muscular activation/support. Some studies simulate singular muscle forces to test for their effect on ligament loads or joint shift. Exemplary, the effect of quadriceps and hamstring muscles are reported in DeMorat et al. (2004), Markolf et al. (2004), Li et al. (1999) and reviewed in Oberhofer et al. (2017);
- changing characteristics due to preparation; for example, dissection of fat, muscles, and capsular;
- age, state, and lack of representativeness of specimens (Woo et al. 1991);
- unclear effects on the characteristics due to the freezing and thawing process (Clavert et al. 2001; Jung et al. 2011; Turner et al. 1988; Moon et al. 2006).



2.2.3 Surrogate Tests

A surrogate or dummy aims to replicate the properties of human anthropometry and physiology.

Dummy Tests

Dummy tests allow a repetitive and systematic test design. Hybrid dummies are well known for their use in car and traffic crash tests. Such dummies can be instrumented with sensors and used in field and laboratory studies. The lack of musculature and the simplification of joints limits the field of investigation. A transfer of dummy results of tested injury scenarios to humans is therefore challenging. The group of Nicola Petrone used such dummies to test skiing safety equipment, like safety barriers (Petrone et al. 2010; Petrone et al. 2011) or helmets (Petrone et al. 2019). In Figure 2-9 B1, a dummy is used for simulating a landing situation. B2 shows the test design for safety net tests. Senner et al. (1996) published a study using a more abstract skier dummy (Figure 2-9 A) to test landing scenarios in skiing. An extensive description can be found in the dissertation of Senner (2001). Yoneyama et al. (2009) built a robot with multiple joints to model a curved ski turn (Figure 2-9 C). The knee joints have 6 degrees of freedom.

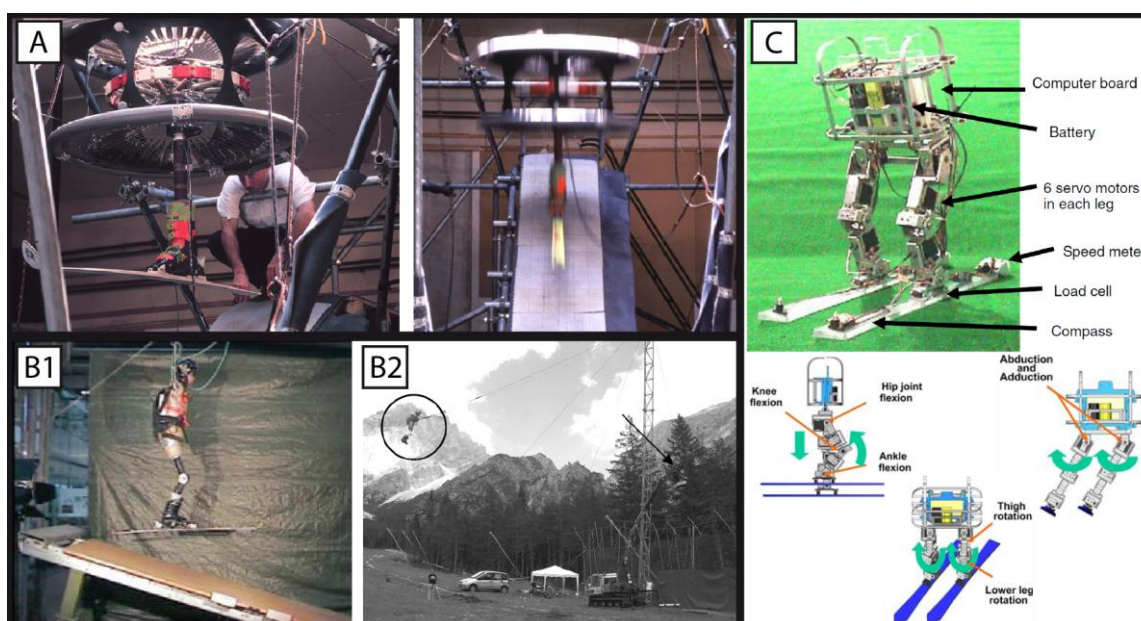


Figure 2-9 Examples for the use of dummies and the different level of abstraction: A) Senner (2001), B1) Petrone et al. (2011)¹, B2) Petrone et al. (2010)¹, C) Yoneyama et al. (2009)². ¹©Elsevier, ²©Springer Nature; all figures reprinted with permission of the respective copyright holder.

Surrogates of knee joints

Most leg surrogates published, were designed for testing knee braces and with a focus on varus-valgus stress (Brown et al. 1990; Daley et al. 1993; France and Cawley 2005; France et al. 1987) or tibial displacement (Glynn et al. 2002; Liggins and Bowker 1991; Liu et al. 1994). Other designs allow to test for combined loads (Cawley et al. 1989; Hochmann 2012; Lunsford et al. 1990; Mathewson and Greenwald 2003; Nusser et al. 2016; Binder et al. 1997)

That these surrogates can be of various levels of biofidelity and complexity is observable in Figure 2-10. Many surrogates do not have the functionality to simulate changing muscle activation. The reproduction of the knee joint is often simplistic (for example a hinge joint) and in some cases, the articulating structures are not present at all.

To overcome some of the limitations of existing surrogates and to allow the investigation of the complex injury mechanisms in alpine skiing Nusser (2016) developed a surrogate, which is of high complexity and will be used for further investigations in this work. The characteristics of her test rig and modifications done for this work will be discussed in chapter 3.1.

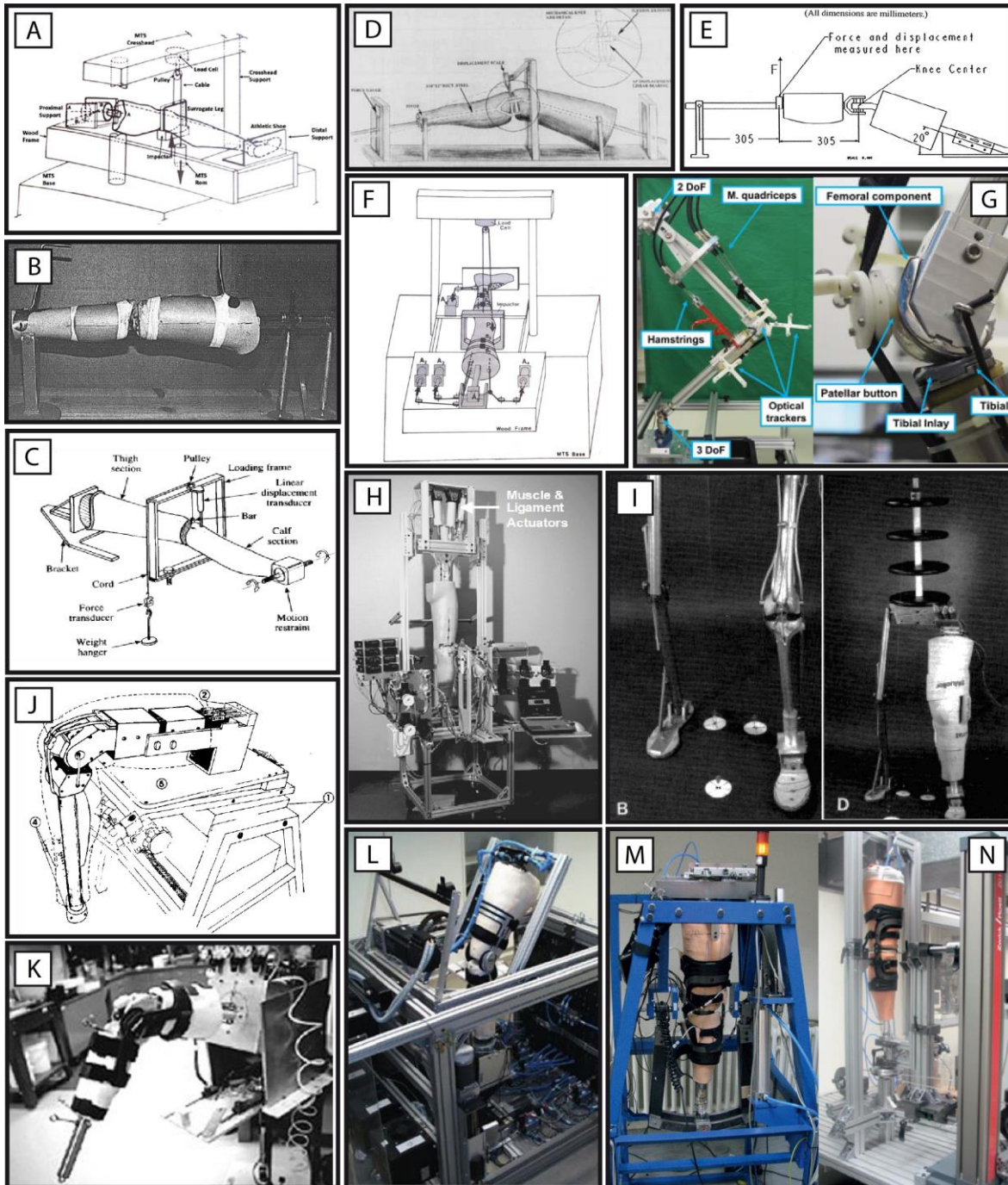


Figure 2-10 Examples of surrogates of various complexity designed for knee brace testing (except G, which was used for a flexion sensor validation): A) Brown et al. (1990)¹, B) Lunsford et al. (1990)², C) Liggins and Bowker (1991)³, D) Liu et al. (1994)², E) Glynn et al. (2002)², F) Daley et al. (1993)⁴, G) Asseln (2019), H) France and Cawley (2005), I) France et al. (1987)³ and more recently used in Mathewson and Greenwald (2003), J) Cawley et al. (1989)⁴, K) Test Rig by DJ Otho, picture found in Hochmann (2012), L) Binder et al. (1997), M+N) two test rigs used by Hochmann (2012). ¹©Elsevier, ²Wolters Kluwer Health, Inc., ³©SAGE Publications, ⁴©ASME; all figures reprinted with permission of the respective copyright holder.

2.2.4 Digital Modelling

Digital (or in-silico) modelling of injuries is a powerful tool, as models can specifically be developed for a research question. In theory, there are no limitations to complexity, and (maybe most valuable) combinations of different modelling tools are possible. For example, a multi-body model of a skier can be combined with a FEM model of the knee to study intra-articular loads of tissue and bones in a skiing situation.

In practice, such co-simulations and even simpler designs are restrained by numerical and processing issues, for example, the availability of eligible solvers for optimization problems. Such solvers are needed because of the complex human anatomy and the reason that human dynamics are usually not deterministic. Especially FEM computations are resource intensive and a single simulation run can take multiple days, and therefore, can make a parameter analysis unrealisable (Kazemi et al. 2013). Not seldom, the essential validation of an in-silico model represents a dilemma, because often, a digital model is selected for the very reason that the intended research question is only investigable by using a digital model. Reasons can be high-risk scenarios, ethical issues, no existing sensor technology, and many more. This consequences in the situation that validating input parameters or results by experimental studies sometimes is impossible or large simplifications and assumptions need to be accepted (Sharkey and Hamel 1998).

If possible, experimental data is used for validation. Two examples are shown in Figure 2-11 A (Ali et al. 2016) and B (Lehner 2007), where cadaver experiments were used to validate a model. The multi-body model of Lehner (Lehner 2007; Senner et al. 2014) shown in Figure 2-11 B1 and B2 takes into account all important anatomical structures (bone structures, soft tissue structures, muscles) of the knee and mathematically describes their visco-elastic material behaviour. These were determined by cadaver studies shown on the left side in Figure 2-11 B1.

The drawback of using experimental data for the validation of digital models is that as a result, the digital model implements the same limitations as the experimental design. As those limitations should be circumvented by the digital model, we find ourselves in a dilemma: experiment is not possible for example due to ethical reasons → digital model is chosen → needs an experiment for validation.

Moreover, a transfer of a model, which was designed to answer a specific research question, to a practical multi-use simulation tool is limited (Lund et al. 2012). Probably

as a result of these limitations, no digital model and results of such were found in the literature research for this work, which gives satisfactory insight into ACL injury mechanisms in alpine skiing.

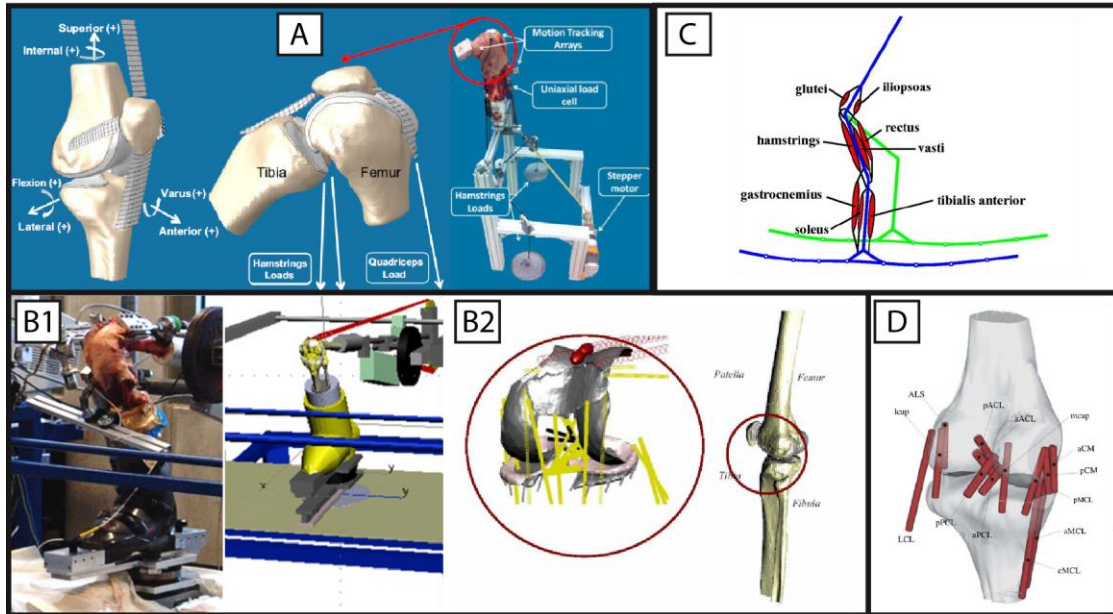


Figure 2-11 Examples of digital models of the knee: A) FEM-Model validated by cadaver study by Ali et al. (2016)¹, B1) Multibody model by Stefan Lehner validated by cadaver study (Senner et al. 2014), B2) Multibody model by Lehner (2007) including various muscle tendons and ligaments, C) planar model by Eberle et al. (2019) for testing dynamic landing situations with muscle agitation, D) multibody model by Shelburne et al. (2004)¹ with a high resolution of ligament bundles used for studying ligament loads in a gait cycle. ¹©Elsevier; all figures reprinted with permission of the respective copyright holder.

2.3 Currently Described Knee Injury Mechanisms in Alpine Ski Sports

Sections of this chapter were published in Hermann and Senner (2020b).

Skiing is a highly complex activity as the skier is interacting with the skiing equipment (boot, binding, ski, poles) and the environment (snow, slope conditions, temperature). All those aspects need to be considered in understanding injury mechanisms in skiing in addition to the kinematic and kinetic of the skier itself. Multitudes of variables influence the knee's safety, both extrinsic and intrinsic. Most vulnerable to injury are especially two ligaments of the knee, ACL, and MCL. The biomechanical interaction of the body structures and their implication on ACL injuries were intensively studied (Ganapathy et al. 2018; Bere et al. 2011), e.g. the influence of knee and hip flexion angle, varus and valgus, internal and external rotation of the tibia, muscle activation of the thigh, as well as external loads on the body.

The strong influence of the knee flexion angle on ACL stress was shown by Wascher et al. (1993), making the knee flexion angle an important variable to consider in a safety system. In the same publication, the group describes the influence of an internal or external rotation and a varus and valgus loading on ACL stress. These loadings result from either the forces and torques acting on the foot or from inertia of the upper body movements.

An additional variable discussed with respect to knee injuries is the ratio of quadriceps (Quad) and hamstrings (Hams) activation. Different ratios of Quad-Hams-activation have either a positive or negative effect on ACL stress (DeMorat et al. 2004; Myer et al. 2009).

Also, individual aspects such as age (Ekeland et al. 2019), gender (Ruedl and Burtscher 2019; Hewett et al. 2006; Wojtys et al. 1998; Shultz et al. 2011), weight, fitness, skill level (Hume et al. 2015), fatigue (Spörri et al. 2017), attentiveness, neuromuscular control (Gruber 2001), and pre-injuries (Paterno et al. 2010) are shown to be important factors related to ACL injuries.

Besides those internal factors related to the skier, external factors (Senner et al. 2014; Spörri et al. 2017), such as snow and course condition, weather, equipment (Senner et al. 2013), and speed, are important to consider.

The focus of this work will be on injury mechanisms of recreational skiers, as a new safety system for this group will have the most beneficial effect on society and a greater number of individuals. Likely, a safety system for professional skiers must be designed differently as the athletes' demand on the performance is extreme and the line between a safe and an unsafe skiing situation is very small.

Injury Mechanisms in Recreational Skiing

The most comprehensive description of injury mechanisms was published by Freudiger and Friedrich (2000). The authors differentiated 17 injury mechanisms and categorized them into four groups (Table 2-3).

Table 2-3 Categorization of 17 injury mechanisms by Freudiger and Friedrich (2000).

I. Knee flexion in combination with	II. External rotation of the tibia in combination with	III. Internal rotation of the tibia in combination with	IV. Extension
<ul style="list-style-type: none"> - anterior-tibial loading e.g., induced by a backward fall. - forced anterior-tibial translation (e.g., boot-induced-anterior-tibial-translation (BIAD)). - hyperflexion. 	<ul style="list-style-type: none"> - hyperextension. - an anterior translation of the tibia. - a valgus with a centre of gravity in front of the ski binding. - a valgus in knee flexion with a centre of gravity in front of the ski binding. - a valgus and an anterior translation of the tibia, centre of gravity in front of the ski binding. - a varus and an anterior translation of the tibia with a centre of gravity clearly behind the ski binding. 	<ul style="list-style-type: none"> - hyperextension. - flexion. - varus with a centre of gravity in front of the ski binding. - varus in flexion with a centre of gravity in front of the ski binding. - valgus in flexion, with a centre of gravity behind the ski binding. - valgus with an anterior translation of the tibia and with a centre of gravity behind the ski binding. 	<ul style="list-style-type: none"> - hyperextension. - hyperextension with internal rotation of the tibia and a varus.

The first group includes various versions of a boot-induced anterior-tibia-translation (BIAD). A BIAD is characterised by an anterior translation of the tibia with respect to the femur due to the fixation of the ankle by the ski boot. This translation leads to high ACL stress. Figure 2-12 (a) illustrates a BIAD resulting from a landing on the back-tip of the ski while being in a backward-leaning body posture. The anterior tibia translation is often amplified by activation of the quadriceps to prevent a fall. Either a hyperflexion or hyperextension of the leg results in even higher ACL stress.

Group two includes external rotations in different combinations, e.g. external rotation + valgus + extension of the leg. Those mechanisms relate to the situation shown in Figure 2-12 (b).

The third group includes internal rotations in different combinations, e.g. internal rotation + varus and relates to the phantom foot shown in Figure 2-12 (c).

The fourth group includes situations with hyperextension of the leg.

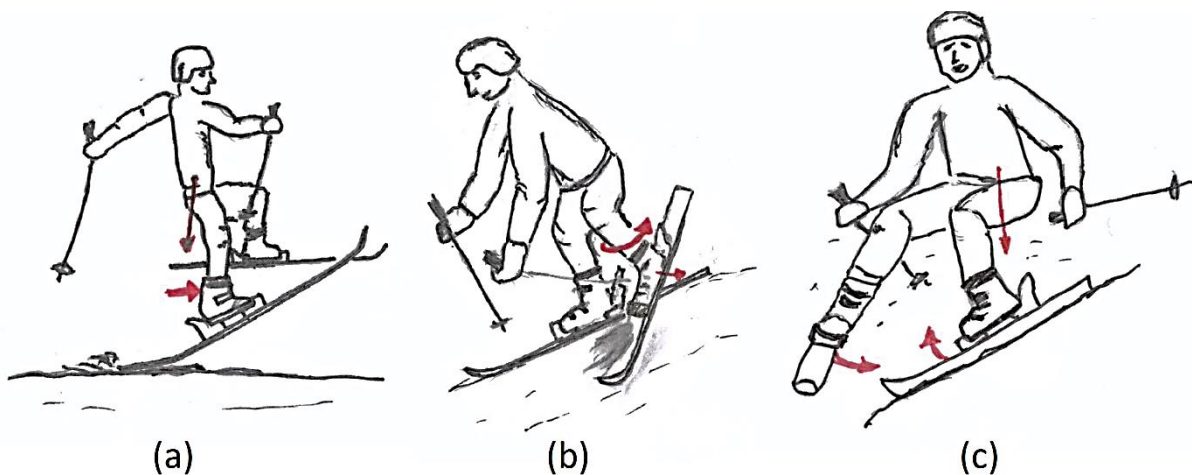


Figure 2-12 Mechanism of anterior cruciate ligament ruptures in skiing. (a) Boot-Induced anterior tibia drawer (known as BIAD), (b) valgus + external rotation, (c) Flexion + internal rotation (Phantom foot).

Injury Mechanisms in Professional Skiing

Even though professional skiing is not the focus of this work, it makes sense to have a comparative look at the situation in high-performance sports.

Three typical injury mechanisms are commonly named with respect to professionals (Bere et al. 2011; Bere et al. 2013; Brucker et al. 2014):

Slip-Catch mechanism (Figure 2-13) - The outer ski is drifting away (A); extension of the leg; followed by an abrupt catch in the inner edge (B) and a forced valgus with internal rotation of the tibia; muscular support of the knee is missing.

Landing Back-Weighted (Figure 2-14) - Landing with an extended leg and a centre of gravity behind the ski binding; initial snow contact with the back tip of the ski (A); followed by increasing knee flexion, an anterior translation of the tibia probably due to strong activation of the quadriceps and/or provoked by the fixed ski boot, and a compressional loading between tibia and femur (B).

Dynamic Snow Plow (Figure 2-15) - Centre of gravity behind the ski binding; inner ski drifts away (A); followed by a very dynamic internal rotation of the tibia and a valgus. According to Senner et al. (2014), a present hyperflexion of the leg and strong activation of the quadriceps contributes to a final occurrence of injury.

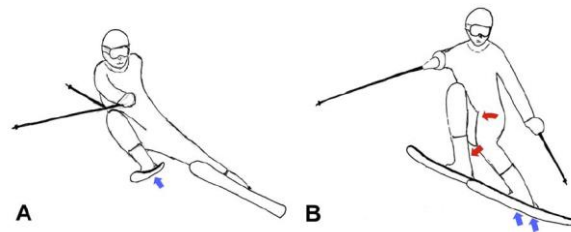


Figure 2-13 Slip-catch-mechanism. ©Elsevier: Reprinted with permission from Brucker et al. (2011)

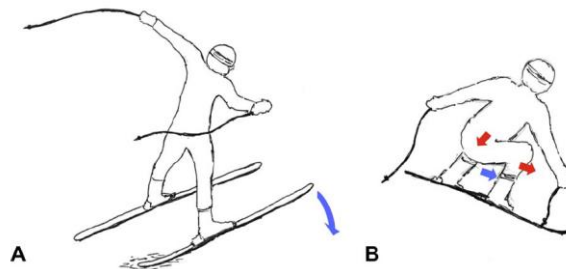


Figure 2-14 Landing Back-Weighted. ©Elsevier: Reprinted with permission from Brucker et al. (2011)

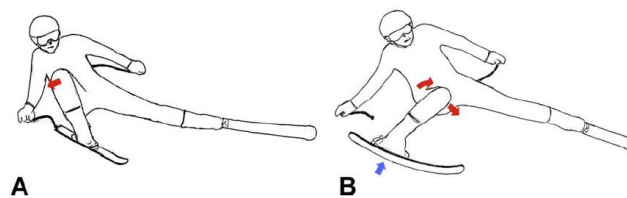


Figure 2-15 Dynamic Snow Plow. ©Elsevier: Reprinted with permission from Brucker et al. (2011)

2.4 Parameters Influencing ACL Loads

2.4.1 Influence of the Quadriceps-Hamstring-Ratio on the ACL

Besides the passive stabilisation by the bones, menisci, ligaments, and capsule, the knee joint is strongly influenced by muscles. Dependent on the knee and hip flexion angle (Koyanagi et al. 2006; Markolf et al. 2004), different activation pattern of quadriceps and hamstring muscles are reported to increase or decrease loads on ligamental structures like the ACL.



A dominant quadriceps loading is reported to increase the risk of injury by producing an anterior shift of the tibia with respect to the femur and thus increasing the load on the ACL (DeMorat et al. 2004; Renström et al. 1986; Markolf et al. 2004; Beynnon and Fleming 1998; Pandy and Shelburne 1997; Draganich and Vahey 1990; Dürselen et al. 1995).



A co-contraction of quadriceps and hamstrings is reported to have a stabilising effect and therefore can help to prevent an injury, as rotational and translational stiffness increases (Li et al. 1999; Louie and Mote 1987; Myer et al. 2009; Withrow et al. 2008; Solomonow et al. 1987; More et al. 1993; Renström et al. 1986; Beynnon and Fleming 1998; Pandy and Shelburne 1997; Draganich and Vahey 1990).

The quantification of the effects of different muscle activation patterns is limited. In most studies, the number of muscles included in the test and the number of activity levels tested for are small. In-vivo studies are restricted to EMG measurements for referencing muscle loads. In-vitro studies, using cadaver legs, can apply defined tension forces on the muscles or their respective tendons. In the reviewed literature, in general, small forces were applied. An exception is a study by DeMorat et al. (2004), where 4500 N quadriceps contraction was simulated, resulting in large anterior tibial translation and ACL injuries of the tested legs.

Using 18 cadaver knees Wascher et al. (1993) tested the influence of 200 N quadriceps force on the ACL load over the full range of knee flexion motion. High ACL loads were measured for knee flexion angles smaller than 20°, decreasing to a non-loaded state

above. For flexion angles higher than 80° ACL loads increased for a single specimen. Above 120° knee flexion, all specimens showed increased ACL strain.

With 13 cadaver knees, Markolf et al. (2004) tested the effect of either 100 N quadriceps load or 100 N hamstrings load in combination with an anterior or posterior tibial force, tibial torques, and varus/valgus moments (Figure 2-16, Figure 2-17 and Figure 2-18). The measurements were performed from -5 to 120° knee flexion. In correspondence to Washer et al., their results show that quadriceps activation is increasing ACL loads for smaller flexion angles. In comparison to measurements with quadriceps loads, measurements with hamstring loads resulted in smaller ACL loads in the same flexion range. In the test case without additional external loads (no rotational or varus/valgus loads) and the test case with sole internal rotation, hamstring activation resulted in a significant, though decent, increase of ACL load in flexion angles above 45° (Figure 2-16).

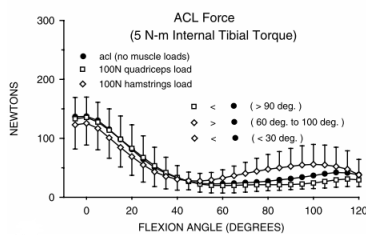


Figure 2-16 Influence of an internal torque plus muscle activation on the ACL load. Source Markolf et al. (2004), reprinted with permission.

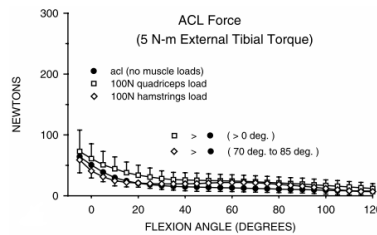


Figure 2-17 Influence of an external torque plus muscle activation on the ACL load. Source Markolf et al. (2004), reprinted with permission.

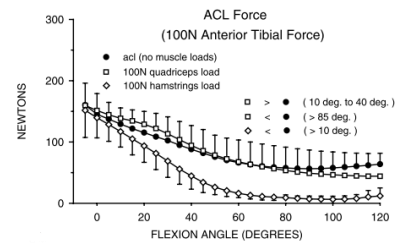


Figure 2-18 Influence of an anterior force plus muscle activation on the ACL load. Source Markolf et al. (2004), reprinted with permission.

A protective potential of hamstring activation was also found by More et al. (1993). The authors increased hamstring loads from 0 to 90 N on ten cadaver knees resulting in a decreasing load on the ACL over all knee flexion angles from 0° to 90°.

In an in-vivo study, Beynon and Fleming (1998) reported comparable results. Additionally, they could show that during flexion movement ACL loads were higher than during extension movements.

In-situ studies using mathematical models are more flexible in the variation of input parameters. Existing studies (Pandy and Shelburne 1997; Shelburne et al. 2004) support the above-mentioned findings.

In alpine skiing, a majority of the known injury mechanisms (see chapter 2.3) include a backward leaning position of the upper body (Freudiger and Friedrich 2000). A backward moving center of mass, which may be behind the foot sole in skiing, is associated with a higher risk of injury. As the hip angle is influencing the trunk orientation, it may be an important factor concerning injury risks (Heinrich et al. 2014). An increased hip flexion lengthens biarticular hamstring muscles and shortens biarticular quadriceps muscles (Visser et al. 1990). Hamstring activation, and the hamstring-quadriceps ratio, are reported to increase with increased hip flexion (Delp et al. 1999; Guex et al. 2012). There is no clear understanding of the effect the hip angle has on ACL loads by altering the force directions of the muscles (Alentorn-Geli et al. 2009).

2.4.2 Influence of Anterior – Posterior Translation, Tibia Rotation, and Varus-Valgus Stress on the ACL

Anterior-posterior tibia translation and internal and external rotation with or without a varus/valgus stress are principal components of ACL injuries (see chapter 2.3 and Table 2-3). It is unlikely that only one of these forces or moments is acting on the knee at any time. In most situations, a combination of forces and moments will be present. Therefore, it is not purposeful to consider these separately from one another.

Available literature bases its investigations mainly on the in-vitro studies by the groups around Markolf and Wascher (Markolf et al. 1981; Markolf et al. 1990; Shapiro et al. 1991; Wascher et al. 1993; Markolf et al. 1995; Markolf et al. 2004; Markolf et al. 2008; Markolf et al. 2018).

The key results of the publications by this group are:



Internal rotations lead to higher ACL loads than external rotations for small flexion angles (Markolf et al. 1990; Wascher et al. 1993; Markolf et al. 2004), see Figure 2-16 and Figure 2-17.



The influence of internal rotation on ACL load increases with increased extension of the leg (Markolf et al. 1990; Markolf et al. 2004), see Figure 2-16.



In 30° flexion, an anterior force results in an ACL load of the same amount as the anterior force applied to the knee, increasing with a further extension of the leg (Markolf et al. 1990; Markolf et al. 1995; Markolf et al. 2004); see Figure 2-18. In contrast, Gabriel et al. (2004) found a decrease in ACL loads for an increasing flexion angle.



An anterior force in combination with an internal torque further increases ACL loads from hyperextension to 20° flexion (Markolf et al. 1995); see Figure 2-22. This combination near full extension was considered to be the greatest risk for injury to the ACL by Markolf et al..



An anterior force in combination with an external torque decreases ACL loads compared to a sole anterior force (Markolf et al. 1995).



Near full extension of the leg, varus stress increases ACL loads more than valgus stress (Wascher et al. 1993); see Figure 2-20 and Figure 2-21. This was also found in the in-silico study of Bendjaballah et al. (1997).

With increasing flexion angle, the influence of a valgus on ACL load stays nearly on a constant level, and the influence of a varus on ACL load decreases (Markolf et al. 1990; Wascher et al. 1993); see Figure 2-20 and Figure 2-21. At 130° knee flexion angle, a sole varus moment results in about 40% decrease in ACL load and a sole valgus moment in a 30 to 80% (depending on quadriceps activation) increase in ACL loads (Lehner 2007).



An anterior force in combination with a varus moment further increases ACL loads compared to a sole anterior force for smaller flexion angles (Markolf et al. 1995).



An anterior force in combination with a valgus moment further increases ACL loads compared to a sole anterior force for flexion angles larger than 10° (Markolf et al. 1995; Berns et al. 1992), see Figure 2-23



An internal torque in combination with a varus moment did not change ACL loads compared to a sole internal torque in a knee flexion range of 1 to 90° (Markolf et al. 1995). Yet, this combination increases ACL loads compared to an unloaded flexion, which was also found by Dürselen et al. (1995). Lehner (2007) found a decrease in ACL loads when an internal rotation was supplemented by a varus moment of 15 Nm at a knee flexion angle of 140°.

A present varus moment is reducing the range of internal rotation at a knee flexion of 100° (Lehner 2007).



An internal torque in combination with a valgus moment increases ACL loads for flexion angles between 10° to 70° (Markolf et al. 1995); see Figure 2-24. Kanamori et al. (2000) also found decreasing ACL forces for increasing flexion angles in a similar load setting. Kanamori et al. (2002) also reported that an internal torque plus valgus leads to higher ACL loading than an external torque plus valgus. At 140° knee flexion angle, Lehner (2007) found the increase of ACL load resulting from a 15 Nm valgus and an internal rotation was present, but not significant.



An external torque in combination with a valgus or varus moment did not change ACL loads compared to a sole external torque in a knee flexion range of 0 to 90° (Markolf et al. 1995). Lehner (2007) found that a varus (significant effect) or valgus (present effect, but not significant in cadaver experiment; significant in in-silico experiment) of 15 Nm supplementing an external rotation increased ACL loads at a knee flexion angle of 130 and 140°. A present valgus moment is reducing the range of external rotation at a knee flexion angle of 100° (Lehner 2007).



A flexion moment leading to hyperflexion of the knee increases ACL loads even more than a hyperextension provoked by a torque of the same amount (Wascher et al. 1993); see Figure 2-19.



Axial compression between femur and tibia leads to increasing ACL stress with increasing knee flexion angle (Markolf et al. 2018).

In an in-vivo study, Shoemaker et al. (1988) reported a range of voluntary generated tibial torques of 24 to 99 Nm (mean values: 40 to 71 Nm) when wearing a ski boot, depending on the test conditions “knee flexion angle” and “restrained or unrestrained torso and pelvis”. The authors assume a maximal external torque of 110 Nm is needed to tear the ACL, as this torque has to overcome about 70 Nm internal torque generated by muscular counteraction in a 45° flexed knee and a ligamental contribution of 40 Nm reported in a previous study of the group (Shoemaker and Markolf 1982). For a voluntary generated external torque with tensed muscles, counteraction was 12%

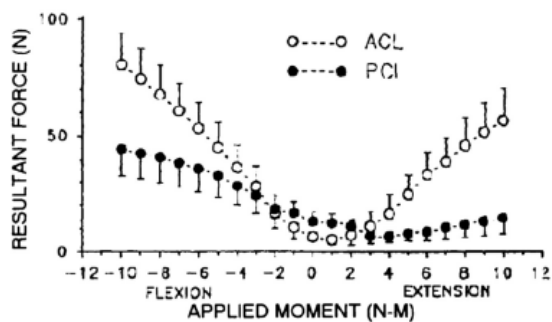


Figure 2-19 Influence of a forced hyperextension / hyperflexion on the cruciate ligaments. Source Wascher et al. (1993), reprinted with permission.

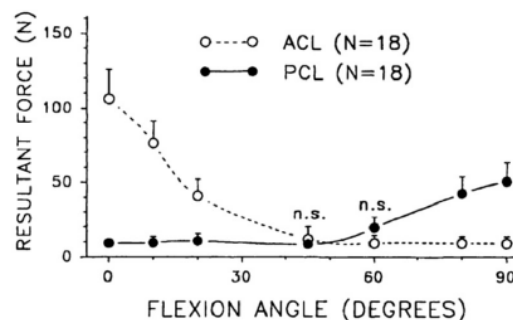


Figure 2-20 Influence of a varus moment of 15 Nm on the cruciate ligaments for different knee flexion angles. Source Wascher et al. (1993), reprinted with permission.

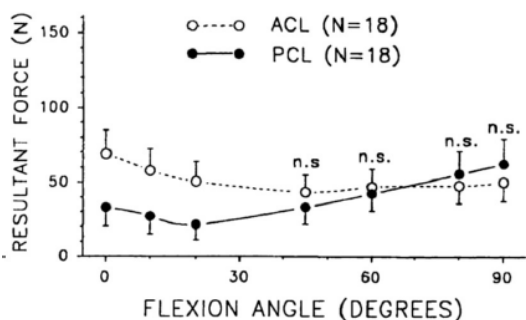


Figure 2-21 Influence of a valgus moment of 15 Nm on the cruciate ligaments for different knee flexion angles. Source Wascher et al. (1993), reprinted with permission.

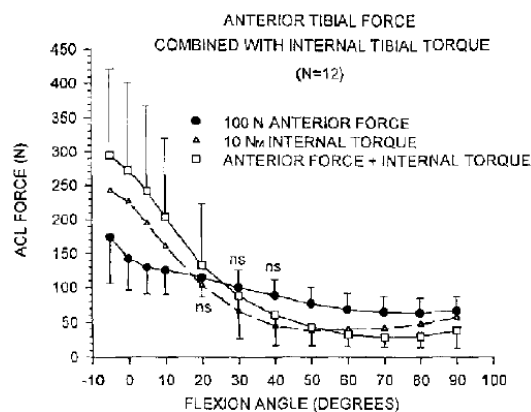


Figure 2-22 Influence of combined load of anterior force and internal torque on the ACL. Source Markolf et al. (1995), reprinted with permission.

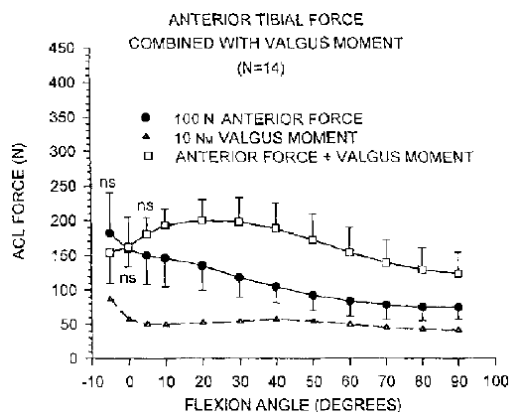


Figure 2-23 Influence of combined load of anterior force and valgus moment on the ACL. Source Markolf et al. (1995), reprinted with permission.

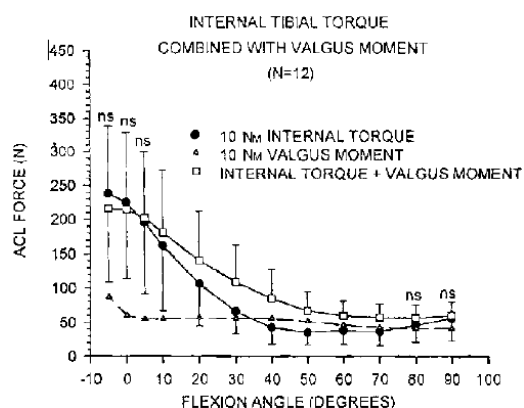


Figure 2-24 Influence of combined load of internal torque and valgus moment on the ACL. Source Markolf et al. (1995), reprinted with permission.

smaller than for the internal torque generation. This indicates that skiers are not able to deal with internal tibia torques to the same extent as for externally acting rotations of the tibia. This is in accordance with the above-mentioned findings that internal torques lead to higher ACL loads than external torques, as the ligament support by the musculature is smaller.

2.5 Summary and Derivation of Research Questions

The previous chapters showed that the understanding of knee injury mechanisms in alpine skiing is limited to descriptions of external observations of the location and dynamics of body parts before and during an injury (assuming the exact time of injury can be determined), the derivation of (bio-)mechanical loads leading to these situations, and a very scattered quantification of influences on ACL loads (mainly obtained from cadaver studies). One of the greatest challenges in extending this knowledge is the multitude of possible scenarios to study, as there are a nearly infinite number of possible kinematic and kinetic scenarios to consider. Also the interaction with the surrounding, for example, the selected equipment and the environment, as well as the interindividual and intraindividual variability complicate things. Quantification of the influences on ACL loads is necessary to allow the development of a safety system that on the one hand can protect the knee when required and on the other hand does not lead to more injuries through overly conservative behaviour. An example of the latter is an inadvertent release of the ski binding because the safety setting was set too low.

The objective of the following chapters is to extend the quantitative knowledge of the interaction of external and muscular loads on the loads in the ACL and thus be able to derive a technical solution to detect and react to a hazardous situation for the knee and especially the ACL.

3 Towards a Comprehensive Understanding of Knee Injury Mechanisms

Key points of this chapter

Surrogate study –

Influence of Quadriceps / Hamstring ratio and Hip angle on the ACL

Findings from the surrogate study demonstrate that an active hamstring can reduce the load in the ACL and a dominant quadriceps increases ACL loads for knee flexions smaller than 40°. Moreover, the ACL is loaded differently in flexion or extension movements with flexion movements mainly resulting in higher ACL loads. No statement can be made for higher flexion angles due to limitations of the study design. The hip angle influences ACL loads, but the relationship should be further investigated. Though a backward-leaning hip position resulted in smaller ACL loads in this study, a forward-leaning may be beneficial for stability and control in alpine skiing.

Multi-Body-Simulation –

Testing Ski Typical Loading Conditions

This simulation study aimed to quantify the effect of combined external loads on the ACL loads, which was achieved for loading scenarios including internal torque, varus and valgus loads, anterior tibial force, and axial compression for five different muscle activation ratios of the thigh. External torque was not simulated, as the model could not be validated for such simulation scenarios.

In summarising, Figure 3-28 (see page 3-82) illustrates the positive and negative influence of the investigated parameters on the ACL loads.

The investigations show that no sole parameter suffices as a control variable for a safety system. It can be stated that the knee flexion angle is the most important parameter with respect to the risk of injury, but ACL load varies greatly for the same knee flexion angle when combined with different muscle activations and external loads.

Derived recommendations to reduce the risk of knee injury in alpine skiing

A takeaway recommendation for every skier is that skiing with moderately flexed legs reduces the risk of injury. Moreover, targeted thigh muscle training allows the skier to increase knee stability and reduces ACL loads through muscle support.

With respect to technological improvements, it is clear, that a safety system monitoring the knee flexion angle, the muscle activity of the thigh, and the external loads acting on the ski could react more adequately in a given situation than a safety system only monitoring the loads acting on the ski. This can only be achieved with a mechatronic ski binding including appropriate sensor systems monitoring these parameters.

The following studies aim to expand knowledge about injury mechanisms of the knee in alpine skiing and quantify the relationships between internal and external influencing parameters and ACL loads. Therefore, studies are carried out using a combination of two different methodologies:

A leg surrogate is used to test the influence of various ratios of quadriceps and hamstring activations in the full range of knee flexion movement and extension movement. This scenario was chosen as existing literature could be used to validate the results². A multi-body simulation model of the same surrogate is developed for further investigations. The simulation model is validated with the results from the surrogate study and then used to investigate the influence of other parameters (rotational loads, applied singular forces) and combinations of parameters representing typical loads in skiing.

² For the validation and discussion of the surrogate study and the multi-body-simulation mainly the studies of Markolf, Washer, and group are used. This deliberately ignores thousands of other publications about the ACL and ACL loading and is explained by the similarity of the measurement principles of the surrogate and Markolf's system. An extensive explanation of Markolf's system and other principles to measure ACL load is given in Appendix 7.3

3.1 Study with a Leg Surrogate to Test the Influence of Muscle Activation on the ACL

Parts of this chapter were published in Hermann et al. (2022b). Minor alterations have been made for reuse in this work.

3.1.1 Introduction

The aim of this study was to quantify the influence of quadriceps and hamstring ratios over the whole range of knee flexion angles on ACL loads using a surrogate with ten motor-driven and force-controlled muscles. In addition, the influence of a hip angle of -20° and $+20^\circ$ and two different pre-loadings of the ACL are studied. A previous version of the surrogate was first published in Nusser et al. (2016).

3.1.2 Method

3.1.2.1 The Surrogate

Bone structures and joints

The tibia, fibula head, and femur of the surrogate consist of aluminum and were derived from a CT-Scan of a 35-year-old healthy male human (Figure 3-3 and Figure 3-4). The tibiofemoral joint and the patella-femoral joint are realized by prosthetic components manufactured by Smith & Nephew (London, UK).

Ligaments

Ligamental structures (ACL, PCL, LCL, MCL, and popliteus tendon) are realised by medical implants by LARS Ligaments (Arc-sur-Tille, France). ACL and MCL are instrumented by custom-made force sensors with a measurement range of 0 to 1.5 kN for the ACL and 0 to 500 N for the MCL. The original design of the surrogate intended to implement the two bundles of ACL and PCL (which would anatomically be more correct). The sensor design and the limited space for the sensor integration led to the integration of one sensor in the femur head and the other sensor in the tibia head. It showed that the integration of a sensor in the femur was impracticable, as the ACL bundle is loading the sensor non-orthogonally for knee flexion angles larger than 0° (Figure 3-1). The strain gauge sensor is not able to record forces parallel to the sensor, thus with increasing knee flexion angle, increasing load components are not “seen” by the sensor, leading to wrong results and interpretations.

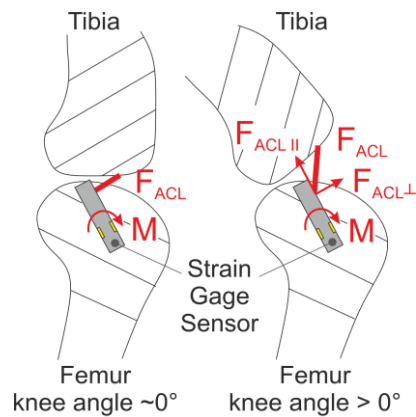


Figure 3-1 Issue of the ACL sensor implemented in the femur head. For knee flexion angles larger than 0° the sensor is not loaded orthogonally but can only measure forces in this direction.

Using a Multi-Body-Model of the surrogate (see Chapter 3.2) the effect of using only one bundle of the ACL was investigated. The results show that the insertion of the ACL bundle in the posterolateral insertion site on the femur and on the anteromedial insertion site on the tibia correspond with a double bundle setting (Figure 3-2).

Therefore, one LARS Ligament bundle was used respectively for ACL and PCL in this study.

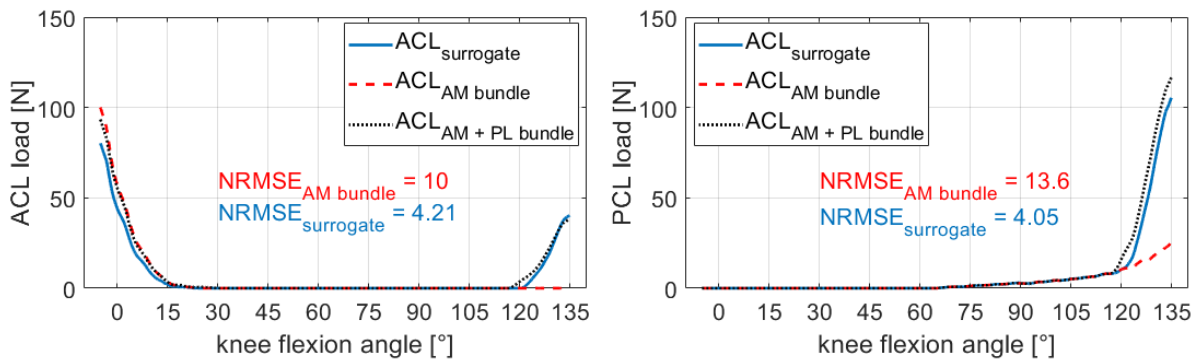


Figure 3-2 Results of a multi-body simulation to investigate the effect of using only one ACL bundle on ACL and PCL loads. Inserting the ACL bundle in the posterolateral insertion site on the femur and the anteromedial insertion site on the tibia (ACL surrogate) corresponds with the results of using a double-bundle (ACL AM+PL bundle). The ACL AM bundle graph represents an anatomical correct implementation of the AM bundle without an implemented PL bundle. Given is the normalized root mean square error (NRMSE) with respect to the ACL AM+PL bundles. For more details, see appendix 7.3.

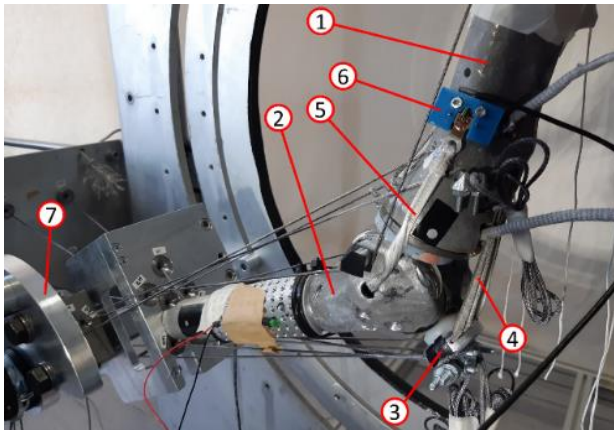


Figure 3-3 Leg surrogate (close-up on the knee). (1) Tibia, (2) Femur, (3) patella, (4) patella tendon, (5) MCL, (6) Force sensor measuring MCL-loads, (7) (part of the) hip. Also visible are the ropes representing the muscles.

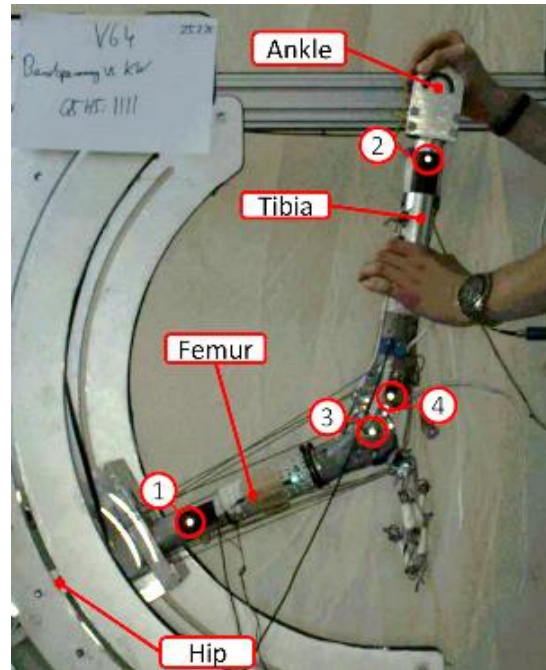


Figure 3-4 View from the medial side of the surrogate leg. The leg is upside down in the room. Points 1-4 are markers used for the camera-based tracking of the knee flexion angle. Femur: Marker (1) and (3). Tibia Marker (2) and (4).

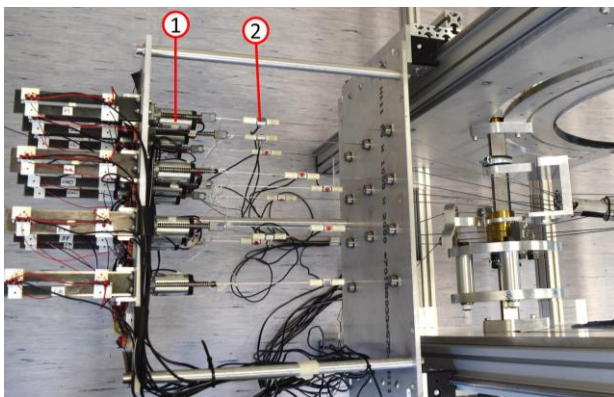


Figure 3-5 DC motors (1) and muscle force sensors (2) of the surrogate to control quadriceps and hamstring forces.

Muscles

Ten major muscles (Table 3-1), supporting the knee kinematic and stabilization are implemented. Muscle forces are transmitted by Dynema ropes and are measured via force sensors (0-5 kN, K-100 ATP Messtechnik, Ettenheim, Germany) in the ropes (Figure 3-5). Applied muscle forces are constantly controlled and kept on the same value by DC motors during a test scenario (knee flexion-extension movement), therefore, allowing studies with the same quadriceps and hamstring ratio over the whole knee flexion range. Correct anatomical insertion sites for the tendons are realized for realistic kinematic and kinetic behaviour.

Table 3-1 Applied muscle forces for quadriceps and hamstrings. Percentage value refers to peak muscle forces stated by Arnold et al. (2010). The peak force for M. vastus medialis is stated with 1444 N. As our surrogate is differentiating between M. vastus medialis longus and obliquus, the peak force was divided equally on both. The peak forces stated for the two heads of M. biceps femoris are summed up.

	100% in N	5% in N	15% in N
Quadriceps (Q) sum of all	5572	278	835
M. Vastus Lateralis	2255	113	338
M. Vastus Intermedius	1024	51	154
M. Vastus Medialis Longus	722	36	108
M. Vastus Medialis Obliquus	722	36	108
M. Rectus Femoris	849	42	127
Hamstrings and Gastrocnemii (H) sum of all	4400	219	659
M. Semitendinosus	302	15	45
M. Semimembranosus	1163	58	174
M. Biceps Femoris	1021	51	153
M. Gastrocnemius Medialis	1308	65	196
M. Gastrocnemius Lateralis	606	30	91

Joint Lubrication

Surrogate studies suffer from realising realistic friction situations compared to in-vivo and in vitro studies. The friction coefficient of the human tibiofemoral joint is reported to be 0.002-0.023 (Charnley 1960; Neville et al. 2007). To reduce friction, lubricant was used in the tibiofemoral joint of the surrogate. To find a suitable lubricant, three eligible products by Klüber Lubrication (Munich, Germany) were compared with bovine synovia taken from the angle joints. A tribological test using an Anton Paar Rheometer MCR 302 (Anton Paar Germany GmbH, Ostfildern-Scharnhausen, Germany) was performed. Material pairing in the test was the same as the implants used in the surrogate (100Cr6 (femur) and PEHD UHMW (tibia)). Test conditions were $T=25^{\circ}\text{C}$; contact pressure = 5.86 MPa; Speed: 0 – 3000 rpm, which equals a velocity of 0-3.3 m/s; Load = 1N; lubricant sample volume 50 μl ; synovial sample volume 100 μl . Results are shown in Figure 3-6. Klüberalfa YVI 93-152 was chosen as a lubricant for the surrogates' joint, as the measured friction coefficient was similar to or lower than the synovia's in the velocity range in which the loads are applied in the surrogate tests (about 0.02 m/s).

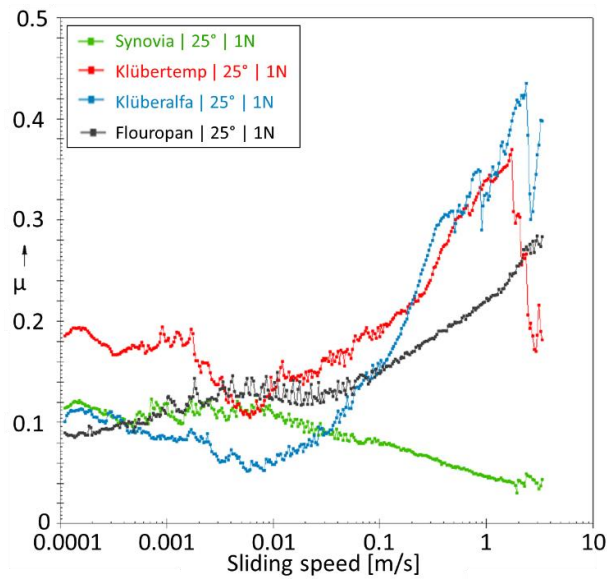


Figure 3-6 Tribological tests with bovine synovia and three lubricants (Klübertemp GR OT & Klüberalfa YVI 93-152 & Flouropan T20 Spray) at a temperature of 25°C. Klüberalfa was chosen as a lubricant for the surrogate, as the measured friction coefficient was similar to or lower than the synovia's.

3.1.2.2 Test Scenarios

Varied parameters are hip angle, quadriceps-hamstring ratio, and two different pre-loadings for the ACL and the MCL. In total 24 different test scenarios were performed resulting from all combinations of the variable settings in Table 3-2. Each scenario was tested five times. All tests were performed in a randomized order. This minimizes

Table 3-2 List of controlled parameters and pre-settings. In total 24 different settings were each tested 5 times in a randomized order (120 tests in total).

Attribute	Settings	Abbreviation
Knee flexion angle	(1) In each test the knee was flexed from total extension to maximum possible flexion (130°-140°)	
Hip angle	(1) -20° (backward leaning) (2) +20° (forward leaning)	
Muscle setup	(1) without muscle forces	Without (w/o)
quadriceps-hamstring ratio	(2) balanced	Q5H5
[%] of maximum forces	(3) only hamstrings	Q0H5
reported by Arnold et al. (2010). See Table 3-1.	(4) only quadriceps	Q5H0
	(5) Hamstrings dominant	Q5H15
	(6) Quadriceps dominant	Q15H5
Pretension of ligaments in 0° knee flexion	(1) ACL 50 N, MCL 45 N (2) ACL 85 N, MCL 75 N	-

effects by repetition of the same test scenario and increases the trustworthiness in repeatability of the results.

Applied Muscle Forces

Maximal muscle forces reported by Arnold et al. (2010) are used in this study. The applied muscle forces were either zero, 5 % of maximal force, or 15 % of maximal force (Table 2). In Arnold et al. (2010), the peak force for M. vastus medialis is stated with 1444N. The surrogate is differentiating between M. vastus medialis longus and obliquus, therefore, the peak force was divided equally on both. Also, the peak forces stated for the two heads of M. biceps femoris are summed up for the “one-headed” biceps femoris of the surrogate.

Pre-tension of ACL and MCL

Two different pre-settings for the ACL and MCL were tested. In setting (1) (see Table 3-2) the pretension of the ACL was set to 50 N. This setting was chosen to replicate results by Wascher et al. (1993). The MCL was set to 45 N to counteract the medial force applied by the ACL. In setting (2) it was aimed to set the ACL pretension to 30 N at 30° knee flexion. This was previously recommended in cruciate ligament replacement surgery (Markolf et al. 1996). This setting could not be reached, due to a too strong medial drift of the tibia, which may be attributed to the missing soft tissue and capsule normally counteracting movement of the joint. In addition, in a flexed state, the MCL is not tensioned and thus not counteracting the ACL. Therefore, the maximum pretension of the ACL at 30° flexion achievable (10 N) was set. This setting resulted in an 85 N ACL load in the extended leg. MCL pretension was set to 75 N in the extended leg to achieve a centred joint. While adjusting both ligament settings no muscle forces were applied.

Flexion-extension

In each test, the knee was flexed and extended manually by the same person. The person was training the procedure before the measurements at least five times in all muscle settings. The flexion movement was performed from an extended leg until the

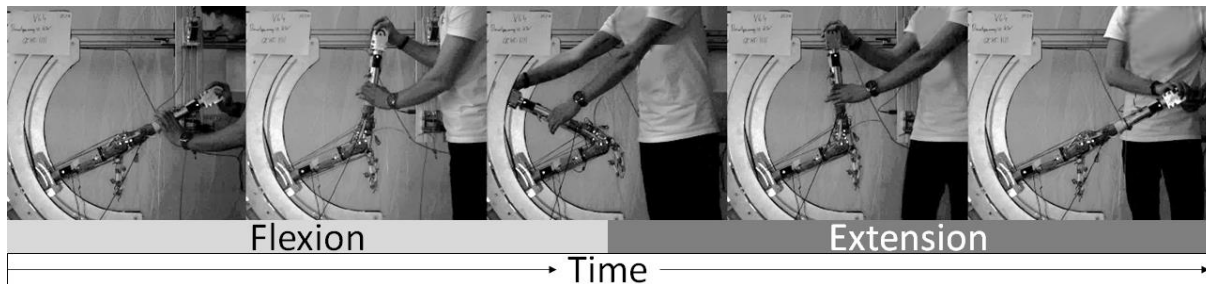


Figure 3-7 Flexion movement from extended leg to maximal possible flexion and vice versa. The flexion was performed by the same person in all tests.

maximal possible flexion angle was achieved and vice versa (Figure 3-7). The flexion range was limited by a bone-to-bone contact, which was varying slightly between the different settings of the musculature and the resulting respective anterior-tibial translation.

The knee flexion angle was recorded using markers (Figure 3-4) and a camera-based tracking system (SIMI Motion, Unterschleißheim, Germany). The camera system was synchronized with the rest of the measurement system. All data was recorded at a measurement frequency of 100Hz.

Data Processing

The mean values of the five repetitions for each setting was calculated for comparison. Moreover, seven knee flexion ranges were defined (-5° to 20° , 20° to 40° , 40° to 60° , 60° to 80° , 80° to 100° , 100° to 120° , $>120^{\circ}$). The mean values of the ACL load for each flexion range and test setting were calculated and compared. To test for significant differences in ACL load due to muscle force ratio, the results of one setting (hip angle $+20^{\circ}$; pre-loads: ACL 85 N, MCL 75 N) were used. This setting is deemed the most relevant for the investigation of skiing injuries due to the high ACL loads and the hip angle tested for. A one-way-ANOVA and a post-hoc Tukey's honestly significant difference test were calculated for each knee flexion range using Matlab. The significance level was set to $p < 0.05$. Flexion and extension movements were tested separately.

3.1.3 Results

The graphs of every individual measurement are provided in appendix 7.5.1 in Figure 7-16 to Figure 7-19.

For flexion angles greater than 90° an increasing external rotation of the tibia (maximum of about 12°, estimated by video data) with increasing knee flexion angle was observed for all tested scenarios with muscle activation (the tibia was unrestricted with respect to rotation).

Without muscle activation

Without muscle activation, the loads on the ACL increased for both an extended leg (knee flexion smaller than 45°) and for flexion angles greater than 100° (Figure 3-8 (a)-(d)). For a hip angle of -20° and higher preloads for the ligaments, the ACL loads increased for flexion angles larger than 80° (Figure 3-8 (c)). In mid-flexion, the ACL experienced no loading. With respect to the direction of the movement, loads were higher for the flexion movement in deeper knee flexion and higher for the extension movement for the more extended leg (see also Figure 3-9). The mean maximal knee flexion angle of each scenario was between 142 to 145° (see Figure 7-16 to Figure 7-19 in appendix 7.5.1).

Quadriceps dominant activation

The dominant quadriceps activation Q15H5 led to the highest ACL loads in all tested scenarios (Table 3-3). This was true, independent of the hip flexion or the preloads of the ligaments. Flexion movements led to higher ACL loads than extension movements for most knee flexions. Maximal ACL load did not occur in the hyperextended leg, but at the straight leg (about 0° knee flexion for +20° hip angle and 2° for -20° hip angle). An active quadriceps was shifting the point of no ACL load to higher knee flexions (Figure 3-8 (a)-(d)). For a hip flexion of +20°, the flexion movement of a Q5H0 ratio had comparable gradients to the flexion movement of an equalized muscle ratio of Q5H5. For a hip flexion of -20° the Q5H0 ratio, which is the only scenario with sole quadriceps activation, shifted the point of no ACL load to higher knee flexion angles to about 45° for the smaller ligament preloads (Figure 3-8 (a) magnification box) and to about 60° for the larger ACL preloads (Figure 3-8 (c) magnification box). This was true

for flexion and extension movements. No notable increase in ACL loads was observable for deeper knee flexions (with a maximal increase to 16 N).

Table 3-3 Maximal ACL loads for the flexion and extension movements.

	ACL=50N/MCL=45N; hip angle = -20°		ACL=50N/MCL=45N; hip angle = +20°		ACL=85N/MCL=75N; hip angle = -20°		ACL=85N/MCL=75N; hip angle = +20°	
max. ACL load [N]	Flex.	Ext.	Flex.	Ext.	Flex.	Ext.	Flex.	Ext.
w/o	48	45	50	54	59	57	79	76
Q0H5	55	66	65	75	112	117	98	105
Q5H15	97	116	136	141	118	138	154	163
Q5H5	98	92	129	120	107	104	151	152
Q5H0	110	101	131	120	142	136	154	147
Q15H5	142	143	186	171	155	150	199	188

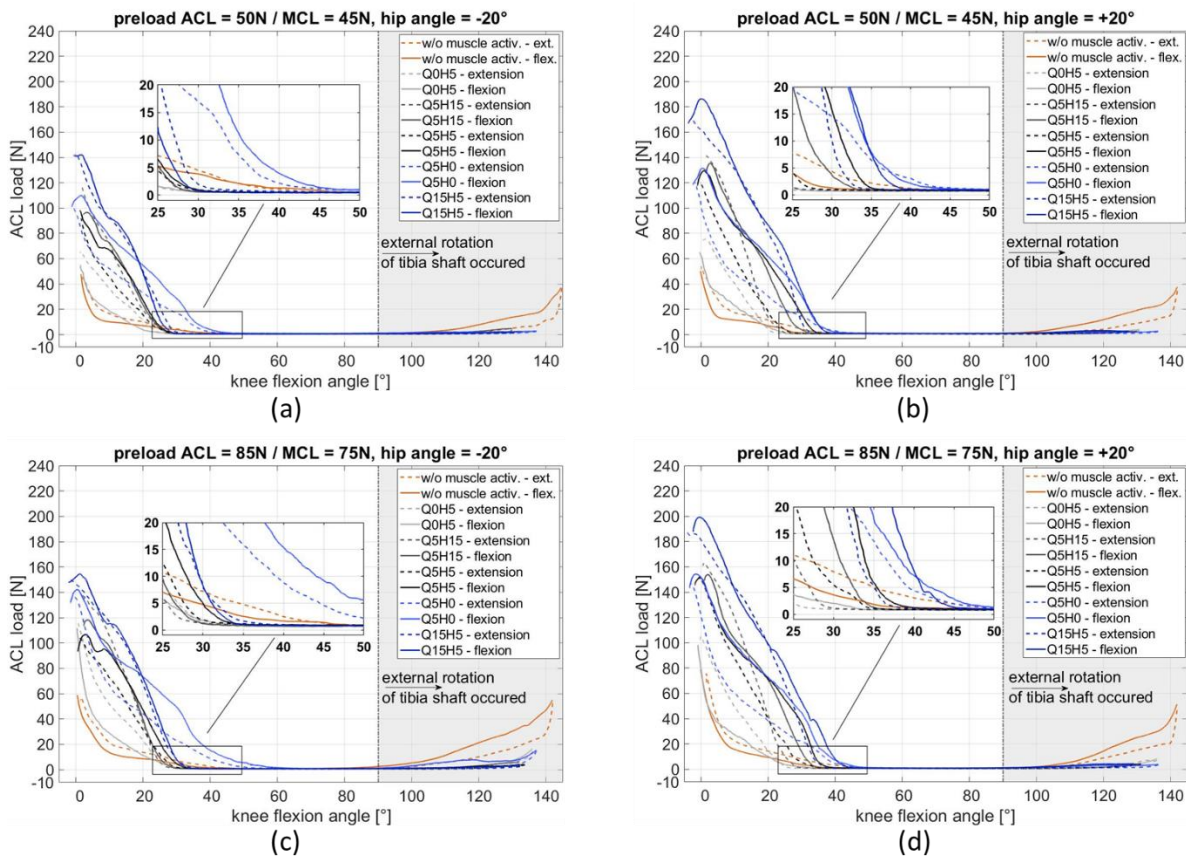


Figure 3-8 Resulting ACL loads over the knee's flexion range for different preloads of the ACL and MCL, different hip angles, and different muscle activations ratios of the hamstrings and quadriceps. The mean of five repetitions for each setting is plotted. The knee flexion was not restricted by external factors. An external rotation of the tibia to an extent of 12° (estimation based on video data) was observable for flexion angles larger than 90° caused by the PCL.

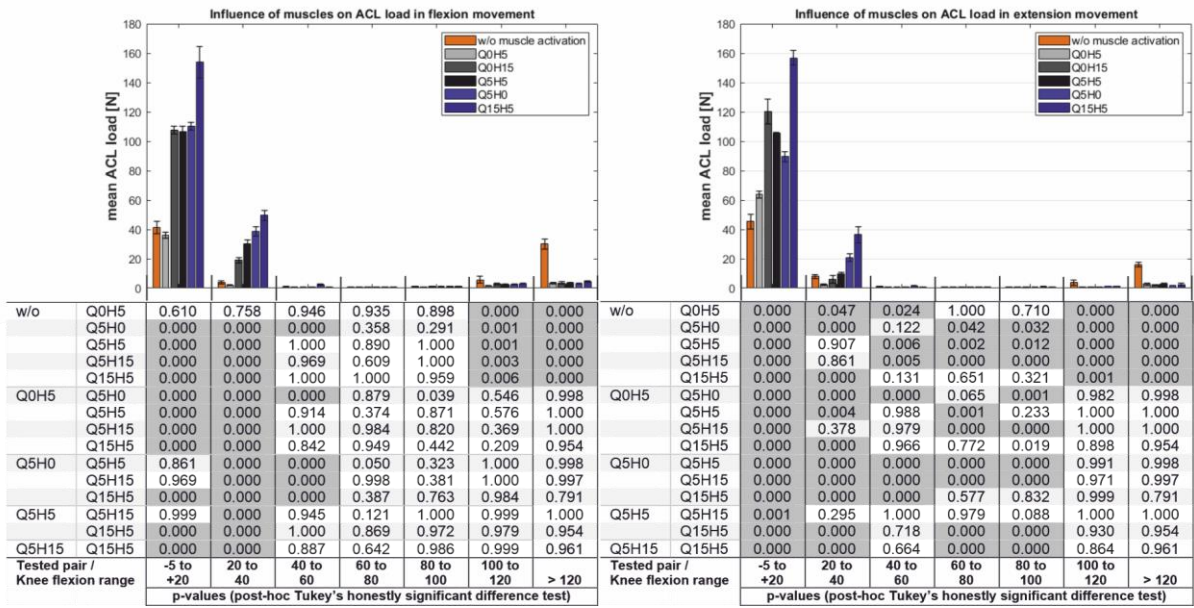


Figure 3-9 Mean ACL loads for different knee flexion ranges for different muscle activation for the setting +20° hip flexion, pre-loads: ACL 85 N, MCL 75 N. Each mean value is calculated from the means of the five repetitions of each setup. For each knee flexion range, the muscle activation was tested with one-way ANOVA and a post-hoc significance test. The p-values are given below each set of bars. Dark grey fields are significant ($p < 0.05$). Left: results for the flexion movement. Right: results for the extension movement.

Hamstring dominant activation

A dominant hamstring activation Q0H5 was loading the ACL only minimally compared to no muscle activation. An exception was the hyperextended leg, which led to the maximal loads of the ACL provoked in the Q0H5 scenarios. Extension movements led to higher maximal ACL loads than flexion movements (Table 3-3). This was true for knee flexions smaller than 10° for all measurements. The flexion movement of a Q5H15 muscle ratio led to similar loading gradients as an equalized muscle ratio of Q5H5 in a flexion movement, having slightly higher values for knee angles smaller than 15 to 18° (depending on the scenario), and smaller values for knee angles above this value. Extension movements in Q5H15 led to higher values than extension movements for Q5H5. In general, a dominant hamstring activation was de-loading the ACL (compared to Q5H5) for knee flexions >10° and shifted the point of an unloaded ligament by 10 to 15° to smaller flexion angles compared to the measurements with no muscle activation (Figure 3-8 magnification boxes). Only a small increase in the ACL load, up to 16 N, was observable for deep knee flexions.

Influence of the hip angle

In the range of -5 to 20° knee flexion, a hip angle of +20° led to 24 to 47 % higher ACL loads than a hip angle of -20° (Figure 3-10 (a)+(b)) for both, extension movements, and flexion movements. In the range from 20 to 40° knee flexion, a hip angle of +20° led to 30 to 110 % higher ACL loads. For flexion angles from 100 to 145° and a hip angle of -20°, the ACL loads were smaller (6 to 57%) in measurements with the smaller preload settings for the ligaments and the ACL loads were larger (20 to 40%) in measurements with the larger preload settings of the ligaments compared to the results with a hip angle of +20°.

Influence of different preloads of the ligaments

On average, larger preloads of ACL and MCL led to higher ACL loads (Figure 3-10 (c)+(d)). In a knee flexion range of -5 to 20°, the increase of 35 N ACL preload and 30 N MCL preload resulted on average in a 13.5 N increase in extension movements and 17.4 N increase in flexion movements.

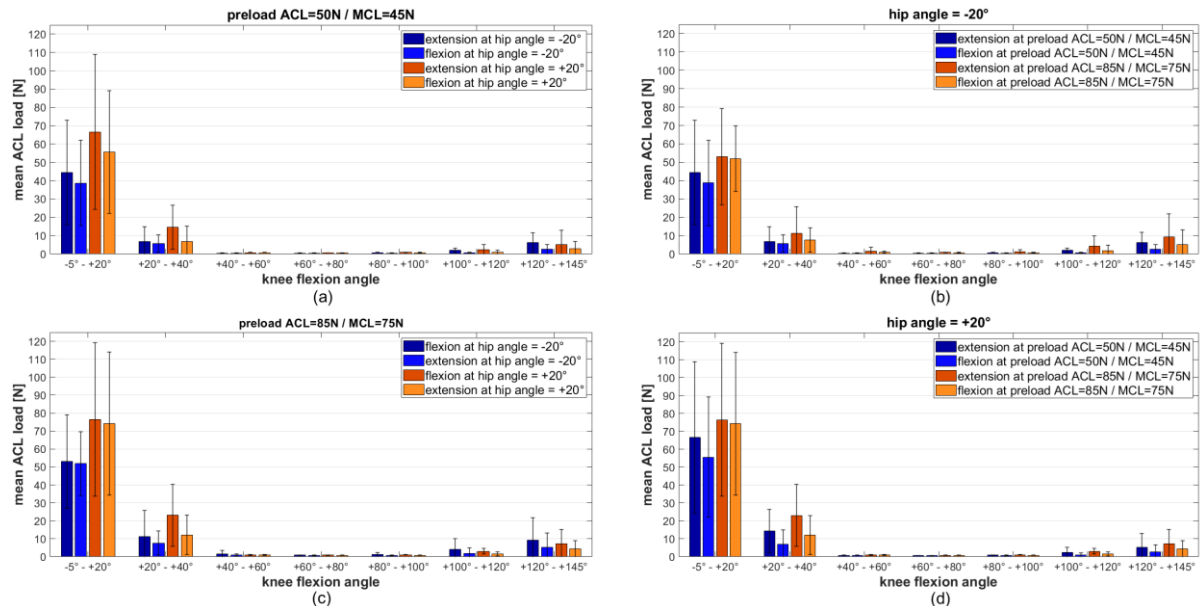


Figure 3-10 Influence of the hip angle (a) + (c) and the ACL/MCL preloads (b)+(d) on ACL loads. Each bar represents the mean and the standard deviation of all measurement points of all muscle set-ups in the given knee flexion range.

3.1.4 Discussion of the Surrogate Study

The used surrogate allowed the investigation of different ratios of quadriceps and hamstring contraction on the ACL. No reference was found that this was done before in surrogate or cadaver studies.

Results show that quadriceps dominance, hamstring dominance, and an balanced co-contraction (in the following text named only as co-contraction) have different impacts on the ACL load. Moreover, a flexion movement and an extension movement result in different ACL loads. In the flexion movement and for flexion angles smaller than 40°, hamstring dominance results in decreased or similar ACL loads compared to a co-contraction, and quadriceps dominance results in increased ACL load compared to a co-contraction.

In the extension movement, quadriceps dominance results in higher ACL loads than hamstring dominance. Compared to a co-contraction, the results depend on the muscle forces applied, the knee flexion, the hip angle, and the pre-loads of the ligaments.

With an increased extension of the leg, the ACL load increased, which reflects results reported by others (Markolf et al. 2004; Wascher et al. 1993). With increased flexion of the leg, the tests without muscle forces led to an increase in ACL loading. Wascher et al. (1993) observed the same for a passively flexed knee. All tests with applied muscle forces showed an increase in ACL loads for deep flexion angles of the knee. Similar results were reported for 100 N hamstring or quadriceps loading by Markolf et al. (2004).

In accordance with the literature, quadriceps loading is increasing the stress on the ACL more than hamstring loadings. But interestingly, this seems to be dependent on the direction of the movement and the hip angle. The extension movement with a +20° hip angle and with a dominant hamstring in the Q5H15 ratio led to higher ACL loadings compared to a sole quadriceps loading Q5H0 or the equalized Q5H5 ratio (co-contraction) in flexion angles < 15° (18° for tests with larger preloads of the ligaments). The same was true for the measurements with a hip angle of -20° with larger preloads of the ligaments, but not for the measurements with the smaller preloads of the ligaments.

A sole hamstring activation (Q0H5) was considerably increasing ACL loads in extension movements compared to the flexion movements. On the other hand, the sole quadriceps activation (Q5H0) was provoking greater ACL stress in flexion movements than in extension movements. This fact was not prominent for the test in which the dominant muscle group was counteracted by the other muscle group (muscle ratios Q15H5 and Q5H15).

This partly contradicts the common statement that the hamstrings are providing a protective contribution to the ACL. The results of this study indicate that always a co-contraction of hamstrings and quadriceps is beneficial for unloading the ACL. A positive effect observable for all measurements with dominant hamstring activation is a shift of the point of no ACL load to smaller knee flexion angles.

Larger preloads of ACL and MCL lead to larger loads of the ligaments throughout the flexion range of the knee. There is little knowledge of the true preloads of the ligaments. Moreover, it was not possible to reproduce surgical recommendations with the surrogate. This could be attributed to the fact that the surrogate knee misses a capsule, the menisci, and muscle volume to stabilize bone positions.

Our results indicate that a more forward flexed hip angle is negatively affecting the ACL loads due to the respective direction of muscle forces. Other authors emphasise that a flexed hip and active hip motion have advantages with respect to balance and shock absorption and are reported to have benefits for reducing ACL injuries (Blackburn and Padua 2008; Alentorn-Geli et al. 2009; Yu et al. 2006). These contradicting results show that the interacting kinematics of the hip and knee are complex and need further understanding.

No statement can be made for flexion angles above 90°. For flexion angles smaller than 90° the PCL is still (partly) relaxed. The increased loading of the PCL leads to the external rotation, as the tibia was not blocked in any direction. If the foot was standing on the floor this rotation would be counteracted by an internal torque due to friction and thus further load the PCL. Thus, the flexion-extension movement can be seen as an open-kinetic-chain. Other studies investigating the influence of open-kinetic-chain exercises on the kinematics of the knee also report external rotation of the tibia for

increasing knee flexions (Jonsson et al. 1989; Keays et al. 2013). As there is still a lack of information about ACL loads for deep knee flexion angles, future investigations with the surrogate in a closed-kinetic-chain setting should be performed.

Simplifications of the surrogate with respect to a real human leg partly limit interpretability. Indeed, several aspects of the surrogate were not considered or addressed in comparison to a human knee joint and lower extremity. Muscle volume change during muscle activation might alter the force direction of the muscle with respect to the bones and ligaments and is not included in the surrogate. Muscle volume may also affect knee kinematics (e.g. rotation centre or translations) due to geometrical boundaries, as the flexion is limited by soft tissue contact. Latter may result in less posterior translation of the tibia or even an anterior push of the tibia and, therefore, in rising ACL loads in deeper flexion angles. Missing structures (for example menisci and capsule) may decrease stabilisation or alter kinematics since these structures were recognized as secondary stabilizers (Ganapathy et al. 2018). The use of only one bone shape does not represent the individual characteristics of different humans. However, these limitations may also be present in cadaveric studies and, even more, in computer simulations. Overall, surrogate studies allow a repetitive investigation of numerous scenarios, without loss of the specimen and provide a valuable contribution to injury research. Surrogate studies have advantages in studying injury mechanisms. Compared to cadaveric studies, no specimens are used, and multiple scenarios can be tested more easily. In future studies, the surrogate used in this study provides the opportunity to test the application of external loads acting on the foot. This will also allow investigating the capability of the different muscles to protect the ACL against these loads. Muscle activation is an important variable with respect to knee injuries. A thorough understanding of the exact interactions will allow us to develop safer sports equipment and training plans to prevent such injuries.

Findings from the presented study demonstrate that an active hamstring activation can reduce the load in the ACL and a dominant quadriceps is increasing ACL loads for knee flexions smaller than 40°. Moreover, the ACL is loaded differently in flexion or extension movements with flexion movements mainly resulting in higher ACL loads. The influence of the hip angle is still unclear and needs to be investigated in future work.

3.2 Studies with a Multi-Body-Simulation-Model

3.2.1 Introduction

A multi-body-simulation-model (MBS-model) of the surrogate used in the previous chapter is used for further investigations. This brings some advantages as an automatised simulation of various scenarios is possible. Not all ligaments of the surrogate are instrumented with a force sensor, making a realistic setting of pre-tension difficult. The MBS-model allows to perform parameter sensitivity studies and, therefore, increases the interpretability and validity of the results of the surrogate. This is also true the other way around. Tests performed with the digital model can be performed with the surrogate for validation. Thus, the combined use of the surrogate and the MBS-model can increase the reliability and significance of the results. A very practical reason for using the MBS-model is that high loads can be tested without fear of damage or breakage of the surrogate.

3.2.2 Method

3.2.2.1 Infrastructure and Simulation Environment

To execute simulations of multiple scenarios in a fully automatised manner, Simpack (Dassault Systèmes, Vélizy-Villacoublay, France) was coupled with Matlab (The MathWorks Inc, Natick, Massachusetts, USA), and Matlab Simulink (Figure 3-11).

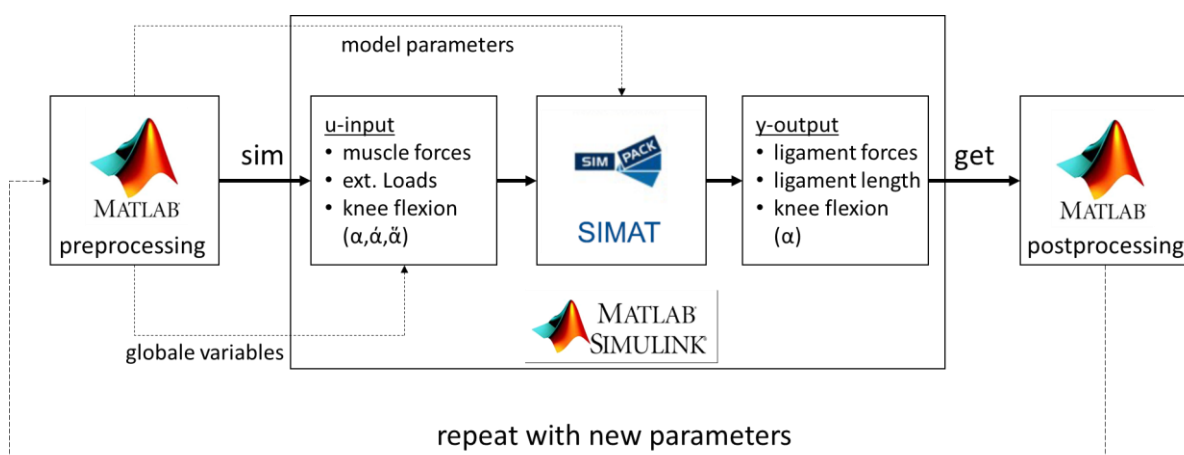


Figure 3-11 Structure of the coupled simulation between Matlab Simulink and Simpack

The simulation is controlled and parameterized in Matlab. The SIMAT-interface is a Matlab Simulink block enabling the co-simulation with Simpack by using the variables u-input and y-output for communication via a co-simulation server provided by Simpack. Moreover, the SIMAT block allows that model parameters (for example the stiffness of the ligaments) can be manipulated in Matlab. The simulation runs at a time resolution of 100 Hz.

3.2.2.2 Model

The MBS-model (Figure 3-12 left) is built (Hermann 2021) with the same CAD-data set used to build the surrogate. Also, the degrees of freedom for the joints are mirrored, with zero degrees of freedom in the hip and the ankle and six degrees of freedom in the knee (Figure 3-12 right). The hip flexion angle can be modified as a model parameter. Collateral and cruciate ligaments connect the tibia and femur and align them anatomically. Internal/external rotation, ad-/abduction, and medio-lateral translation are restricted by maximal ranges (based on Jagodzinski et al. (2016)), which are given in Table 3-4. The use of these limitations is necessary, to compensate for the increase of stiffness of the joint by the missing structures (like menisci, and capsule). Without the limitations, the model can become unstable for extreme test scenarios. The patellofemoral joint has six degrees of freedom (Figure 3-12 right).

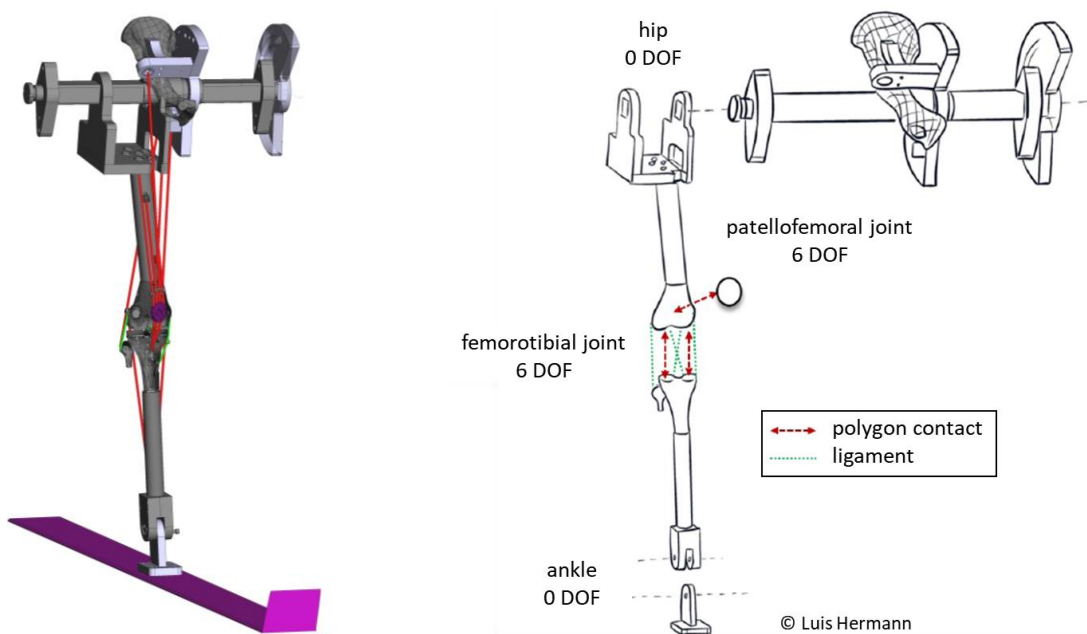


Figure 3-12 Picture of the MBS-model (left) and shema of the kinematics (degrees of freedom- DOF) of the model (right).

Table 3-4 Limitations of the knee's degrees of freedom. Selection of limits is based on Jagodzinski et al. (2016).

Degree of Freedom	Limit
Internal / External rotation	$\pm 30^\circ$
Ad-/Abduction (Varus / Valgus)	$\pm 30^\circ$
Medio-lateral translation	± 5 mm

The medio-lateral translation is limited to ± 5 mm to compensate for the missing stabilisation by the capsule, thigh muscles, and medial patellar retinaculum.

Joint surfaces

The articular surfaces of the femoro-tibial joint and the patellofemoral joint are modelled by polygon contacts (Figure 3-12 right and Figure 3-13). The polygon mesh is as smooth and homogenous as possible to prevent numerical problems.

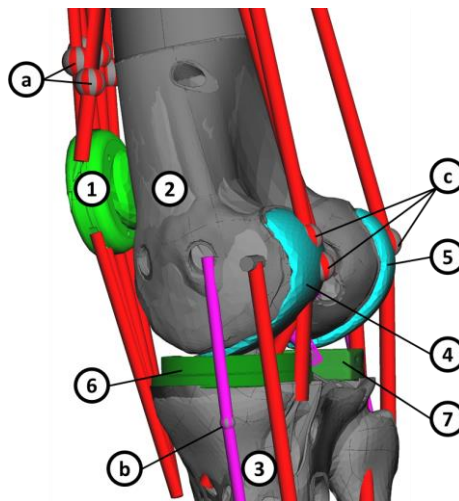


Figure 3-13 MBS-model of the knee. (1) Patella; (2) Femur head; (3) Tibia head; (4) medial femur condyle (prosthetic implant); (5) lateral femur condyle (prosthetic implant); (6) medial tibia plateau (prosthetic implant); (7) lateral tibia plateau (prosthetic implant); (a) dummy bodies quadriceps tendon; (b) dummy body medial collateral ligament; (c) dummy bodies hamstring muscles. The femoro-tibial joint and the patellofemoral joint are described by polygon contacts between (1)-(2), (4)-(6), (5)-(7), (a)-(2), (b)-(3); between (c)-(2) a point-surface contact is modelled.

In the surrogate model, both tibial plateaus and the sliding surface of the patella are made of polyethylene. In the MBS-model, these elements are assigned a modulus of elasticity of 1350 MPa with a layer thickness of 4mm. The metal components of the surrogate model are assigned an E-module of 210000 MPa with a layer thickness of 5 mm (medial and lateral femoral condyle, femur with embedded sliding surface for the

patella, cover of the patella). A damping coefficient for compressions of 5 Ns/mm^3 is assumed for all polygon contacts. A dynamic friction model with a static and dynamic coefficient of friction of $\mu = 0.01$ is assumed between the interfaces. This value is based on a lubricated friction pairing of polyethylene and steel (Uetz and Wiedemeyer 1984).

Ligaments

Collateral and cruciate ligaments are implemented as viscoelastic parallel spring dampers (Kelvin-Voigt point-to-point elements). The model parameters for each ligament are given in Table 3-5. The mathematical background, as well as the determination of the parameters for stiffness k , the initial length of the ligaments l_0 , and the parameter ε_l , is described in appendix 7.6.1 to 7.6.3. Simulation results using these parameters were compared in a sensitivity study to results with parameters reported in literature and parameters defined by the LARS Ligaments implants used in the surrogate studies (see chapter 3.1.2.1). The parameter sensitivity study was performed with respect to the characteristic parameters of ACL, PCL, LCL, and MCL and can be found in appendix 7.6.4.

The MCL consists of a medial and lateral part connected by a dummy body (see sphere (b) in Figure 3-13), which allows depicting the wrapping of the ligament around the tibia head by a polygon contact between the tibia and the dummy body. The collateral ligaments are implemented in two optional ways (Figure 3-14), as a double bundle and as a single bundle as instrumented in the surrogate. Results of the latter option are presented in the following, as this will allow validating the simulations in future tests with the surrogate.

Table 3-5 Parameters of the non-linear-elastic model of the ligaments as used in the MBS-model. The MCL is separated by a dummy body in a distal and proximal part.

Ligament	k [N]	ε_l	l_0 [mm]
MCL	13967	0.03	51.6 + 43.5
ACL	17296	0.03	29.8
PCL	22449	0.03	30.6
LCL	27160	0.03	71.7

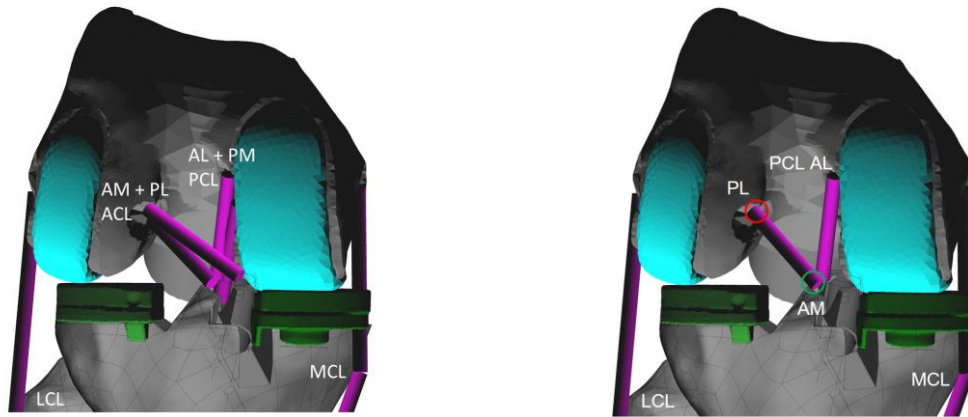


Figure 3-14 The two implementations of the collateral ligaments in the digital model: As a double bundle and anatomically correct (left) and as a single bundle mirroring the implementation in the surrogate. The latter is used for the following tests. See also the results of a comparative simulation in Figure 3-2.

Muscle implementation and tested muscle forces

The simulated muscles of the quadriceps and hamstrings and the tested muscle forces correspond to the set-up of the surrogate (Table 3-1) and anatomical insertion points are taken from the same CAD-dataset. The wrapping of the muscles around the bones over the flexion movement is made possible by using dummy bodies (shown in Figure 3-13 (a) and (c) and Figure 3-15). These dummy bodies separate the muscles in a tendon section with a linear-elastic behaviour and a muscular section implemented as a force vector. Dummy body-to-bone contact is modelled as polygon contact for the quadriceps and as point-surface contact for the hamstrings (to reduce computing effort). Wrapping of gastrocnemius medialis and lateralis is neglected and both are modelled as point-to-point force vectors between insertion points.

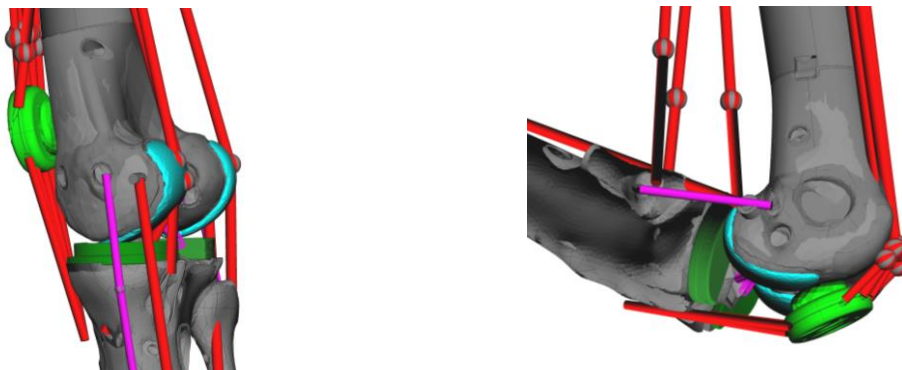


Figure 3-15 In the extended position, the dummy bodies of the hamstrings have bone contact (left). In the flexed knee, the quadriceps wrap around the femur, which is made possible by dummy bodies, the hamstring dummy bodies lose contact with the bone.

Flexion angle

To model a continuous flexion movement, a dummy tibia is used (green shape in Figure 3-16). The original tibia is fixed to the dummy tibia in the ankle joint. The dummy tibia rotates around an idealized pivot point of the knee joint and, thus, drags the tibia bone with it, which might have a different pivot point, due to the interactions with other structures. The simulated flexion range is -5 to maximal 135° and flexion and extension are applied with 3.5°/s.

Application of external loads

A model of an anterior or posterior force, a varus or valgus moment, and an internal or external rotation is implemented (Figure 3-17). Those loads can also be simulated in combinations. The anterior/posterior force is decoupled from the tibia by use of an auxiliary body (cuboid around the tibia head in Figure 3-17) to ensure that the force always acts in the sagittal direction of the femur.

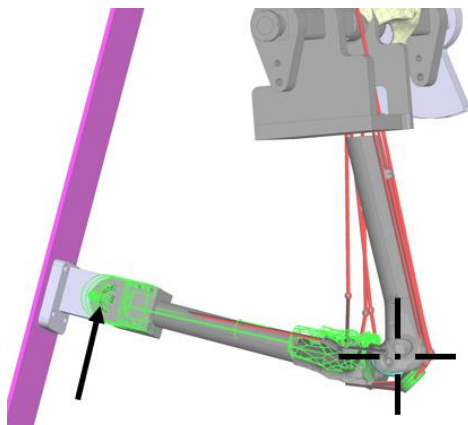


Figure 3-16 To model a continuous flexion movement a dummy body (green) is used, which rotates about the idealised pivot point (black cross) and is fixed to the tibia in the ankle joint, thus dragging the tibia with it (black arrow).

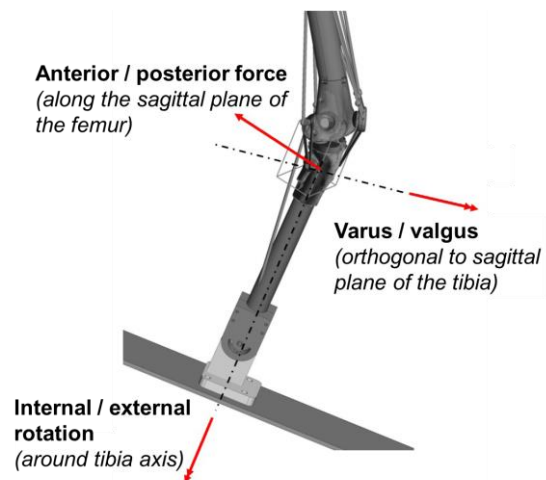


Figure 3-17 Definition of the effective direction of the external loads. The picture shows an internal rotation of the knee.

3.2.3 Model Validation

3.2.3.1 Test Scenarios

The model is validated against the results of the surrogate tests (chapter 3.1.3) and literature results.

Replication of the surrogate studies

The surrogate tests with the ligamental pre-tension of 50 N for the ACL and 45 N for the MCL are replicated. The tested scenarios and settings are given in Table 3-6.

Table 3-6 Scenarios and parameter settings of the surrogate studies replicated for the validation of the digital model.

Attribute	Settings	Abbreviation
Knee flexion angle	0°-130°	
Hip angle	+20° (forward leaning)	
Muscle setup quadriceps-hamstring ratio [%] of maximum forces reported by (Arnold et al. 2010). See Table 3-1.	(1) without muscle forces	Without (w/o)
	(2) balanced	Q5H5
	(3) only hamstrings	Q0H5
	(4) only quadriceps	Q5H0
	(5) Hamstrings dominant	Q5H15
	(6) Quadriceps dominant	Q15H5
Pretension of ligaments in 0° knee flexion	ACL 50N, MCL 45N	-

Replication of the studies testing external loads

(Markolf et al. (1990) and Markolf et al. (2004))

The study designs by Markolf et al. (1990; 2004) are replicated to validate the behaviour of the digital model in scenarios with external loads. The external loads used in the tests are given in Table 3-7, the muscle forces and setups are given in Table 3-8. The simulated knee flexion ranges from -5° to 135°.

Table 3-7 External loads used in the validation tests to replicate the studies of Markolf et al. (1990; 2004).

Load	Setting
Anterior / posterior force	± 100 N
Varus / valgus moment	± 5 Nm
Internal / external rotation	± 5 Nm

Table 3-8 Muscle setups with respective muscle forces used in the tests to replicate the studies of Markolf et al. (1990; 2004).

	M0: w/o muscle activation [N]	M1: Hamstring activation 100 [N]	M2: Quadriceps activation 100 [N]
Quadriceps (Q)			
M. Vastus Lateralis	1	1	20
M. Vastus Intermedius	1	1	20
M. Vastus Medialis Longus	1	1	20
M. Vastus Medialis Obliquus	1	1	20
M. Rectus Femoris	1	1	20
Hamstrings and Gastrocnemii (H)			
M. Semitendinosus	1	33	1
M. Semimembranosus	1	33	1
M. Biceps Femoris	1	33	1
M. Gastrocnemius Medialis	0	0	0
M. Gastrocnemius Lateralis	0	0	0

3.2.3.2 Results

Replication of the surrogate studies

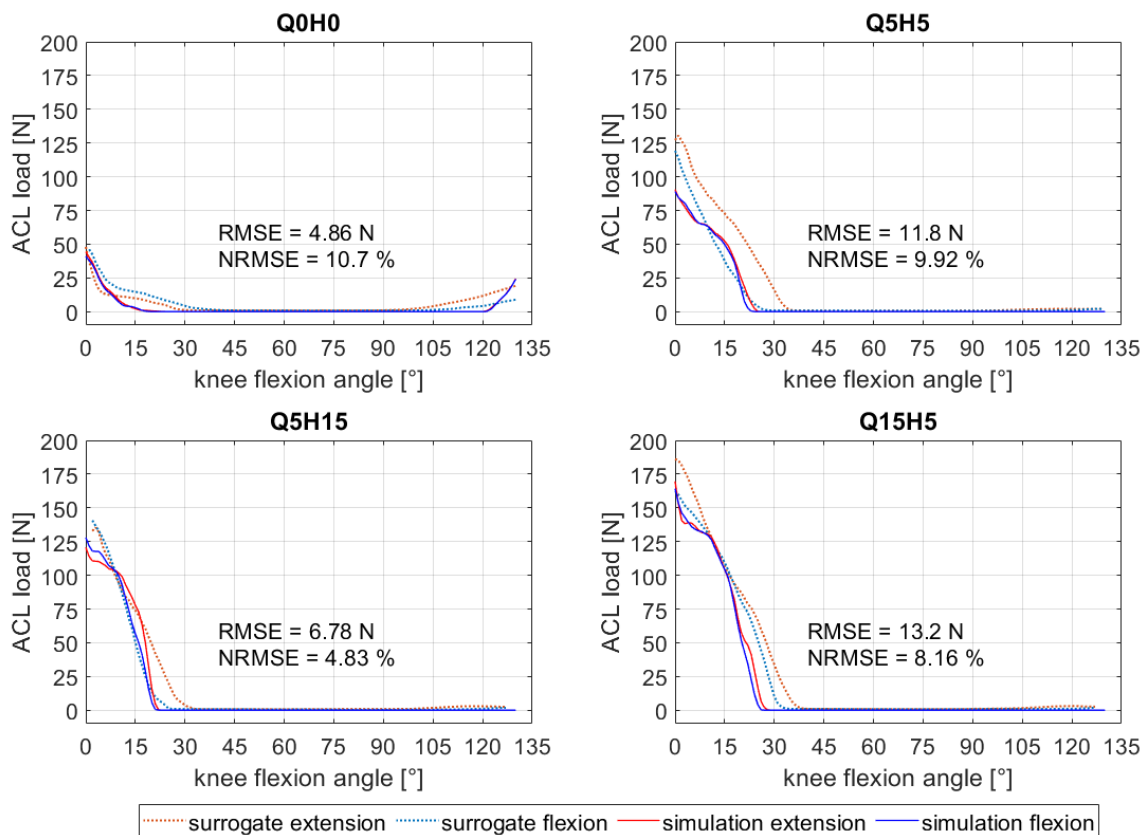


Figure 3-18 Comparison of the results of the surrogate study and its replication with the digital model.

Qualitatively, the curves of the ACL load of the simulation results are very similar to those of the surrogate tests for all four setups of muscle forces (Figure 3-18). However, a shift of the flexion angle where the ligament is unloaded towards smaller flexion angles can be observed. Also, in the Q0H0-setup, the point in deep flexion, where the force increases again, shifts towards larger flexion angles. It is also noticeable that the simulation results show a significantly lower hysteresis (difference in ligament forces between flexion and extension) in contrast to the surrogate test results. The simulation underestimates especially ACL loads in extension movements.

For all four tested muscle setups, the RMSE is equal to or below 13.2 N and the NRMSE is equal to or below 10.7 %.

*Replication of the studies testing external loads
(Markolf et al. (1990) and Markolf et al. (2004))*

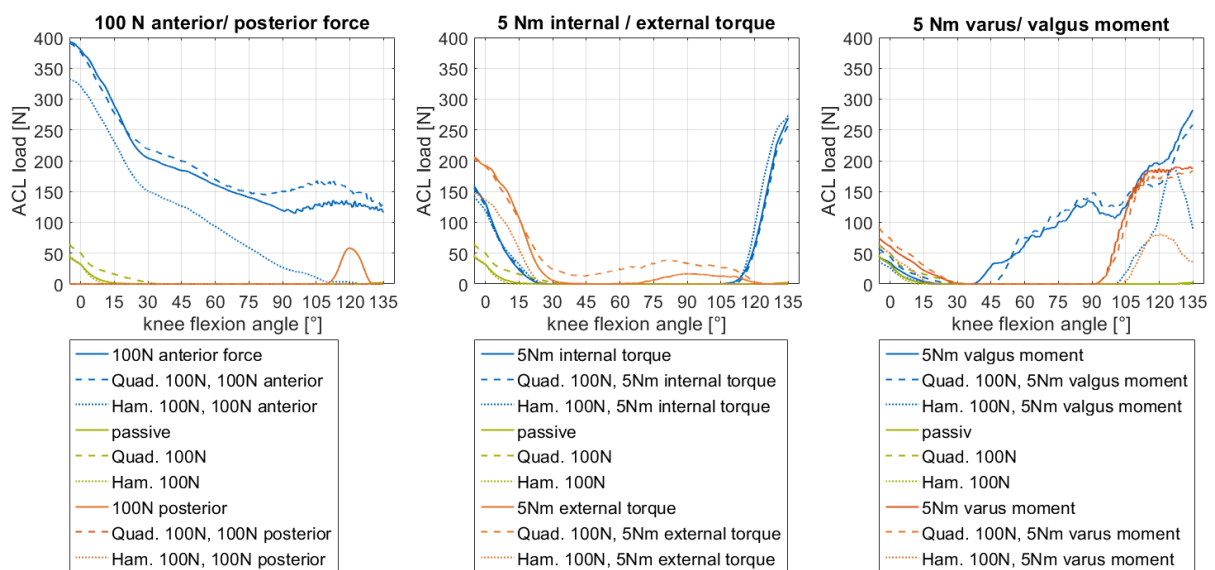


Figure 3-19 Simulation results of ACL loads resulting due to different external loads and load combinations which were also studied by Markolf et al. (1990; 2004), see chapter 2.4.



In a passive flexion (no muscle activation), the ACL loads decrease with increasing flexion. At a flexion angle of about 15° and above, the ACL is unloaded. (Figure 3-19 green line)



A quadriceps activation of 100 N increases ACL loads for flexion angles smaller than 30° and shifts the point of an unloaded ACL to higher flexion angles (~30°). (Figure 3-19 green dashed line)



The effect of isolated 100 N hamstring forces on ACL loads is small with a minimal decrease in ACL loads. (Figure 3-19 green dotted line)



A force in the anterior direction significantly increases ACL loads over all flexion angles. The effect lessens with increasing flexion angle. A posterior force results in complete relaxation of the ACL for flexion angles smaller than 110°. In passive flexion, an increased ACL load is observable due to a posterior force between 110° to 130°, which is not present if either a 100 N quadriceps or hamstring force is applied. (Figure 3-19 left)



A 100 N quadriceps activation in addition to an anterior force increases ACL loads for knee flexion angles above 20° additionally to the high load due to the anterior force alone. (Figure 3-19 left)



A 100 N hamstring activation in addition to an anterior force decreases ACL loads over all flexion angles compared to a sole anterior force. The effect is increasing with increasing knee flexion angle. At 30° knee flexion, the ACL load is three-quarters compared to a sole anterior force. At 90° knee flexion, the ACL load is one-quarter and at a knee flexion angle of 120°, it is 2% compared to a sole anterior force. (Figure 3-19 left)



At a straight leg, a 5 Nm internal torque increases ACL loads on a level three times as high compared to the unloaded knee. An increase in ACL loads is present for knee flexion angles smaller than 30°. Above 105° knee flexion, the ACL load increases dramatically and reaches five times the highest value measured without a rotational torque. (Figure 3-19 middle)



A quadriceps force in addition to an internal torque does not significantly affect the ACL loads, compared to a sole internal torque. (Figure 3-19 middle)



A hamstring force in addition to an internal torque does not significantly affect the ACL loads, compared to a sole internal torque. (Figure 3-19 middle)



In this study, an external torque increases ACL loads for flexion angles smaller than 30° even more than internal rotations. Moreover, ACL load increases for flexion angles greater than 70° to 120° . Above 120° no loading of the ACL was present. (Figure 3-19 middle).



For flexion angles smaller than 20° an additional 100 N quadriceps force to an external torque does not affect ACL loads compared to a sole external torque application. In contrast, for flexion angles between 20° to 120° the ACL load increases. (Figure 3-19 middle)



A 100 N hamstring force in addition to an external torque reduces ACL loads throughout all flexion angles of the knee (by approximately a quarter) compared to a sole external torque. (Figure 3-19 middle)



A sole valgus load significantly increases ACL loads for flexion angles above 40° (increasing with increasing flexion) and reaches a maximal load comparable to the maximal load resulting from an internal torque for very deep knee flexions. (Figure 3-19 right)



A varus moment increases ACL loads for knee flexion angles smaller than 30° . The increase is approximately 25 % for a hyperextended leg. ACL loads increase rapidly with increasing knee flexion angles above 90° reaching high loads of close to four times the pre-tension of the ACL at a straight leg. (Figure 3-19 right)



A 100 N quadriceps force in addition to a varus or valgus moment does not significantly alter ACL loads. (Figure 3-19 right)



A 100 N hamstring force can eliminate all ACL loads produced by a varus or valgus in a knee flexion range from 30° to 100° . Above 100° knee flexion angle, ACL loads resulting from a varus moment are more than halved by the hamstring activation. In addition, valgus loads are reduced but, nevertheless, reach higher loads. (Figure 3-19 right)

3.2.3.3 Discussion

The aim of the investigation was the validation of the multi-body-model. For most tested scenarios, the simulation results with the digital model are comparable (see summary

in Table 3-9) to results presented in the cadaver studies by Markolf et al. (1990; 2004). Only the simulation of an external torque on the tibia is in contrast to the literature. With respect to knee injuries in alpine skiing following findings are particularly important: A protective ability of the hamstrings against an anterior force acting on the knee is clearly observable. Moreover, a protective effect of activating the hamstrings in presence of a varus / valgus moment is apparent in the simulation results. In addition, the steady increase of ACL loads in mid flexion for a valgus loading is of relevance, as most other loading scenarios (internal and external torque and varus moment) are affecting the ACL only in small and high knee flexions. An anterior tibial load is negatively affecting the ACL over the whole flexion range of the knee.

Table 3-9 Comparison of results of replicated loading simulations and the reported results in the literature: Effect of external forces applied on the knee on the ACL loads.

Results Parameter	small knee flexion		medium knee flexion		large knee flexion	
	Literature	Simulation	Literature	Simulation	Literature	Simulation
Anterior force	- - -	- - -	- -	- - -	- -	- -
Posterior force	+	+	0	+	0	0/-
Internal torque	-	-	0	-	- -	- -
External torque	0/-	- -	0/-	- -	0	0
Varus moment	-	-	0	-	- -	- -
Valgus moment	0/-	0/-	- -	0/-	- -	- -

+ decrease; - increase; - - strong increase; - - - extreme strong increase; 0 no effect; in conflict with literature

With respect to the influence of the musculature, anterior loading simulations show qualitatively similar behaviour compared to the results of the cadaver studies by Markolf et al. (2004) but is showing higher ACL loads for an extended knee (about 400 N in the simulation versus 150 N in Markolf et al. (2004) and less than 200 N in Markolf et al. (1995)). This may be attributed to missing structures in the simulation model. The present protective ability of the hamstrings against an anterior force acting on the knee confirms results by Markolf et al. (2004).

In literature, there is limited quantification of the effect of a varus or valgus load on the ACL over the whole flexion range of the knee, and no study was found providing information on flexion angles above 90°. In the simulations, a valgus moment increases the loads in the ACL only slightly for small flexion angles. In medium and large flexion, ACL loads increase significantly. This behaviour was also reported by Markolf et al.

(1990; 1995) and Wascher et al. (1993) for flexion angles up to 90°. However, the increase in ACL loads for small flexion angles shown in the simulation results is more pronounced than reported in the named literature. A varus moment increases the loads in the ACL significantly more than a valgus moment.

In medium flexion, the ACL is completely relaxed under a load of a varus moment and is only loaded again in greater flexion (>90°). Markolf et al. (1990; 1995) and Wascher et al. (1993) report this phenomenon for small and medium flexion angles up to 90°.

A protective effect of activating the hamstrings in the case of a varus / valgus moment is apparent in the simulation results. No in-vitro study can be found which investigates such loading conditions to validate these results. However, this effect can be supported by the general understanding of the hamstring geometrical interactions with the ACL (Ganapathy et al. 2018).

The popliteus tendon, which is implemented in the surrogate, is missing in the digital model. This tendon is acting against external torques and anterolateral translation (Jagodzinski et al. 2016). This may partially explain the high ACL loads resulting in the simulation due to a 5 Nm external torque (Figure 3-19 middle), which is in contrast to Markolf et al. (2004), who reported lower ACL loads resulting from an applied external torque than an applied internal torque of the same magnitude. The increase of ACL loads due to an internal torque is confirmed by the cadaver studies by Markolf et al. (1990; 2004) and Wascher et al. (1993). Also, the decrease of ACL loads in larger flexion with a quadriceps activation in addition to the internal torque is observable in the simulation results and shown by Markolf et al. (2004). Activation of the hamstrings in addition to an internal torque is reported to decrease ACL loads in smaller flexion angles and increase ACL loads in higher flexion angles Markolf et al. (2004), which can only be confirmed to a limited extent due to the very small differences in the force values of the simulation.

The digital model does not consider the wrapping of the cruciate ligaments, which are acting against internal rotation. This wrapping increases axial compression of the knee, which may result in a reduced load of the ligaments as the rotational load is transmitted through other structures. In external rotation, this mechanism is not present, as the cruciate ligament unwinds. No multi-body-model was found in the literature that modelled the wrapping of the cruciate ligaments. Even in most presented finite-

element-models, wrapping is neglected and only a few studies can be found, which include it. A reason for the negligence of wrapping is the high computational costs (Naghbi Beidokhti et al. 2017). As computational power steadily increases, hopefully, effective wrapping simulations will be possible soon, as the mechanisms play a major role in knee kinematics.

The simulations are validated against cadaver studies. As tissue of cadavers has altered properties compared to living tissue, differences in the extent of ACL loads are tolerable and a stronger focus should be on the qualitative comparison of results.

The presented digital model is a model of a model, the surrogate leg. The surrogate itself is a simplification of a real human leg. There is a risk that by modelling this surrogate, through further simplification or assumptions made, errors may add up and validity of interpretations made of the results may not be given.

The main limitations (of both models) are missing structures of the knee that play major roles in the knee joint kinematics in certain loading conditions. For example, the menisci, the capsule, as well as smaller ligaments and muscles will increase rotational stability (Jagodzinski et al. 2016).

The small NRMSE for the results of the digital model compared to the results of the surrogate tests indicate similar representability of both models. The digital model, compared to the surrogate, shows a shift of the point of the unloaded ligament towards smaller flexion angles. For interpretation with respect to skiing safety, these results of the digital model are more optimistic (smaller range of knee flexion angles with the loaded knee). Therefore, the data of the digital model should be interpreted more conservatively.

Despite the named limitations, the digital model is a valid tool to study injury mechanisms in alpine skiing for most scenarios. External torques are overestimated and therefore should not be included in further simulations or should be interpreted with care. A double-check of the results with studies carried out with the surrogate model would be desirable to further check the validity of the digital model.

3.2.4 Testing Ski Typical External Loads

In the previous chapters the interactions between elementary external loads acting on the knee and the ACL loads were discussed. In the three graphs in Figure 3-19, it is observable that in deep knee flexion an internal rotation, but also a valgus and an anterior force significantly increase ACL loads, which is amplified by a quadriceps activation. Even though this is highly relevant information, further quantification and a more distinct resolution of this interaction are necessary to allow the derivation of technological measures to reduce ACL injuries. If, for example, the decision algorithm of a safety device is relying on the knee flexion angle, the device must know the threshold for the knee flexion angle that is defining the difference between uncritical and critical knee flexion as precisely as possible. From the previous results and from the fact that existing ski bindings, which only act on singular external loading conditions, do not prevent knee injuries satisfactorily (see chapter 4.1), it is apparent that such a device should not rely on a singular parameter, instead a combination of parameters needs to be considered.

The following investigations use the digital model to further quantify the effect of combined loadings of the knee, as such commonly occur in alpine skiing (see chapter 2.3 and Table 2-3).

3.2.4.1 Test Scenarios

As shown in the previous study, the digital model overestimates the effect of external torques at the tibia on the ACL loads, therefore, only studies with internal torques are presented. The aim of the study is to quantify the influence on the ACL loads of

- an internal torque acting on the tibia,
- an internal torque + valgus loading,
- an internal torque + valgus loading + anterior force,
- an internal torque + varus loading,
- an internal torque + varus loading + anterior force,
- an anterior force,
- axial compression of the knee

over a flexion angle from 0 to 135° and different activation ratios of quadriceps and hamstrings. An overview of the parameter settings used in the simulations is given in Table 3-10.

Table 3-10 Parameters varied in the simulations of ski typical loads of the knee.

Attribute	Settings	Abbreviation
Knee flexion angle	0°-135°	
Muscle setup	(1) without muscle activation	
quadriceps-hamstring ratio	(2) balanced	Q5H5
[%] of maximum forces reported by (Arnold et al. 2010). See Table 3-1.	(3) Hamstrings dominant	Q5H15
	(4) Quadriceps dominant	Q15H5
	(5) strong co-contraction	Q15H15
Internal torque	0 Nm 30 Nm 70 Nm	IT
Varus / Valgus moment	0 Nm 20 Nm 40 Nm	Var / Val
Anterior tibial force	0 N 100 N	ANT
Axial compressive force	10 N 100 N	AXC

In the flexion movement simulation, the patella left the intercondylar notch between 35° to 75° flexion in simulations with high external loads (internal torque / valgus & varus). This is attributed to the bone geometry and missing ligamental and capsular structures. As this effect did not occur in the extension movement, only the results of the extension movement are presented in the results section. Because of the neglectable hysteresis between flexion and extension simulations, the impact of this effect on the results is estimated to be small. Nevertheless, further model development must investigate the issue and address it by implementing further ligamental or capsular structures which may counteract the movement of the patella.

3.2.4.2 Results

To allow an easy interpretation of the interactions between internal torque, varus or valgus moments, axial compression, anterior tibial force, muscle forces, and ligamental loads, the results are presented in grouped graphs in Figure 3-20 to Figure 3-27.

Internal torque + valgus (Figure 3-20)



An increasing internal torque increases ACL loads for flexion angles smaller than 30° and larger than 105°. In contrast, valgus loads affect the ACL mainly in medium knee flexion angles. The highest ACL loads are provoked by a pure valgus moment, which increases ACL loads for flexion angles larger than 30° for situations with no or small muscle activation or quadriceps-dominant muscle activation. An additional internal torque reduces the ACL load provoked by the valgus moment, with the effect that with 70 Nm internal torque and 40 Nm valgus moment the ACL loads only

increase for flexion angles smaller than 30° and larger than 100° (except for the situation without muscle activation).

Internal torque + valgus + anterior tibial force (Figure 3-21)



In general, an anterior tibial force significantly increases ACL loads over nearly all flexion angles if the muscles are inactive or in the case of a dominant quadriceps. For larger valgus moments (also in combination with internal torques), high ACL loads (> 500 N) are observable for knee flexion angles above 50° (for quadriceps-dominant activation only to 105°). Especially for larger flexion angles, hamstring activation is reducing ACL loads to a level that is comparable to a situation without anterior tibial force. For the hyperextended leg, an anterior tibial force increases the ACL load two to eight times, depending on the muscle activation.

Internal torque + valgus + axial compression (Figure 3-22)



Axial compression of the knee reduces ACL loads in all investigated scenarios.

Internal torque + valgus + anterior tibial force + axial compression (Figure 3-23)



Axial compression of the knee reduces ACL loads in all investigated scenarios compared to results without axial compression shown in Figure 3-21. The effect size varies for the different loading scenarios and is especially strong for medium valgus moments in the knee flexion range between 30° and 105°.

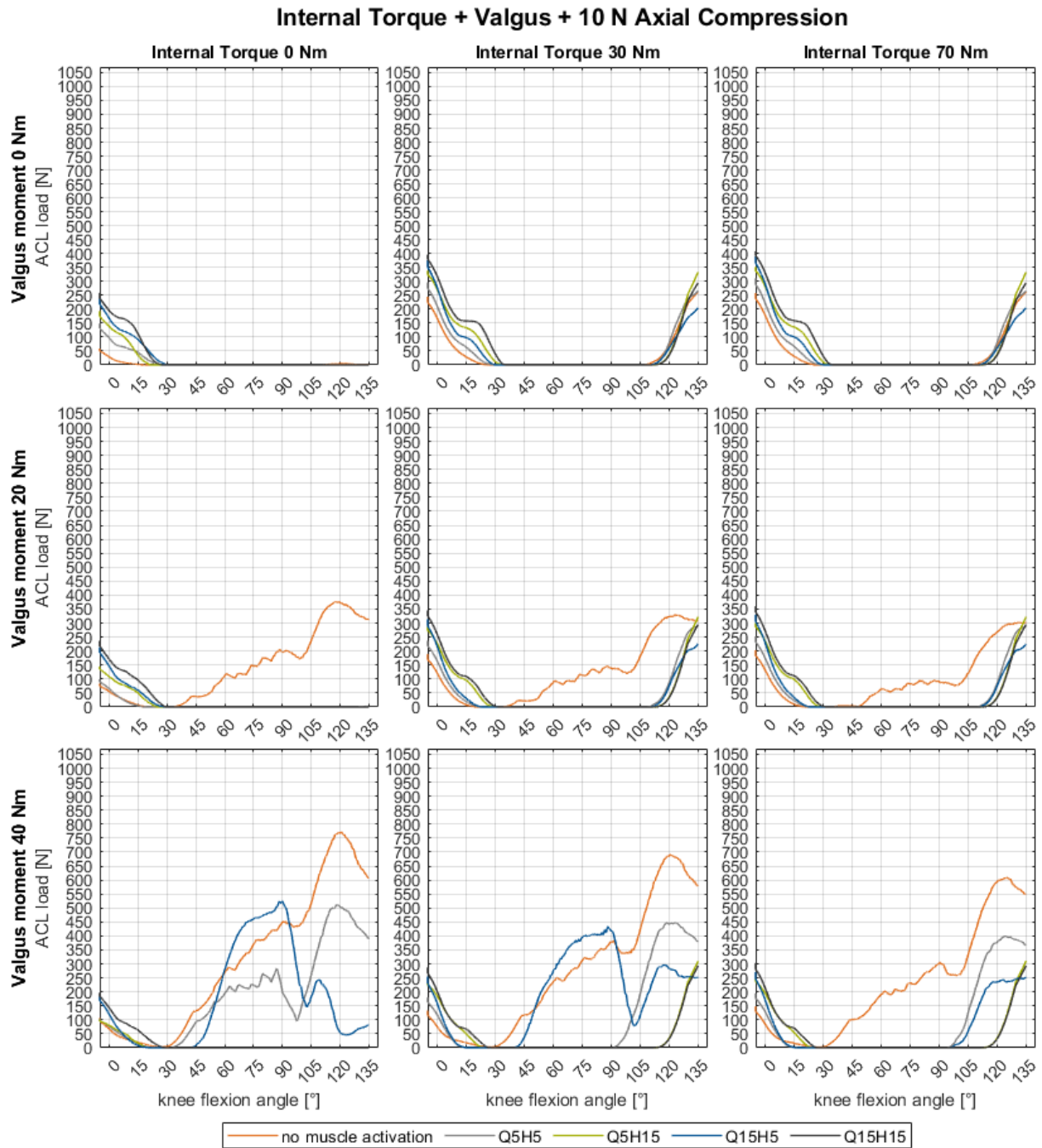


Figure 3-20 ACL load for different combinations of valgus loadings and internal torque acting on the knee for different muscle activation patterns (Table 3-10). No anterior force and 10N axial compression is acting on the knee.

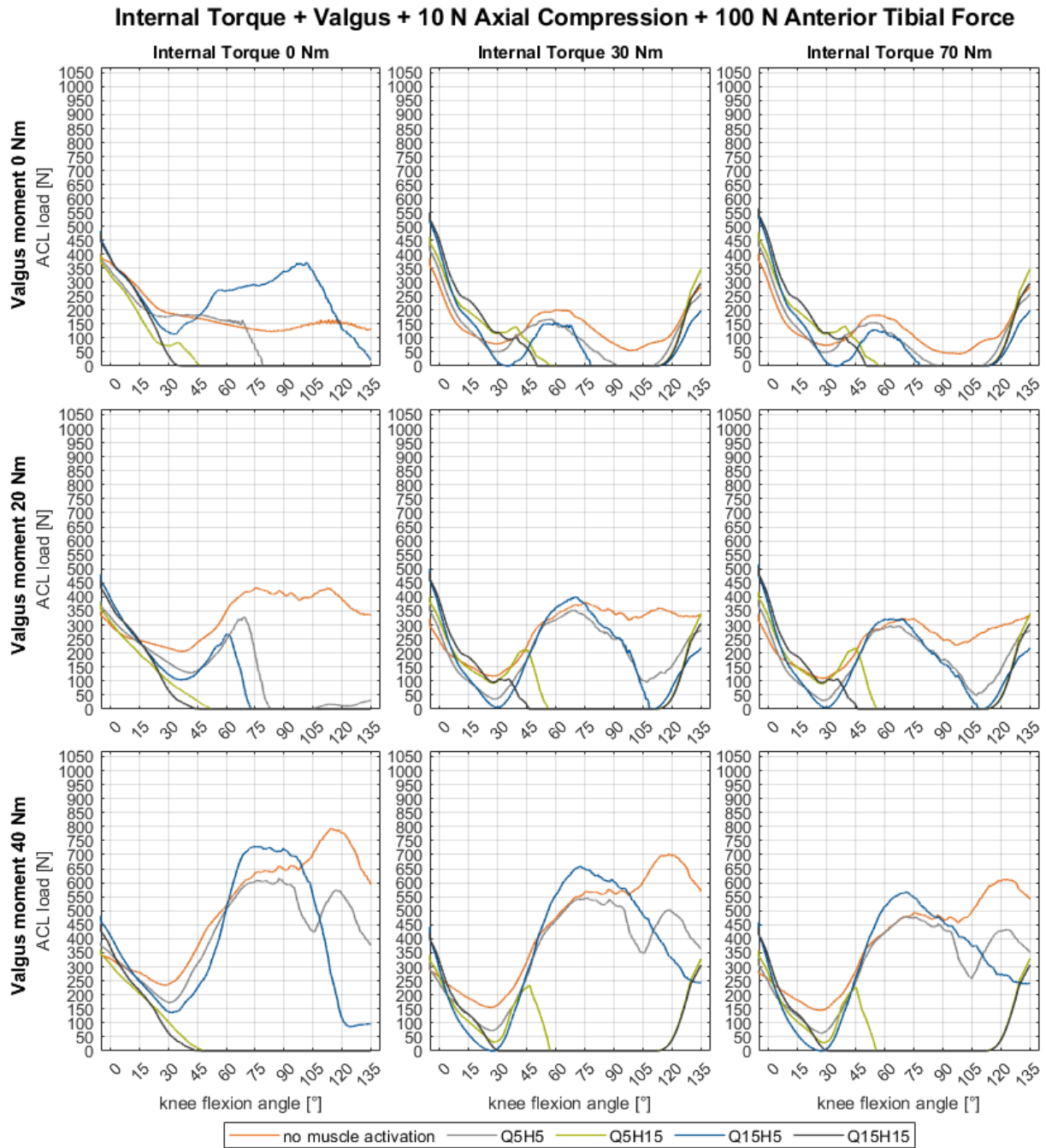


Figure 3-21 ACL load for different combinations of valgus loadings and internal torque acting on the knee for different muscle activation patterns (Table 3-10). 100 N anterior force and 10 N axial compression is acting on the knee.

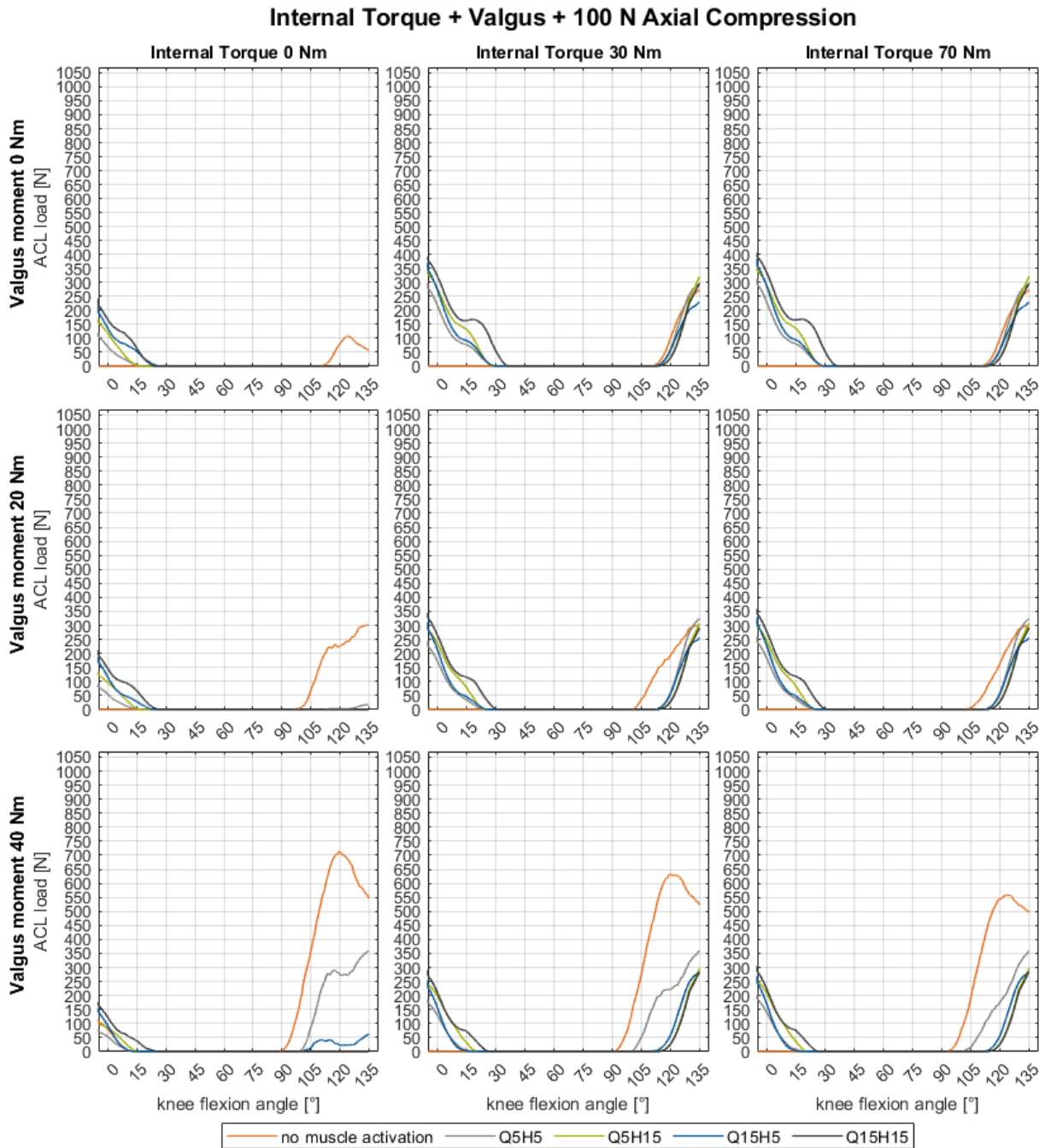


Figure 3-22 ACL load for different combinations of valgus loadings and internal torque acting on the knee for different muscle activation patterns (Table 3-10). No anterior force and 100 N axial compression are acting on the knee.

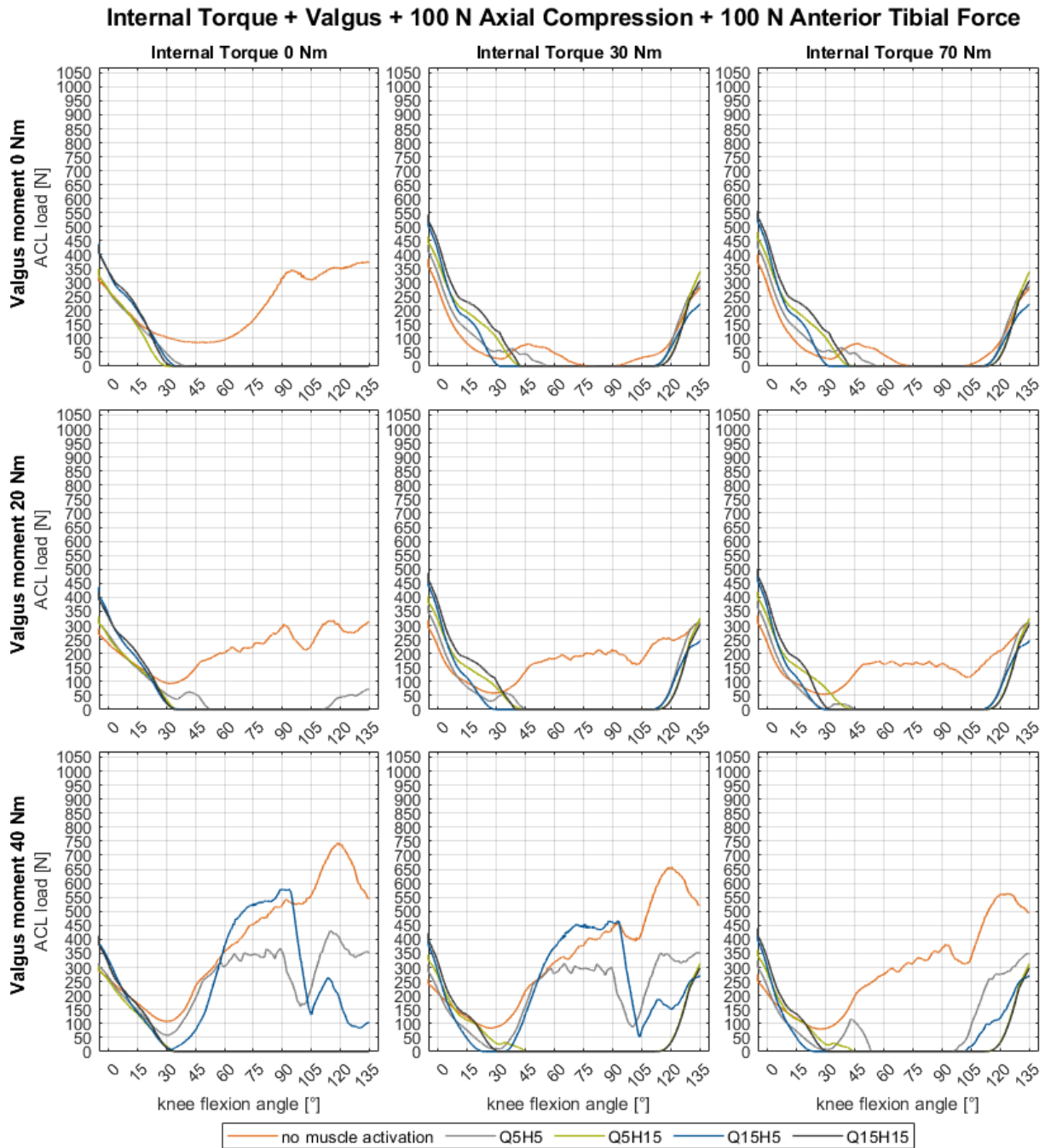


Figure 3-23 ACL load for different combinations of valgus loadings and internal torque acting on the knee for different muscle activation patterns (Table 3-10). 100 N anterior force and 100 N axial compression are acting on the knee.

Internal torque + varus (Figure 3-24)

A combination of internal torque and varus leads to an increase of ACL loads for knee flexion angles between -5° to about 40° and 80° to 135° . The ACL is unloaded in the flexion range between 40° and 80° . This is true for all Quad-Ham-muscle activation ratios. A negative effect of a varus moment is more pronounced at higher flexion angles. An additional varus load to an internal torque leads to a decrease in the maximal flexion angle of an unloaded ACL from 110° to 80° . Therefore, ACL loads increase for flexion angles above 80° . In case of no or small muscle activation, a sole varus moment (absent internal torque) increases ACL loads over all knee flexion angles. This effect is not present for higher muscle activations or in combination with an internal torque. Muscle activation leads to higher ACL loads for small flexion angles. For high flexion angles, increased muscle activation reduces ACL loads (especially the quadriceps has a stronger effect).

Internal torque + varus + anterior tibial force (Figure 3-25)

For a pure varus moment (absent internal torque), an anterior tibial force significantly increases ACL loads over nearly all flexion angles if the muscles are inactive or in the case of a dominant quadriceps. The effect is extreme for a situation with dominant quadriceps and reaches loads above 500 N for knee flexion angles larger than 75° / 45° for 20 Nm / 40 Nm varus moment. In the case of a combined varus moment and internal torque, ACL loads increase only moderately in all knee flexion angles. Compared to a combined valgus moment / internal torque, which showed to strongly impact ACL loads for medium (above 30°) flexion angles, a combined varus moment / internal torque is mainly influencing the ACL for smaller ($< 45^\circ$) and larger ($> 80^\circ$) flexion angles.

Internal torque + varus + axial compression (Figure 3-26)

An additional axial compression does not affect ACL loads, compared to the same scenarios without axial compression, for most tested scenarios. One exception is a pure varus moment in case of no muscle activation. In this case, the additional axial compression increases ACL loads for knee flexion angles larger than 75° . A second exception is a pure varus moment

with small muscle activation in co-contraction (Q5H5). In this case, the additional axial compression reduces ACL loads over all flexion angles.

Internal torque + varus + anterior tibial force + axial compression (Figure 3-27)



The most prominent effect of axial compression is the elimination of high ACL loads in a situation with quadriceps dominant muscle activation (Q15H5) and absent internal torque. In the other tested scenarios, the effect of an additional axial compression is very moderate (decreasing ACL loads) or not present at all.

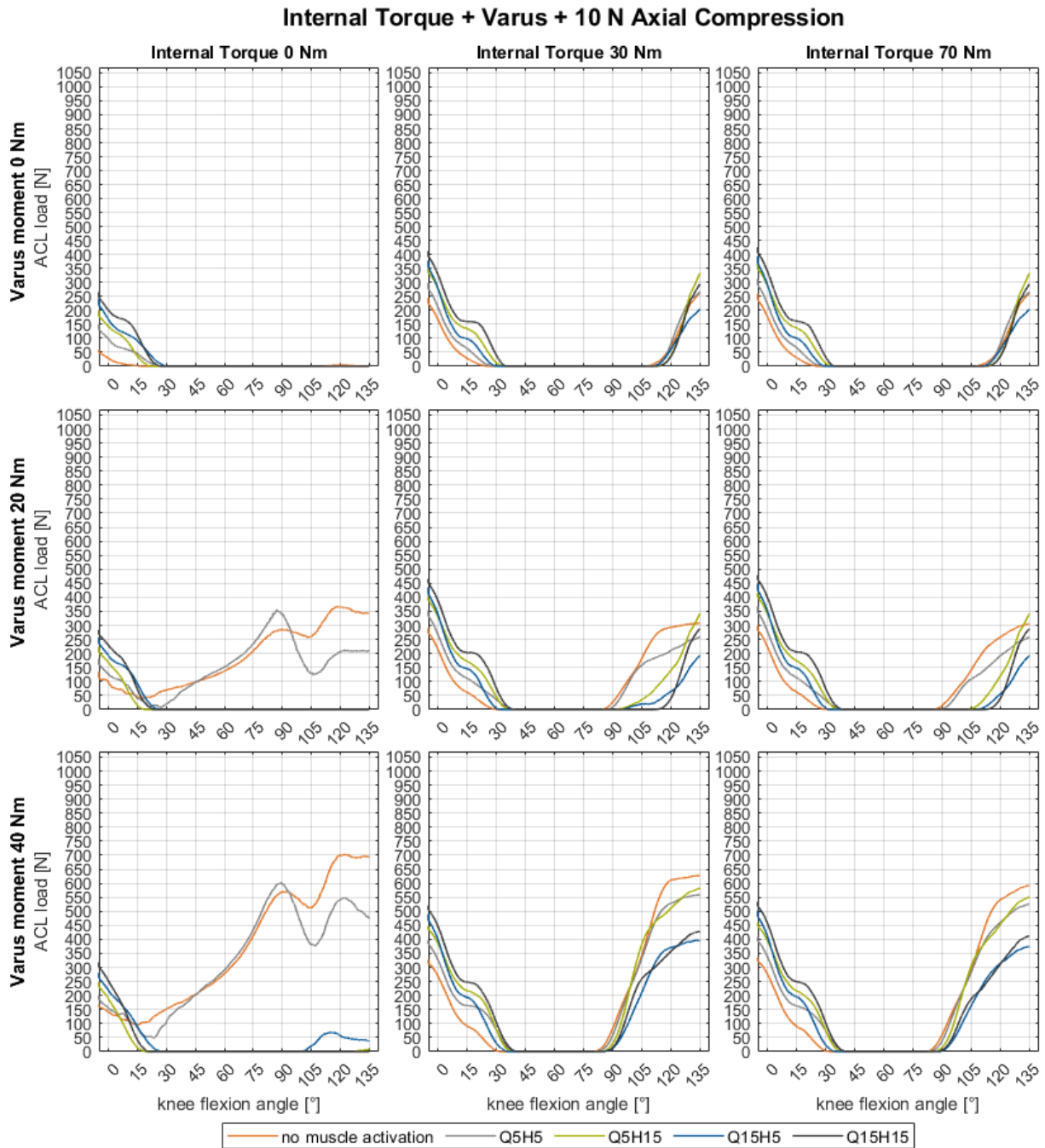


Figure 3-24 ACL load for different combinations of varus loadings and internal torque acting on the knee for different muscle activation patterns (Table 3-10). No anterior force and 10 N axial compression are acting on the knee.

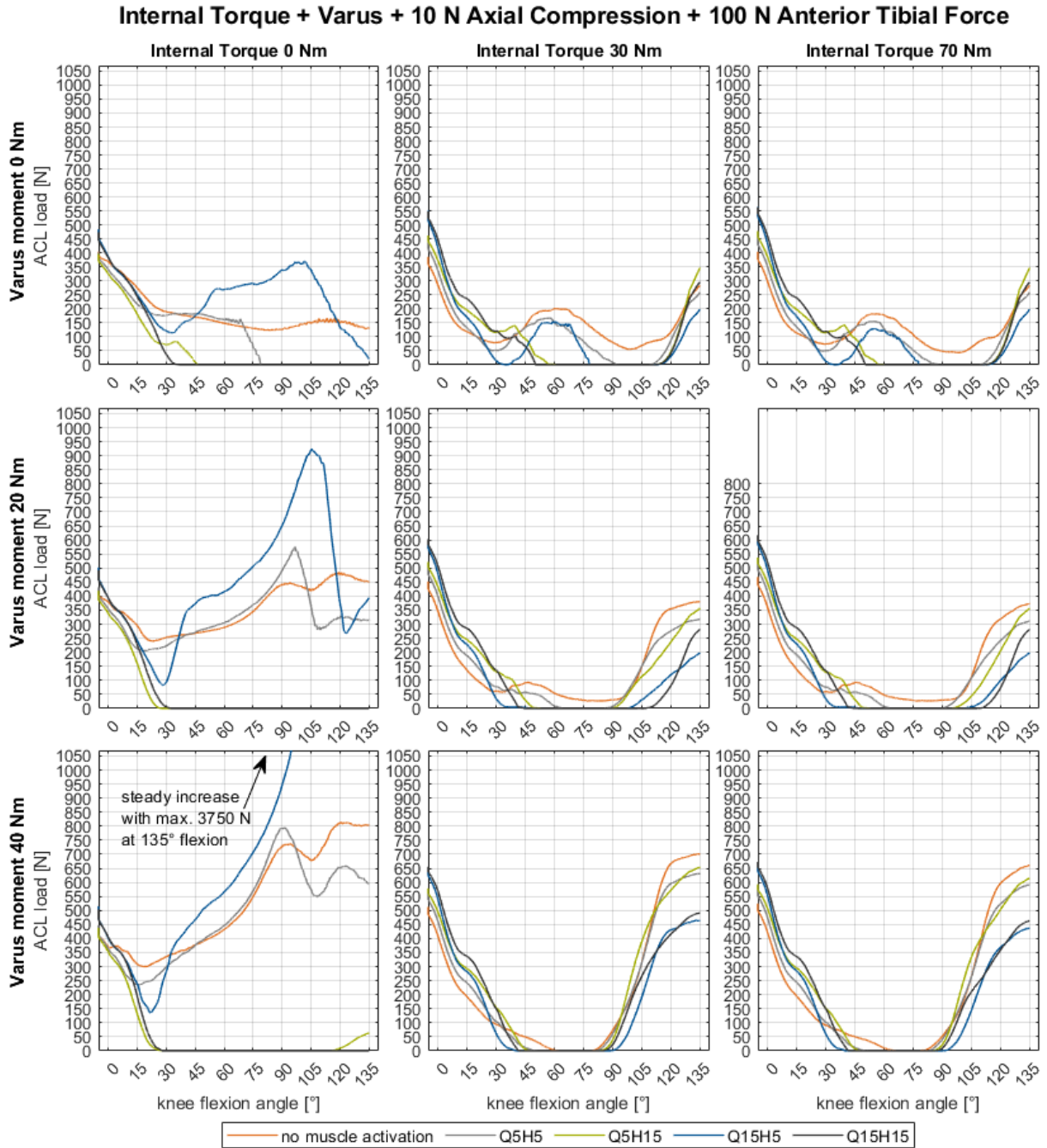


Figure 3-25 ACL load for different combinations of varus loadings and internal torque acting on the knee for different muscle activation patterns (Table 3-10). 100 N anterior force and 10 N axial compression are acting on the knee.

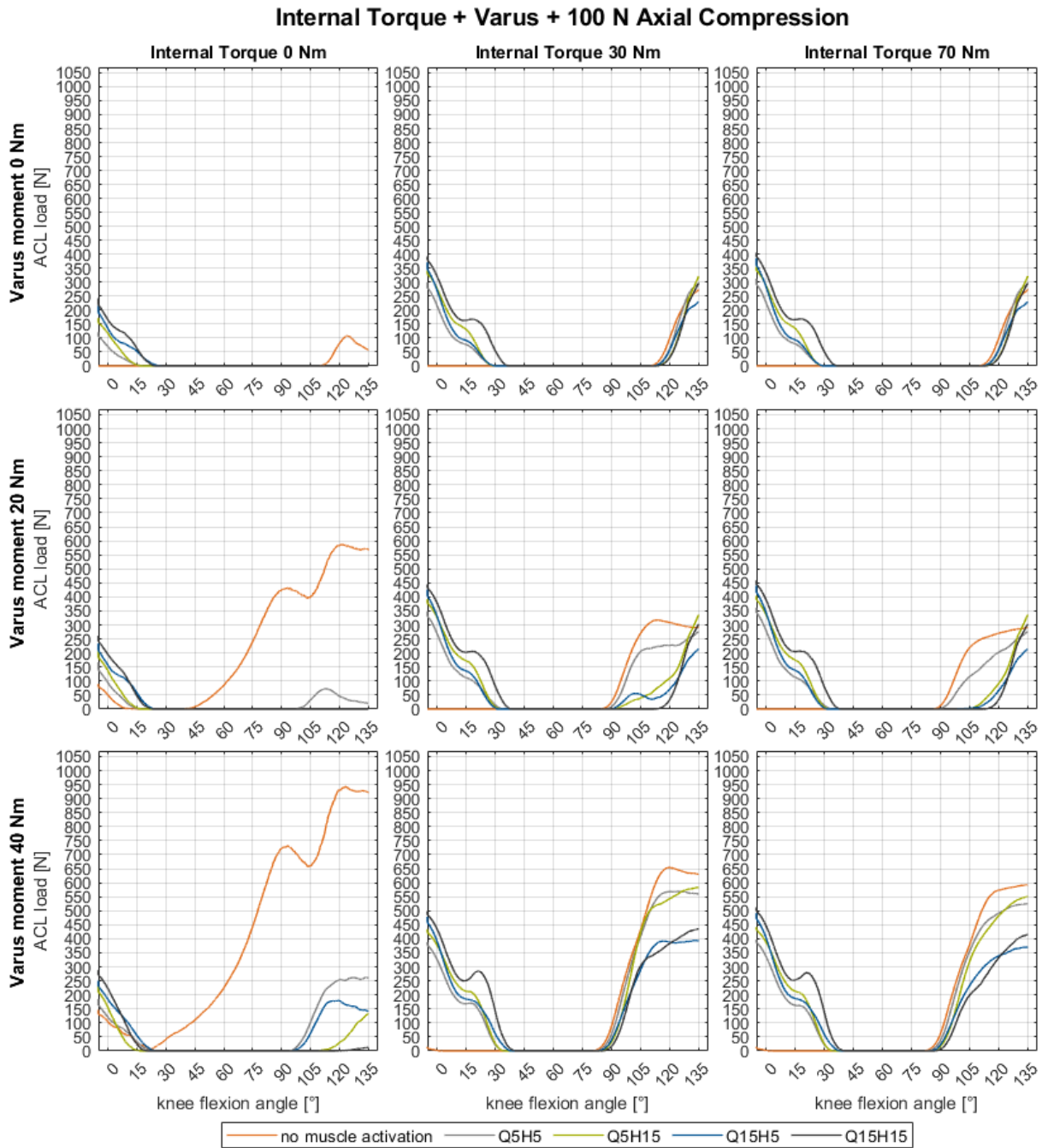


Figure 3-26 ACL load for different combinations of varus loadings and internal torque acting on the knee for different muscle activation patterns (Table 3-10). No anterior force and 100 N axial compression are acting on the knee.

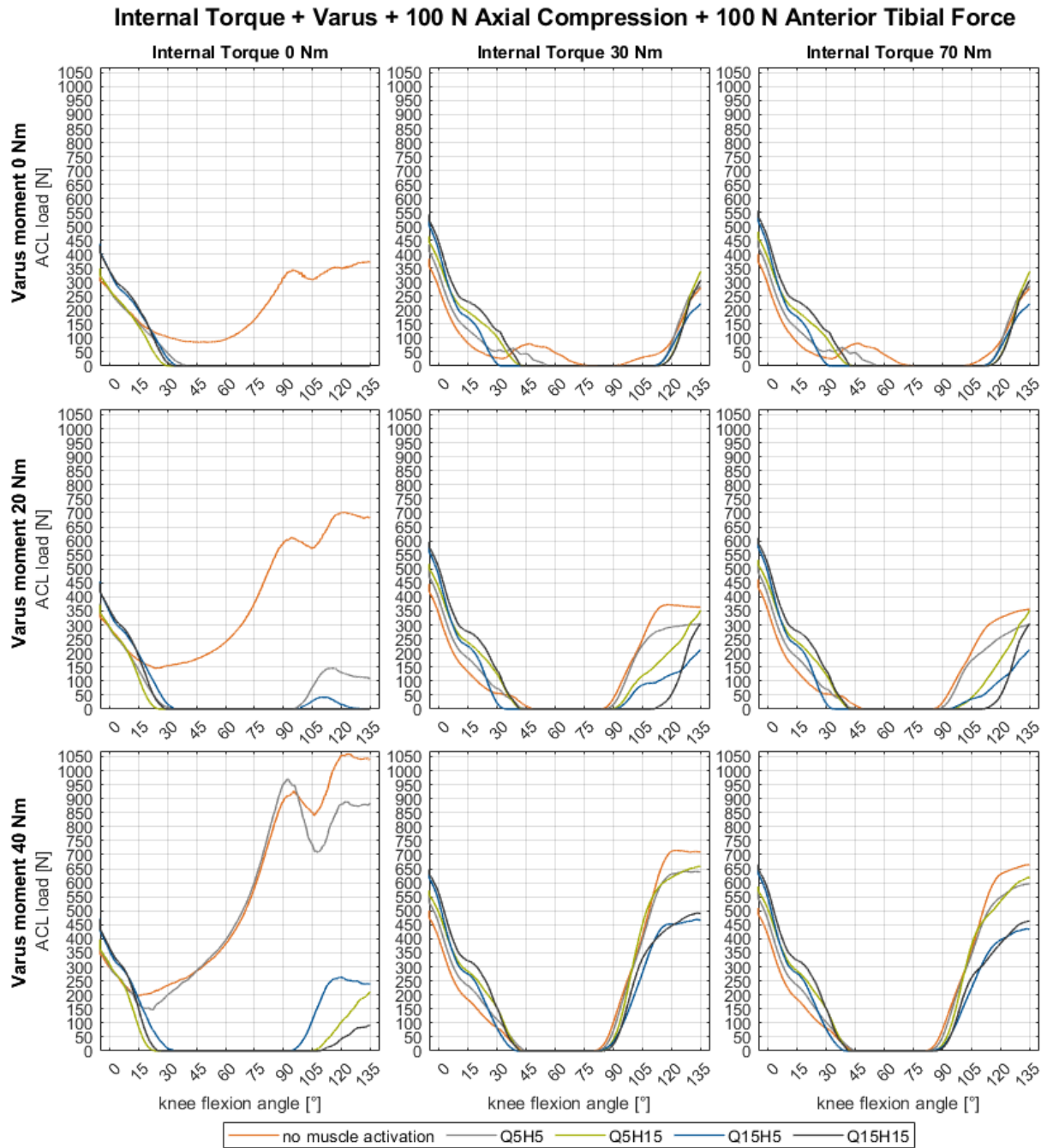


Figure 3-27 ACL load for different combinations of varus loadings and internal torque acting on the knee for different muscle activation patterns (Table 3-10). 100 N anterior force and 100 N axial compression are acting on the knee.

3.2.4.3 Discussion

This simulation study aimed to quantify the effect of combined external loads on the ACL loads, which was achieved for loading scenarios including internal torque, varus and valgus loads, anterior tibial force, and axial compression for five different muscle activation ratios of the thigh. External torque was not simulated, as the model could not be validated for such simulation scenarios.

One widely described injury mechanism is the phantom foot (see Figure 2-12 (c), page 2-27, Järvinen et al. (1994)) which is an internal rotation of the tibia plus valgus in deep knee flexion (backward fall). The criticality of such a situation can be verified by the simulations, especially in the case of low muscle activation. It is likely that in the situation of a phantom foot, an additional anterior tibial force is acting on the knee, which is induced by the stiff ski boot (known as BIAD, see Figure 2-12 (a), page 2-27). If so, the knee is even more at risk as a quadriceps activation (skier tries to stand up) increases the load on the ACL. Maybe the finding that the quadriceps is 'only' amplifying existing high ACL loads produced by other parameters, can solve the argument if a quadriceps-induced ACL rupture exists (DeMorat et al. 2004) or not (Aune et al. 1995).

The combination of valgus moment, internal torque, and anterior tibial force was previously described as a known injury mechanism by Freudiger and Friedrich (2000) (see Table 2-3, page 2-9). The simulations can confirm this statement only for investigations with no or low muscle activation and quadriceps domination. In the case of hamstring domination or a strong co-contraction of the muscles, the ACL loads are eliminated or reduced to low (uncritical) values. This emphasizes the results of the surrogate study (see chapter 3.1.3) showing the importance of a co-contraction of quadriceps and hamstrings as a significant factor to reduce ACL loads.

Compared to the results testing a 5 Nm valgus (see chapter 3.2.3), the negative effect on ACL loads of a sole valgus moment with no muscle activation is increasing with increasing valgus moment. It is controversial that in the simulations with 20 Nm valgus and additional quadriceps-domination at knee flexion angles larger than 30°, no ACL load can be seen. In contrast to this, in the simulations with a 5 Nm valgus moment and with a 40 Nm valgus moment, a strong negative impact on the ACL can be

observed. The reason for this discrepancy is unclear but may be attributed to geometrical influences of the model. An internal torque in addition to a valgus moment leads to smaller ACL loads than the pure valgus moment.

Freudiger and Friedrich (2000) define an internal torque in combination with a varus moment as critical if the centre of gravity is in front of the ski binding (see Table 2-3, page 2-9). This can be either in an extended or flexed knee.

The simulation results show a small increase of the ACL load for a present varus moment in the extended leg with an approximately 50 N increase compared to the unloaded knee (depending on muscle activation). In combination with internal torque, the increase due to a varus moment is approximately 100 N compared to a sole internal torque. The negative effect on the ACL by a varus moment in combination with an internal rotation is even more pronounced for increasing flexion angles above 90° / 105°, depending on the loading level.

In skiing, the latter case could result like this: the outer edge of the ski tip gets caught while the knee is in deep flexion (perhaps after a landing with a backward fall), which leads to internal rotation with varus while the body (still in a low position) slides/falls forward over the stuck ski.

For knee flexion angles above 15° and absence of internal torque, the ACL load increases drastically for an increasing varus moment, which is even amplified by an anterior tibial force (in combination with a dominant quadriceps) leading to the highest loads of this investigation.

The results indicate that varus loads can be counteracted by strong muscle activation. Especially a strong quadriceps activation or a strong co-contraction reduces loads provoked by a combination of varus moment and internal rotation. As the quadriceps is amplifying the ACL load of a sole varus moment, this is controversial (also found by Aune et al. (1997)) and might indicate that the protective effect actually results from an increased axial compression caused by the muscle activation.

In the performed simulations axial compression reduced ACL loads. This may be attributed to increased friction. In a slip-catch situation in skiing, this indicates that the ACL likely is injured before the knee is loaded again. However, even if the ACL loads are reduced by axial compression, other structures of the knee (for example menisci or the bones) are increasingly stressed.

3.3 Discussion of the Performed Studies with Respect to Knee Injury Prevention

The surrogate study (chapter 3.1) and the simulations (chapter 3.2) show that the interactions between external loads, muscle activation, and knee flexion angle are complex. In the following graph (Figure 3-28), generalized rules of these interactions are illustrated to allow the interpretation with respect to an injury prevention system. These rules are simplifications and need to be handled with care. Due to the multitude of possible loading scenarios, the schema is not comprehensive and is only based on the investigations of this work. Investigations of higher loads (>5Nm) for external torques are missing (see chapter 3.2 for more information).

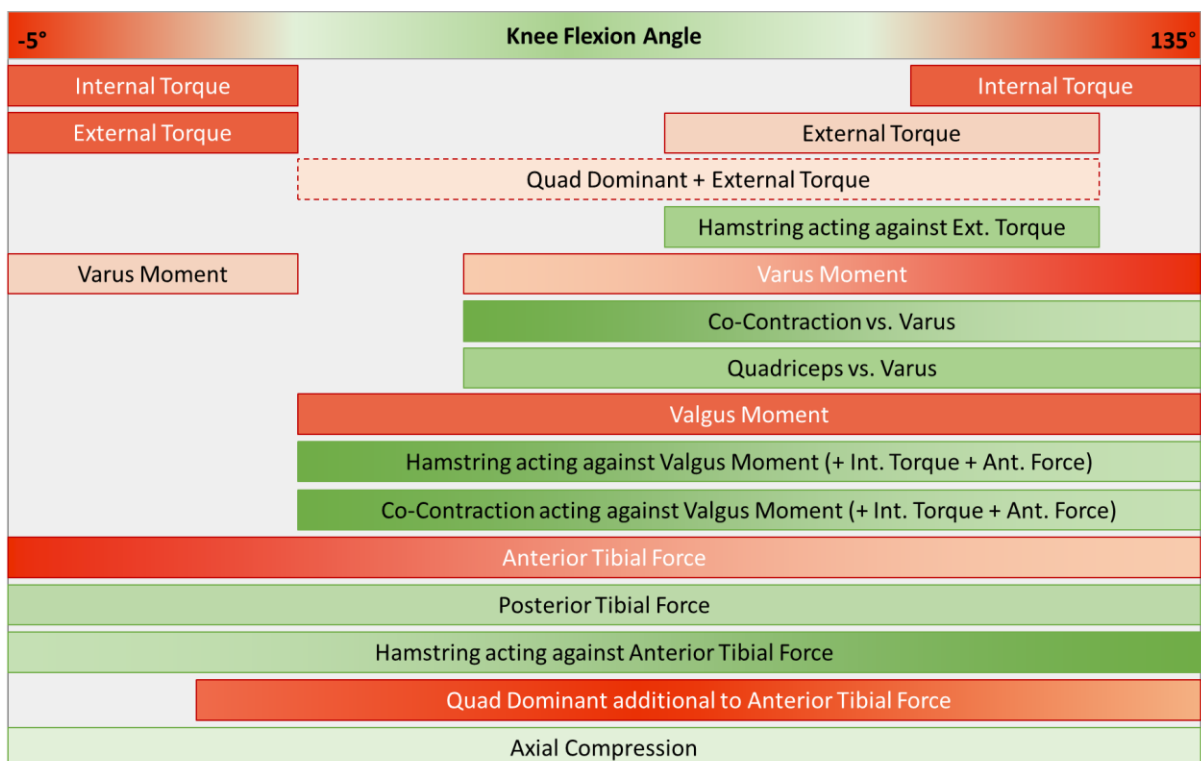


Figure 3-28 Generalized schema of the effect of various parameters on the ACL loading over the knee flexion range. Red: negative effect; Green: positive effect; light to dark coloring: weak to strong effect. Due to the multitude of possible loading scenarios, the schema is not comprehensive and is only based on the investigations of this work. Investigations of higher loads (>5Nm) for external torques are missing (see chapter 3.2).

The previous investigations show that no sole parameter suffices as a control variable for a safety system. It is obvious that such a system needs information on the loads acting on the ski, as these are the origin of all reaction loads of the ACL and the other body structures. However, the effects on the ACL by the same external loads are extremely different for different knee flexion angles or different muscle activations (Quadriceps-Hamstring-Ratio).

This means that a safety setting of the ski binding will successfully protect the knee in a given situation but may not be able to protect it in another, just slightly different, situation. For example, a skier at the beginning of the skiing day may ski with slightly flexed knees of about 30° and actively uses his/her muscles (for example a Q15H15 ratio). In such a situation, the ACL sees close to no or only a small loading in nearly all studied loading situations. As the skiing day progresses (or even during a long slope run), the skier gets tired and, hence, will not react with the proper amount of muscle activation anymore (for example a Q5H5 ratio). To save energy, the skier will take a more upright body posture and now skis with about 10° knee flexion. The ACL is now constantly loaded with 300 N or more. A slip of the outer ski will easily bring the knee into hyperextension and further increase the load of the ACL even to an injury level. Tired muscles may also lead to a situation, where the skier will fall into deep knee flexion angles (for example due to a landing after a small drop). The ski boot may then induce an anterior tibial force. If the ski catches in the snow and induces an internal torque about the tibia in addition to a valgus or varus moment, the ACL may be exposed to critical loading probably leading to an ACL rupture.

Well-trained leg musculature is a benefactor to many described risk factors, as the hamstrings and quadriceps can counteract many different forces. Nevertheless, it is unlikely that the majority of skiers adequately train their musculature before or during the ski season.

If a future safety system would monitor muscle activation ratios and muscle fatigue, such a system could give feedback to the skier in case of fatigue and adapt the safety settings according to the use of the musculature.

Based on the performed investigation, it can be stated that the knee flexion angle is the most important parameter with respect to the risk of injury. It is clearly visible in Figure 3-28 that the ACL is more prone to injury for a hyperextended and extended knee, as well as for the knee in deep flexion. Therefore, skiing with moderately flexed

legs reduces the risk of injury. A safety system also monitoring the knee flexion angle could react more adequately in a given situation than a safety system only monitoring the loads acting on the ski.

The investigations were performed using two different methods: a surrogate (physical model) and a digital multi-body-simulation model of the same surrogate. As discussed before (chapters 3.1.4 and 3.2.3.3) both methods have advantages and drawbacks, and only the combined use of multiple methods will successfully lead to a comprehensive understanding of injury mechanisms in skiing and other sports. In future work, the studies carried out in the simulations can reduce the number of situations to be examined with the surrogate to the critical situations. Investigating these situations with both methods serves to validate the results.

An improved digital model is needed to test for external torques, as these are reported to play a role in various injury mechanisms (Freudiger and Friedrich 2000).

Both used methods are quasi-static and extended simulation models need to be developed to test higher dynamics.

Computational power is a major limiting factor when performing simulation studies. If such power will be more abundantly available in the future, the interactions of the entire human body as well as environmental structures (such as snow conditions) and the equipment would ultimately be possible.

4 Towards a Knee Injury Preventive Ski Binding

Key points of this chapter

Proposed Concept to Reduce Knee Injuries in Alpine Skiing - Mechatronic Ski Binding

The previous studies on injury mechanisms show that the interaction between external and internal loads on the skier and the risk of ACL injury is complex. Conventional mechanical ski bindings cannot react optimally in all situations. A mechatronic ski binding includes sensors providing valuable information to improve the mode of operation and an actuator to adapt the release values of the binding.

Input Parameters

Sensory input parameters for the proposed mechatronic system are the *knee flexion angle*, *muscle activation* of the thigh, *loads acting on the foot*, and *skiing velocity*. For each parameter, a prototype is presented and tested for possible implementation in a mechatronic ski binding. Recommendations are made for future designs. In addition, information about the skier (age, gender, weight, body height, skiing level) is used in the control algorithm.

Algorithm and Validation

An *algorithm based on fuzzy controllers* is proposed, due to the advantages of such a design to cope with the individuality of skiers and the ability to define threshold values for input parameters and critical conditions. A first comprehensive draft of such an algorithm is presented in this thesis. The algorithm is applied to a data set of case reports provided in literature to demonstrate the mode of operation and allow a discussion of the design. In future work, the optimization of the design and validation must include the acquisition of field data by using the sensor systems with a standard mechanical ski binding in order to avoid injuries due to incorrect behaviour of the mechatronic solution. The complete mechatronic system should only be implemented after several iterations of improvement. The design can include artificial intelligence to optimally train the algorithm.

The previous studies on injury mechanisms show that the interactions between external and internal loads on the skier and the determination of the risk of an ACL injury are complex. Therefore, the mechanical ski binding that is common today, though succeeding in preventing tibia breakages, cannot protect the knee satisfactorily, since the information of the binding loads in two directions is insufficient to cope with the complexity.

An ideal safety system needs to consider the kinetical and kinematical complex mechanisms which lead to injuries and react accordingly. Realizing this with a purely

mechanical solution is not possible. Sensors are required on the skier or in the ski equipment and, therefore, only a mechatronic system comes into question (Senner et al., 2014). As the unnatural extension of the foot length because it is connected to the ski is the main reason for the great stress on the body structures, separating the ski from the skier, when there is a risk of a knee injury, is the most effective way to reduce knee injuries. On the other hand, the separation must not happen unintentionally, because a fall may also lead to injuries. A mechatronic binding with a carefully designed and trained algorithm may be the only approach that can handle this complexity.

4.1 Overview of Existing Binding Concepts

Parts of this chapter were published in Hermann and Senner (2020b). Minor alterations have been made in these sections for reuse in this work.

Senner et al. (2013) differentiate between six categories of ski bindings (Figure 4-1). The first three categories refer to mechanical concepts, and the other three to mechatronic concepts.

Mechanical Ski Bindings

Purely mechanical concepts of ski bindings distinguish themselves by the number of degrees of freedom (DoF), which quantifies the number of movement directions leading to a release of the binding. Most common bindings on the market have 2 DoF, a lateral/medial release at the front (toe) element of the binding and a vertical release at the back (heel) element of the binding. There are also 3 DoF-bindings with either a lateral release at the back element or a vertical release at the front element. The latter type allows the binding to release in a backward fall. Until today, there is no guideline for release settings for the third release mode, leaving the user to gradually adjust the values until no inadvertent release occurs.

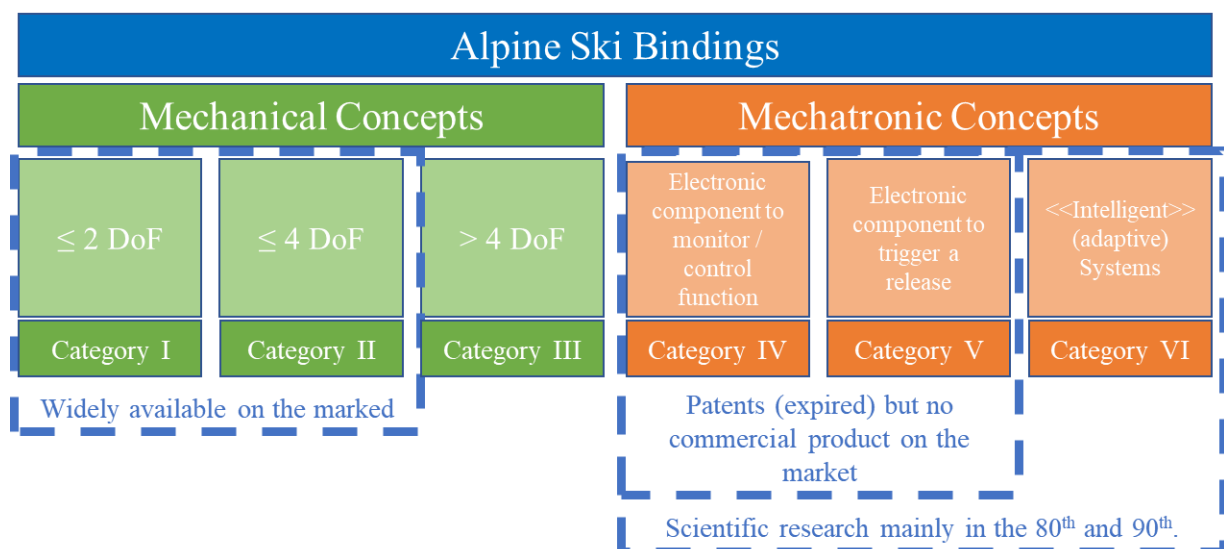


Figure 4-1 Categories of ski bindings. Originally from Senner et al. (2014) and modified by Hermann and Senner (2020b). © Elsevier 2020, reprinted with permission.

Mechatronic Ski Bindings

A mechatronic concept has an electronic component in the ski binding system. The idea of a mechatronic binding is not new, and there are various concepts and patents in the literature, which will be discussed in the following:

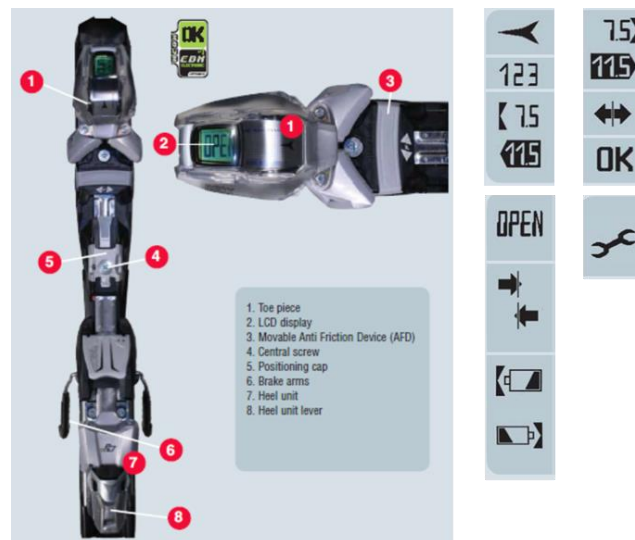


Figure 4-2 Atomic Neox EBM Manual, 2004 (Atomic Austria GmbH 2004); Patent released 2006 (Holzer 2006).

Category IV: A Category IV binding has an electronic component only to monitor or control a function. In a basic form, it could be a display in the binding, informing the skier about the proper condition of the binding, the right contact pressure, release setting, or inspection interval. Atomic made an attempt with a category IV binding in 2004, with a binding called NEOX EBM (Figure 4-2).

Category V: In a more advanced state, the binding includes sensors monitoring certain skiing variables and an actuator, which triggers a release of the binding. Various patents (Smolka 1971; Flock 1992; Ettliger and Dodge 2007; Platter and Rosenich 1989) and publications (Wunderly and Hull 1989; Wunderly et al. 1988) in the early 90th did not result in any product on the market. Nevertheless, the presented binding concepts in these documents are still valuable.

In an early patent, Smolka (1971) brought up the idea to use the muscle activity of the foot or leg as a control variable for the release mechanism (Figure 4-3 (C)). The patent is rather unspecific about the selection of muscles, which should be used to control the

binding. Moreover, no information is given, on which states of muscle activity should result in a release.

In multiple publications, Wunderly and Hull with team (Wunderly et al. 1988; Wunderly and Hull 1989) presented a binding concept relying on an electronic release mechanism (Figure 4-3 (A)). Therefore, boot loads are recorded with a 6 DoF dynamometer as part of the binding itself.

Flock (1992) patented the idea (Figure 4-3 (B)), to measure the knee flexion angle and to determine a risk of injury followed by a retention or release decision.

Ettlinger et al. (2010) developed and patented (Ettlinger and Dodge 2007) a binding that measures the shear force under the foot to determine the force application point. If the force application is at the inner edge of the rear ski area the retention values of the binding should be lowered. The release thresholds with respect to the force application point are shown in Figure 4-3 (C).

Platter and Rosenich (1989) describe a three-level release controller (active / counter delayed release / instant release) which adapts to measured forces acting on the binding (Figure 4-3 (E)). It is not mentioned how these forces are to be recorded.

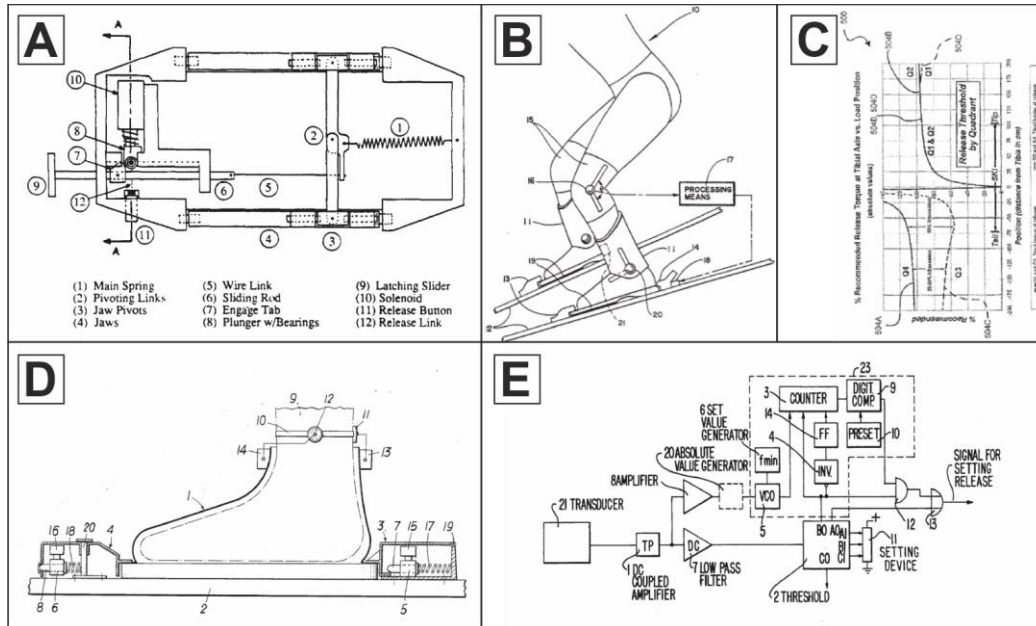


Figure 4-3 Examples of Category V binding concepts: (A) Binding with force sensor and programmable release by Wunderly et al. (1988)¹ and Wunderly and Hull (1989), (B) Knee angle controlled release; US Patent 5,295,704-1994 (Flock 1992), (C) Shear loading controlled release; patent WO 2008/021813 A3 (Ettlinger and Dodge 2007), (D) Bio adaptive binding; US Patent 3,776,566-1973 (Smolka 1971), (E) measured force triggered binding; US patent 5,064,215 .1991 (Platter and Rosenich 1989).
¹©Elsevier; reprinted with permission.

Category VI: In the most advanced state, the binding has an intelligence, allowing the system to adapt. 40 years ago Lieu and Mote, JR. (1980) described a concept of an EMG-controlled binding (Figure 4-4 (A)). 12 years later, a design concept of a binding using load cells and EMG was presented by Neptune and Hull (1992). The release controller is relying on data of dynamometers in the binding and the neuronal stimulation of the quadriceps (Figure 4-4 (B)).

More recently, various patents were filed describing Category VI bindings (Pantazelos et al. 2020; Reiter et al. 2017; Bauer+Kirch GmbH 2015; Riedmayer 1998) or related topics (Barden et al. 2016; Senner and Schott 2017, 2009; D'Antonio et al. 1980), but no prototypes or proofs of concepts have been released to the public. Kos and Umek (2018) presented a prototype of an instrumented ski with the aim to build a feedback system.

In 2009 Salomon SAS (Annecy, France) presented a prototype (Merino et al. 2009), which can be seen as a category VI binding (Figure 4-4 (C)). In their patented work (Laurent et al. 2007), Salomon used a pragmatic approach by collecting data and then trying to categorize it into non-critical for normal skiing and critical, for situations, when a release was expected. Regrettably, none of these systems was released on the market.

In contrast to a pragmatic approach towards a mechatronic ski binding and the release-retention algorithms, which focuses on typical and atypical skiing forces, a biomechanical approach focuses on movement patterns that cause injuries. In the following, such a concept is presented including prototypes of necessary sensor systems and an algorithm design.

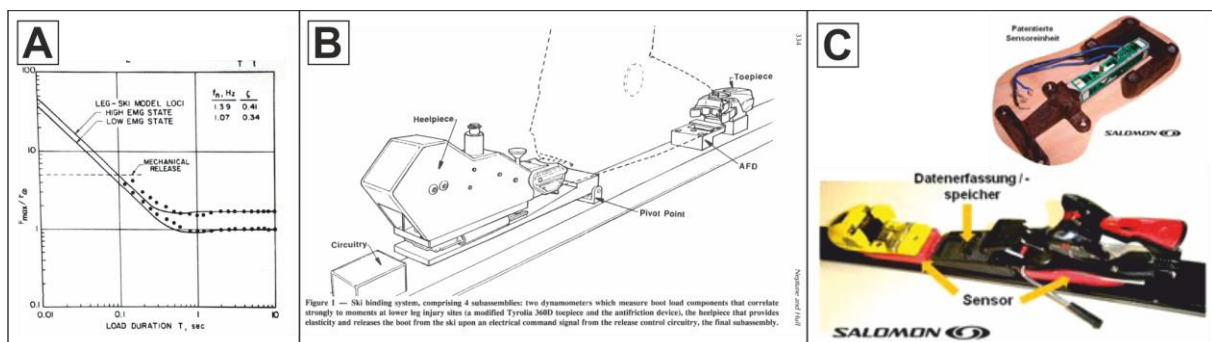


Figure 4-4 Category VI binding concepts: (A) EMG controlled binding by Lieu and Mote, JR. (1980)¹, (B) Force and EMG controlled binding by Neptune and Hull (1992)², (C) Force controlled binding concept of Salomon SAS (Merino et al. 2009; Laurent et al. 2007).¹©ASME, ²©ASTM; reprinted with permission of the respective copyright holder.

4.2 Biomechanical Design Concept of a Mechatronic Ski Binding

Sections of this chapter were published in Hermann and Senner (2020b). Only minor alterations have been made for reuse in this work.

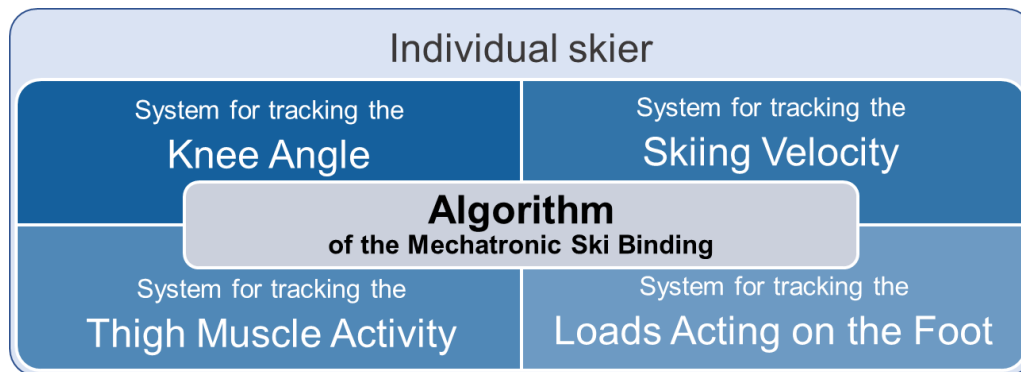


Figure 4-5 Four sensor systems are the basis for an algorithm for a mechatronic ski binding. The algorithm also includes information of the individual skier, for example age, fitness, gender, and more.

Based on the known mechanisms of knee injuries, which are described in the literature (see Chapter 2.3) and based on the results of the studies with the knee surrogate (Chapter 3.1) and the digital model (Chapter 3.2), a set of five input parameters is considered necessary to be integrated into a mechatronic ski binding system (Figure 4-5):

- (1) the knee angle,
- (2) the muscle activity of the thigh,
- (3) the forces and torques acting on the foot, including the force application points and the centre of gravity,
- (4) the skiing speed and
- (5) information about the individual (age, gender, weight, body size, skill level, previous injuries).

This list is based on the current understanding of injury mechanisms and the assumption that other parameters can be predicted by these. For example, the hip angle, as an indicator of a forward or backward leaning, can often be anticipated by the centre of gravity. Future research might prove this assumption being false and demand the consideration of more (or less) parameters to achieve a safe mechatronic system.

In contrast to highly accurate scientific systems, the focus in the development of sensors for these parameters must be on practicability and usability in real life skiing. Former would not be applicable in a future mechatronic system on the market, due to size, price, and processing power necessary.

In the following chapters, examples of possible sensor systems for parameters (1) to (4) are developed, validated, and discussed. In addition, a design proposal for an algorithm that controls the binding is presented. Such an algorithm constitutes the core of every mechatronic system and is likely to be optimized as more information becomes available. The presented systems serve as proof of concept. The development of fully functional systems, of a quality level that would allow the integration in a market-ready system, would require a joint effort by the sports industry, manufacturing industry, and research institutes and can, therefore, not be achieved within the frame of this work.

4.2.1 System for Tracking the Knee Flexion Angle

This chapter was published open access in Hermann et al. (2020). Minor alterations have been made for reuse in this work. The original work also includes supplementary video material, which can be viewed on the website of the journal³.

To measure the knee angle while skiing, it is important to have a wearable system. The skier moves around in a huge special area, making external systems, like camera-based motion tracking, not applicable. Optimal would be the integration of sensors in already existing equipment, like skiing pants or underpants.

Standard electro-goniometers are precise tools to measure one or two-dimensional flexion (Bronner et al. 2010; Rowe et al. 2001). In some studies, stiff components are attached to the leg to decrease movement artifacts (Petushek et al. 2012). Most of these sensors are inappropriate for integrating into textiles, like ski base layer pants, due to the size, weight, and need to remove them when washing. Stiff components could restrict the movement of the knee, may not align well with the changing shape of the body, and might be dangerous for the wearer. One option could be to use inertial measurement units (IMU), which can be accurate for measuring joint angles for several minutes (Yoshioka et al. 2018; Fasel et al. 2017a, 2017b; Supej 2010). The drawback of IMU systems is that the measurement drift is hard to control over a period longer than one slope run.

In contrast, wearable textile-based sensors are flexible, making them suitable for measuring joint flexion angles during skiing. Examples of such sensors (Pettys-Baker et al. 2017; Mattmann et al. 2008; Yamada et al. 2011; Bergmann et al. 2013; Munro et al. 2008; Shyr et al. 2014; Tognetti et al. 2014) have been developed with flexible and stretchable polymers with either capacitive or resistive principles. In most cases, those sensors are made of silicon filled with carbon black. The measurement principle is similar to a strain gauge. For such sensor types, no signal integration is needed, which would result in drift over longer time periods. In this study, silicon-based sensors of both principles measuring strain were chosen. Silicon-based resistive sensors are inexpensive and, therefore, preferable for future mass production. Disadvantages of resistive sensors include sensitivity to temperature changes, strain rate, and drift over

³ <https://link.springer.com/article/10.1007/s12283-020-00336-9#Sec19>

time (Qiu et al. 2019). On the other hand, silicon-based capacitive sensors are more expensive and need more intensive computations. However, they are not sensitive to drift over time and strain rate and are less sensitive to temperature and humidity. More information about the sensor principles, which are redundant to the sensor principles used in chapter 4.2.3 for measuring pressure, can be found in Appendix 7.7.

The concept of measuring the knee flexion angle via a strain sensor is based on the simplification that the knee joint is a hinge joint. Ideally, the stretchable sensor is placed on or close to the skin, while the two endpoints keep a constant position relative to the bones. Due to the elongation of the sensor in knee flexion, the electrical resistance/capacity changes, and (linearly) correlates with the knee flexion angle. If calibrated, the knee flexion angle can be calculated from the measured electrical variable.

This study focuses on the development of two compression pants that measure knee flexion using either a silicon-based piezo-resistive sensor (RS) or a silicon-based capacitive sensor (CS). The presented underwear-sensor-systems will be compared on their ability to measure the knee joint angle in dynamic movements.

4.2.1.1 Prototypes

To evaluate the reliability and accuracy of the RS and the CS, the study was performed as follows: (1) Testing the linearity of the sensor; (2) Developing the prototype of compression ski base layer pants, thereby considering the requirements due to the environment, usability, and integration of the sensors and electronic components; (3) Evaluating the prototypes using a test rig consisting of a leg surrogate, which can be flexed automatically at various speeds; (4) Evaluating the knee angle measurements of the prototypes in a human participant study (n=20).

Sensors

Both sensor types were silicon-based. The silicon fibre for the RS is produced by REHAU AG, Muri bei Bern, Switzerland. The CS is a customised commercial product by LEAP Technology, Aabenraa, Denmark.

The linearity of the sensors was tested by stretching the sensor in one cm increments (five repetitions / sensor was held in each position for 60 seconds before the value was

taken; Figure 1 (b) and (d)). Both sensors showed linear behaviour (Figure 4-6 (a) and (c)). The RS needs to be pre-tensioned to about 20% of its initial length (Figure 4-6 (a)) and can be stretched up to 200%, which reflects the typical mechanics of elastomeric fabrics (Munro et al. 2008; Gioberto et al. 2016). Between 120-200% elongation, the maximal variation of values was $\pm 4\%$ of the mean value for each measurement point. No pre-tension is necessary for the CS and maximal elongation is 150%. The maximum variation of values was $\pm 0.5\%$ of the mean value for each measurement point.

To calculate the knee angle, a calibration of the sensors before usage on the ski slope is necessary. This calibration must be repeated each time the pants are put on, as the relative position of the sensors to the knee joint may be different each time the system is used. In a practical application, the number of calibration coefficients should be two. Otherwise, a multi-control point calibration process is needed, which is too complicated to perform on the ski slope. In a two-point calibration, the wearer must take two postures at pre-defined knee flexion angles, e.g. 0° and 90° . The corresponding sensor values (S_i) are stored, and the calibration coefficients (k_0 and k_1) are calculated. The flexion angle (φ_i) at each measurement point (i) while skiing is then calculated

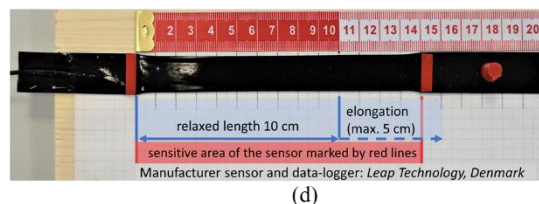
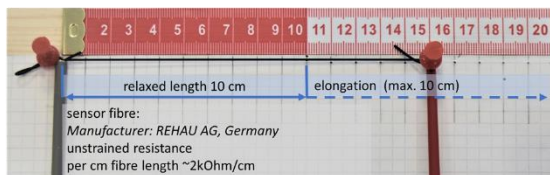
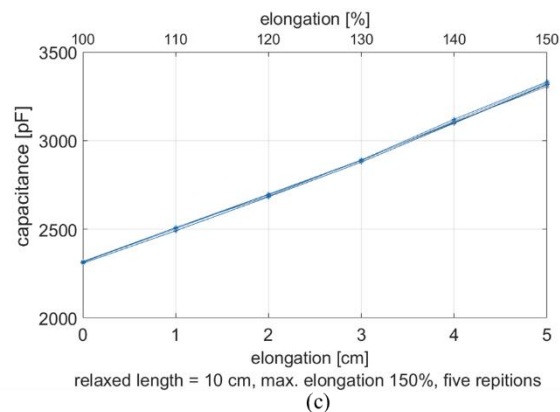
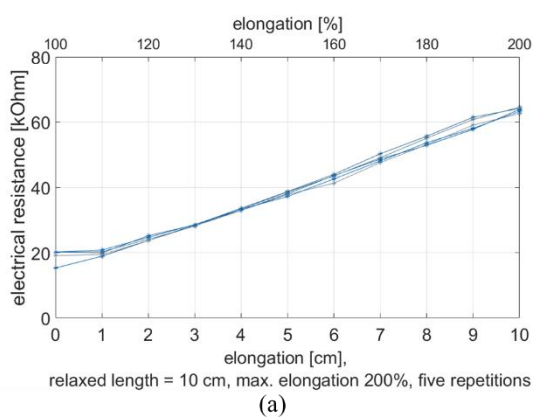


Figure 4-6 (a) relationship between elongation and RS-values; (b) RS-fibre and measurement setup; (c) relationship between elongation and CS values; (d) CS-sensor and measurement setup, data logger not shown.

with the formula (4-1):

$$\varphi_i = k_1 * S_i + k_0 \quad i = 1, \dots, n. \quad 4-1$$

Prototypes of measuring pants

For the best measurement results, the sensors should be directly attached to the skin. As this is impractical, integration in a knee bandage or attaching the sensor to compression pants are viable alternatives. The bandages or compression pants must stick to the skin to prevent dislocation of the respective sensor and, for the RS-prototype, to keep the RS in the pre-tensioned state. Figure 4-7 (H) shows the self-designed RS-underpants made of PA and elastane, for which the School of Textiles and Design, Reutlingen University, performed the integration in a textile and electronic wiring. The RS is incorporated in the knee area. Figure 4-7 (I) shows a commercial compression garment (2XU, Melbourne, Australia) with the CS sewn over the knee region. The mechanical stiffness of both sensors is negligible compared to the stiffness of the textile in which they are attached (stiffness increases by 4 % when the sensor is integrated in the textile for the CS prototype and less than 1 % for the RS prototype). For best results, the sensors were positioned over the patella, as this is where elongation during knee flexion is highest. Due to the small diameter of the RS-fibre, the RS-prototype includes two fibres parallel to each other. Thus, it was ensured that at least one fibre was always positioned over the patella. For calculating the knee angle, the fibre with a greater change of resistance, meaning more elongation, was used.

4.2.1.2 Validation Study: Methodology

Artificial leg tests with the prototypes

For the validation tests, single-leg prototypes were used. On a knee flexion test rig (Figure 4-7 (A-G)) the prototype was tested for functionality. The custom-made test rig consists of an upper leg and a lower leg made of silicon (Figure 4-7 (A)) connected by a hinge joint (Figure 4-7 (B)). The gap between the upper and lower leg is bridged by wires running in tubes (Figure 4-7 (A)). The entire leg is enclosed by black tights (Figure 4-7 (C)), which prevents the prototypes from getting caught in the gap. A pneumatic cylinder powered flexion and extension movement in the range of 0 to 60°. The velocity of the flexion/extension movement was varied by controlling the air pressure that supplies the cylinder. A rotary sensor (RFD-4000 hall sensor,

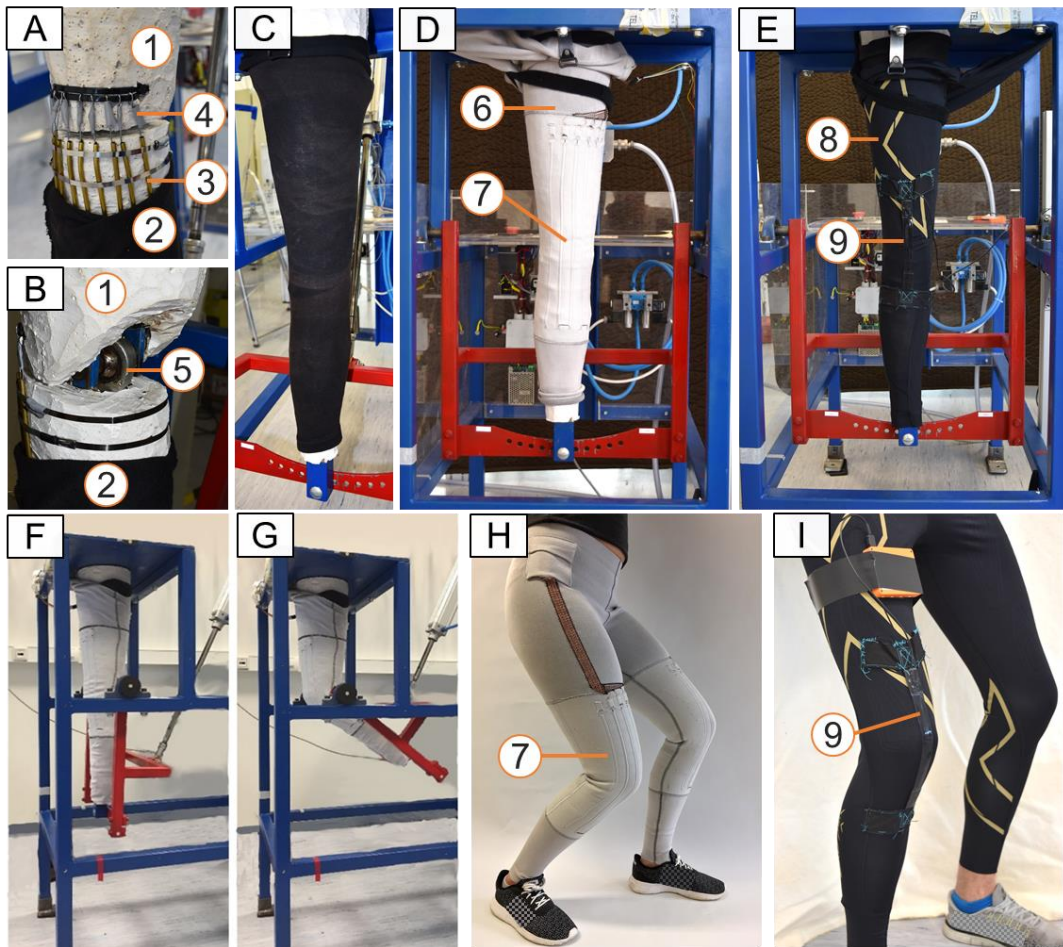


Figure 4-7 (a) frontal knee part of the knee flexion test rig; wires (4) running in tubes (3) bridge the gap between the silicon thigh (1) and shank (2), (b) hinge joint (5) of the knee flexion test rig, (c) thin tights covered the silicon so the prototypes did not catch the knee gap or the wires, (d) prototype of RS-pants (6) in test rig; knee part (7) include the RS-fibres, (e) prototype of CS-pants (8) in test rig; CS (9) stretched over the knee part, (f) knee flexion test rig with the leg in 0° flexion and (g) 60° flexion, (h) participant wearing RS-pants, (i) participant wearing CS-pants.

novotechnik, Ostfildern, Germany) with an accuracy of 0.1° was used to record the amplitude and velocity of the movements of the test rig. Videos of exemplary recordings are provided in the supplementary materials of the published version of this study on the publisher's website⁴.

The following tests were performed:

- (1) Test for the influence of different velocities: A two-point calibration was performed, with 0° and 60° followed by multiple flexions at three velocities: slow

⁴ <https://link.springer.com/article/10.1007/s12283-020-00336-9#Sec19>

(2 bar), medium (3.5 bar), fast (5 bar). The resulting angular velocities are given in Figure 3 (a) for RS and (c) for CS. RS and the rotary sensor were synchronously recorded at 1 kHz using a 16-bit data logger NI-USB 6212 (National Instruments, Austin, Texas, USA) and the software LabView 2018 (National Instruments, Austin, Texas, USA). CS was recorded at 100 Hz using the data logger provided by the sensor manufacturer which runs a standalone LabView application. In post-processing, the CS data were linearly interpolated to 1kHz and synchronised with the rotary sensor data by calculating the time lag through cross-correlation. No filters were used on the data. MATLAB R2017b (The MathWorks Inc, Natick, Massachusetts, USA) was used for processing the data and generating the graphs.

- (2) Long term test: The prototypes were calibrated at 0° and 60°. Then a three-hour measurement was recorded with a continuous flexion between 0° and 60 in the 'slow' setting (about 6,100 flexions and extensions) and a measurement frequency of 100 Hz, for both RS and CS measurements. No filter was used.

Human participant study

This study received ethical clearance by the Ethics Commission of the Technical University of Munich (Ref.nr.: 38/20 S). All participants were informed about the goals and risks of this study and gave their written consent. Twenty participants (7 males, 13 females, mean age 23.3 ± 6.23 years, no self-reported injuries, self-reported high fitness level) performed flexion-extension movements wearing both prototypes. For the RS only the knee part of the pants was used (see Figure 4-9 (e)). The participants were asked to stand in a ski binding on a platform with an inclination of 15°, wearing the same ski boot model in their shoe size (Mindbender, K2, Seattle, Washington, USA; Flexion Index 130 for male and 110 for female). This setup was chosen to simulate ski-like flexion behaviour and to represent the fixation of the ankle by the ski boot.

The maximal and minimal values of the first flexion were used to calibrate the respective system. Camera-based automatic 2D-Motion-Tracking (Contemplas, Kempten, Germany) was used as the reference system (MTS). For the tracking, markers were attached to the condylus lateralis femoris (red marker) and 15 cm in both directions on the axis between the first marker and the trochanter major femoris (green marker) and the first marker and the malleolus lateralis (blue marker) (Figure 4-9 (e))

and (f)). A manual trigger was used to mark the start and end of the measurement and turn on an LED attached to the ski boot. Measurement frequencies were 500 Hz for the CS-prototype, 1 kHz for the RS-prototype, 100 Hz for the MTS. MATLAB was used for the post-processing. MTS data was up-sampled by linear interpolation to 500 Hz and 1 kHz for comparison with CS and RS-data. For the synchronisation, the data was shortened using the trigger and LED signal, then cross-correlation was calculated to determine the time lag between MTS and the respective elongation sensor. The first flexion was used to calibrate the sensor. Bland-Altman-plots (Bland and Altman 1986) were used to compare elongation sensor and MTS results over the whole range of the KFA. Before the start of the measurement, the participants were asked to perform two squats so the pants and sensors could align. At the start of the measurement, the participants were asked to flex the knee as deep as they voluntarily could (~120°), followed by ten squats to about 90° KFA. A metronome of 50 beats per minute gave an orientation for the speed of flexion for these ten squats. Each beat marked a turning point from flexion to extension and vice versa. Participants were asked to hold their arms horizontally, so as not to interfere with the MTS. Exemplary video recordings of the human participant test are provided in the supplementary materials of the published version of this study on the publisher's website⁵.

4.2.1.3 Validation Study: Results

Results artificial leg tests with the prototypes

Influence of velocity

Figure 4-8 (a) and (c) show the calibrated KFA of RS (KFARS) and CS (KFACS) against the 'true' KFA. In the upper graph, a linear trend for each velocity setting is plotted to allow better comparison. The respective lower graph shows the timeline of the same test. The RS-system was sensitive to the velocity of the flexion-extension movement (Figure 4-8 (a)). The sensor signal drifted to higher values for higher velocities, reflecting mechanical properties of RS reported by others (Bergmann et al. 2013). The influence was greater for smaller flexion angles (<30°). A 5° increase of the trendline values from slow to medium speed and again from medium to fast speed at 0° KFA was observable. For 50° KFA there was only a 1° increase for the trendline values for both speed steps. A repetition of the slow speed setting resulted in the same

⁵ <https://link.springer.com/article/10.1007/s12283-020-00336-9#Sec19>

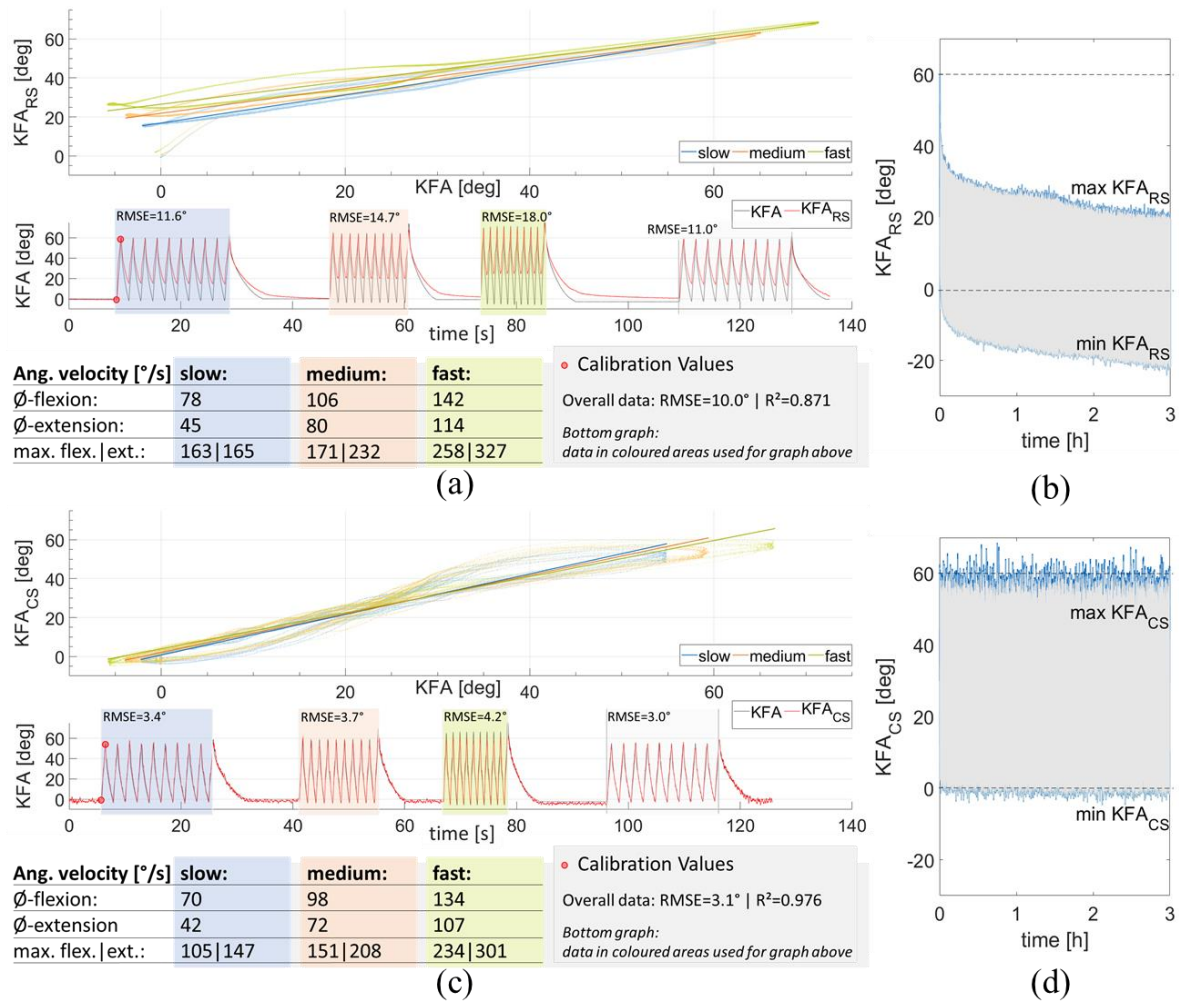


Figure 4-8 (a)+(c) Results for the RS and CS-system on the knee flexion test rig for three different speed settings (slow, medium, fast). The setting ‘slow’ was repeated at the end to test for repeatability. RS/CS-values calibrated with the min. and max. values of the first flexion (red markers in graph (a) and (c)). Mean and maximal angular velocities for the three speed settings are given below the graphs. The top graph shows the dependence on the flexion/extension velocity. The bottom graph shows a comparison of KFA and RS-values (a) and CS-values (c). The black line shows the true KFA measured by a hall-sensor goniometer: the red line shows the respective RS/CS-values. (b) long time drift of the sensor signal of the RS in a constant flexion-extension of the KFA between 0°-60° for 3 hours. (d) long time behaviour of CS.

value range as before (similar root mean squared error (RMSE) of 11.6° vs 11.0°; see Figure 4-8 (a)). Hysteresis was higher for KFA between 0-30° than for larger KFA.

Hysteresis increased with velocity for the RS. R² of KFA and KFARS over the whole measurement was 0.871, RMSE was 10.0 °.

The velocity dependence for the CS was smaller than for the RS (Figure 4-8 (c)), with a 1° increase of the trendline values for both velocity steps at 0° KFA and a 1.2°

decrease for both velocity steps at 50° KFA. At 30° KFA no influence was observable. This point marked the turning point from an increasing effect of the velocity to a decreasing effect. At the same KFA, the hysteresis was the smallest. The effect of the velocity on hysteresis was small for the CS. R² of KFA and KFACS over the whole measurement was 0.976, RMSE was 3.0°.

Long-term test.

The behaviour of maximum and minimum flexion values of the long-term tests are shown in Figure 4-8 (b) for RS and (d) for CS. A relaxation of the RS-signal over 3 hours of 40° for the maximum values and 20° for the minimum values was observed (Figure 4-8 (b)). No large displacement of the prototype relative to the leg surrogate was observed during the measurement, which could have explained the relaxation. The CS showed close to no relaxation during the 3h-test (Figure 4-8 (d)) but showed considerable variation for the maximum and minimum values.

Results human participant study

Figure 4-9 (a-d) show the results for a male participant doing the eleven flexion-extension movements wearing the RS-prototype and CS-prototype, respectively. As observed in Figure 4-9 (a) and (c), the RS is constantly overestimating the flexion angle for the ten movements following the first flexion by $12 \pm 7.5^\circ$. The CS (Figure 4-9 (b) and (d)) shows superior behaviour, with a mean deviation of $-3.3 \pm 5.6^\circ$. However, in Figure 4-9 (d), the CS-values of the flexion appear to overestimate, and the CS-values of the extension underestimate the true KFA.

Across all tests by sensory type, the mean deviation between sensor and MTS system was $10.6 \pm 7.5^\circ$ for RS and $3.4 \pm 5.1^\circ$ for CS. The mean R² across all participants is .92 for the RS-prototype, and .97 for the CS-prototype. Mean angular velocities were $53 \pm 6.5^\circ/\text{s}$ and $-55 \pm 7.4^\circ/\text{s}$ for flexion and extension (Table 4-1). Maximal angular velocities were $197 \pm 27^\circ/\text{s}$ to $-199 \pm 49^\circ/\text{s}$ for flexion and extension (Table 4-1).

4.2.1.4 Discussion

Artificial leg tests

The RS was sensitive to the speed with which the elongation was applied, as well as a long-term drift, which reflects the typical mechanics of elastomeric fabrics (Mattmann et al. 2008; Gioberto et al. 2016; Tognetti et al. 2007). In future skiing applications, the

calibration would take place before skiing in a quasi-static way. Thus, the velocity dependence would not allow reliable determination of the KFA in dynamic skiing afterwards. Perhaps modelling the dependence could improve results, but a critical concern is the long-term relaxation of the signal, which leads to more substantial errors as the time from the last calibration increases. If the dynamic and long-term characteristics of the RS-fibre could be modelled, the prototype could be promising: RS-fibre and its textile integration show positive attributes for wearability, washability, and the simple measuring principle requiring only standard and robust electronics.

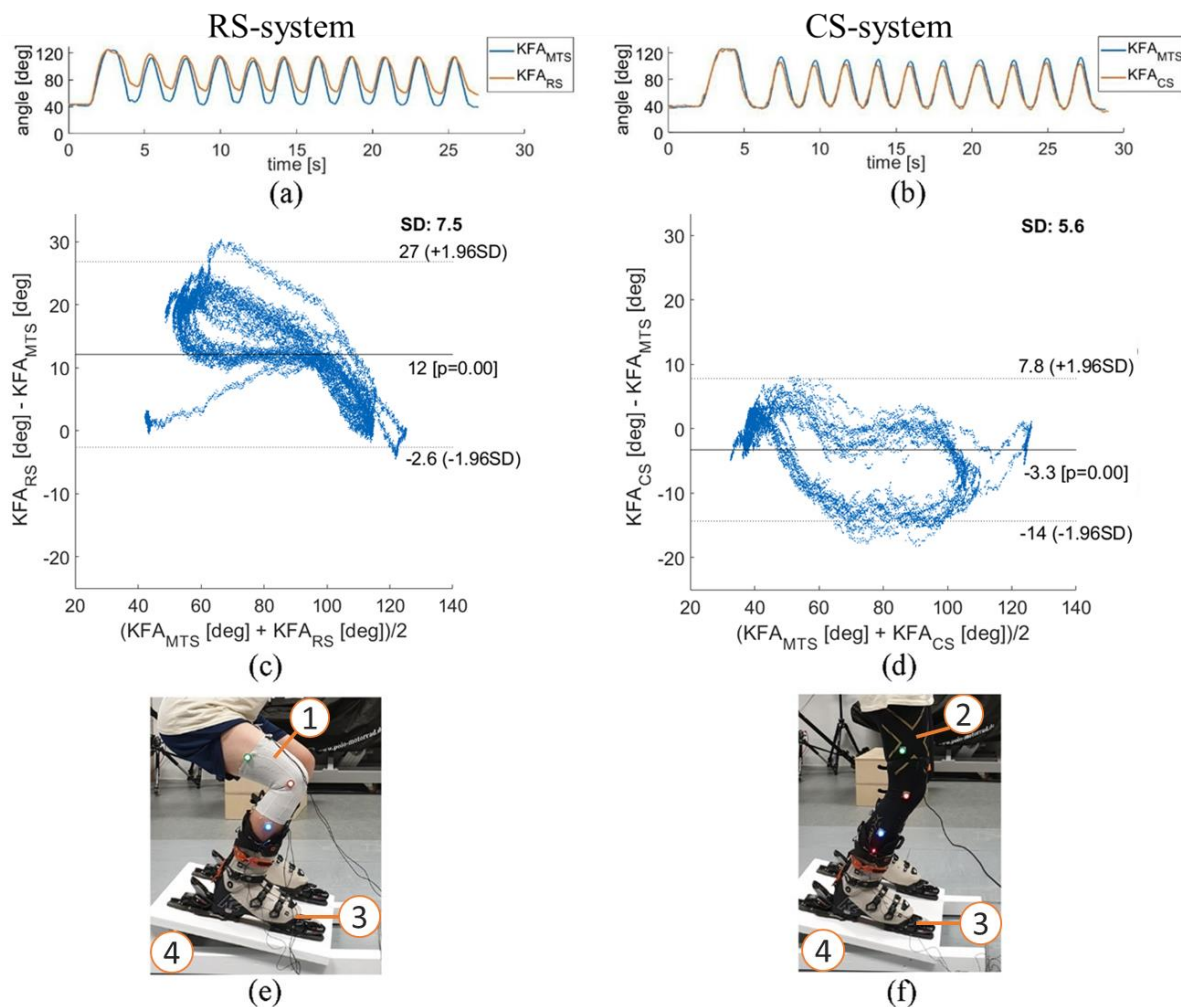


Figure 4-9 Exemplary results for a male participant: Measurements (a) with the RS and (b) with the CS vs. the knee angle recorded by the camera-based MTS, Bland Altman diagram (c) of the results of the RS, and (d) of the CS after knee angle calculation using a two-point calibration, (e) participant wearing the RS-System (1), (f) participant wearing the CS-system (2). Participants wore ski boots in a ski binding (3), which was fixed on a platform (4) with a 15° inclination. The three coloured LED-markers (green, red, blue) are used by the MTS to determine the KFA.

Table 4-1 Results of comparison test; n=20 participants. RS: piezo-resistive sensor system; CS: capacitive sensor system. Reference system: Camera-based 2D tracking.

participant (gender)	mean absolute deviation [deg]		standard deviation [deg]		root mean squared error [deg]		R ²	
	RS	CS	RS	CS	RS	CS	RS	CS
1 (f)	20	1.1	9.5	4.6	8.7	4.3	0.87	0.97
2 (f)	12	-2.9	6.5	5.8	6.5	4.6	0.92	0.96
3 (m)	19	-1.2	9.7	5.5	8.7	4.2	0.92	0.98
4 (f)	6.7	-13	6.7	6.7	6.6	5.1	0.94	0.95
5 (f)	10	-4	4.8	7.5	4.6	5.8	0.96	0.92
6 (m)	5.7	-5.6	4.6	3.2	4.5	2.9	0.97	0.98
7 (f)	10	-0.91	5.8	2.5	5.2	2.2	0.95	0.99
8 (m)	5.4	-5.3	11	10	6.8	5.3	0.87	0.91
9 (m)	-0.32	-4.8	5.6	5.7	5.5	5	0.94	0.96
10 (f)	5.5	-5.3	6.6	4.3	5.6	3.6	0.95	0.98
11 (f)	15	0.27	7	4.2	6.3	3.6	0.92	0.97
12 (f)	12	-3.3	7.5	5.6	5.6	4.8	0.94	0.97
13 (f)	20	1.4	11	2.4	9.5	2	0.89	0.99
14 (f)	5.4	-5.3	11	10	6.8	5.3	0.87	0.91
15 (f)	1,8	0.97	4.8	4.5	4.8	4.2	0.94	0.98
16 (m)	11	1.4	6.6	3	6.3	2.6	0.95	0.99
17 (m)	17	-3.6	8.6	4.4	8.5	4.1	0.89	0.96
18 (f)	17	-1	7.4	3.6	7.2	3.5	0.92	0.98
19 (f)	15	0.49	11	3.2	9	2.5	0.84	0.99
20 (m)	4	-7	4.2	6	3.8	3.9	0.97	0.96
max (abs)	20	13	11	10	9.5	5.8	0.97	0.99
min (abs)	0.32	0.27	4.2	2.4	3.8	2	0.84	0.91
mean (abs)	10.64	3.44	7.50	5.14	6.53	3.98	0.92	0.97

The CS was superior, with less drift and an overall RMSE of 3.0° compared to the RS, with an overall RMSE of 10°, and thus is recommended for use in skiing underpants. The CS prototype shows a limitation to accurately record maximum and minimum values. Besides sensor inherent characteristics, attributes of the garment and the type of attachment to the garment may be reasons for this behaviour. Future research will need to address this aspect. Disadvantages of CS compared to RS include more complex electronics necessary for capacitive measurements, a limited sample rate, and a more complex integration in the textile.

The mean velocities of the test rig for CS were 5-10% slower than for RS. This may result from a different stiffness of the pants and the limitation of using an analogue manometer for setting the pressure, which may impact repeatability. Also, the test rig reached higher flexion angles for higher velocities (about 5 to 7° increase for each

velocity step) due to imperfect control of the pneumatic system. This could influence the results but was neglected as both sensor systems were affected by it.

Calibration process

The calibration process is critical for the accuracy of the knee angle measurements for both systems. A two-point calibration was used in this study, which is easy to perform but has limitations. As the knee is not a hinge joint, the postulation of the linear relationship between the elongation of the sensor and the knee flexion angle is incorrect, and non-linearities might increase measurement errors. For a skier, it may be challenging to take the exact positions for calibration. The calibration should be repeated throughout the ski day to correct errors due to the potential movement of the garment and sensors relative to the body, as well as potential sensor drift. A possible calibration procedure for a two-point-calibration could be that the skier is asked to stand straight and sit on a bench or chair lift with 90° KFA. If the calibration is not performed with great precision, this procedure might lead to large errors in the determination of the calibration coefficients. For a future commercial product, different and more robust calibration procedures should be considered or developed. For example, a dynamic calibration in which the skier performs (multiple) flexions in the knee's full range of motion. This dynamic calibration, possibly combined with a learning algorithm, would therefore include viscoelastic behaviour. The resulting sensor values would not be absolute values for the knee flexion but a normalised value of the individual's flexion range.

Human subject study

Results of the human subject tests are comparable to results by Petushek et al. (2012), who used a goniometer with an RMSE of $7.03^\circ \pm 2.69^\circ$. The accuracy of both systems was lower for a straight leg compared to a leg in medium or deep flexion. One reason might be that the pants textile is tighter on the skin in a flexed state due to muscle volume change. The design of the textile's stretching behaviour has a high impact on the measurements. Anisotropic stretch-design could improve the quality of measurements with a stiffer design in the circular direction. Current research is working on more suitable materials (Li et al. 2020) and textile integration (Gioberto et al. 2016; Wang et al. 2020) for more accurate and robust sensors for human motion tracking.

Harms et al. (2010) provide an example of more complex sensor modelling to improve results by modelling textile wrinkles. Nevertheless, Harms et al. do not aim to measure absolute angles but only recognise postures.

General discussion

The current system tested only addresses flexion and extension of the leg in a limited knee flexion range of 0 to 60° knee angle. Maximum ACL-loading in skiing occurs in hyperextension and hyperflexion of the leg combined with tibial torque (and rotation) (Hame et al. 2002). As this study was a pilot study to test the feasibility of the two different sensor principles, the exposure of the participants to the risk of injury by testing hyperflexion movements was kept to a minimum by asking them for only one deep flexion movement. Also, our flexion test rig is limited to the tested flexion range. Future work should consider more critical situations with respect to knee angle and angular velocities that result in knee injuries. For flexion movements, the experimental maximal angular velocities of the test rig and the human subject study were within the range of velocities measured on the slope by Petrone et al. (2013), who used biplanar electrogoniometers. For extension movements, the maximal angular velocities are slower than reported by Petrone et al..

More than one sensor is needed to cope with the complex characteristics of human motion (e.g., measuring rotation, flexion, and ad-/abduction of the tibia vs. femur), which requires sensor fusion and effective algorithms (Mendes et al. 2016). In this study, the influence of knee movements in other dimensions than the sagittal plane was not investigated. Rotations of the tibia and abduction and adduction of the knee will likely influence the sensor output. Quantification and control of such will be necessary for successful integration in a wearable system. Pilot tests to measure tibial rotation with our two proposed sensors were unsatisfying. Soft tissue artefacts and relative movement between skin and textile heavily impacted the results. A small stretchable sensor based on carbon black filled silicon for measuring rotations was presented by (Li et al. 2019). The proposed method should be modified and tested for human motion tracking.

4.2.1.5 Conclusion with respect to a mechatronic ski binding

For a mechatronic safety system, knowledge about the knee angle is of great importance (see chapter 3.3), as the influence of external loads and muscle activation varies greatly with the knee angle. The reached RMSE 3° of the CS-system might be accurate enough for the integration on a mechatronic system but less optimal accuracies are to be expected for the handling of such systems outside the controlled laboratory study design. Extended studies on the slope need to prove if the calibration process can be successfully applied by the skiers.

The challenges of measuring joint angles with textile-integrated sensors are still manifold (Qiu et al. 2019; Wang et al. 2020; Muhammad Sayem et al. 2020). Nevertheless, more and more technical textiles appear on the consumer market (Muhammad Sayem et al. 2020) that reach an applicable state and fulfill the customer's needs. The most promising solution for joint angle determination could be the hybrid use of IMUs and a stretchable CS. IMUs are accurate and can record rotations and translations in all directions. A CS and a Kalman filter could control the drift of the IMU. The integration of such a hybrid sensor system in skiing underpants would be similar to the presented prototypes and could be integrated into a mechatronic ski binding system via wireless data transmission.

4.2.2 System for Tracking the Muscle Activity of the Thighs

This chapter was published open access in Hermann and Senner (2020a). Minor alterations have been made for reuse in this work.

In the past, measuring muscle activity required expensive equipment and appropriate experience in its application. The integration of sensors that measure muscle activity into garments or wearables provides individuals with an easy-to-use approach and thus opens up the technology for new fields of application in sports, medicine, rehabilitation, and ergonomics. In alpine skiing, the muscle activity of the thigh has a great influence on the safety or risk of injury of the knee. Therefore, the integration of information on thigh activity in a mechatronic safety system makes sense, as the control algorithm could adapt the safety settings of the system accordingly. Electromyography (EMG) is the standard method for measuring muscle activity. It is differentiated into two main kinds of EMG: surface EMG and intramuscular EMG. Only surface EMG systems are suitable for integration into a sports garment because intramuscular EMG is invasive and medical supervision is therefore mandatory. In surface-EMG, electrodes are applied to the skin surface to measure muscle activation. It is important to understand that by EMG, not muscle strength is measured, but muscle activation. Even if those two are highly correlating, the interpretation of measurements differs. The EMG-force relationship is linear for most voluntary isometric muscle activations but non-linear for specific muscles, muscle loads, and movement velocity (Alkner et al. 2000; Bigland and Lippold 1954).

For more details on the principles of muscle activation and the basics of EMG measurements, the reader is encouraged to refer to standard literature, e.g. the recommendations of the Seniam Project (Freriks and Hermens 2000) or the EMG-Fible (Konrad 2011).

The recently published review paper by Guo et al. (2020) summarises research into textile electrodes between 2007 and 2018, listing 41 publications. Of these, only 14 were published in peer-reviewed journals, showing that textile-integrated surface EMG and its application remain a niche subject. Publications relating to sports applications are even rarer. Excluding papers on material or system design, only four publications focus on garments specifically designed for use in sports (Guo et al. did not assign the

system design paper of Finni et al. (2007) in their “sports” category, even though, the Myontec Mbody pants, shown in Figure 4-10 (left), subsequently resulted from it). Of these four papers, two (Colyer and Mc Guigan 2018; Tikkanen et al. 2012) used commercial products (Myontec) in the study, and the other two (Shafti et al. 2017; Ribas Manero et al. 2016) used the same custom-made pants (same research group; papers published at the same conference).

Two examples of commercially available products for measuring muscle activity in consumer sports garments by Myontec (Finland) and Athos (USA) are shown in Figure 4-10. Both companies provide pants, as well as shirts, for measuring muscle activity.



Figure 4-10 Commercially available sports garments for tracking muscle activity of the tights by Myontec (left) and Athos (right). Pictures taken from the websites www.myontec.com and shop.liveathos.com on the 21.03.2020.

The company Myontec is a spin-off of the University of Jyväskylä of the group of Prof. Taija Finni (Juutinen). The company lists 11 publications on the website backing the design, functionality, and validity of its product, including the three publications mentioned above. Athos names one publication (Lynn et al. 2018) to prove the validity and reliability of their product. Three of the authors are employed by the manufacturer.

The publications backing the applicability of those products may well be biased due to conflicts of interest. As these products are health-related, independent validation is necessary. In general, there is a lack of studies comparing textile-based EMG garment solutions with established scientific systems. The few existing papers largely validate textile electrodes not yet integrated in a garment. For example, Li et al. (2011) and Sumner et al. (2013) confirm that measurements with textile electrodes are

comparable to ones with standard EMG electrodes. Both studies are limited due to the fact that only six individuals were tested.

The purpose of this study is to validate the concept of using textile electrodes embedded in garments. Self-designed EMG-measuring pants incorporating stainless steel electrodes are tested.

4.2.2.1 Prototype

In this study, self-produced EMG-pants for measuring quadriceps and hamstrings activation using stainless steel electrodes are tested. Stainless steel electrodes are cheaper than the more commonly used silver electrodes and therefore would be an attractive alternative. The electrodes consist of a polyester fabric, with stainless steel wires (0.05 mm²) wound twice around the polyester threads. For the quadriceps, the skin contact area of each of the two electrodes is 30 mm x 165 mm. For the hamstrings, the skin contact area of each of the electrodes is 30 mm x 105 mm. The dimensions were chosen to optimally match the respective muscle regions. A textile patch was applied to prevent skin contact (visible in Figure 4-11 top-left picture) over an additional area of 30 mm x 30 mm of each electrode. In this area a button was attached to route the signals to the outside of the pants for attachment of an EMG sensor module. The commercially available Myon EMG Mobile System (Myon, Switzerland) was used as sensor module for signal amplification and wireless transmission to the computer. As the measuring pants used were not compression pants, standard compression pants made by 2XU were used as a second layer to improve electrode-skin contact. The prototype is shown in Figure 4-11. Sizes available were S, M, L, and XXL. A pre-test showed good washability of the electrodes. Three electrodes were washed in four handwash cycles using chlorine-free washing solutions. The electrodes showed no change in electrical resistance. Similarly, the use of disinfection spray did not alter the electrical resistance (measured after the pants were dry again).



Figure 4-11 MG-pants prototype using stainless steel electrodes (top-left). The electrodes are connected via buttons on the outside of the pants (bottom-left) to a sensor module (top-right) by Myon (Myon EMG Mobile System: amplifier, wireless transmission). Standard compression pants were used as a second layer (bottom-right) to improve electrode-skin-contact.

4.2.2.2 Validation Study: Methodology

Participants

In total 28 participants (9 female/19 male) between 20 and 35 years of age (mean 25.3 years) were enrolled in the study. Before the start of the experiment, all participants gave their informed consent. The participants were free of injuries, had not undergone ACL surgery, and had no orthopaedic or neuromuscular damage to the knee or leg muscles. Table 4-2 summarises the activity levels of the participants.

Table 4-2 Number of days per week with sportive activity

	none	1-2 times	3-4 times	> 4 times
male	2	6	8	3
female	1	3	2	3

Study design

Each participant underwent five test scenarios in a randomised order, with each scenario involving one of the following electrode settings:

- 1) Quadriceps: standard electrodes; application of electrodes as recommended by SENIAM as shown in Figure 4-12 in the left picture. Short pants were not interfering with the electrodes.
- 2) Quadriceps: standard electrodes; row-application; application of electrodes corresponding to the arrangement of the textile electrodes in the measuring-pants as shown in Figure 4-12 in the middle picture. Short pants were not interfering with the electrodes.
- 3) Quadriceps: measuring pants with textile-integrated electrodes.
- 4) Hamstrings: standard electrodes; application of electrodes on the biceps femoris and the semitendinosus, as shown in Figure 4-12 in the right picture.
- 5) Hamstrings: measuring pants with textile-integrated electrodes.

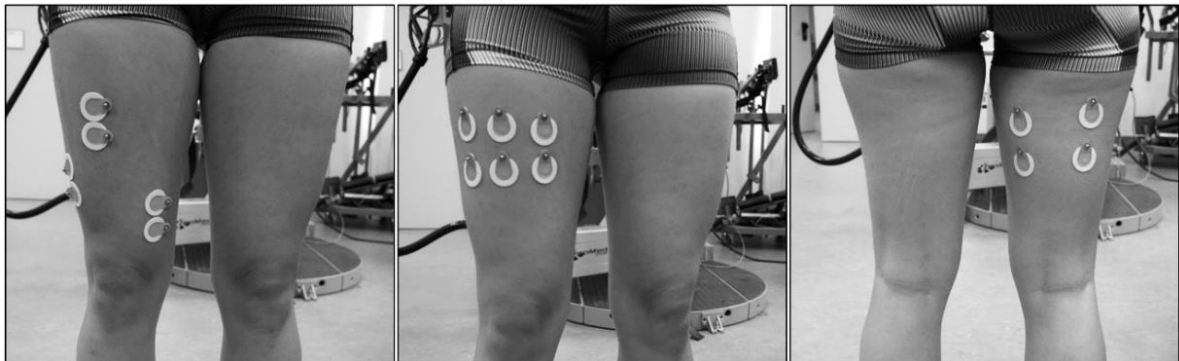


Figure 4-12 Left: SENIAM recommended application for the quadriceps. Middle: row-application; electrodes applied to the quadriceps corresponding to the electrode layout of the measuring pants. Right: hamstring application (SENIAM).

EMG measurements were taken for isometric muscle activation for five activity levels using a standard EMG system by Myon (Switzerland) as shown in Figure 4-14. The data acquisition rate was set at 1000 Hz. The knee's flexion/extension moment was recorded using an Isomed 2000 dynamometer (D&R Festl GmbH, Germany, see Figure 4-13). Activity levels were 100%, 80%, 60%, 40% and 20% of maximum voluntary performance of a flexion/extension knee moment. Figure 4-15 shows a typical test protocol. The participants always started with an application of 100%

maximum voluntary performance, followed by a stepwise lowering of the moment and a second maximum voluntary performance with two more decreases.

Measurements on the quadriceps were performed with an angle of 60° between femur and tibia and measurements on the hamstrings with an angle of 90° between femur and tibia (180° would be a straight leg, see Figure 4-16). Those angles were chosen as a compromise between comfort, optimal angle for the respective muscle to generate maximum force, and the need to prevent interaction between the seat and the sensor areas.

A graphical feedback interface helped the participants to control the activity level. They were asked to maintain each activity level for 3 s.



Figure 4-13 Isomed 2000 (D&R Festl GmbH, Germany)



Figure 4-14 Myon EMG Mobil System (1)+(2) and Ambu BlueSensor P Electrodes (3)

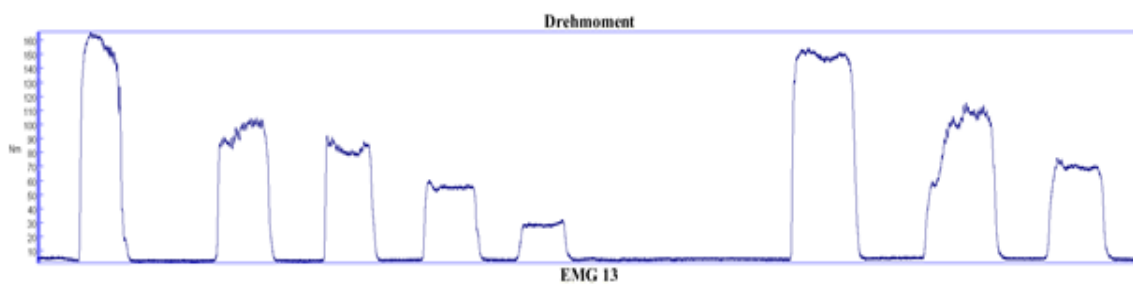


Figure 4-15 Typical test record, starting with 100% maximum voluntary performance, followed by stepwise 20% decreases and a second maximum voluntary performance with two decreases.

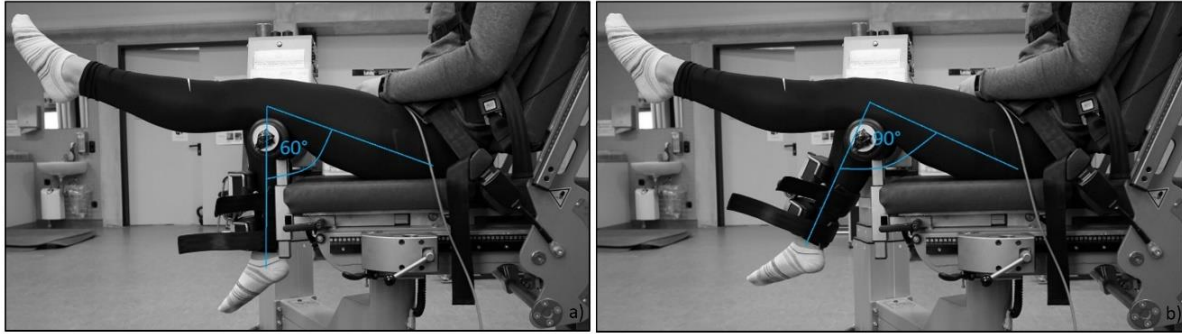


Figure 4-16 Selected angles between femur-tibia for the measurements. Left: 60° for quadriceps activation; Right: 90° for hamstrings activation. 180° would be a straight leg.

The test procedure steps for each participant were:

- 1) Selection of the appropriate size for the pants.
- 2) Adapt settings of the Isokinet on the participant.

Followed by repetitive steps for the five randomized test scenarios:

- 3) Skin preparation according to SENIAM standards.
- 4) Application of electrodes/pants.
- 5) Warm up (flexion/extension movements against a small force).
- 6) Test following the protocol in Figure 4-15.

Data processing

All measurements, except the hamstring measurement of one participant, were completed and included in the analysis. The EMG data was rectified and filtered using a second order Butterworth low pass filter (cut-off frequency 200 Hz) and a root mean square (window size 20 ms) filter. The sum of the signals from the three electrode-pairs of the quadriceps, respectively two electrode-pairs of the hamstrings (see Figure 3), were calculated to allow comparison with the signals from the measuring pants. The signal was cut to segment the activity levels, using thresholds of 8 Nm for quadriceps and 11.3 Nm for hamstrings measurements, which is equal to 90% of the smallest respective moment measured across all participants. A mean value was calculated for each activity level measurement. EMG values and values of flexion/extension moments were normalised using the higher of the two maximum voluntary performances of the respective flexion/extension. For each measurement, a linear regression (least-square-method) of normalised EMG vs. normalised moment was calculated.

Average EMG and flexion/extension moment were calculated for each participant for the SENIAM-application and the pants. To reduce the influence of the applied flexion/extension moment, also the EMG/moment ratio (EMG normalised by the moment) was calculated. Bland-Altman plots (Bland and Altman 1986) were used to compare the two measurement methods.

4.2.2.3 Validation Study: Results

In Figure 4-17 and Figure 4-19 the EMG measurements are plotted against the applied flexion/extension moment for each activity level of all participants. For hamstrings and quadriceps, the absolute values of the pants are smaller than the values of the SENIAM-electrode-application. The row-application of standard electrodes on the quadriceps results in the highest EMG values. As observable in the normalised data in Figure 4-18 and Figure 4-20, all measurement methods have similar linear behaviour. For the hamstrings, the measurement amplitude for pants is about 60% of the SENIAM amplitude.

In Figure 4-21, the Bland-Altman plot for the average EMG values of each participant is shown. The mean difference between the two systems is 0.237 V, with a width of the 95% limits of agreement of 0.591 V. In the Bland-Altman plot Figure 4-22 the EMG-signal/moment ratio is compared. The mean difference is 0.0043 V/Nm, the width of the 95% limits of agreement is 0.0102 V/Nm. It is also notable that the difference between the systems increases with increasing muscle activity.

4.2.2.4 Discussion

The aim of this study was to validate the concept of using textile electrodes embedded in garments. The easy application of textile electrodes allows the use in amateur sports like skiing. For the intended use in a mechatronic ski binding, no qualified knowledge about electrode application procedures and data processing is needed and no normalising procedure is necessary, therefore enabling all athletes an easy use.

The large electrode surface does not allow statements about single muscles. However, it is even more suitable for the recording of muscle regions like the quadriceps or hamstrings in total. This is reflected by the fact that the row-application of electrodes, which corresponds to the arrangement of textile electrodes in the pants achieved higher signals than the SENIAM-application (in both cases the sum of three pairs of electrodes).

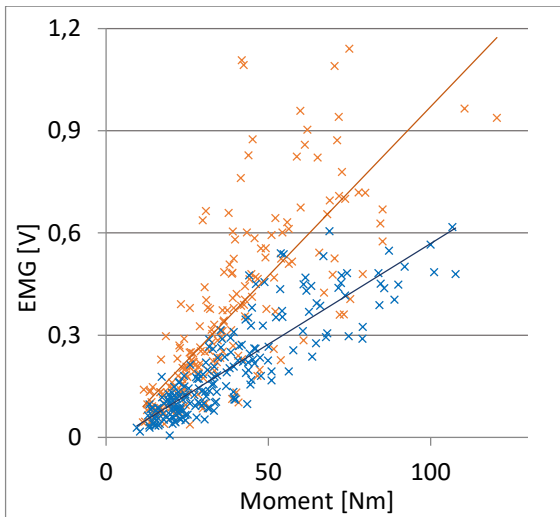


Figure 4-17 Hamstrings: regression of non-normalized values of EMG and flexion moment. Orange: standard electrodes (SENIAM). Blue: Pants

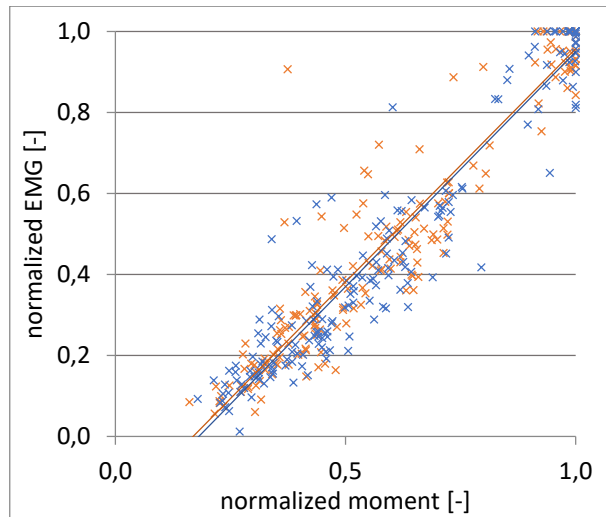


Figure 4-18 Hamstrings: regression of normalized values of EMG and flexion moment. Orange: standard electrodes (SENIAM). Blue: Pants

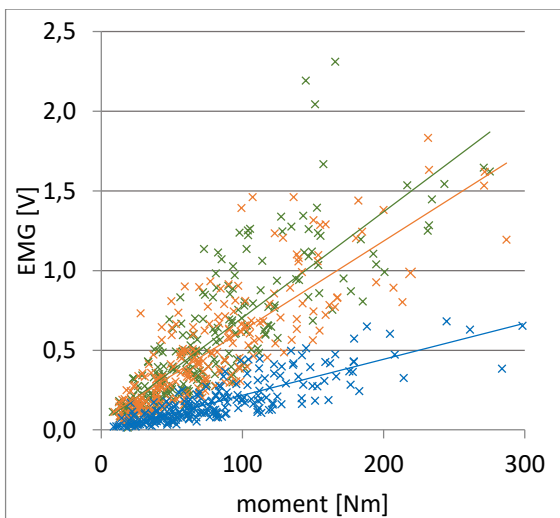


Figure 4-19 Quadriceps: regression of non-normalized values of EMG and flexion moment. Orange: standard electrodes (SENIAM). Green: standard electrodes applied in a row. Blue: Pants

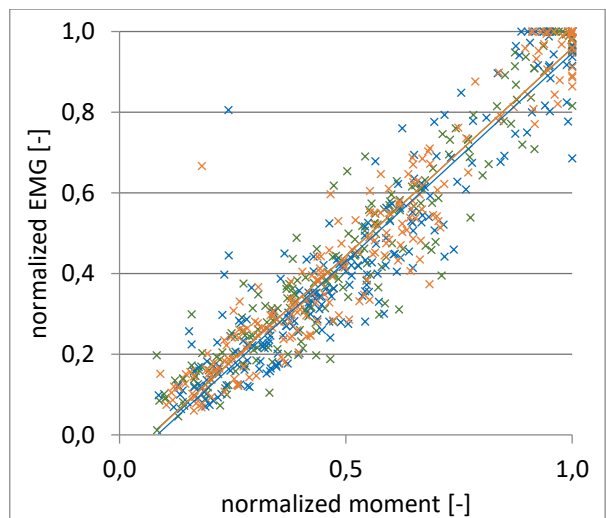


Figure 4-20 Quadriceps: regression of normalized values of EMG and flexion moment. Orange: standard electrodes (SENIAM). Green: standard electrodes applied in a row. Blue: Pants

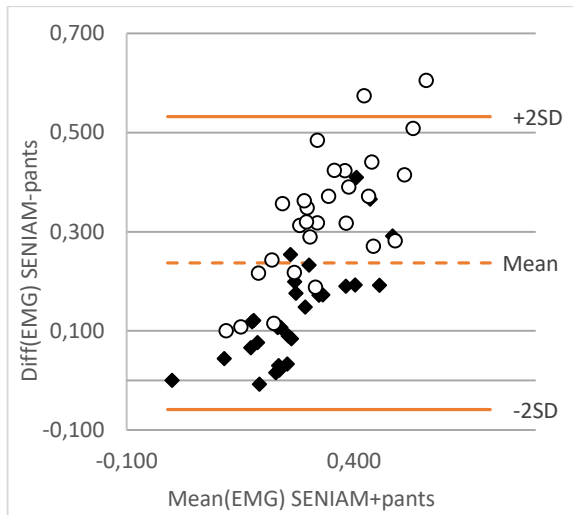


Figure 4-21 Bland-Altman-Plot of rectified, average EMG of each participant; dots: Hamstrings; squares: quadriceps.

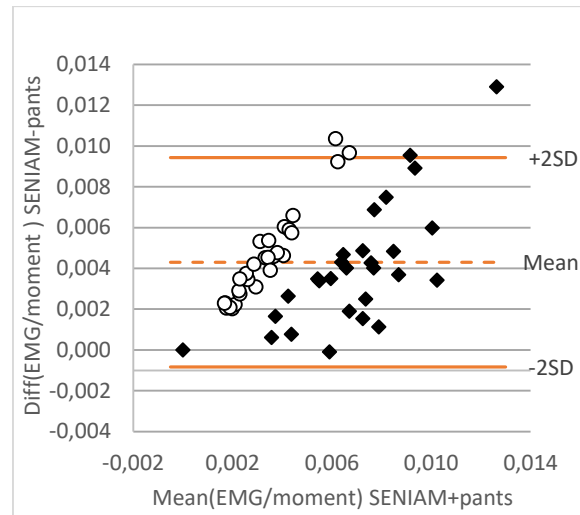


Figure 4-22 Bland-Altman-Plot of ratio (EMG/applied moment) of each participant; dots: hamstrings; squares: quadriceps.

Even though the surface of the textile-integrated electrodes is bigger, signal amplitudes of the textile-integrated electrodes were smaller compared to standard electrodes. Moreover, the Bland-Altman plots demonstrate an increasing difference between the signal amplitude of the textile-integrated electrodes and standard bipolar electrodes for increasing muscle activation. As both systems showed a comparable linear behaviour, this increasing difference does not impact a feasible textile solution and could easily be addressed by increased amplification of the signal. Also, by using gel or wetting the electrodes, signal attenuation could be decreased (Pani et al. 2019). In this study a very simple textile prototype was used. Different materials, or more sophisticated textile sensors, or improved integration of the sensors in the garments could also lead to reduced signal attenuation. In addition to the electrode itself, the design of the textile in which the electrodes are embedded is of great importance. The electrode-skin contact pressure is a critical parameter influencing the signal quality that is achieved through an optimal textile design (Kim et al. 2020).

While stainless-steel electrodes are washable and corrosion-resistant, they may not be the optimum solution for the integration in pants. Applications using gold, silver, nickel, copper or carbon-filled silicon can be found (Awan et al. 2019; Guo et al. 2020; O'Brien et al. 2019). The choice of material is influenced by multiple and varying factors such as price, location of integration, carrier textile, expected mechanical properties

(e.g. flexibility due to the required range of motion), and biocompatibility. Textile and materials research is highly active in developing better materials suited for wearable and textile integration (Gehrke et al. 2019; Lee et al. 2020). The electrodes were made of polyester threads around which metallic threads were wound. Such threads can break and thus lose conductivity. Also, they become uncomfortable for the user because the broken threads penetrate the skin. There are more suitable production methods, e.g. coating, for producing electrodes directly on or in the textile.

When performing EMG measurements, multiple interfering influences must always be taken into consideration: crosstalk, individual anatomical and physiological differences, subcutaneous fat and fatigue to name but a few. EMG-pants will have to overcome with all these. In this study, an influence of the dynamometer electric motor was apparent. However, because the influence was comparable in all measurements, we considered it acceptable.

The study cohort generally practices sports, had a mean age of 25.3 and a mean body-mass-index of 24.2. Therefore, it does not represent the population in general. Further tests are required especially involving heavier participants. As surface-EMG is highly influenced by subcutaneous fat, its applicability to heavier persons will certainly be limited. Therefore, wide use of EMG-wearable textiles in health and rehabilitation will not be without challenges. For sports applications, especially for professional or keen amateur athletes, such systems could be beneficial in training and injury prevention. The self-produced EMG-pants were tested in an isometric setting. Therefore, the interpretation of results is only valid for the use of such garments in similar settings e.g. isometric training and rehabilitation. Nevertheless, transferability of results to EMG measurements of more dynamic movements is likely possible. Future research must prove the validity of such measurements because dynamic measurements are per se subject to more interfering artefacts (Farina 2006). In addition to those artefacts, which also apply to measurements using standard electrodes, motion artefacts resulting from electrode-skin displacement might have a strong impact on the feasibility of garments with textile-integrated electrodes (Zhang et al. 2011).

4.2.2.5 Conclusion with respect to a mechatronic ski binding

Especially when comparing larger muscle groups, EMG-garments are an easy-to-use tool for the researcher, athletes, or patients undergoing rehabilitation. Scenarios such as recording the ratio of quadriceps and hamstrings activation, which do not need a normalisation procedure, enable athletes to use the approach without having qualified knowledge about electrode application procedures and data processing.

These are prerequisites for the use in a mechatronic ski binding. Moreover, EMG-pants are already available as consumer goods, therefore, having already a high level of development. Electrodes for recording muscle activity place similar demands on the carrier textile (e.g. close fitting) as sensors for recording the knee angle. Therefore, a combined integration in measuring trousers is conceivable.

4.2.3 System for Tracking the Loads on the Feet

Sections of this chapter were submitted and accepted for publication (Hermann et al. 2021). Alterations have been made in these sections for reuse in this work.

Like a mechanical ski binding, a mechatronic ski binding needs to consider the forces acting on the ski. An optimal sensor system would not only allow to measure these forces, but also calculate the resulting torques at the binding, and the force application points. This information allows to make assumptions about the body position (for example a possible backward-lean due to a vertical force application load behind the ski binding) and resulting loads at the knee (e.g. valgus/varus due to a high side-load on the ski).

Tracking skiing loads is normally done with specially developed equipment. The use of standard laboratory dynamometers is not applicable, as the system must be carried by the skier or attached to the skiing equipment.

Several custom-made systems were developed for recording the forces and moments acting on the ski (Figure 4-23). Most systems are based on strain gauge sensors for measuring the forces between the ski and the ski binding or between the ski binding and the ski boot. In many systems, forces and moments are recorded separately for the front and back component of the ski binding (Schwameder et al. 2001; Falda-Buscaiot 2017; Saito et al. 2015; Stricker et al. 2010). This is advantageous if the force transmission through the two binding components is investigated, but susceptible to provoking and recording constraint forces in the ski-boot-binding-complex, as the system is statically overdetermined, thus limiting the interpretability of the results. Other systems only use one sensing component (Kiefmann et al. 2006), thus measuring the absolute skiing loads.

Such “measurement bindings” can give highly accurate information about the forces, moments, and the instantaneous point of force application along the longitudinal axis of the ski. Thus, such a system would be perfect as input for a mechatronic ski binding, but these bindings are unhandy to use, as they are stiff, large, and heavy. Moreover, they are unique and of a complexity that does not allow widespread use in skiing as a consumer product.

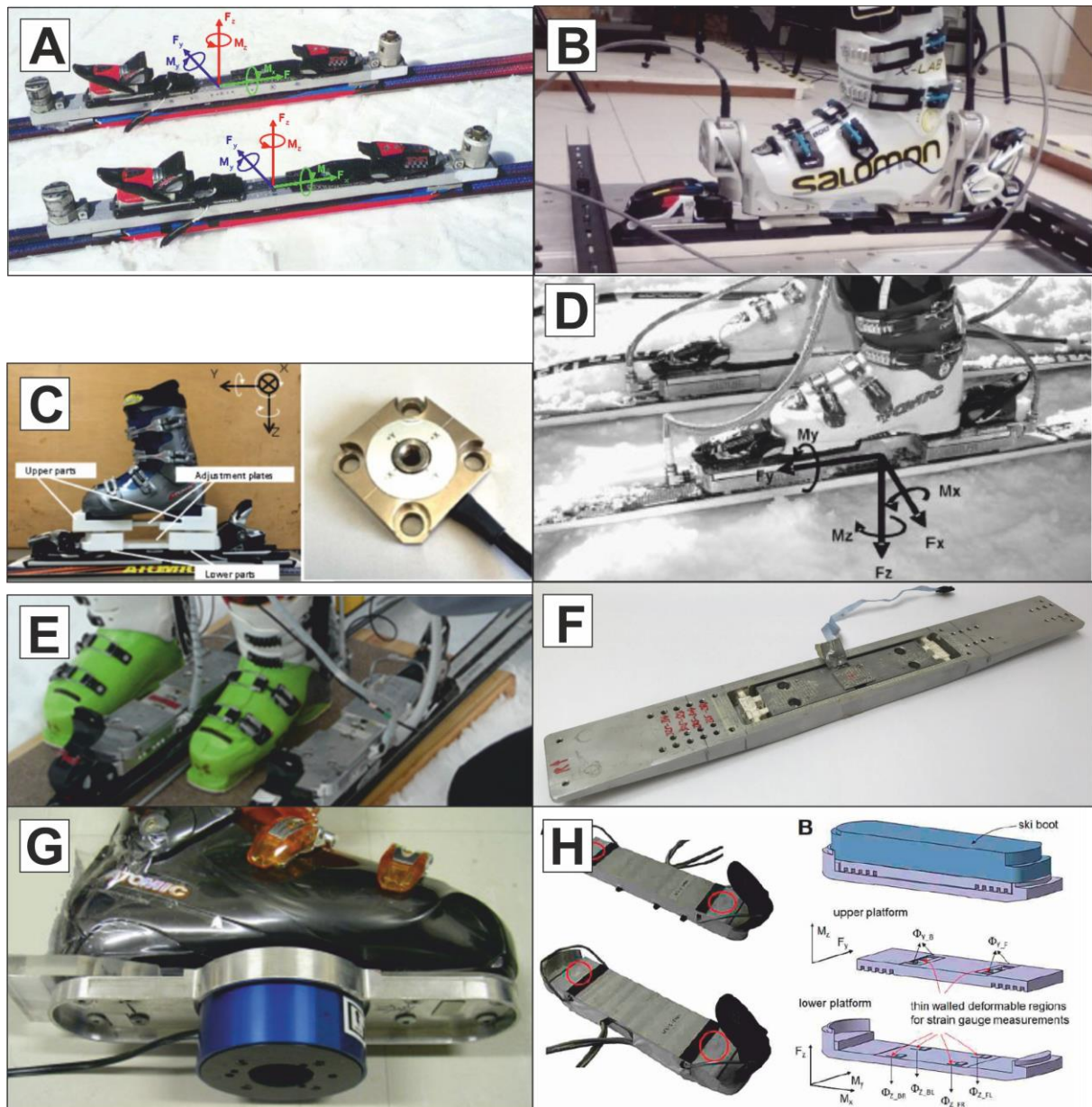


Figure 4-23 Selection of measurement systems to record skiing loads. Systems recording loads on the two binding components separately: (A) Schwameder et al. (2001), (B) Falda-Buscaiot (2017), (C) Saito et al. (2015), (D) Stricker et al. (2010)¹; Systems recording absolute loads for the whole binding: (E) system of the Technical University of Munich first published in Kiefmann et al. (2006), (F) system of MARKER Deutschland GmbH, Penzberg, Germany (unpublished), (G) Hirose et al. (2015), (H) Meyer et al. (2019) and Meyer (2012). ¹©Taylor & Francis; all figures reprinted with permission of the respective copyright holder.

One option to reduce weight and size is to reduce the degrees of freedom measured by the system. However, systems measuring only the vertical force (Figure 4-24 (A)+(B)) are still heavy and need to be very stiff due to the measurement principle. For

example, the system by Wimmer and Holzner (1997) shown in Figure 4-24 (B -right) had a total weight of 990g.

An alternative to force measurement is the measurement of pressure. With a known measurement surface and pressure distribution, the acting forces and moments can theoretically be calculated. Pressure sensors are cheaper and can be very thin and therefore minimise a possible restriction of the athlete by the system itself. A flexible design of pressure sensors is possible and allows the integration inside a ski boot. Various systems of different sensor types (resistive, capacitive, hydro cells) have been used in research (Figure 4-24 (C)-(G)) and are also available as commercial products.

Drawbacks of pressure sensors are the limitation on unidirectional measurements and the reduced measurement frequency compared to force sensors (depending on the measuring principle and the number of sensors used but usually lower than 250 Hz). Moreover, further limitations are a difficult calibration when inside the boot (due to shoe buckles and changing position of the foot inside the boot), and the difficult determination of the force application points (only possible for forces inside the sensing area). As with all sensor systems, a compromise between spatial resolution, time resolution, measurement accuracy, robustness, and usability must be found for the intended use.

Nevertheless, pressure insoles were successfully used in skiing research for various reasons. Krueger et al. (2006) determined the edging angle and the ground reaction force with a 24-sensor insole. Raschner et al. (2001) used insoles with 99 capacitive sensors to compare carving turns to (at that time) traditional turns. Spitzenpfeil et al. (2006) tracked mechanical loads in alpine ski racing and derived implications for safety and material considerations and Lafontaine et al. (1998) conducted a study with PEDAR pressure measuring soles (Novel, Munich, Germany) with professional ski instructors. The maximum and average vertical forces, the maximum pressure, the pressure distribution, and the trajectory of the centre of pressure (COP) were calculated for different turns. In their congress abstract, Brodie et al. (2008) propose that pressure insoles can provide insight into possible stance alteration to reduce knee torques or aid preventive programs. An interesting work was presented by Holleczeck et al. (2010) who used self-made pressure sensors (Holleczeck et al. 2009) and artificial

intelligence to detect snowboard turns. Falda-Buscaiot et al. (2017) studied the influence of slope angle, foot position, and turn phase on the plantar pressure distribution.

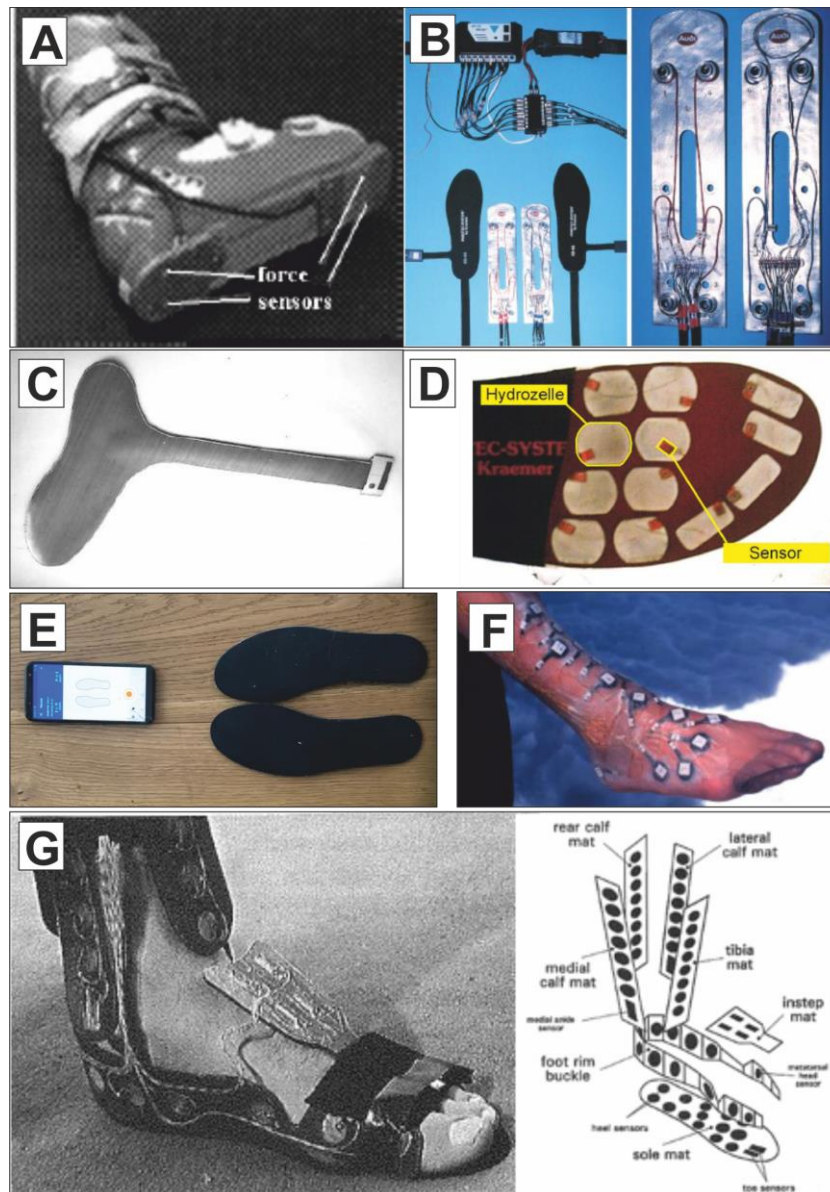


Figure 4-24 Force and pressure sensor systems to measure vertical loads in skiing and pressure distribution in the ski boot. Systems based on force sensors: (A) Rađenović et al. (2001), (B) ski boot integrated force measurement plates (right) presented by Wimmer and Holzner (1997) and PAROTEC pressure insoles with 16 sensors (see D) - picture taken from Senner (2001); Systems based on pressure sensors: (C) PEDAR sensor insole by Novel GmbH, Munich, Germany used by (Raschner 1997), (D) PAROTEC sensor Insole by Paromed, Neubeuern, Germany (Senner 2001), (E) MOTICON sensor insole and mobile app by Moticon ReGo AG, (F) single pressure sensors around the leg and foot to measure pressure in the ski boot (Senner 2001), (G) Sensor “sock” for measuring pressure in a ski boot presented by Schaff et al. (1997).

Stricker et al. (2010) compared forces calculated with data from pressure measurement soles with forces recorded by 3D dynamometers (see Figure 4-23 (D)). The compressive force measured by the soles was on average between 21% (outer ski) and 54% (inner ski) lower than that measured by the 3D dynamometers. The authors attribute this to the different positions of the measuring systems, as well as to the fact that part of the force is absorbed in the boot shaft. However, a high degree of similarity between the force-time curves of the pressure measuring pads and the dynamometers was found.

A sophisticated pressure sensing system (see Figure 4-24 (G)) was presented by Schaff et al. (1997), who used a measurement sock with 64 sensors attached beneath the foot, as well as around the lower leg, the instep, and medially and laterally at the foot.

Aim of the following study

The use of pressure sensors not only in the plantar region of the foot but also in the shaft can add valuable information and may allow the estimation of all force and moment components acting on the foot. For a mechatronic ski binding, a system working on pressure sensors is preferable to a system based on force sensors because it would be easier to integrate it into the existing equipment and would be a lot cheaper. In particular, an integration into the outer shell of the ski boot would be relatively easy to manufacture and may have advantages to an integration in the soft boot or sock with respect to manufacturing and sensor robustness. On the other hand, the pressure amplitude certainly is diluted through the different material layers from the foot to the outer shell. To test this, self-made prototype systems to measure pressure distribution in the ski boot were developed. The main goal was to find the number of sensors and the location of those sensors needed to optimally estimate skiing loads.

In total three systems for the right foot were built:

- PTBoot: Pressure sensors attached to the plastic shell of the **boot**, between the shell and the inner soft boot.
- PTSock: Pressure sensors attached to the inside of the soft boot, between the soft boot and the ski **sock**.
- PTFoot: Pressure sensors directly attached to the **foot**.

This allowed to investigate the best location for the sensors around the leg and test the loss of pressure amplitude from one (material) layer to the next. In a laboratory study, simulated skiing movements were recorded simultaneously with all three systems and a 6 DOF-measurement binding (Kiefmann et al. (2006); see Figure 4-23 (E)), which acted as reference system. Based on the results, a recommendation for a reduced number of sensors is given. Fewer sensors allow higher measurement frequencies and reduce the complexity of a to-be commercial measurement boot and the required microcontrollers.

The value-output of the 17 sensors of each prototype was correlated with the loads measured by the measurement binding.

4.2.3.1 Prototypes

Selection of a sensor technology for the prototypes

For the development of the prototypes for measuring the pressure distribution in a ski boot, either capacitive or resistive sensors are applicable. More detailed information about pressure sensing technologies and their respective properties, advantages, and drawbacks can be found in appendix 7.7.

The two technologies each have advantages and drawbacks (Table 4-3) and the decision for a technology depends on the application and the resulting requirements. The most important requirements for pressure sensors as well as their practical application are summarised by Razak et al. (2012) and mainly concern hysteresis, linearity (see also appendix 7.7), temperature sensitivity, and the pressure range of the sensor. In addition, the two pressure measurement methods differ fundamentally with respect to the measurement results. While resistive sensors measure the peak pressure of the entire sensor surface, the result of the capacitive measurement is the average pressure over the sensor surface (Ashruf 2002).

The aim of this work is to develop prototypes to determine the optimal placement of sensors inside a ski boot. Focus, at the early stage of the investigations, is to have a system design that is as easy to implement as possible. Therefore, for the easy structure of the sensor and the logging module, a resistive solution was chosen, even though this may not be applicable in a marked-ready product, as the impact of humidity and temperature may require a capacitive sensor design.

Table 4-3 Advantages and disadvantages of resistive and capacitive pressure sensors

Resistive	Capacitive
<ul style="list-style-type: none"> + simple sensor design + simple data logger design + large measurement range + fast reaction time - non-linear - sensitive to temperature and humidity 	<ul style="list-style-type: none"> + not sensitive to temperature and humidity - complex data logger design - sensor thickness
<i>o records maximal pressure acting on the sensor</i>	<i>o records mean pressure acting on the sensor</i>



Figure 4-25 SHEMA of the pressure sensor (left) and steps of manufacturing: centre left: foils with conductive tracks; centre right: wired sensor foils; right: finished sensor with pressure sensitive conductive material layer over the foils with the conductive tracks and protective, non-conductive foils laminated on both sides of the sensor.

The two types of self-made sensors have a circular design with a sensitive area of 30 mm in diameter and a surface of 707 mm² (Figure 4-25) for a larger sensor and 20 mm in diameter and a surface of 314 mm² for the smaller sensor. The sensors consist of a flexible carrier foil of 25 µm thickness with 18 µm thick copper tracks printed on it. The tracks form two interlocking combs. The two conductive tracks are wired for the connection to the data logger and a reference conductor. Velostat (electrically conductive foil due to a carbon black impregnation) was used as pressure-sensitive conductive material. Three layers, each 0.1 mm thick, were placed on the conductive side of the foil. All layers were fixed and isolated by laminating them with conventional laminating film. A voltage divider circuit with a 100 Ω reference conductor was used to record the sensor signal (see section: *Data processing of the pressure sensing systems* and equation 4-3, page 4-128).

The sensor characteristics were determined (Figure 4-26) and an approximation curve was calculated using equation 4-2 with the curve fitting tool of Matlab 2020a (MathWorks, Natick, Massachusetts, USA).

$$y = ae^{-bx} \quad 4-2$$

with y being the pressure seen by the sensor, x being the electrical resistance of the sensor, and the parameters $a = 5.065 * 10^7$ and $b = 0,1475$ for the large sensor type, having a correlation of $R^2 = 0.9527$ between pressure and electrical resistance.

Due to the small number of small sensors used (see next section: *Placement of the Sensors*), the sensor characteristic for each of these sensors was determined individually and is given in Table 4-4.

Table 4-4 Parameters for the sensor characteristic approximation for the four small sensors used. Parameters refer to equation 4-2.

Sensor	a	b	R²
PTSock 6	125.1	0.01671	0.9286
PTSock 10	115.8	0.008495	0.9588
PTFoot 6	95.98	0.001639	0.9743
PTFoot10	370.5	0.0364	0.9775

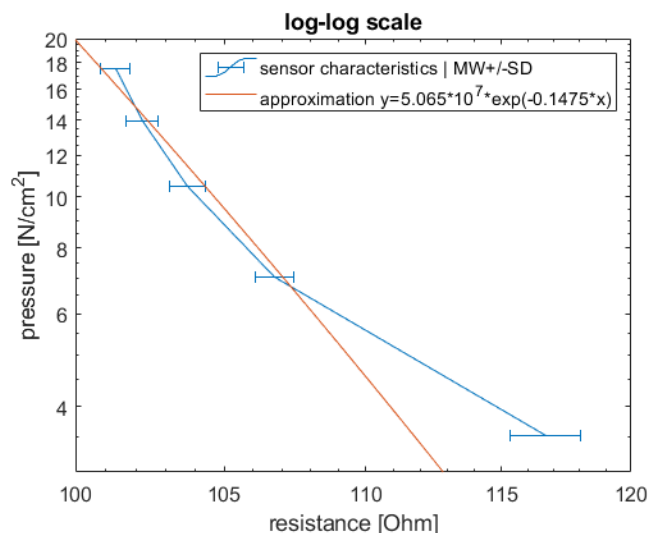


Figure 4-26 Sensor characteristic of the large sensor type derived of 5 of the self-made pressure sensors.

Placement of the Sensors

The placement of the sensors was determined based on preliminary tests and considerations with regard to an optimal detection of following loads acting on the foot, which are forward/backward leaning (M_y) / rotation torque (M_z) / edging loads (M_x / F_y) / ground reaction force (F_z) with the coordinate system according to Figure 4-29.

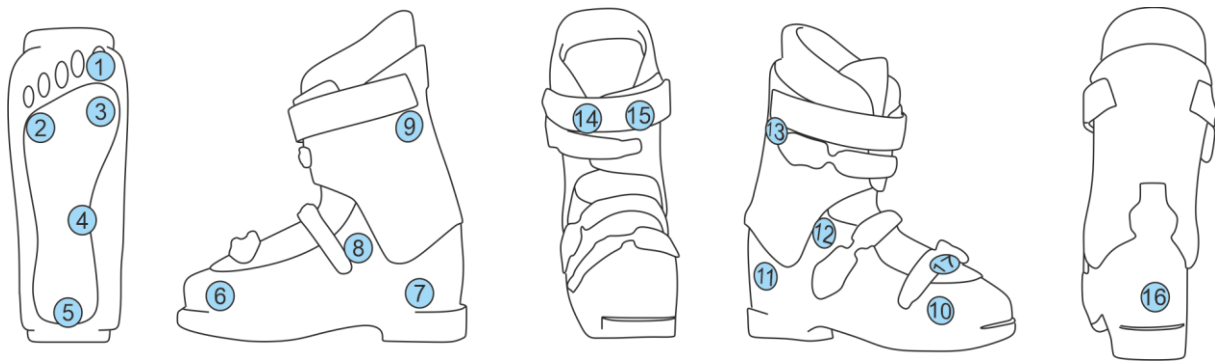


Figure 4-27 Placement of the 17 pressure sensors of ski boot prototype 'PTBoot' (placed on the inner side of the hard shell of the boot). At the same positions, sensors of the two other prototypes were placed (outside the ski sock and at the skin of the foot; see Figure 4-28).

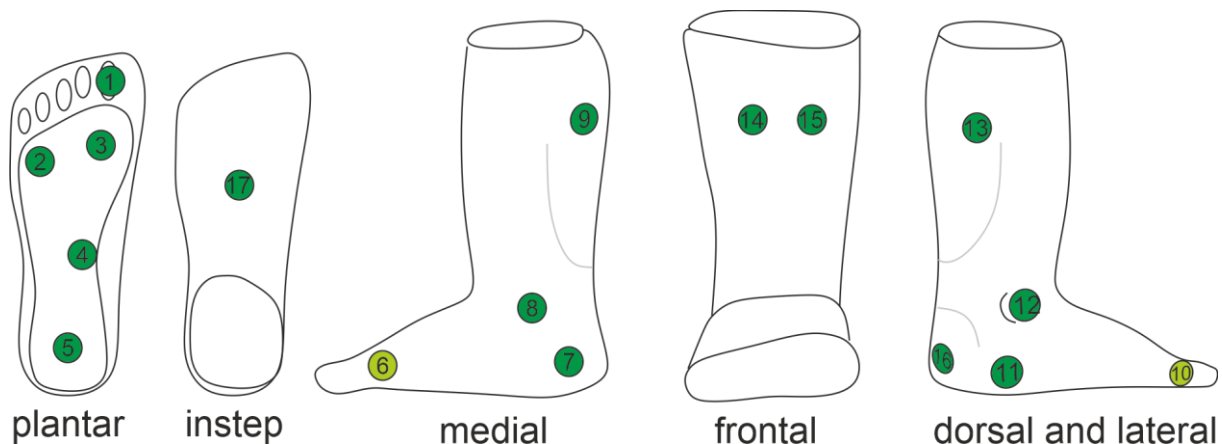


Figure 4-28 Placement of 17 pressure sensors in the sock prototype 'PTSock' and the placement of the sensors directly on the skin of the foot 'PTFoot'. Sensors 6, and 10 are of a smaller diameter (20 mm). All other sensors have a diameter of 30 mm. Positions of sensors 1-17 correspond to positions of the sensors of the ski boot prototype (Figure 4-27).

For all three prototypes, 17 sensors were distributed around the foot and lower leg (Figure 4-27 and Figure 4-28). Four sensors were placed on both the medial and lateral side of the foot, five sensors were placed in the plantar region, two sensors on the tibia shaft, one sensor at the heel, and one sensor above the instep. For PTKSock and

PTFoot the sensors in the toe region no. 6 and 10 (see Figure 4-28), have a smaller diameter of 20 mm, due to space limitations.

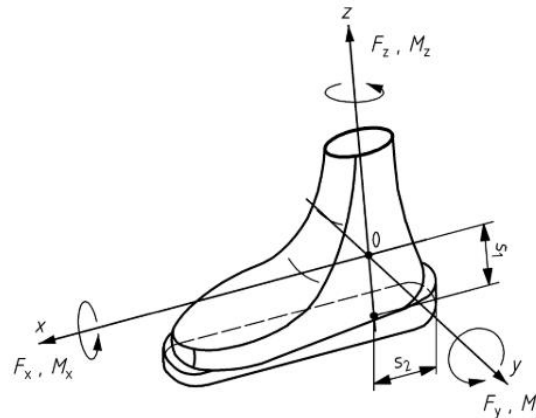


Figure 4-29 Coordinate system of the measurement binding according to DIN:ISO 9462:2017 picture taken from (DIN ISO).

Data processing of the pressure sensing systems

A myRio-1900 (National Instruments, Austin, Texas, USA) was used for A/D conversion, processing, and logging (Figure 4-30). To allow the logging of all sensors, multiplexers (MUX, CD74HC4051E, Texas Instruments, Dallas, Texas, USA) were used with reference conductors ($R_{Reference} = 100\Omega$) for each MUX. The sensors were supplied with $U_0 = 5V$. The resistance of each sensor R_{Sensor} is calculated with equation 4-3, where U_{Sensor} is the measured signal in Volt.

$$R_{sensor} = \frac{U_{Sensor} * R_{Reference}}{U_0 - U_{Sensor}} \quad 4-3$$

A LabView 2015 (National Instruments, Austin, Texas, USA) program was running on the myRio. Measurement frequency was set to 10Hz (limited by the number of sensors and the hardware, e.g., switching time of the MUX). Data was saved on a USB-stick plugged into the myRio-module.

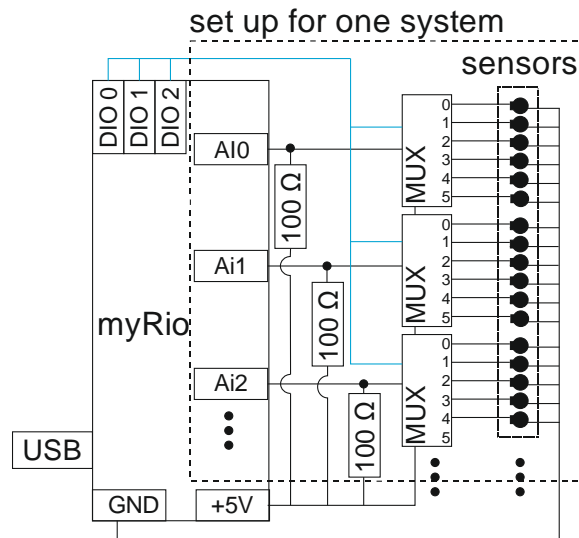


Figure 4-30 Set up of the data logger showing a system with 17 sensors.

4.2.3.2 Validation Study: Methodology

All three pressure sensing prototypes (Figure 4-31 (A-C)) were used simultaneously with a 6 DOF measuring binding (first presented by Kiefmann et al. (2006); see Figure 4-23 (E)). The measurement binding is attached to a pair of skis via a standard ski binding (Figure 4-31 (D)) and is controlled by a tablet running a LabView program, which records at a frequency of 500Hz. The pressure sensing prototypes and the measurement binding are synchronized via a manually activated trigger. The setting of the data collection is stationary. One participant simulates ski-typical body postures by shifting body weight and using muscle activation (Figure 4-32). Simulated postures are backward-leaning (Figure 4-32 (A)), forward-leaning (Figure 4-32 (B)), left curve (inner edge of the measurement boot), right curve (outer edge of the measurement boot) (Figure 4-32 (C)), internal rotation, and external rotation (Figure 4-32 (D)). Each position was held for 5 seconds.

Postprocessing

For comparison with the pressure systems, the data of the measurement binding was down smoothed using a moving average window of 25 (0.05 s). The pressure values were calculated using equations 4-3 and 4-2 with the respective equation parameters of the above-mentioned sensor characteristic. For the correlation with the measurement binding, the pressure values (10 Hz) were linearly interpolated to 500 Hz. All calculations were performed using Matlab.

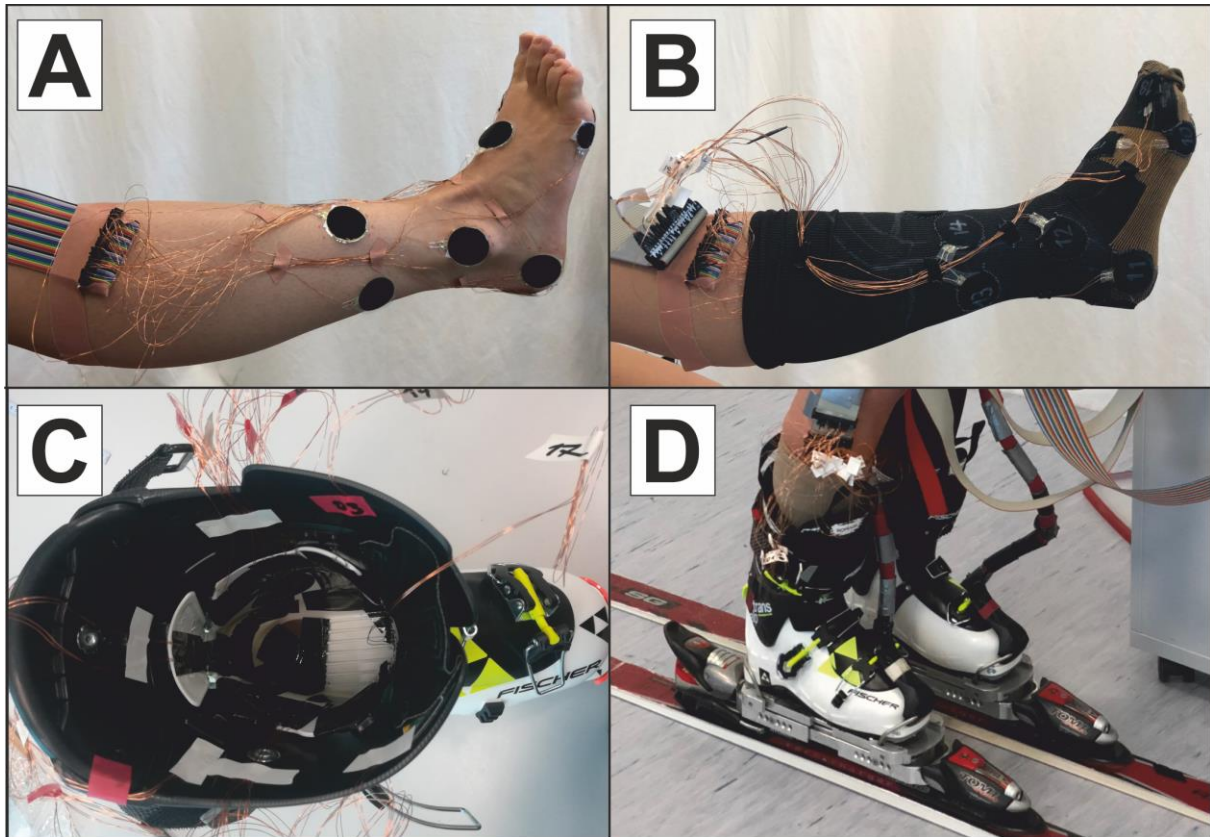


Figure 4-31 The three sensor prototypes and the test set up with the participant wearing all prototypes and standing in the measurement binding. (A) sensors attached to the skin of the foot; (B) measurement sock; (C) view in the outer shell of the measurement boot. The sensors are visible; (D) test set up with measurement binding.

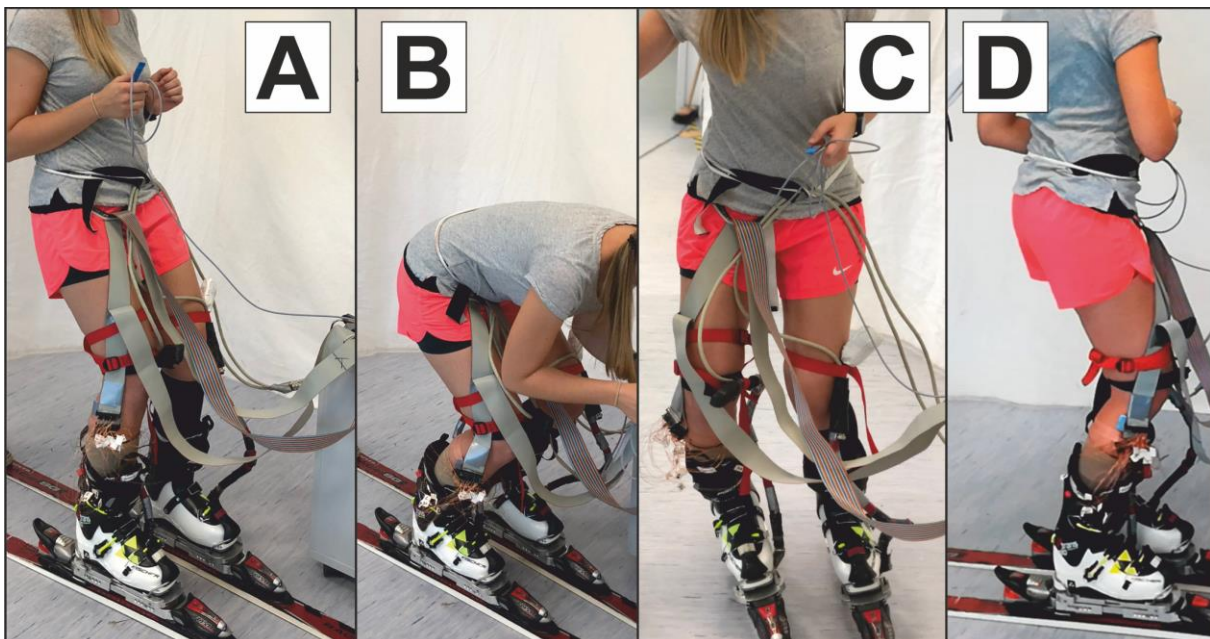


Figure 4-32 Simulation of ski-typical body postures to test the sensors. (A) backward-leaning; (B) forward-leaning; (C) left curve / edge force (respective movement for right curve); (D) simulation of internal/external rotation.

4.2.3.3 Validation Study: Results

Comparison between the pressure sensing systems

The comparison of the respective values of each sensor of the different prototypes at the same position indicates qualitative similarity between the pressure curves with a loss of amplitude from PTFoot to PTSock to PTBoot (Figure 4-33). The loss is not the same for each sensor position. The pressure recorded by PTBoot is low with values smaller than 0.125 N/cm^2 for most of the sensors and not exceeding 10 N/cm^2 in any sensor. The pressure range for PTFoot and PTSock is mainly between 0 and 40 N/cm^2 . Higher values are reached by PTFoot sensor 2 (positioned under the outside edge of the ball of the foot), which reaches 68 N/cm^2 , and PTFoot sensor 6 (positioned at the medial side of the ball of the foot), which reaches a maximum of 83.4 N/cm^2 . These unrealistic high values indicate that the sensors were preloaded, locally deformed (wrinkled), or damaged and, therefore, the sensor characteristic may have changed (see discussion).

Both sensors under the ball of the foot (sensors 2 and 3) show the highest pressure values in the plantar region and have a distinguishable resolution of the measured manoeuvres in all three systems. The sensor positioned under the heel (sensor 5) hardly measures any pressure for PTBoot but has higher values (about 10 N/cm^2) for PTFoot and PTSock. The sensors under the big toe (Sensor 1) of PTFoot and PTSock show only small pressure responses to the six skiing manoeuvres, with the highest values for the time spans of the transition from one manoeuvre to another. The same sensor of PTBoot shows nearly no signal. The different skiing manoeuvres are not prominently expressed in the sensor data under the arch of the foot (sensor 4), which recorded small pressures over the total measurement. On the medial and lateral side, the higher positioned sensors 8 and 12 of PTBoot show higher pressures than the lower positioned sensors 6, 7 (medial), and 10, 11 (lateral) of PTBoot. The same sensors of PTSock and PTFoot give more pronounced values than the sensors of PTBoot, but some signals of sensors 6, 7, and 12 seem to be influenced by disturbances as they show unexpected or unrealistic behaviour (see discussion). Even though the sensors at the calf (9 and 13) show high pressures for PTFoot and PTSock, only low values are recorded by PTBoot. At the tibia (sensors 14 and 15), the sensors of all three prototypes are sensitive to the six skiing manoeuvres. Sensors 16 (backside

of heel) and 17 (instep) record high pressure and allow the skiing manoeuvres for PTFoot and PTSock to be distinguished but record only low values for PTBoot.

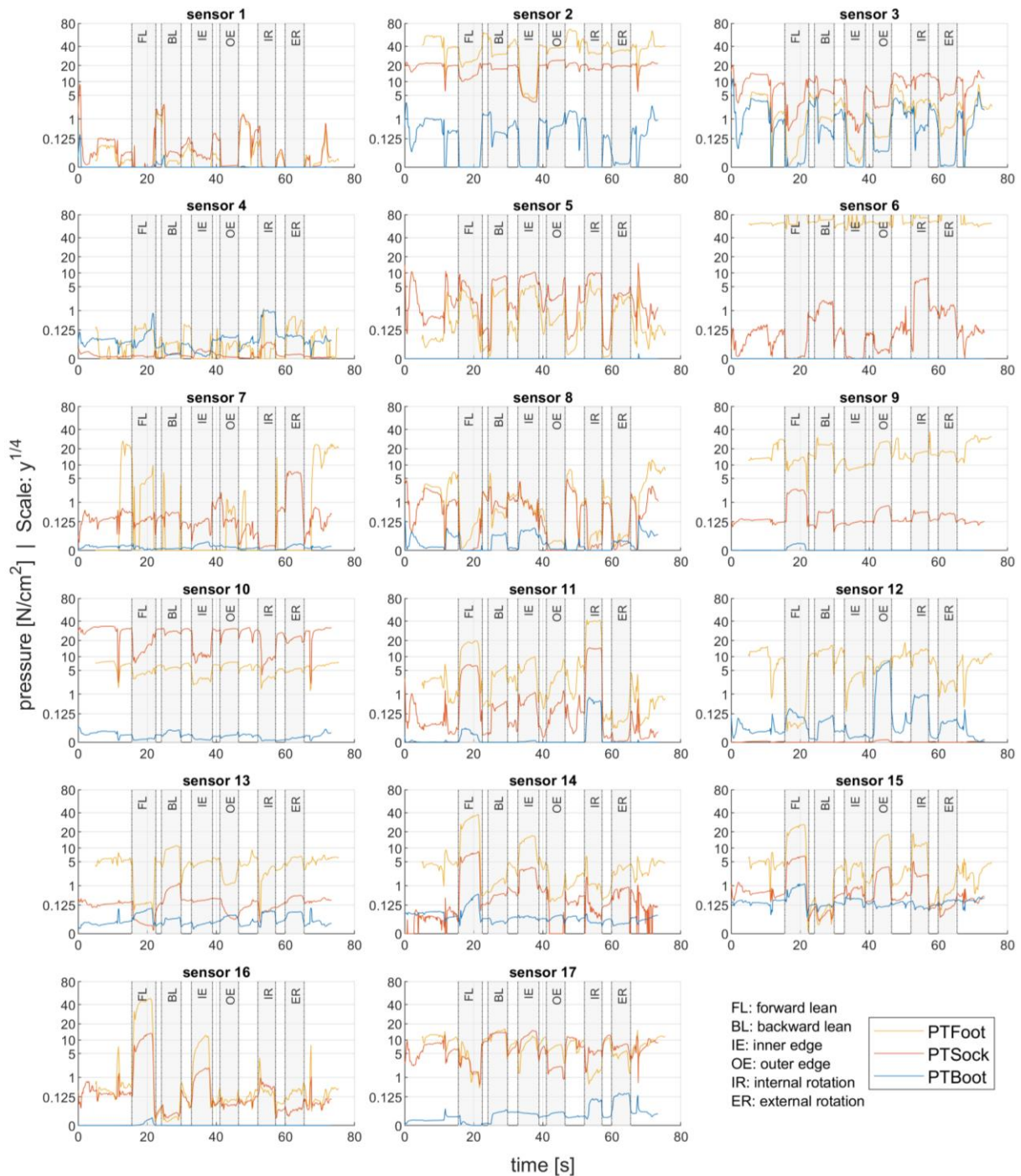


Figure 4-33 Comparison of the pressure sensor values of the three prototypes. The grey areas and a respective annotation indicate the six skiing positions.

Correlation of the pressure sensing systems with the measurement binding

The Pearson correlation coefficients (testing for linear relationship) between the pressure sensors and the forces and moments measured by the measurement binding are overall small to medium large with only singular sensors reaching values between 0.5 and 0.8 (Figure 4-34). A Spearman correlation test (testing for a monotonous, (also non-linear) relationship) is also not more successful in finding a strong connection of specific sensors to external loads (Figure 7-37 in Appendix 7.8).

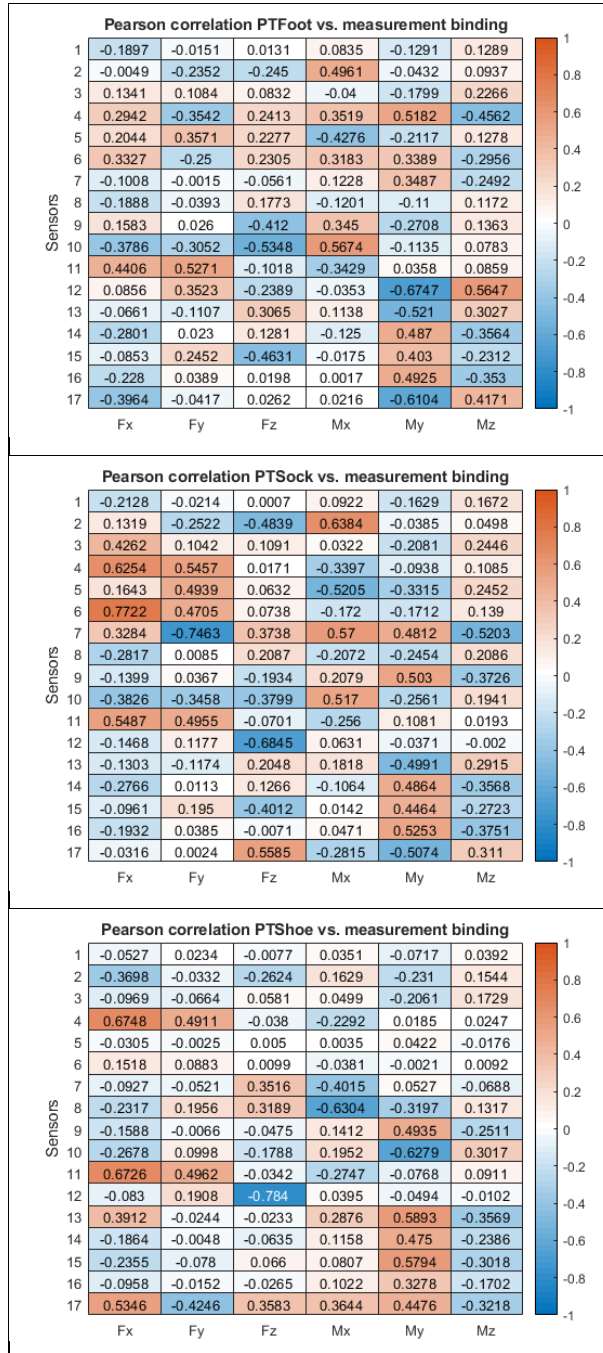


Figure 4-34 Pearson correlations between all sensors of each of the three prototypes and the measurements of the measurement bindings.

4.2.3.4 Discussion

In this study, PTBoot measured only very small pressure values and the loss of amplitude from PTFoot to PTBoot is large. Therefore, sensors for a to-be measuring boot or sock need to be designed very specifically with respect to resolution and sensitivity, and probably different sensor designs are needed for different sensor positions in the boot. It may be advisable to design the shell shape in such a way that the liner transfers a large part of the force to the shell on defined surface areas on which the sensors are placed.

In general, the sock prototype produced more reliable results than both the other prototypes. Therefore, an integration of a pressure measurement system in the sock or the inner boot of the ski boot would be more expedient than the integration between the hard shell and the inner boot of the ski boot. On the other hand, with respect to robustness and easy manufacturing, a pressure sensing boot is preferable to a pressure sensing sock.

The qualitative determination of specific skiing manoeuvres with a pressure measurement system in the ski boot is possible. Based on the results of the investigations with the three prototypes, it is possible to reduce the number of pressure sensors needed. A recommendation of sensor positions is given in Table 4-5.

Table 4-5 Recommendation of the placement of pressure sensors to determine skiing manoeuvres based on the results with the three prototypes.

Detection of	Sensor	Sensor position
Forward / backward lean	(2), (3), 9, 13, 14 , 15 , 16, 17	(ball of foot), calf, tibia shaft , heel, instep
Left / right curve	8, 9 / 12, 13	Upper part of the lateral and medial side of the foot, near the bend of the foot and the calf.
Internal / external rotation	6, 11 / 7, 10	Lower part of the lateral and medial side of the foot.

To detect a forward or backward-leaning body position the tibia shaft may be better suited than a position at the calf or the plantar region. The sensors at the calf are not only influenced by the leaning position, but also by muscle activation. The sensors in the plantar region may be non-optimal as they may give misleading information in some situations. For example, the sensors under the ball of the foot may be unloaded even though the skier is leaning forward. In such a case, the skier presses the tibia in the

boot and pulls the toes up to increase this pressure on the tibia by increasing the pressure on the heel.

The exact selection of a sensor position at the outer sites of the foot may heavily influence the quality of results in detecting curves or rotation movements. One reason to consider is the very individual geometry of the foot, another reason is the clamping of the foot in the boot, which varies for different skiing positions and manoeuvres but also as a result of deliberate force production to control the ski.

A relationship between individual pressure sensors and a distinct force or moments measured with the measurement binding cannot safely be made with the data produced in this laboratory study. A reason may be the complex and non-optimal behaviour of the resistive sensor design (for example non-linear behaviour, the influence of temperature, bending, and local pressure maxima). Another reason is that one sensor is influenced by more than one force component.

Nevertheless, the medium-high correlations of the sensors at the calf and the tibia with the moment in the sagittal plane (M_y) are highlighted. Being able to measure M_y would be of high relevance for a mechatronic ski binding, as this would also allow to estimate the centre of gravity of the skier's body and thus, estimate if the skier is in an upright position or in a forward- or backward-lean.

If exact pressure values or loads should be determined (in contrast to the estimation of body position only), a great challenge will be the calibration of the sensors (offset) in the boot. A commonly used procedure for plantar pressure measurements is that the person's foot is in the boot or shoe and the person lifts the foot for a static and unloaded recording which is then used to 'zero' the sensors. In the following, these values of the static recording are subtracted from the later recorded values to determine the loads acting on the foot. This procedure is not possible in the prototypes used in this study. Even though the lifting of the foot unloads the sensors placed under the foot, the sensors positioned in other regions are loaded. Moreover, a tight setting of the buckles of the ski boot can produce high pressure values which may even bring the sensors to saturation.

The aforementioned recommendation may only hold for the detections of isolated and very specific movements and will probably not be applicable if multiple movement

patterns occur simultaneously. A possible solution approach to this could be the use of artificial intelligence with a well-trained neuronal network. As attractive as such a solution is, the training of such a network would need sufficient real-life data which also has to be labeled labour-intensively.

Due to the design of the study, no high dynamics are apparent, and the loads and pressures measured with the measurement binding and the prototypes are relatively low with most sensors measuring values below 5 to 10 N/cm² and only singular sensors reaching values of 20 to 40 N/mm². The values are small compared to maximal (only plantar) pressure values reported in on-slope skiing of 28 to 38 N/cm² (Lafontaine et al. 1998).

As only the local maximal pressure of each resistive sensor at each time is recorded, the system is prone to large errors due to wrinkles in the sock, a small hard object pressing on the sensor (for example a stiff seam of the sock or inner boot or a bone of the foot) or bending of the sensor. This may also be a reason for the significantly higher pressure signals of single sensors of PTFoot compared to the other prototypes (for example sensors 2, 3, 5, 6, 12). Therefore, the use of capacitive sensors would be advantageous, as local pressure peaks at the sensor surface are filtered and the mean pressure of the sensor surface is measured. Capacitive sensor designs however are more complicated and need specific experience.

The self-designed sensors used in this study are non-linear and the approximation is not ideal. This may lead to large errors in the calculation of pressure values, especially for very small and very high sensor values. This is a result of various aspects of the sensor design and, therefore, could be addressed in multiple ways. For example, by replacing the Velostat layers with a carbon black silicon compound, potential contact loss between the Velostat layers themselves and between Velostat and the printed circuit board material may be prevented. This contact loss results in higher electrical resistance and thus lower pressure values.

To tackle the various challenges with respect to an optimal sensor design (for example, measurement range, saturation, and sensor size), field data will be needed to allow more insights.

4.2.3.5 Conclusion with respect to a mechatronic ski binding

Injuries to the knee in alpine skiing often result from a backward-leaning position (Freudiger and Friedrich 2000). Therefore, the implementation of a measurement boot in a mechatronic ski binding recording external loads and body positions will help to detect risky situations. But for a future mechatronic ski binding, the design of a sensor system measuring the loads at the binding or boot might be the most challenging task. A combination of force sensors measuring torques about the vertical axis and pressure sensors used to predict forward and backward lean and torques in the sagittal plane might be a possible compromise.

Artificial intelligence may allow to cope with the high complexity due to imperfect defined sensor characteristics. A neuronal network with a small number of pressure sensors at defined positions could be trained with skiing loads (M_y , M_z , F_y , F_z) recorded by a measurement binding. With sufficient training data, the neuronal network will predict the skiing loads using the pressure sensor data. This has been successfully done for a snowboard binding by Holleczeck et al. (2010).

4.2.4 System for Tracking the Skiing Speed

4.2.4.1 State of the Art

Relationship between skiing speed and ACL injuries

With increasing speed of the skier, acceleration due to slope roughness and excitations from bumps require the binding to absorb more energy without release (these short-time peak forces are uncritical to the bone and ligaments). Binding settings for these reason have to be a compromise to prevent the binding from unwanted release at higher speed and non-release in situations when an injury threshold is reached

Therefore, the retention value of the ski binding must not be too low, otherwise the risk of an inadvertent release increases. When the skier is, however, very slow, the available energy may not be enough to open the binding, and thus increases the risk of ACL injury. Especially for beginners and intermediate skiers, it is reported that a person falls while skiing slowly or is even standing still (Merino et al. 2007). In such a situation, the acting forces are either too small or the force application points are at a point, where the resulting release moments are small. This conflict shows that it is important to record the speed of the skier and consider it in the algorithm of a mechatronic ski binding.

Ruedl et al. (2016) questioned 498 skiers with an acute ACL injury, to report their own perceived speed and if a failure of binding release occurred (Table 4-6). In only 110 cases of all falls that had lead to the injury, the binding did release. Lower perceived speed was significantly ($p=0.003$) associated with an increasing proportion of failure of binding release.

Table 4-6 Self-perceived speed and binding release/non-release at moment of ACL injury. Data originally published in Ruedl et al. (2016)

Self-perceived speed in the moment of injury	Failure of binding release	Binding released
	77.9% (n=388)	22.1% (n=110)
Very fast (n=16)	56.2% (n=9)	43.8% (n=7)
Fast (n=76)	65.8% (n=50)	34.2% (n=26)
Moderate (n=192)	78.1% (n=150)	21.9% (n=42)
Slow (n=154)	84.4% (n=130)	15.6% (n=24)
Very Slow (n=51)	84.3% (n=43)	15.7% (n=8)

A generalisation, however, that the retention settings of the ski binding should be adapted to the speed of the skier alone is not possible:

Scher and Mote Jr. (2001) had 15 skiers perform slow manoeuvres like walking on skis (sideways and in V-position), hopping, skating, and turning on the spot. 11 of the 15 skiers achieved higher binding values in the slow manoeuvres than compared to downhill skiing (the skiers were instructed to ski aggressively). In the same publication, Scher and Mote Jr. report that 15 of 32 skiers, which performed downhill skiing, could have decreased the retention values of the lateral toe force by at least 35%. In addition, 15 skiers could have lowered the settings of the heel piece by 50% for downhill skiing. Even though the tested slow manoeuvres were no “downhill” skiing manoeuvres, these findings are partially in conflict with the assumption that higher velocities generally require higher retention values at the binding and they suggest that (a complex interaction of) various parameters need to be considered to define the retention values of the ski binding for the different skiing situations. For example, besides speed as an influencing parameter, the aforementioned studies by Ruedl et al. (2016) and Merino et al. (2007) also report a significant influence of the type of fall, gender, and skill level.

State of the art to measure the speed of skiing

Various studies used differential GNSS (global navigation satellite system), also in combination with IMU (Inertial Measurement Units) sensors and achieved good results in determining the speed of alpine skiers (Fasel 2017; Wägli 2009; Skaloud and Limpach 2003). Wägli (2009) presents a system using a differential global positioning system (DGPS) in combination with an inertial sensor system and achieves a promising accuracy of 0.2 m/s. DGPS (as other differential GNSSs⁶) uses a reference station with a fixed position to achieve higher accuracy. Such systems are expensive and would require additional equipment / infrastructure placed in the ski area.

Unfortunately, sensor signals by smartphones and sport watches are not sufficient for speed tracking, either. Even though, they are used for tracking in various Apps, the measurement frequency of these devices is only 1 Hz and thus too slow to be of use for an algorithm for a mechatronic binding. The most promising solution might be a combination of a low-cost GPS (global positioning system) sensor and one or several IMUs. IMUs are multi-sensor-modules consisting of acceleration sensors, gyroscopes,

⁶ GNSS is a collective term for all satellite systems, which are GPS, GLONASS, Galileo, and Beidou.

and magnetometers. A sensor fusion of the GPS signal, acquiring position data, and the signals of the IMU, acquiring linear acceleration, rotary velocity, and orientation, is achieved with a Kalman filter. The settings of this filter are very important for a reliable system and the adjustment of these settings is affected by several challenging factors, such as:

- availability of GPS signals,
- dynamics of the skier (style, equipment, snow conditions, body movements),
- IMU drift,
- characteristics of the sensors,
- environmental influences.

For use in a commercial product in sports, the IMUs need to be lightweight, small and should be cheap. Prices have been decreasing rapidly for such sensors, allowing the design of low-cost systems. Within the last years, new production technologies led also to increased performance of such sensors.

Zihajehzadeh et al. (2015) used a Kalman filter for a low-cost GPS and an IMU in downhill snowboarding and reported velocity errors smaller than 0.35 m/s in the horizontal plane, which are comparable with results by Wägli (2009). For the velocity in the vertical direction, the authors recommend the use of a barometer, as the accuracy was low due to the small number of visible satellites. Wägli simulated GPS loss of 15 seconds and still achieved small errors of 0.57 m/s by using a Kalman filter. In the following study, a low-cost GPS-IMU system is validated for use in alpine skiing.

4.2.4.2 Validation Study: Methodology

Prototype

The prototype of a low-cost GPS-IMU sensor system is shown in Figure 4-35. It consists of an Arduino Zero microcontroller, a GPS receiver (Ardufruit Ultimate GPS Logger Shield FGPMMPA6H, 10hz), a barometer (Bosch BMP 280), and an IMU (Bosch BNO055, 100Hz). A display is used for visualising error messages, calibration status, and speed. The earphones can be used to communicate status messages while skiing. A standard power bank is used for the power supply. A 3D printed housing protects the electronics. An external antenna allows the application on the helmet or other regions of the skier. The sensor data is stored on an SD card for postprocessing.



Figure 4-35 Low-cost GPS-IMU prototype.

Output data of the prototype

GPS allows for recording according to two different NMEA⁷ codes, GGA and RMC. The respective information stored in each code is given in Table 4-7. The GGA code provides information about the geographical location (longitude, latitude, and altitude) but no information about the speed. The RMC code also provides the speed over ground but does not give information about the altitude. Due to the needed processing and writing times of the data and to achieve to highest possible data acquisition rate (100Hz IMU data and barometer and 10Hz GPS data) only one of the GPS codes can be stored together with the IMU data. For the integration in the Kalman filter the GGA code is used because the change in altitude is an important factor in skiing and the resulting absolute speed, which might significantly differ from the speed over ground provided by the RMC code. Nevertheless, the accuracy of the speed measurements provided by the RMC code will be compared to the speed resulting from the data fusion by comparing it to the speed calculated with the reference system data. The raw data of the prototype is stored in .txt file on the SD Card. In the postprocessing, the data is transferred to the computer, synchronized with the reference system, and filtered.

Reference System

As reference system (see Figure 4-36) two Leica GS-14 receivers are used in a real-time-kinematics (RTK) differential setting in which one receiver is used as reference station and one as rover carried by the skier. The acquisition rate is set to 20 Hz. The manufacturer names a mean error of the position data of <2 cm. Synchronisation with the low-cost system is done by the time stamp of the satellites.

⁷ Quick information about the different types of GPS codes can be found here: <http://www.nmea.de/nmea0183datensatze.html> (last visited on 22.09.2021)

Table 4-7 Information stored according to the two possible GPS codes of the prototype as defined by the manufacturer (GlobalTop Technology Inc. 2011).

\$GPGGA essential fix data which provide 3D location and accuracy data

Example output:

```
$GPGGA,111250.900,4727.6968,N,01212.4245,E,2,10,0.97,1627.7,M,47.1,M,0000,0000*58
```

111250.900	Fix taken at 11:12:50,900 UTC
4727.6968, N	Latitude 47 deg 27.6968' North
01212.4245	Longitude 12 deg 12.4245' East
2	2 = DGPS fix
10	Number of satellites being tracked
0.97	Horizontal dilution of position
1627.7, M	Altitude, Metres, above mean sea level, unit (metres)
47.1, M	Height of geoid (mean sea level) above WGS84 ellipsoid, unit (metres)
0000	Null fields when DGPS is not used
0000	Null fields when DGPS is not used
*58	The checksum data, always begins with *

\$GPRMC recommended minimum data for GPS (provides position, speed, and time)

Example output:

```
$GPRMC,162614,A,5230.5900,N,01322.3900,E,10.0,90.0,131006,1.2,E,A*13
```

162614	Fix taken at 16:26:14,000 UTC
A	A=data valid of V= data not valid
5230.5900, N	Latitude 52 deg 30.5900' North
01322.2900, E	Longitude 13 deg 22.2900' East
10.0	Speed over ground 10.0 knots
90.0	Course over ground 90.0 deg
131006	Date "ddmmyy"
1.2, E	Magnetic variation 3.05 deg, west
A	Mode A / D / E = autonomous / differential / estimated
*58	The checksum data, always begins with *

Participant

As test skier one female participant carried the backpack shown in Figure 4-36.



Figure 4-36 from left to right: reference station, rover and low-cost prototype in the backpack carried by the test skier, test skier

Kalman Filter

The inertial sensor data from the IMU and the data from the GPS are filtered by a loosely coupled linear Kalman filter. The principle is visualized in Figure 4-37. The IMU data is used for the prediction of the position and velocity of the skier. This prediction is corrected by the Kalman filter using the GPS data and a weighting of uncertainties of the initialisation of the sensors, the estimated errors of the IMU signals, and the accuracy of the GPS signal. The estimated error of the IMU signals includes:

- the position error,
- the velocity error,
- the orientation error,
- the noise of the accelerometer,
- and the noise of the gyroscope.

The barometer was not included in the Kalman filter. The reason was that the measurements of the barometer showed a large time latency. The Kalman filter was developed using Matlab (MathWorks, Natick, Massachusetts, USA).

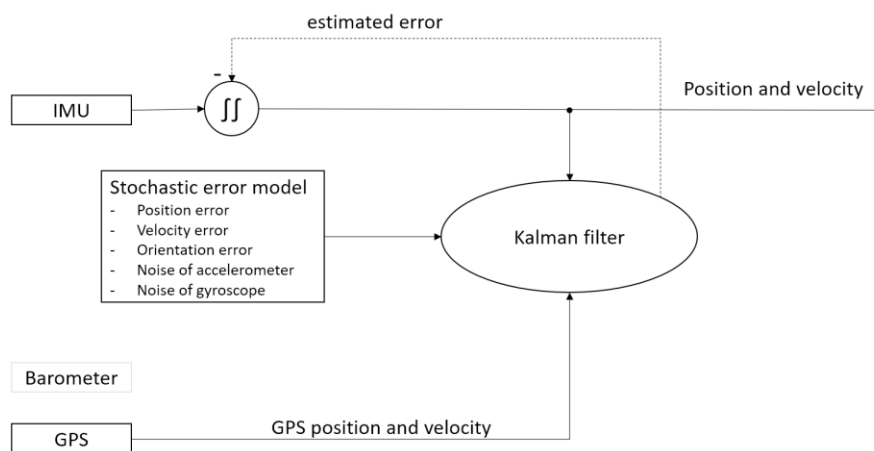


Figure 4-37 Overview of a linear Kalman filter, based on a loosely coupled integration of IMU and GPS. The barometer was not used in the Kalman filter.

Study protocol

The ten different scenarios shown in Table 4-8 were tested.

Scenarios A and B test the influence of different skiing styles, which are also associated with different skiing speeds. The root mean square error (RMSE) was calculated. for

Table 4-8 Different test scenarios

Scenario	Aim	GPS settings	Scenario runs
A	Validation of the Kalman filter for different skiing styles/speed levels	GGA	A1 plow (2 runs) A2 short turns (2 runs) A3 long turns (2 runs) A4 speed run (2 runs)
B	Reference measurement using the GPS integrated speed determination (RMC code)	RMC	B1 plow (1 run) B2 short turns (1 run) B3 long turns (1 run) B4 speed run (1 run)
C	Testing for the influence of vegetation and constructions at the site of the skiing slope	GGA	Multiple runs on the same slope (3 runs + 1 speed runs of A4)
D	Real ski day.	GGA; No reference used	Testing for incidences of GPS loss during half a day of skiing without restriction on slope selection and skiing style

each skiing style, giving the deviation of the speed calculated by the Kalman filter (Scenario A), respectively the speed given by the RMC GPS code (Scenario B), with respect to the speed calculated from the reference system data. In addition, a Bland-Altman plot (Bland and Altman 1986) is used to investigate the accuracy of the Kalman filter results (Scenario A) for the different skiing styles with respect to the speed calculated using the reference system data.

Scenario C consists of four runs on the slope with a focus on the influence of forested areas and buildings to provoke GPS loss. Potential areas of weak GPS signal quality are marked in Figure 4-39 (red circles). To quantify the influence of obstacles, the number of satellites seen by the prototype over the runs is used as well as the horizontal dilution of position (HDOP)⁸ of the GGA GPS. In addition, the absolute error of the speed calculated by the Kalman filter with respect to the speed calculated using the reference system data is determined.

Scenario D is representing a half-a-day of skiing, with uncontrolled influences to test how often, and how long GPS-loss occurs. No reference system is used in scenario D.

⁸ The HDOP: is a quality parameter for the calculated position and is dependent on the position of the satellites towards each other (0 = best possible value). The closer the satellites used for the calculation stand to each other the worse the HDOP (higher values) will be. The HDOP is no error but will "multiply" (add uncertainty to) other errors, e.g. clock errors, errors due to the ionosphere and troposphere, and errors due to multipath effects.

All runs of scenarios A, B, and C were performed on the same slope, Kälbersalvenabfahrt Nr.2b, Ski area Wilder Kaiser -Brixental in Hochbrixen (shown in Figure 4-38). The location of the reference station, as well as the start and end point of the recordings of scenarios A, B, and C is shown in Figure 4-39. The measured distance is 1.03 km and the difference in altitude is 276 m (as recorded by the reference system). Before each run, a ten-second period for the calibration was needed, requiring that the skier stands still in starting direction. During the half-day of skiing for scenario D six runs were performed, which are characterised in Table 4-9. The recordings of scenario D were started before each run and stopped at the end of the ski slope. All runs were recorded between December 28th, 2017 and January 7th, 2018.

Additional investigations

The performance of the Kalman filter during GPS signal loss is investigated in a pilot test by simulating the loss of GPS for different speed levels.

To investigate possible advantages of integrating a barometer, simultaneous altitude measurements of the GPS, the DGPS, and a barometer are compared. Moreover, the influence of the skiing speed on the altitude measurements is tested.

Table 4-9 Characteristics of the six runs performed during scenario D.

Slope	Heading / category	Surrounding Terrain	Duration of run	Map (see Appendix 7.9.1)
Zinsbergbahn (top) to Jochbahn (bottom)	South slope / blue and red	longer forest passages at the end of the run	289.5 s	Figure 7-38
Jochbahn (bottom) to Südhangbahn (bottom)	North-west slope to Skihütte Marchental, afterwards south slope / blue	Scattered trees	317.8 s	Figure 7-39
Südhangabfahrt 2	South slope / red	Small forest in the upper part of the run otherwise free terrain	105.5 s	Figure 7-40
Talabfahrt Scheffau	North slope / black and red	Over the whole run strongly forested	606.8 s	Figure 7-41
Gondel Scheffau (top) to Eibergbahn	East slope / blue	Free terrain	160.4 s	Figure 7-42
Aualmbahn (top) to Kälbersalvenbahn (bottom)	South-east slope / blue and red	Repeated forest passages	378 s	Figure 7-43



Figure 4-38 Section of the pist map of the ski area showing slope Kälbersalvenabfahrt Nr. 2b (<https://www.bergfex.at/brixen/panorama/>, September 18th 2020)

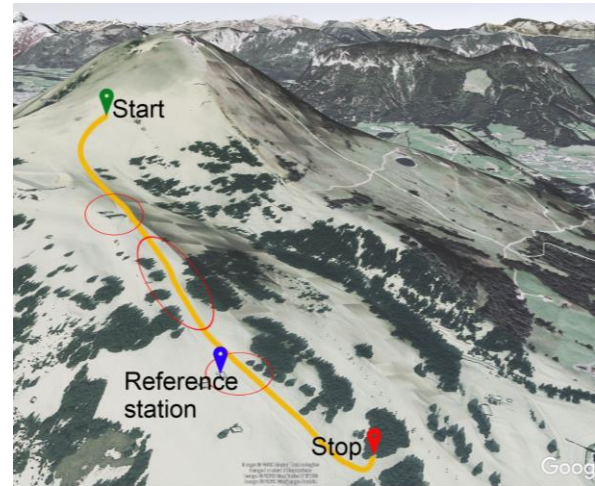


Figure 4-39 Kälbersalvenabfahrt. Green Pin: start of recorded run, blue pin: location of the reference station, red pin: end of the recorded runs. Red circles mark areas with potential GPS loss due to buildings or forests (picture modified from Google Earth. Snow situation not necessarily representing the situation on the test days)

4.2.4.3 Results

Scenario A – Influence of the skiing style and the speed level

The profile and speed ranges for the four different skiing styles are shown in Figure 4-40. In total, the RMSE of the results of the Kalman filter was 0.76 m/s. As observable in the Bland-Altman plot, the filter shows a trend towards better performance for higher speed levels (Figure 4-41). The RMSE for the four different skiing styles are given in Table 4-10.

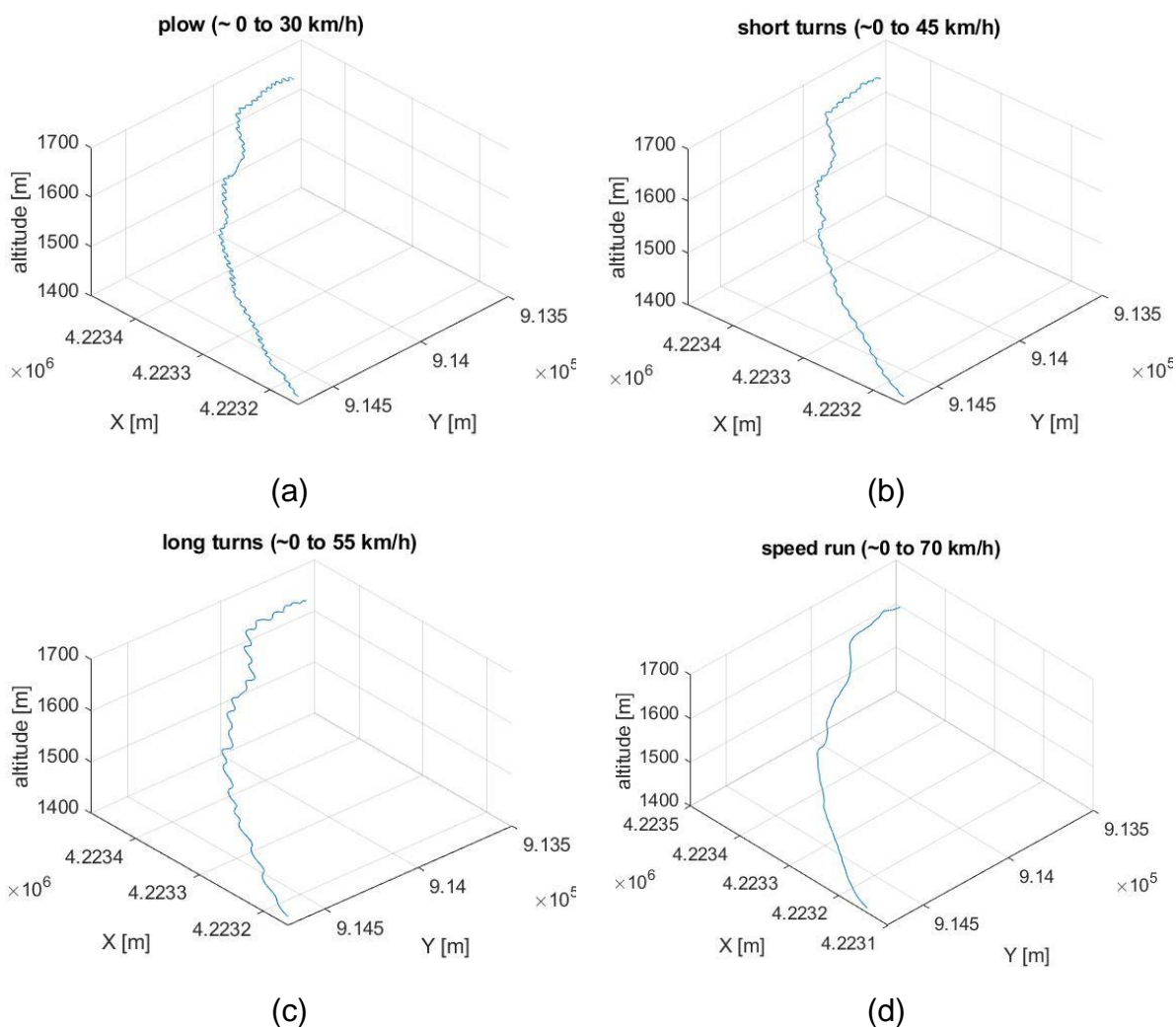


Figure 4-40 Profiles and speed ranges of the ski runs for the different skiing styles (a) plow, (b) short turn, (c) long turn, (d) speed run on the slope shown in Figure 4-39.

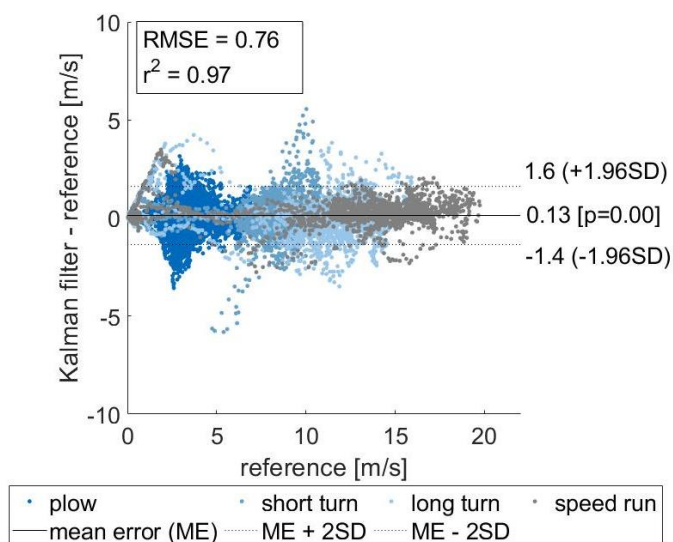


Figure 4-41 Bland Altman plot for eight runs in four different skiing styles (two runs each).

Scenario B – Accuracy of speed determination by the Kalman filter vs. RMC GPS

Table 4-10 lists the RMSE for the speed determined by using different GPS settings compared to the speed calculated using the data from the reference system. Using the RMC GPS code leads to better results for the plow, short turn, and long turn skiing style compared to when using the GGA GPS code. For the plow setting (slowest skiing speed) the speed calculation with the RMC code performed best. If the GGA code is used in the Kalman filter the errors decrease and results get better than the RMC results for the faster skiing styles short turn, long turn, and speed run.

Table 4-10 RMSE of the speed [m/s] for different skiing styles

RMSE [m/s]	RMC	GGA	Kalman Filter
plow	0.67	0.75	0.74
short turn	0.93	1.05	0.82
long turn	1.11	1.15	0.88
speed run	0.97	0.87	0.66

Scenario C – Influence of the vegetation and buildings

In Figure 4-42 to Figure 4-45 the speed of four runs calculated by the GGA code and the Kalman filter is compared to the speed calculated using the reference DGPS. Moreover, the number of satellites seen by the prototype over the runs and the absolute error between the two speed values are shown. The time points where the skier passes the two buildings on the slope and the area with forest on the side of the slope are marked in the graphs.

In all runs, GPS availability was good with nine or more satellites visible. The exception is run 2 (Figure 4-43), where temporarily the number of satellites viewed by the GPS logger drops to seven or eight satellites in the area with forest on the lower part of the ski slope. The HDOP for all measurements was always better than 1.5, which signifies excellent GPS reception. The absolute error of the speed calculated by the Kalman filter is in a range of -11 m/s to +4 m/s in the first run. The error is getting larger at the end of the run. In run 2 the error is smaller than ± 3 m/s, and in run 3 and 4 smaller than ± 2 m/s.

TOWARDS A KNEE INJURY PREVENTIVE SKI BINDING

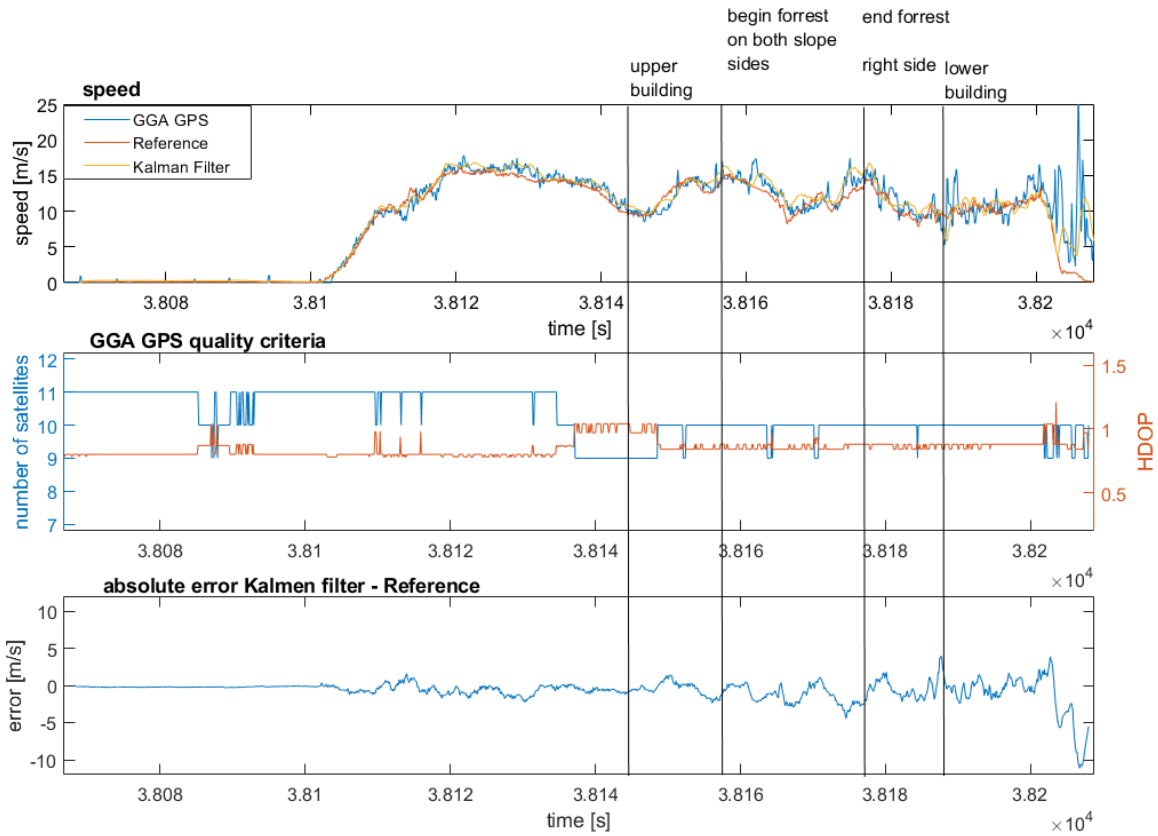


Figure 4-42 Speed, number of satellites seen by the prototype, horizontal deviation, and absolute error of the speed of one run 1.

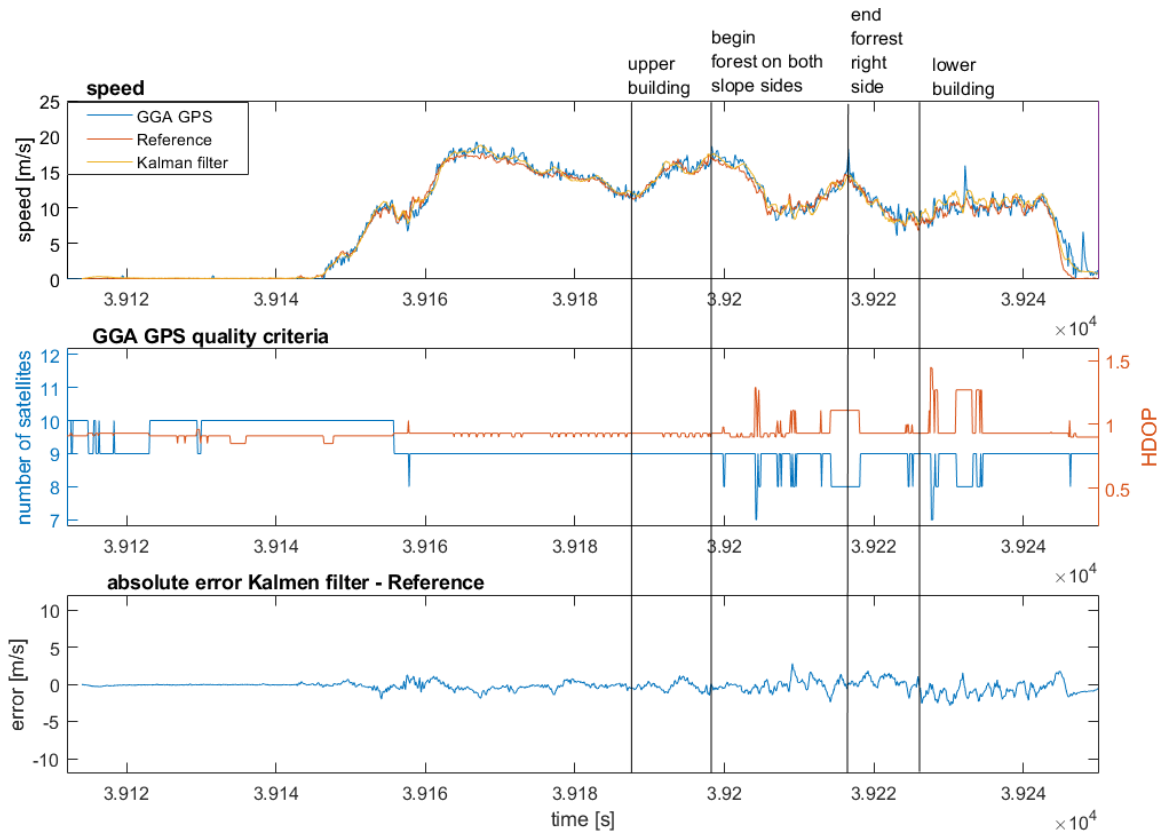


Figure 4-43 Speed, number of satellites seen by the prototype, horizontal deviation, and absolute error of the speed of one run 2.

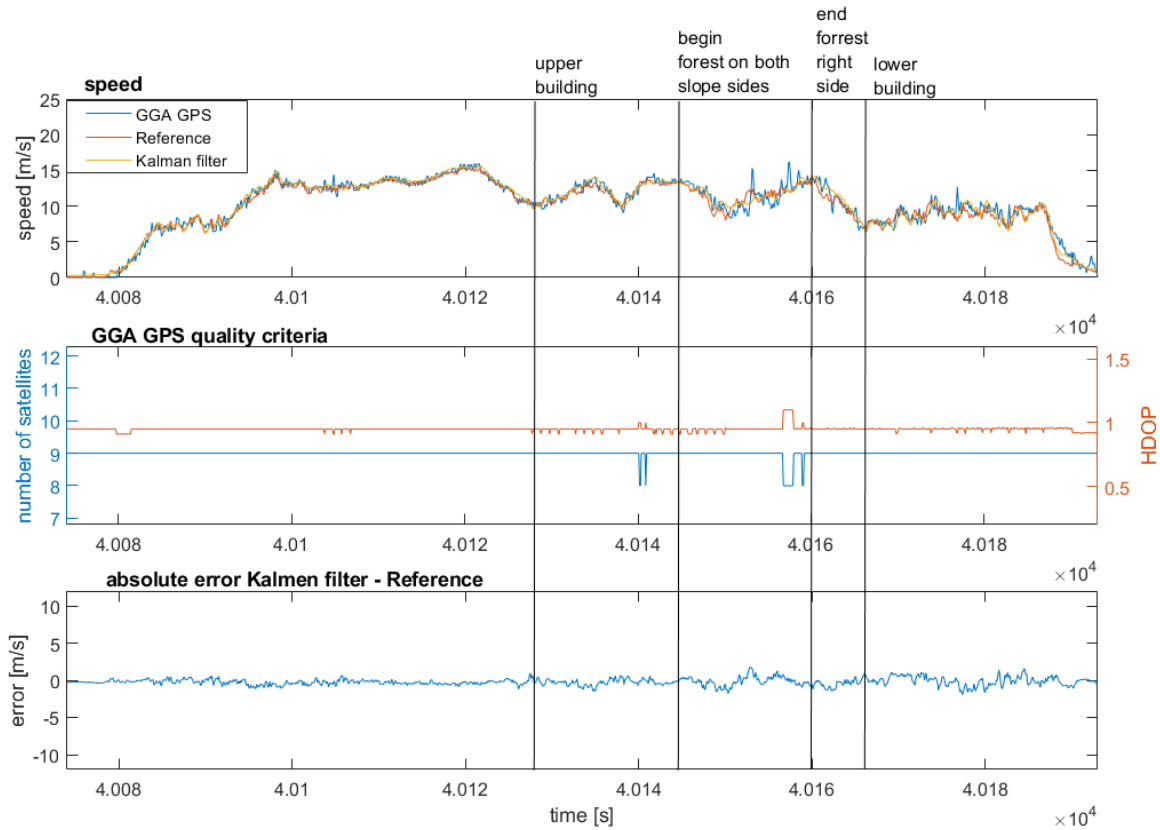


Figure 4-44 Speed, number of satellites seen by the prototype, horizontal deviation, and absolute error of the speed of one run 3.

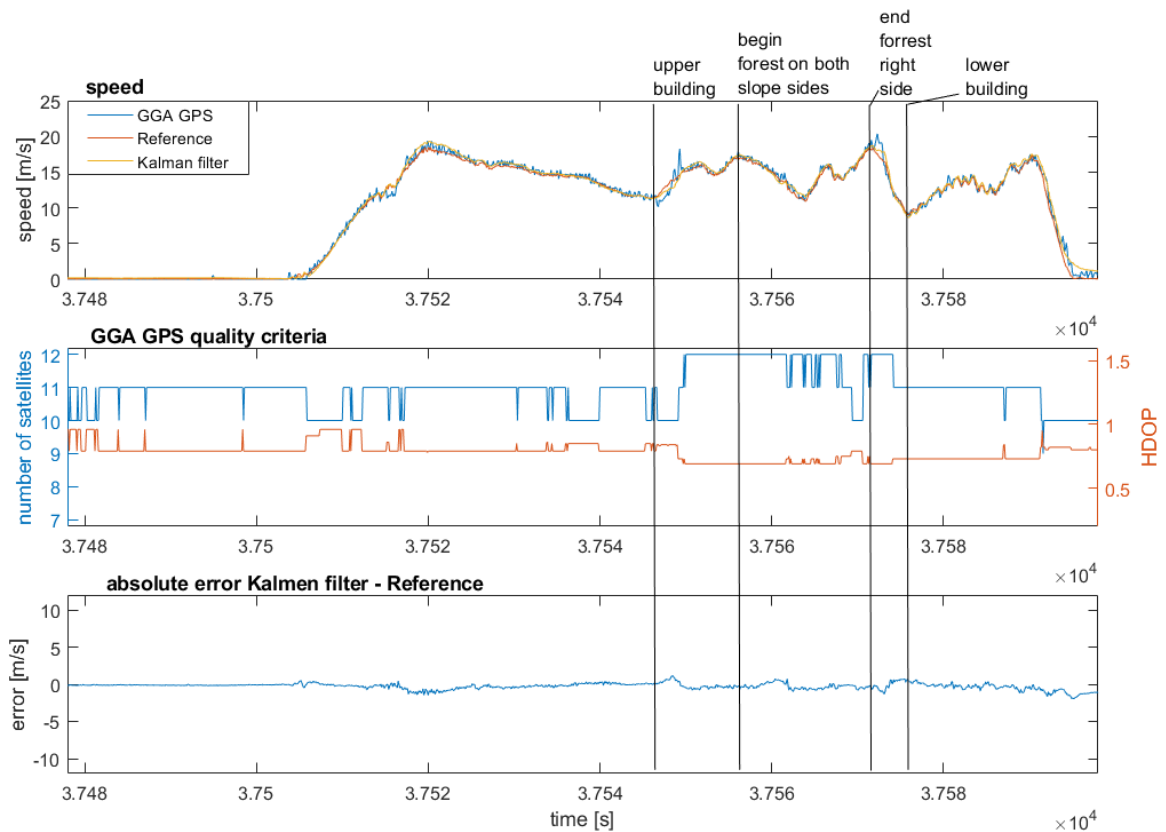


Figure 4-45 Speed, number of satellites seen by the prototype, horizontal deviation, and absolute error of the speed of one run 4 (speed run).

Scenario D – real skiing day

During the six runs of scenario D, GPS loss occurred two times. Each only results in the loss of a single GPS output (duration of 0.1 s). Both times, the loss occurred, while the skier was making a short stop. The first loss occurred on the run from Zinsbergbahn to Jochbahn, the second on the run from Südhangabfahrt. With the loss of altitude, the number of satellites decreases, which is visible in the example of the run on the slope “Talabfahrt Scheffau” visible in Figure 4-46. This is to be expected due to a narrowing of the visible sky for the GPS receiver by the mountains. Throughout all runs, the visible number of satellites remained high (>7).

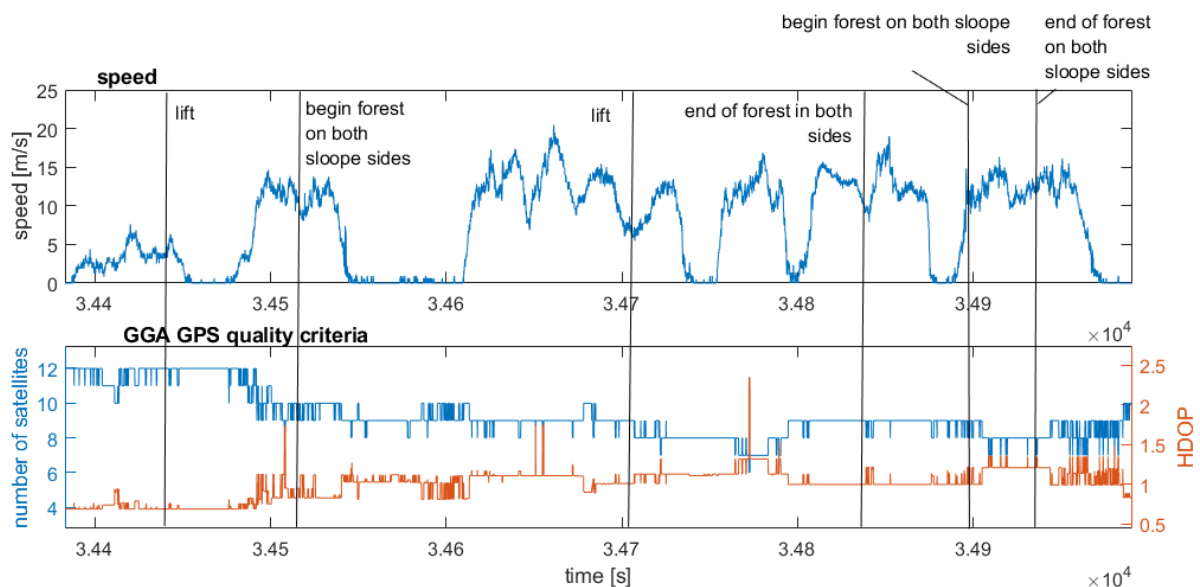


Figure 4-46 Example of the decreasing number of satellites likely due to the descend on the slope Talabfahrt Scheffau (see map in the appendix 7.9.1, Figure 7-41).

Additional investigations

Figure 4-47 shows the performance of the Kalman filter after a simulated GPS loss for three different situations. The filter can calculate reasonable values for speed for approximately 5 s after the GPS loss before the drift gets too large. Especially, if the Kalman filter is already performing slightly oscillating / unstable (right graph of Figure 4-47) the GPS-loss results in increasing drift and large errors after a short time period.

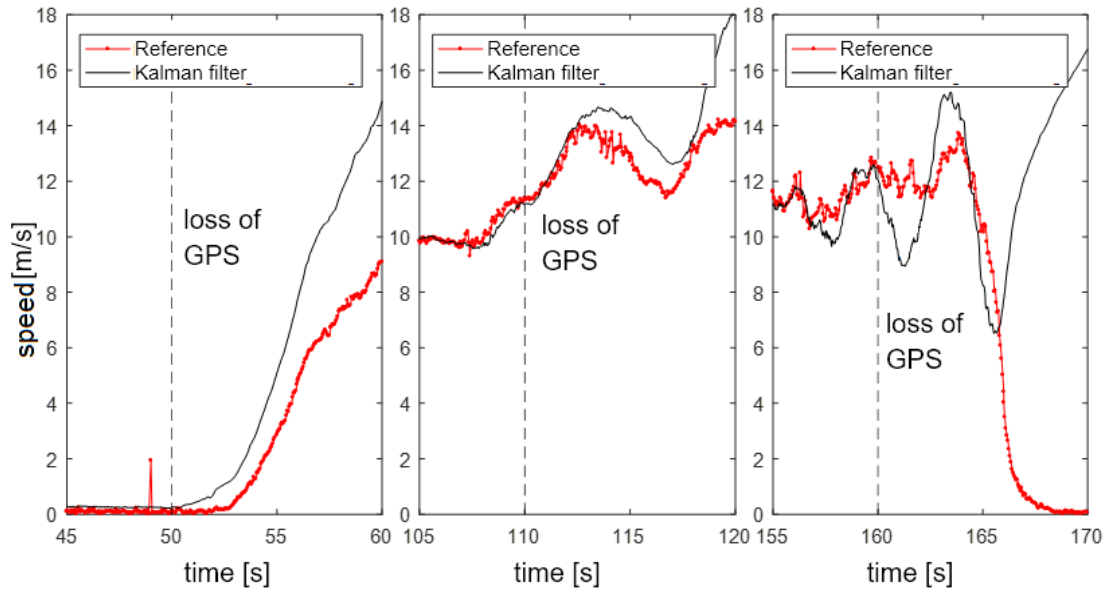


Figure 4-47 Exemplary investigation of the performance of the Kalman filter after a simulated GPS loss at three different speed levels. Left: GPS is lost at the time the skier starts skiing; Middle: GPS is lost at a higher speed while still accelerating; Right: GPS is lost at a higher speed with a slightly unstable speed estimation of the Kalman filter.

Altitude measurements using a barometer, the GPS, and the DGPS are compared in Figure 4-48. In the run shown, the maximal error in the altitude of the barometer was about 10 m, and the maximal error in the altitude of the GPS was about 56 m.

The influence of the skiing speed on the accuracy of altitude of the barometer and GPS is given in Figure 4-49 with the DPGS as the reference system.

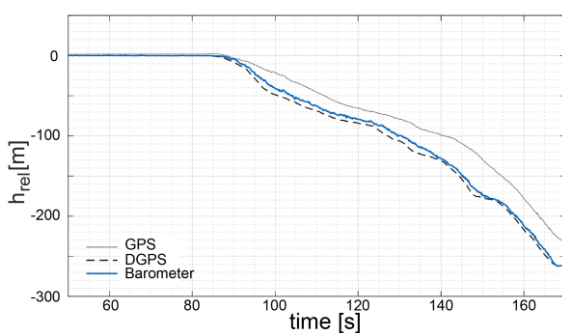


Figure 4-48 Relative altitude loss during a ski run measured by GPS (grey line), differential GPS (dotted line), and a barometer (blue line).

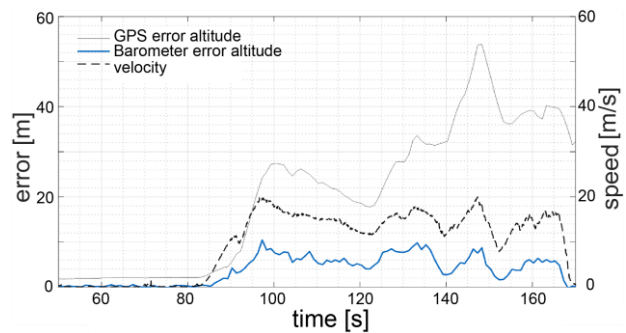


Figure 4-49 Relation between the speed (dotted line) and the errors in altitude measured with the barometer (blue line) and the GPS (grey line).

4.2.4.4 Discussion

Influence of skiing style / speed

The low-cost GPS system used in combination with a loosely coupled linear Kalman filter performed better than the GPS alone. The achieved RMSE of 0.76 m/s compared to the speed calculated using the reference system data would not be sufficient for speed recording in professional competition. For the intended use in a mechatronic ski binding, the accuracy would be good enough, as the general state of kinetic energy and skiing situation can easily be determined. For lower velocities, the RMC code of the GPS provided more accurate data. As the speed determination included in the RMC code does not include vertical velocity, singular use of this code in alpine skiing is limited and absolute velocities of higher values will always be hard to determine. The main advantage of a Kalman filter is that the integrated IMU may enable it to bridge losses of GPS. In the case of GPS loss, the Kalman filter can rely only on the IMU data. In the given exemplary investigation of the performance of the Kalman filter in the case of GPS loss, the filter can calculate reasonable values for the speed for approximately 5 s after GPS loss. This time span will be enough to cope with GPS loss due to buildings on the ski slope or smaller forests.

Even though most GPS losses in skiing are shorter than 5 s (Wägli 2009), the example in the right graph in Figure 4-47 demonstrates that longer losses of GPS are critical, as the Kalman filter drifts rapidly to higher values for the speed, though the actual speed goes to zero. If such would happen in the mechatronic ski binding, the behaviour would most likely be wrong and could lead to malfunction of the system. As the behaviour of the Kalman filter relies strongly on the inherent models of the sensors, and the skier's dynamics, better-suited parameters might be found to prevent such behaviour. Redundant use of multiple IMU sensors (of different resolutions) may allow determining an IMU drifting in the "wrong directions" (Bancroft and Lachapelle 2011).

Influence of the surroundings and the skier

No clear influence of the forest or the buildings could be determined in Scenario C. As observable in the loss of satellites, while descending the slopes in Scenario D, such good GPS reception is not usually available. The geographical position and orientation of a skiing slope influence satellite visibility. Thus, a future Kalman filter needs to be tested in many different ski areas and slopes, and the settings of the filter should be

optimized in a way that the filter can be used globally on any ski piste. The same is valid for the different kinds of skiers. Every person has her or his skiing style, which is affecting the IMU sensors. Therefore, a Kalman filter optimized for one person, may not work for another. If a database of runs of as many persons and locations as possible could be set up, optimizers or artificial intelligence tools (e.g. Neuronal networks) could help to find optimal settings. The main limitation in the development of such a database is that a reference system would always be needed to provide the accurate speed. To make the filter more robust, knowledge about the skier's dynamics, like the repetitive and alternating patterns of turns, could be used to proof-check the output of the IMU sensors. Another solution to get more reliable information about the speed of the skiers would be, to have reference stations for differential GPS openly accessible in every ski resort.

Use of a barometer

Due to the large time latency of the barometer data, the barometer was not used in the Kalman filter. It is unclear what the reason for this latency was. It is possible that the placement of the sensor in the plastic cover and inside the backpack was not optimal and pressure changes outside of the backpack were only measurable with a delay inside the backpack. Moreover, the measurements of the barometer correlated with the speed of the skier (Figure 4-49), which may imply that the barometer was not only measuring pressure changes due to the altitude, but also a drag. Still, the barometer was more accurate in determining the altitude than a GPS sensor (Figure 4-48), and, therefore, can improve the determination of the vertical velocity. In the run shown in Figure 4-48, the maximal error in altitude of the barometer was about 10 m and the maximal error in altitude of the GPS was about 56 m. A drawback of the barometer is that the sensor is very sensitive to weather changes, which may lead to errors over the skiing day.

4.2.4.5 Conclusion with Respect to a Mechatronic Ski Binding

Although there are numerous established measuring systems for speed measurement, it is difficult to determine the speed when skiing. The reasons for this are the difficult boundary conditions caused by the environment (for example forest, height differences, obscuration of the satellites by the mountains) and by the skier (for example high dynamics, relative movements of the body to ski). In addition, high processing power is needed for real-time calculations of GPS and IMU data making the use of a Kalman filter in an embedded real-time system challenging. Differential satellite navigation provides highly accurate data. For an initial integration in a mechatronic ski binding, ski resorts could offer base stations that provide correction data information to all skiers using a suitable system. For use regardless of the ski area infrastructure, the algorithm could dispense with an exact specification of the skiing speed and only use more abstract information like “fast” (e.g.>10 km/h) and “slow” (e.g.<10 km/h) and thus accept measurement inaccuracies to a high degree.

4.3 Design Concept of an Algorithm

Sections of this chapter are published in Hermann and Senner (2020b) and were submitted as congress paper (Hermann et al. 2022a) and are under review (submitted on August 31th, 2021). Minor alterations have been made in these sections for the reuse in this work.

The algorithm is key to a successful mechatronic system. The task of the algorithm is to determine a risk of injury and either adapt the retention values of the binding or release the ski. At the same time, an inadvertent release due to a too conservative system needs to be prevented. A resulting fall can also lead to injuries. Besides the four previously described input parameters *knee flexion angle*, *loads on the foot*, *muscle activity of the thigh*, and *skiing speed*, individual aspects of the skier need to be considered by the algorithm. Examples are age, gender, skill, and known previous injuries. Figure 4-50 shows an exemplary structure of an algorithm, based on our nowadays knowledge of injury mechanisms. Due to the complexity of the injury mechanisms in skiing and the multiple parameters which need to be considered, the design of such an algorithm will be partially based on expert knowledge. Therefore, a fuzzy controller, which enables the formulation of knowledge-based rules, is proposed as a core element of the algorithm.

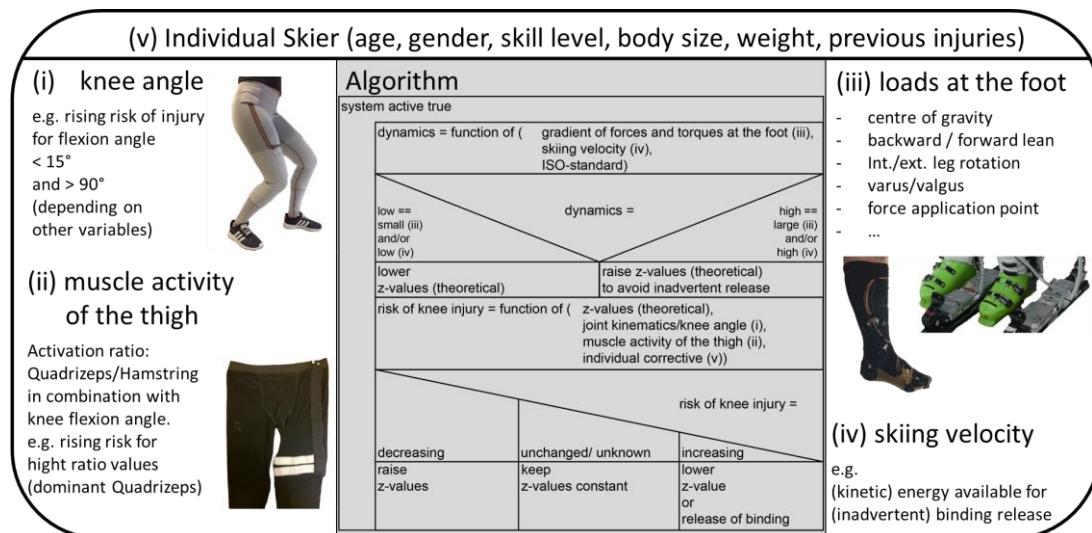


Figure 4-50 Concept of a mechatronic ski binding algorithm and the input variables. For input variables (i–iii) pictures of self-designed sensor-systems are given. Taken and adapted from Hermann and Senner (2020b). © Elsevier 2020, Reprinted with permission.

4.3.1 Basics of Fuzzy Controllers

The following sections will give a short introduction to fuzzy controllers. Moreover, a design of a fuzzy controller for a mechatronic ski binding will be described by using the “Fuzzy Logic Toolbox” of Matlab (MathWorks, Inc., Natick, Massachusetts, USA).

In classical control engineering, the behaviour of a system is first described by means of differential equations and the strategy for control is modelled mathematically. This requires that the behaviour of the system can be described sufficiently accurate by means of differential equations. (Borgelt et al. 2003)

In contrast, the approach of fuzzy logic is to use colloquially formulated knowledge directly for the design of a control system. Thus, the mostly fuzzy and vague description of concepts used by humans does not have to be transferred into concrete values and binary logic first but can be used directly for the creation of logic and qualitative rules (Michels et al. 2002).

This feature makes the fuzzy controller attractive for the use in a mechatronic ski binding because for many of the parameters suggested for implementation in the control algorithm no simple relationship between the parameter value and a true-false decision with respect to a risk of injury can be made.

Fuzzy Membership Function

The key to fuzzy logic is the definition of membership functions. In a classical control function thresholds are defined. For example: knee flexion $<30^\circ \rightarrow$ critical knee flexion = true. With a Fuzzy membership function, no such “crisp” thresholds are needed. Figure 4-51 gives an example: The fuzzy membership functions maps each element of an input parameter (here: *knee flexion*) to a degree of membership (normally between 0 and 1; here to the *criticalness of knee flexion*), thus forming a fuzzy set.

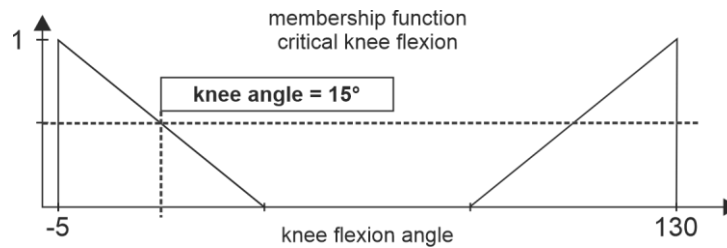


Figure 4-51 Example of the Fuzzy membership functions for the knee flexion angle to the Fuzzy set “critical knee flexion”: The “membership degree” of a knee angle of 15° is about 0.5 in the Fuzzy set.

Fuzzy Logic and Fuzzy Interference Process

There are numerous different methods (fuzzy-interference-processes) of computing an output parameter from the membership functions of different input parameter sets. In this work, a Mamdani Max-Min interference method is used, and the following examples and explanations apply to this method. The fuzzy system is based on “if-then”-rules, which link the antecedent (if-part) to the consequent (then-part). An exemplary rule could be:

"If the knee joint is hyperextended, then the tension in the ACL is high" and as a result the release torque of the ski binding must be lowered.

As such rules normally are not as simple, multiple fuzzy sets (inputs) can be connected by AND or OR conjunctions. As the proposed algorithm for the mechatronic ski binding will only apply AND conjunctions, a closer look is taken at them in the following. Figure 4-52 gives an example of a Fuzzy system, where the *risk of injury* is defined on basis of the *knee flexion angle* and the *rotational torque* on the tibia, which are connected by the logical AND. The *risk of injury* can take values on a scale between 0 and 30 (a self-defined scale with an appropriate resolution). Three rules are formulated (see lines in Figure 4-52) as antecedents:

1. If knee flexion angle is in “hyperextension” AND torque is “high internal”, then the risk value is “high (30)”
2. If knee flexion angle is in “hyperflexion” AND torque is “high external”, then the risk value is “medium (18)”
3. If knee flexion angle is a “small knee flexion” AND torque is “high internal”, then the risk value is “medium (16)”

Like the antecedents, which can be partially satisfied, the consequents also have a membership function, which defines the degree of membership of the risk value to the statements “high” and “medium” (see Figure 4-52 last column). A min-interference between the antecedents and the consequent is applied for the AND operator (implication operator), meaning that the output Fuzzy set is truncated to the minimum of the fuzzy membership values of the different antecedent values. The outputs of all rules are combined in the aggregation process which combines the Fuzzy sets representing the outputs of each rule into a single Fuzzy set (see the last graph of the last column in Figure 4-52). In the defuzzification process, the centroid of the aggregate output set is calculated to obtain a single output value (other methods of defuzzification are possible).

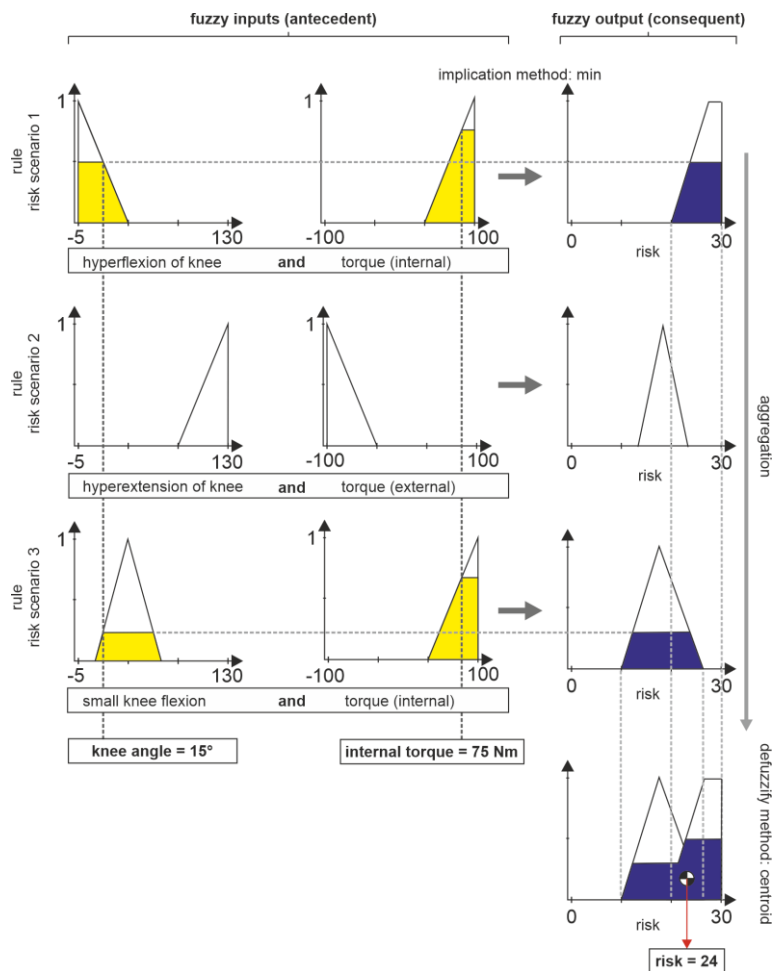


Figure 4-52 Example of a Mamdani Max-Min inference system for a Fuzzy logic with three rules for the two antecedents (input parameters) knee angle and tibia torque which are connected by an AND conjunction (meaning the minimum of the membership values of the two antecedents is used to define the consequent (output) membership value). The output of the fuzzy controller is an injury risk value between 0 and 30 and results from the centroid of the aggregated risk values for each individual rule.

4.3.2 Exemplary Fuzzy Controller for a Mechatronic Ski Binding

The task of a fuzzy controller for the mechatronic ski binding is the determination of a risk of injury and the adaption of the retention values of the ski bindings in a way that an injury is prevented. The design of such a fuzzy controller requires a comprehensive knowledge of injury mechanisms and the conditions leading to a high risk of injury. This knowledge can then be implemented by defining membership functions and fuzzy rules (Baumeister 2018).

4.3.2.1 Structure

Based on the knowledge about knee injuries in skiing described in the previous chapters of this manuscript a structure of an algorithm based on a fuzzy controller is proposed as shown in Figure 4-53.

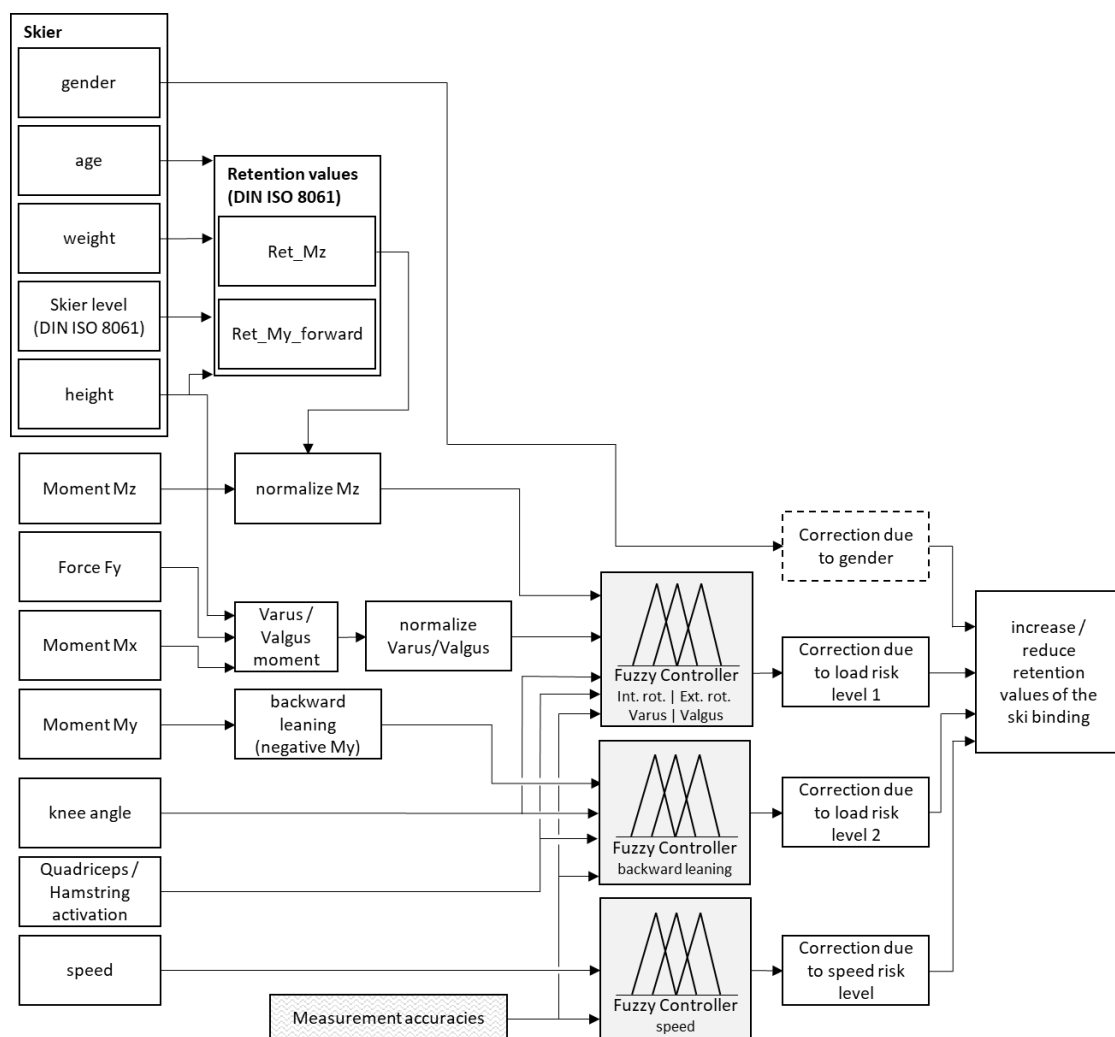


Figure 4-53 Proposed structure of a Fuzzy controller algorithm for a mechatronic ski binding.

Input variables

As described in chapter 4.2, five sets of input parameters are proposed for the implementation in the algorithm. Certain information about the individual skier needs to be stated before the use of the system. The sex of the skier is a direct input for a correction value determination due to *gender*. The parameters *age*, *weight*, *height*, and *skier level* allow the calculation of the retention values defined in the standard *Skibindungen für den alpinen Skilauf - Auswahl von Auslösedrehmomentwerten (ISO 8061) 2020*. The four other parameter sets *knee flexion angle*, *loads on the foot (Mx, My, Mz, Fy)*, *muscle activity of the thigh (quadriceps-hamstring-ratio)*, and *skiing speed* need to be recorded in real-time by sensor systems similar to the systems introduced in chapter 4.2. The moment Mz gives information about an internal or external torque acting on the tibia. The moment Mx and the force Fy, as well as the body height of the skier, and the height of the ski, are used to calculate the acting varus or valgus moments (using equation 7-20 given in appendix 7.10.4). The moment My in the sagittal plane is of utmost interest if negative, as this indicates a backward leaning position and a possible anterior tibial shift due to a boot-induced drawer.

As input for the muscle activity, the ratio of muscle activation of quadriceps and hamstrings with respect to the total activation of the thigh is expected (defined in equation 4-4). The knee flexion angle is expected to be in degree with a straight leg meaning zero degree and an increased flexion of the leg an increasing value. The speed of the skier is expected to be in km/h. Measurement accuracies of the sensor systems can be taken into account.

Risk values

A total of 30 load cases were defined and respective risk values for these load cases were assessed. The procedure is described in appendix 7.10.1. The risk values for the load cases internal/external rotation, varus/valgus moment, quadriceps/hamstring activation, and anterior tibial displacement and the possible combinations thereof are given in Table 7-14 to Table 7-17 in the same appendix.

Processing

The (pre-processed) input variables are processed in three independent Mamdani fuzzy controllers, each giving a *risk level* as output. A first fuzzy controller determines

load risk level 1, which represents the risk due to an *internal/external torque*, a *varus/valgus moment*, the *knee flexion angle*, and *muscle activation* in all possible combinations. *Load risk level 2* is determined by a second fuzzy controller and represents the risk due to a backward leaning position. It is assessed by the input parameters *negative My*, *knee flexion angle*, and *muscle activation*. In addition, a third fuzzy controller with the speed as the sole input parameter determines a *speed risk level*. The risk levels defined by the fuzzy controllers (and by gender) are added up and used for a decision on the adjustment of the retention values of the binding.

Adaption of retention values

Current standards (*Skibindungen für den alpinen Skilauf - Auswahl von Auslösedrehmomentwerten (ISO 8061) 2020*; *Skibindungen für den alpinen Skilauf - Auswahl von Auslösedrehmomentwerten mittels Tibia-Verfahren 2018*) allow a reduction of the release torques by 15%. Therefore, at this early stage of algorithm development, the adaption of the retention values should only be modified within these limits.

It is reported that females have a 2-3 times as higher risk of ACL injury compared to males (Ekeland et al. 2017; Ruedl et al. 2011) and an adaption of the retention values for females is recommended by Ruedl and Burtscher (2019). The reduction of 15% due to sex is implemented in the algorithm.

Risk levels above 10 are assigned as “critical” and the release torques *My* and *Mz* are adjusted by reducing them by 15 %. Though implemented, there is no gradual adaption at this stage of the proposed algorithm (for example a reduction of 5% would be conceivable for risk levels between 11 and 15, a reduction of 10% for risk levels between 15 and 20, etc.). A final implementation of a gradual adaption may be considered, as soon as more experience is available with respect to the relationship of the critical loads and the defined (or redefined) risk values. For known measurement accuracies of the sensor systems, the fuzzy system calculates the worst-case scenario, which then is used for the adaption of the retention values (see discussion).

4.3.2.2 Membership Functions and Fuzzy Rules

For the knee flexion angle, seven membership functions are defined (Figure 4-54; see Table 7-18 in appendix 7.10.2 for the rationale). The membership functions for the normalized parameter *internal/external torque* are given in Figure 4-55. *Skibindungen*

für den alpinen Skilauf - Auswahl von Auslösedrehmomentwerten (ISO 8061) 2020 allows a reduction of the retention values of the ski binding of up to 15% (even 30% possible, because additional 15% can be adapted on skiers wish). Therefore, a “high torque” is defined as 85% of the retention value as recommended by the standard and the input signal of M_z is normalized on this value. A detailed description of the definition of the membership functions for the parameter *internal/external torque* is given in appendix 7.10.3

The membership functions for the normalized parameter *varus/valgus moment* are given in Figure 4-56. A moment of 33.8 Nm is defined as “high varus/valgus” and used as the norm. A detailed description of the definition of the membership functions for the parameter *varus/valgus moment*, the rationale for the high value, and the calculation of the varus/valgus moment are given in appendix 7.10.4. The membership functions for the parameter *quadriceps-hamstring-ratio* are given in Figure 4-57. A “high quadriceps activation” is assumed if the ratio of quadriceps activation related to total muscle activation of the thigh reaches the value 1. A “high hamstrings activation” is assumed when the ratio of hamstring activation to total muscle activation of the thigh reaches the value 1. The input to the membership functions is calculated using equation 4-4, resulting in negative values for hamstring dominance.

$$QuadHam = \frac{Activation\ Quadriceps - Activation\ Hamstrings}{Activation\ Quadriceps + Activation\ Hamstrings} \quad 4-4$$

The membership function for the parameter *negative moment M_y* is given in Figure 4-58 and is normalized by 120 Nm, which is based on the lowest retention value for M_y used by Bally (1996).

The membership function for the parameter *speed* is given in Figure 4-59. A speed below 10 km/h is defined as slow. A speed above 30 km/h is defined as fast.

The output membership functions of the fuzzy controllers correspond to the defined risk values (see the previous section and appendix 7.10.1).

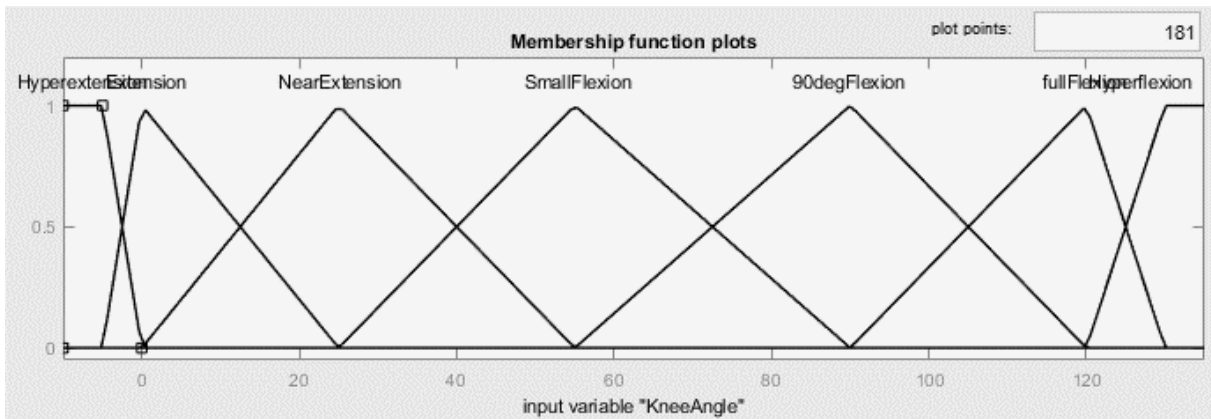


Figure 4-54 Membership functions of the parameter Knee Angle; input values are the current knee angles in degree; membership functions are Hyperextension, Extension, NearExtension, Small Flexion, 90degFlexion, FullFlexion, Hyperflexion.

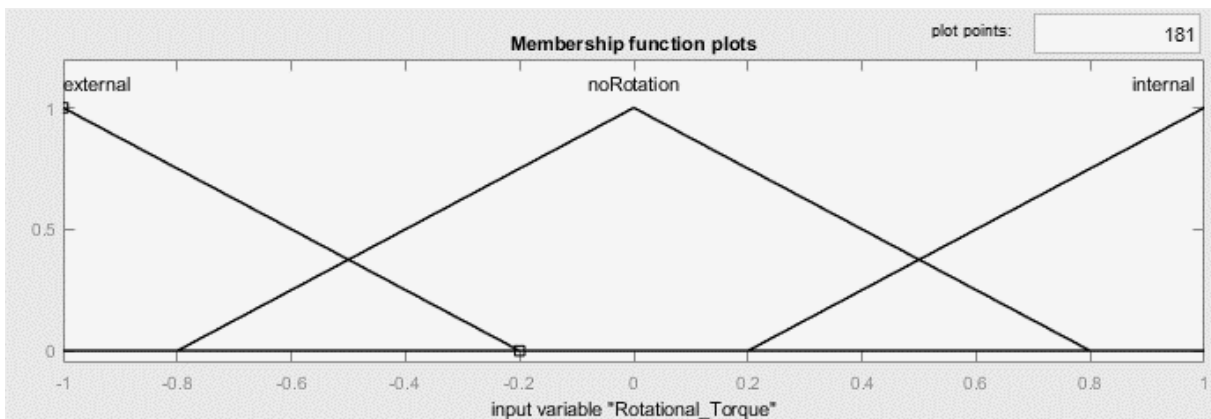


Figure 4-55 Membership functions of the parameter internal/external rotational torque; scaled input value of the moment M_z (for example measured by means of a measurement binding).

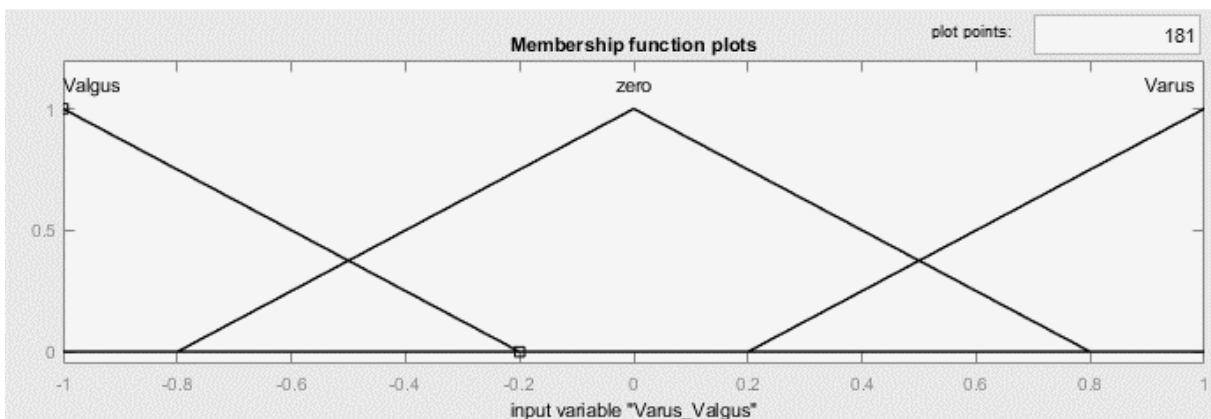


Figure 4-56 Membership functions of the parameter varus/valgus moment; scaled input value of the varus/valgus moment (for example calculated from moment M_x and force F_y measured by means of a measurement binding).

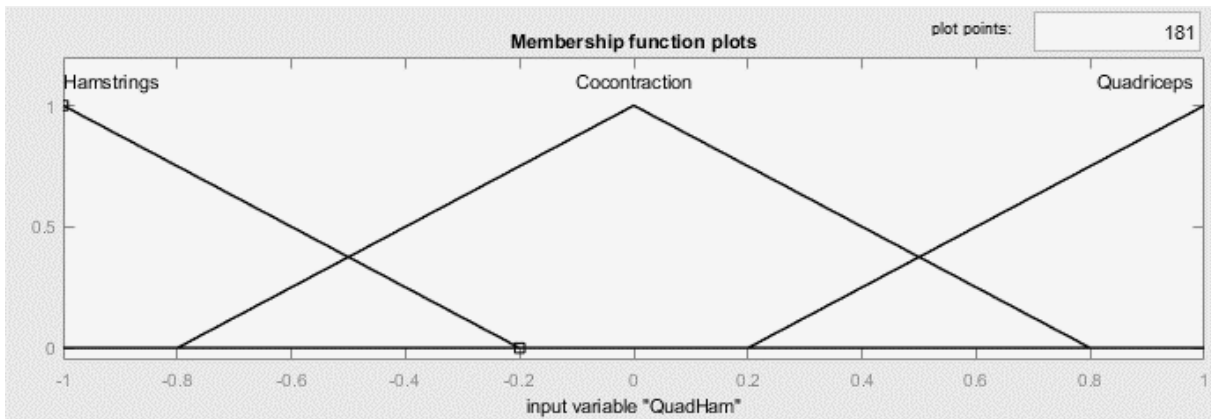


Figure 4-57 Membership functions of the parameter quadriceps/hamstrings activation; horizontal axis: scaled input value of the quadriceps/hamstrings ratio (measured by measuring pants (for example see chapter 4.2.2)).

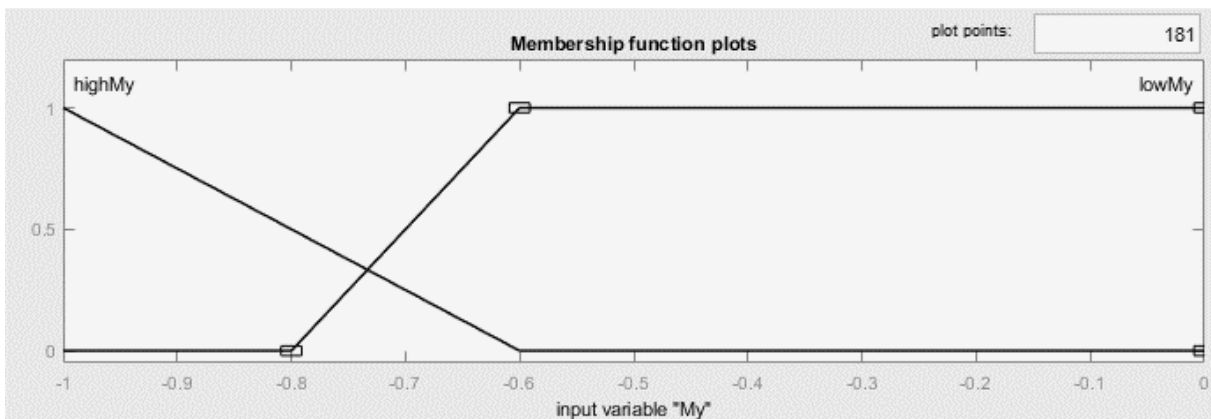


Figure 4-58 Membership functions of the parameter negative moment M_y ; scaled input value of the moment M_y (for example measured by means of measurement binding).

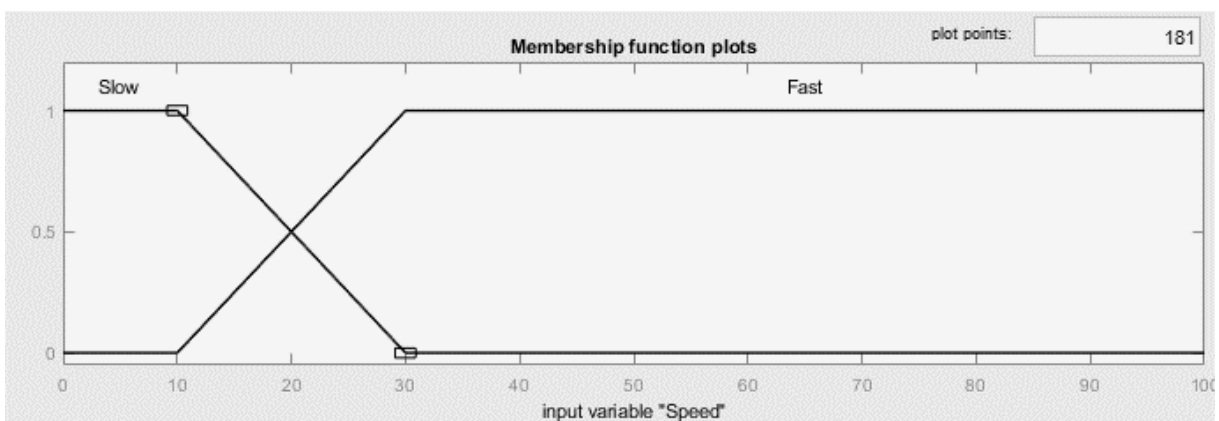


Figure 4-59 Membership function of the parameter "speed"; input value is the speed of the skier (for example measured by means of a GPS-IMU-system).

Fuzzy rules

In total, 231 fuzzy rules are formulated as a consequence of the 30 load cases and membership function for the parameter “speed”. For given input values that have a known measurement error, these rules are applied multiple times to test the most critical value when considering measurement error limits.

Figure 4-60 illustrates the relationship between the selected membership functions and the associated fuzzy rules resulting in the output of a risk level.

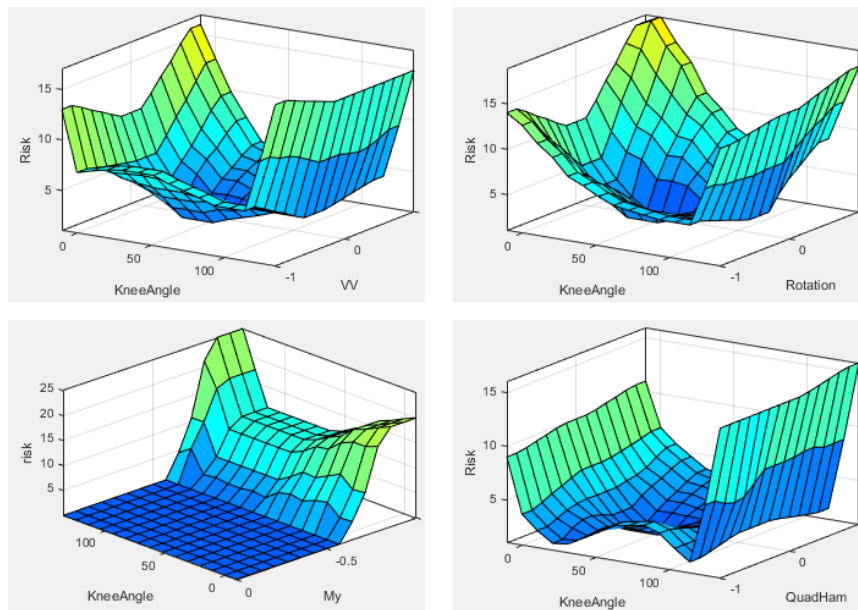


Figure 4-60 Examples of outputs surfaces provided by Matlab illustrating the relationship of the input membership functions and the fuzzy rules. Top-left: output surface for the inputs “knee angle” and “varus/valgus” and the output parameter “risk”. Top-right: output surface for the inputs “knee angle” and “rotation” and the output parameter “risk”. Bottom-left: output surface for the inputs “knee angle” and “negative My” and the output parameter “risk”. Bottom-right: output surface for the inputs “knee angle” and “Quadriceps/Hamstring activation” and the output parameter “risk”.

4.3.3 Example of Application

To test the algorithm, it is applied to a data set of case studies of six patients who have suffered an ACL injury while skiing. This data set published by Fischer et al. (1996) provides information about the skier and the injury mechanism (Table 4-11). No information about muscle activation and binding loads is available, therefore, a co-contraction (QuadHam value = 0) and high loads for Rotational_Torque (Mz), Varus_Valgus (Mx, Fy), and My are assumed (see Table 4-11). Skier no.1 was

assigned a medium-high value for Mz. For skiers no. 2 and 4 two knee angles, 120° and 130°, are tested because the defined risk values for these two angles differ greatly in all defined load cases (see appendix 7.10.1). The load risk levels 1 and 2 are investigated (see again Figure 4-53). Gender and speed risk level are neglected.

*Table 4-11 Results of the application of the algorithm on a data set of six patients who have suffered an ACL injury while skiing as reported by Fischer et al. (1996). Information marked with * are provided by the case report. Only risk value 1 and risk value 2 are represented. The speed risk value is not used. Risk values >10 would lead to a reduction of the retention value.*

No.*	Age*	Sex*	Skier's skill* (**)	Reported Knee angle at injury [°]*	Injury mechanism*	Loads involved centred in the ankle joint*	Assumed binding loads and knee angle (KA) (***)	Load risk level 1	Load risk level 2	Reduction of retention value due to algorithm	Retention value accord. DIN 8061 (Mz_s), and with adaptation (Mz_w) [Nm]
1	43	m	expert	90 to 110	Valgus, little external rotation	Fy, Mz	Fy: -100 N Mz: -40 Nm KA: 100°	6	0	no	Mz_s: 72.7 (#) Mz_w: 72.7
2	26	m	intermediate	>120	Internal rotation, anterior drawer	Fz, My	Fy: -100 N My: -120 Nm KA: 120° KA: 130°	11.4 17	18 25	yes yes	Mz_s: 53.3 (#) Mz_w: 37.6
3	41	f	advanced	0 to 30	Internal rotation, valgus	Fx, Fy, Mz,	Fx: - Fy: -100N Mz: 65 Nm KA: 15°	18.9	0	yes	Mz_s: 63.2 (#) Mz_w: 53.7
4	39	m	expert	>120	External rotation, valgus, anterior drawer	Fy, Fz, (My) Mz,	Fy: -100 N Fz: - My: -120 Nm Mz: 75 Nm KA: 120° KA: 130°	12.5 17	18 25	yes yes	Mz_s: 63.2 Mz_w: 53.7
5	29	m	advanced	90 to 110	External rotation, anterior drawer	Fz, My, Mz,	Fz: - My: -120 Nm Mz: 75 Nm KA: 100°	8	11	yes	Mz_s: 63.2 (#) Mz_w: 53.7
6	18	m	expert	~90	Internal rotation, valgus	Fz, My, Mz,	Fz: - My: - Mz: 75 Nm KA: 90°	7.5	0	no	Mz_s: 72.7 (#) Mz_w: 72.7

(**) Skier's skill is allocated to the skier level according to DIN ISO 8061 as follows:

intermediate: 1; advanced: 2; expert: 3

(***) a measurement accuracy of ±5° is assumed for the knee flexion angle and the most critical result is used.

(#) skiers no. 1,3,5, 6 used higher release levels as recommended, skier no 2 a low level (Fischer et al. 1996)

Results

For four of the six skiers, the algorithm would have proposed a reduction of the retention settings of the binding (Table 4-11, last two columns).

Interpretation

For skier no. 1 a risk level of 6 is determined by the fuzzy controller by the activated rules (combination of *external rotation and valgus* moment; individual load *external rotation*; individual load *valgus moment*). Even if an additional strong quadriceps activation would be assumed, the resulting risk level of 7.3 would not result in an adaption of the binding settings. This scenario shows that the risk values for the load case *external rotation and valgus* need to be redefined. The information regarding ACL loads for this load case currently available is not sufficient to do this. Therefore, further studies to investigate these load cases are encouraged.

The results for skiers no. 2 and 4 show the high dependency of the algorithm output on the knee flexion angle.

Skier no. 3 was a woman and would have assigned a reduced binding setting by the algorithm for this reason alone. Moreover, the resulting load risk level 1 of 18.9 would also result in an adaption. Fischer et al. (1996) presume that a force F_x was involved in the injury mechanism. The algorithm is not including information about F_x and it stands for discussion if F_x should be implemented. A similar scenario for skier no. 6 results in no adaption of the binding settings due to the higher knee flexion reported. The adaption of the binding settings for skier no. 5 was triggered by load risk level 2, which tests for a high negative M_y . The high external torque considered by load risk level 1 did not result in a reduction by itself (but in combination with load risk level 2). The small risk levels for this case highlight the fact that the algorithm is very sensitive to the definition of risk values.

For most of the skiers, the reported release level settings of the bindings deviate from the recommended setting. For these reasons, it is not possible to assume that the algorithm would have performed better in preventing the injuries than the standard's recommendation. Moreover, muscle activation is not considered in the results. If those were available, the results would likely be different. Nevertheless, this example gives

a good impression of the principles of the algorithm and the challenges involved in the design.

4.3.4 Discussion of the Proposed Algorithm

The design of the algorithm is based on the available literature providing information about injury mechanisms in skiing, the involved loading situations, and the relationship towards the loading of the ACL. Since the information is incomplete, the proposed design and in particular the defined risk values should only be viewed as a starting point for a mature development of a mechatronic ski binding.

In most publications the loads tested for are small. For estimating critical loads for some input variables, a linear relationship between the loads acting on the ski or foot and the load on the ACL was assumed. This must be questioned and, therefore, should be investigated by performing further studies.

For the calculation of the varus and valgus moment, the calculation of the lever arm is based on the height of the skier and must be adapted to the actual skier. To be more accurate it should include the knee flexion and ankle flexion in future versions. When calculating the lever arm, the assumption was made that the knee joint is directly above the measurement binding. Due to the different shaft inclinations of a ski boot, this is a simplification. In addition, the lever arm is calculated from the body height, which does not take into account that the ratio of the lower leg length to the body height differs from person to person.

As the current standards allow the reduction or increase of the release torques by 30%, a maximum adaption by the proposed algorithm is limited to this value.

As the experience with the system grows the adaption of the retention values outside the 15% or 30%-limit or even a complete release of the ski from the boot triggered by the algorithm are thinkable. One example in which this would be advantageous is if the force application point of F_y at the ski edge is at (or close to) the projection of the lower leg axis. Then the torsional loads on the tibia disappear, but the valgus and varus moments do not. In such a situation, due to the current binding design of a single M_z release at the front part of the binding, the binding might not release even for high loads and a low retention value.

The reduction of 15% due to sex is implemented in the algorithm. This could also be pre-set at the ski binding. Thus, no algorithmic processing is needed. The question of a general gender-specific binding setting should be clarified by the standards committees.

When calculating the release torque, according to the standard a different value is calculated for each difference in weight of a skier. In contrast, the parameters age and skier level have a stepwise influence on the setting by 15% with certain values. A situation can be imagined in which a skier on the same ski holiday has to lower the z-value of his ski binding by 15% because he is 49 years old on one day and 50 on the next. Using the algorithm, a continuous transition would be feasible, for example, by implementing that the adaptation takes place continuously from the 45th to the 50th year of life.

Continuous adjustment during skiing is conceivable for the parameter skier level. The sensors used in the mechatronic binding system could be used to define a momentaneous skier level using the speed, acceleration, and movement pattern of that skier, and the parameters could be adapted (even during a day of skiing).

Because the release torques can be reduced by a maximum of 15%, it cannot be guaranteed that the reduction is sufficient. It is conceivable that further lowering would have to take place in order to prevent damage to the ACL. On the other hand, it would have to be examined in more detail whether the risk of injury is to be assessed as being higher than the risk of false activation in the situations in which the release torque is reduced.

Therefore, the main challenge will be a real-life validation of the algorithm. It is unacceptable to provoke risky situations to test the correct behaviour of the algorithm. Data of many skiing days need to be recorded using the complete sensor systems however skiing with a traditional ski binding. Followed by a review of the behaviour of the algorithm and an iterative adaption.

There are many points in the algorithm design, where the behaviour can be adjusted. The adaption of the release torque is highly influenced by the pre-defined risk values, the definition of the membership functions, and the definition of the fuzzy rules. The efficiency of these risk values may not be independent of the individual skier. It will be impossible to manually define risk values for individuals, but it is possible that a limited

number of risk value sets can be defined or that some kind of weighting of the fuzzy rules according to specific information about the individual is implemented. Besides using expert knowledge from different disciplines and results from further scientific investigations, artificial intelligence may be a powerful tool towards this goal.

The definition of the membership functions in the proposed algorithm is based on conservatively chosen “high values”, which can result in high risk levels for small loads (for example, the “high value” for a negative M_y is probably too low and may result in inadvertent releases). These values must also be questioned, and replaced by new values if further scientific research suggests.

The algorithm development must also be attuned to the sensor systems used. For example, the calculation of the muscle activation ratio according to equation 4-4 disregards the different muscle volumes, the number of muscles that contribute to the system, and different electrode sizes for the muscle groups. As the quadriceps group is larger and more numerous than the hamstring group of muscles, and electrode sizes are respectively different, this will result in values favouring the quadriceps. This imbalance can be addressed at various points of the mechatronic ski binding design. On the sensor system side, the electronics or the preprocessing of the sensor system could consider this imbalance, for example by using different amplifications, normalising with respect to electrode surface, or the definition of an empirical defined constant equalising the differences. On the algorithm side, the membership functions could be designed or the fuzzy rules defined accordingly to the desired output.

Maybe more (or less) input variables may be needed for a successful algorithm. For example, Senner et al. (2014) discuss the implementation of the angular velocity of the knee motion.

The proposed algorithm considers measurement accuracy by calculating the worst-case scenario. By doing so, the problem arises that the resulting adjustment of the retention value may be too conservative or too progressive. Moreover, if numerous sensor systems are used and several assumptions are made, there is a risk that errors can add up (or cancel each other) due to error propagation. Therefore, it would be desirable that the sensor systems have a well-defined accuracy and reliability and

provide a factor of trustworthiness for the provided sensor signal in real-time (as is already provided by many GNSS systems), which then could be considered by the algorithm.

5 Discussion

This discussion summarises the discussions that have already been held in detail in the respective chapters of this work. It concludes key statements and recommendations for future steps on the way to reducing knee injuries in alpine recreational skiing and the realisation of a mechatronic ski binding.

Knee injury mechanisms in recreational alpine skiing

Knee injuries have remained the most common injury in alpine skiing for decades. Previously published ideas of technological-based prevention systems were unsuccessful and did not reach the market. The complexity of the injury mechanisms and the limitations in measuring in-vivo forces acting on and within the skier lead to an incomplete understanding of the kinematic and kinetic interactions involved. Only a combination of multiple research methods will allow to overcome this limitation. This includes in-vivo, in-vitro, surrogate, dummy, and in-silico studies. In this work, a combination of a surrogate study and multi-body simulation was used to quantify the influence of muscle activity of the thigh, the knee flexion angle, and of external loads acting on the foot on ACL loads. This was achieved for five different muscle activation ratios of the thigh for loading scenarios including internal torque, varus and valgus loads, anterior tibial force, and axial compression. External torque was not simulated, as the multi-body model could not be validated for such simulation scenarios.

The main finding of the investigations of knee injury mechanisms is that no sole parameter suffices as a control variable for a safety system.⁹ It can be stated that the knee flexion angle is the most important parameter with respect to the risk of injury, but ACL load varies greatly for the same knee flexion angle when combined with different muscle activations and external loads. A takeaway recommendation for every skier is that skiing with moderately flexed legs reduces the risk of injury. Moreover, targeted thigh muscle training allows the skier to increase knee stability and reduces ACL loads through muscle support. With respect to technological improvements, it is clear that a safety system monitoring the knee flexion angle, the muscle activity of the

⁹ An intensive discussion of the performed studies on knee injury mechanisms is given in the discussion sections of the respective study in chapter 3 and is summarised in chapter 3.3.

thigh, and the external loads acting on the ski could react more adequately in a given situation than a safety system only monitoring the loads acting on the ski. This can only be achieved with a mechatronic ski binding including appropriate sensor systems monitoring these parameters.

Derivation of a safety system – mechatronic ski binding

Recent developments in sensor and micro-electronic technologies allow the integration of smaller and cheaper systems in sports equipment and fabrics. Therefore, a mechatronic ski binding is becoming technically and economically feasible. The necessary biomechanical variables can be measured by using available measurement principles and low-cost sensors. To give proof of feasibility, four sensor systems were developed and tested. The systems measure the knee flexion angle and muscle activity of the thigh with sensors integrated into the skiing pants. The loads on the foot are measured with pressure sensors in the ski boot. Additionally, a low-cost system to measure the speed of the skier was built and tested. The measurement reliability and accuracy of systems presented in literature and of the self-developed systems in this manuscript are promising but should be improved in further work for implementation in safety equipment.¹⁰ With respect to a mechatronic ski binding, a system-based development is important. This means that the individual sensor systems and the algorithm of the mechatronic ski binding cannot be developed independently, as the characteristics of the sensor systems have to be taken into account by the algorithm. Still, most important for a successful mechatronic ski binding is an increased understanding of the injury mechanisms and the relationship between the proposed variables and the risk of injury. This understanding is key to a reliable algorithm that safely adapts binding retention values without provoking inadvertent releases. The iterative development of such an algorithm can only be achieved through a large number of test skiers using the sensor unit of the mechatronic ski binding to collect data while skiing with a conventional mechanical ski binding as a safety system. By retrospective analysis of the data and recording eventual injury events, the algorithm can be adapted until it behaves correctly. This seems the only ethical way to implement the full mechatronic system, including the actuators, needed to modify retention values.

¹⁰ The individual sensor systems are discussed in detail in the respective section in chapter 4.

In addition to the challenges discussed before, a power supply for the sensors and actuators and a concept for an actuator also needs to be considered. Cold temperatures, long skiing days, and the distribution of the sensors in skis, bindings, boots, and fabrics require either multiple power sources or interfaces between the different parts of the equipment. A release of the ski binding needs to be executed within a few milliseconds demanding either a complete redesign of the ski binding towards a system purely controlled electronically or the inclusion of strong and fast actuators able to work against the retention forces of the binding. Preferably, the final system has a mechanical backup in case the electronic parts or the power supply fail.

Stakeholders and liability

The first two questions asked when discussing the idea of a mechatronic system are:

“What if the mechatronic system does not work properly?” and

“What if the sensors are not accurate enough?”

These important questions have to be addressed but should not lead to the rejection of the idea at hand. Otherwise, no progress will be made and progress with respect to knee injury prevention in the skiing industry has been slow and inadequate over the last decades. It should be the aim of engineers and researchers of all disciplines to find solutions for challenging and complex systems and develop them to be safe and effective. We may not be able to save all ACLs from injuries, however, the first step leads to the next and so even a simpler design of a mechatronic system than the one proposed in this work may be beneficial to the skiing community and helps to push technology beyond current boundaries.

A successful development of a mechatronic ski binding will need the inclusion of many stakeholders. Formerly foreign industries, such as the textile and electronics industry, need to work closely together with universities and research institutes. An open mind and a willingness to take economical risks are necessary to ensure that safety equipment of such complexity can be developed and brought to a reliable and robust state. The current trend for digitalization is putting increasing pressure on the sports and garment industry. This will hopefully lead to improved technologies and new

materials in the future, allowing for more robust and accurate sensor systems. Moreover, the possibilities of artificial intelligence will lead to better algorithms, compensating for weaknesses and uncertainties like low measurement accuracy and the individualities of skiers.

It is important that the standards committees expand the considerations regarding the implementation or creation of mechatronic systems standards concerning ski bindings. In addition, considerations about legal issues such as liability should be clarified and a legal basis for mechatronic systems should be created. For the first approval of a standard of a mechatronic ski binding, it could be justified that the release torques can only be altered within the already permitted range until more knowledge is available. For liability reasons it is expected that a new system needs to be as safe or safer than the existing system and fearing liability claims prevents many stakeholders to take the next step. However, progress may bring us to the point when the situation turns around and the ones who did not dare to develop may be facing damage compensation demands because they do not provide the safety standard, which will then be the status quo. To reach this point, clear scientific evidence of the advantages of a mechatronic concept compared to traditional mechanical ones must be published and the feasibility must be proven in a thorough process.

Current research in skiing injuries mainly focuses on injury epidemiology and understanding injury mechanisms. For many years, only a few works on technological improvements or new systems were published. Linking the efforts of understanding injury mechanisms and sensor development, to make those mechanisms measurable in real-life skiing will be the fastest way to successful solutions.

Even though there are multiple challenges on the way to a mechatronic ski binding, the effort will be worthwhile, as it will make skiing safer (and more fun).

6 Conclusion

The high number of knee injuries in alpine skiing demands the development of a new safety system. This work addresses the two main challenges on the way to such a system:

The first challenge is the incomplete understanding of the injury mechanisms of the knee. This challenge was addressed by surrogate studies and multi-body simulations investigating these injury mechanisms in alpine skiing. It was shown that a high number of parameters influence knee injuries. Derived from the performed studies and from the state of knowledge reported in the literature, the recommended input parameters for a safety system are the knee flexion angle, the muscle activity of the thigh, the loads acting on the feet, the skiing speed, and individual information about the skier. Only a mechatronic ski binding concept will allow coping with such complexity. Further quantification of the relationship between the input parameters and ligamentous loads is necessary for a safe design of an algorithm for a future mechatronic ski binding.

The second challenge concerns the technological requirements with respect to sensor systems and algorithms. Only recent development in the microchip industry provides the necessary miniaturised and cost-effective sensors and microprocessors, making a mechatronic ski binding a feasible concept. For each measurable input parameter recommended for the mechatronic ski binding, a sensor system prototype was presented in this work proving the concept and stating challenges that need to be overcome for a successful product. Moreover, an algorithm design was presented based on fuzzy logic that combines the sensor values with an estimated risk level and a decision to adjust the retention settings of the binding.

The future validation of a mechatronic ski binding requires the collection of field data with the sensor systems while using a classical ski binding. This data must be used to adapt the control algorithm until it behaves correctly, meaning it releases in case of overloads but does not provoke inadvertent releases. Only then can the full mechatronic system including the actuators be implemented in a market-ready product.

This work outlines a possible way towards an economically feasible system enabling safer skiing, but should be seen as starting point and proof of concept only. A successful development of a functional mechatronic ski binding can only be achieved

CONCLUSION

by a combined effort of industry, research institutes, standards committees, and other stakeholders.

Since 2019, based on the work in this manuscript a research cooperation between the industry und university is funded by the Bayerische Forschungsstiftung (Grant no. AZ-1375-19; Titel: Mechatronische Skibindung).

.

List of Figures

- Figure 1-1 This manuscript is structured in three main blocks..... 1-4
- Figure 2-1 Bones and structures of the bones of the knee joint. Source: Wurzinger L. Kniegelenk (Articulatio genus). In: Aumüller et al. (2017). ©Thieme 2017, reprinted with permission. 2-6
- Figure 2-2 A frontal view in the knee joint (right leg). The cruciate, the collateral ligaments and the menisci are observable. Source: Kohn (2005), page 23. ©Thieme 2004, reprinted and modified with permission. 2-8
- Figure 2-3 Tearing force of the human ACL as reported in different publications. Original graphic by Lehner (2007) p.30, modified and translated. 2-8
- Figure 2-4 Main degrees of freedom of the knee (right leg | tibia is moved & femur is fix). To a small extent translations in the other directions are also possible. 2-10
- Figure 2-5 Torsional stiffness (rotational laxity) of the knee joint. The stiffness of the knee increases with increasing rotation and can be divided into two approximately linear areas (primary and secondary stiffness). The hysteresis that occurs when the leg is turned back can also be seen. Taken and adapted from (Louie and Mote 1987), p. 294. 2-11
- Figure 2-6 Results of various studies testing the torsional stiffness of the knee. The variation of the respective results shows the complexity of the knee's kinematics, but also the influence of the study's methodology on the results. Each number in the legend is associated with a study referenced in Table 7-1 in appendix 7.2. Studies 2, 5, and 6 are plotted with a line. Due to the used methodology, the results of these three studies are estimated to be very accurate, but they do only describe the torsional stiffness for specific tested conditions (knee flexion angle / external loads / muscle activations). 2-13
- Figure 2-7 Exemplary test designs of different in-vivo studies with applications of external loads: A) Haughom et al. (2012)¹, B) Park et al. (2008), C) Rottometer by Almquist et al. (2013)², D) Lorbach et al. (2009b)¹, E) Branch et al. (2010)¹, F) Li et al. (2008)³, G) Beynnon et al. (1997)⁴, H) Louie and Mote (1987)³, I) Hull and Johnson (1989)⁵.

1©Springer Nature, 2©John Wiley and Sons, 3©Elsevier, 4©SAGE Publications, 5©ASTM; all figures reprinted with permission of the respective copyright holder.....	2-16
Figure 2-8 Examples of cadaver test rigs by: A) Cassidy et al. (2013) ¹ , B) DeMorat et al. (2004) ² , C) Erickson et al. (1993) ² , D) Hangalur et al. (2016) ² , E) Alam et al. (2011) ² , F) Li et al. (1999) and Hsu et al. (2006) ² , G) Kiapour et al. (2015) ³ , H) Withrow et al. (2008) ⁴ , I) Woo et al. (1991) ² , J) Lorbach et al. (2009a) ⁵ , K) Markolf et al. (2004) ² , L) Yildirim et al. (2009) ⁶ , M) Lehner (2007), N) Zavatsky (1997) ³ . 1©ASME, 2©SAGE Publications, 3©Elsevier, 4©Wolters Kluwer Health, Inc., 5©Springer Nature, 6©John Wiley and Sons; all figures reprinted with permission of the respective copyright holder.	2-19
Figure 2-9 Examples for the use of dummies and the different level of abstraction: A) Senner (2001), B1) Petrone et al. (2011) ¹ , B2) Petrone et al. (2010) ¹ , C) Yoneyama et al. (2009) ² . 1©Elsevier, 2©Springer Nature; all figures reprinted with permission of the respective copyright holder.....	2-20
Figure 2-10 Examples of surrogates of various complexity designed for knee brace testing (except G, which was used for a flexion sensor validation): A) Brown et al. (1990) ¹ , B) Lunsford et al. (1990) ² , C) Liggins and Bowker (1991) ³ , D) Liu et al. (1994) ² , E) Glynn et al. (2002) ² , F) Daley et al. (1993) ⁴ , G) Asseln (2019), H) France and Cawley (2005), I) France et al. (1987) ³ and more recently used in Mathewson and Greenwald (2003), J) Cawley et al. (1989) ⁴ , K) Test Rig by DJ Otho, picture found in Hochmann (2012), L) Binder et al. (1997), M+N) two test rigs used by Hochmann (2012). 1©Elsevier, 2Wolters Kluwer Health, Inc., 3©SAGE Publications, 4©ASME; all figures reprinted with permission of the respective copyright holder.....	2-22
Figure 2-11 Examples of digital models of the knee: A) FEM-Model validated by cadaver study by Ali et al. (2016) ¹ , B1) Multibody model by Stefan Lehner validated by cadaver study (Senner et al. 2014), B2) Multibody model by Lehner (2007) including various muscle tendons and ligaments, C) planar model by Eberle et al. (2019) for testing	

dynamic landing situations with muscle agitation, D) multibody model by Shelburne et al. (2004)¹ with a high resolution of ligament bundles used for studying ligament loads in a gait cycle. ¹©Elsevier; all figures reprinted with permission of the respective copyright holder. 2-24

Figure 2-12 Mechanism of anterior cruciate ligament ruptures in skiing. (a) Boot-Induced anterior tibia drawer (known as BIAD), (b) valgus + external rotation, (c) Flexion + internal rotation (Phantom foot)..... 2-27

Figure 2-13 Slip-catch-mechanism. ©Elsevier: Reprinted with permission from Brucker et al. (2011) 2-28

Figure 2-14 Landing Back-Weighted. ©Elsevier: Reprinted with permission from Brucker et al. (2011) 2-28

Figure 2-15 Dynamic Snow Plow. ©Elsevier: Reprinted with permission from Brucker et al. (2011) 2-28

Figure 2-16 Influence of an internal torque plus muscle activation on the ACL load. Source Markolf et al. (2004), reprinted with permission. 2-30

Figure 2-17 Influence of an external torque plus muscle activation on the ACL load. Source Markolf et al. (2004), reprinted with permission. 2-30

Figure 2-18 Influence of an anterior force plus muscle activation on the ACL load. Source Markolf et al. (2004), reprinted with permission. 2-30

Figure 2-19 Influence of a forced hyperextension / hyperflexion on the cruciate ligaments. Source Wascher et al. (1993), reprinted with permission. ... 2-34

Figure 2-20 Influence of a varus moment of 15 Nm on the cruciate ligaments for different knee flexion angles. Source Wascher et al. (1993), reprinted with permission. 2-34

Figure 2-21 Influence of a valgus moment of 15 Nm on the cruciate ligaments for different knee flexion angles. Source Wascher et al. (1993), reprinted with permission. 2-34

Figure 2-22 Influence of combined load of anterior force and internal torque on the ACL. Source Markolf et al. (1995), reprinted with permission. 2-34

Figure 2-23 Influence of combined load of anterior force and valgus moment on the ACL. Source Markolf et al. (1995), reprinted with permission. 2-34

Figure 2-24 Influence of combined load of internal torque and valgus moment on the ACL. Source Markolf et al. (1995), reprinted with permission. ... 2-34

Figure 3-1 Issue of the ACL sensor implemented in the femur head. For knee flexion angles larger than 0° the sensor is not loaded orthogonally but can only measure forces in this direction..... 3-40

Figure 3-2 Results of a multi-body simulation to investigate the effect of using only one ACL bundle on ACL and PCL loads. Inserting the ACL bundle in the posterolateral insertion site on the femur and the anteromedial insertion site on the tibia (ACL surrogate) corresponds with the results of using a double-bundle (ACL AM+PL bundle). The ACL AM bundle graph represents an anatomical correct implementation of the AM bundle without an implemented PL bundle. Given is the normalized root mean square error (NRMSE) with respect to the ACL AM+PL bundles. For more details, see appendix 7.3..... 3-40

Figure 3-3 Leg surrogate (close-up on the knee). (1) Tibia, (2) Femur, (3) patella, (4) patella tendon, (5) MCL, (6) Force sensor measuring MCL-loads, (7) (part of the) hip. Also visible are the ropes representing the muscles. 3-41

Figure 3-4 View from the medial side of the surrogate leg. The leg is upside down in the room. Points 1-4 are markers used for the camera-based tracking of the knee flexion angle. Femur: Marker (1) and (3). Tibia Marker (2) and (4)..... 3-41

Figure 3-5 DC motors (1) and muscle force sensors (2) of the surrogate to control quadriceps and hamstring forces. 3-41

Figure 3-6 Tribological tests with bovine synovia and three lubricants (Klübertemp GR OT & Klüberalfa YVI 93-152 & Flouropan T20 Spray) at a temperature of 25°C. Klüberalfa was chosen as a lubricant for the surrogate, as the measured friction coefficient was similar to or lower than the synovia's. 3-43

Figure 3-7 Flexion movement from extended leg to maximal possible flexion and vice versa. The flexion was performed by the same person in all tests. 3-45

Figure 3-8 Resulting ACL loads over the knee's flexion range for different preloads of the ACL and MCL, different hip angles, and different

muscle activations ratios of the hamstrings and quadriceps. The mean of five repetitions for each setting is plotted. The knee flexion was not restricted by external factors. An external rotation of the tibia to an extent of 12° (estimation based on video data) was observable for flexion angles larger than 90° caused by the PCL.	3-47
Figure 3-9 Mean ACL loads for different knee flexion ranges for different muscle activation for the setting +20° hip flexion, pre-loads: ACL 85 N, MCL 75 N. Each mean value is calculated from the means of the five repetitions of each setup. For each knee flexion range, the muscle activation was tested with one-way ANOVA and a post-hoc significance test. The p-values are given below each set of bars. Dark grey fields are significant (p<0.05). Left: results for the flexion movement. Right: results for the extension movement.	3-48
Figure 3-10 Influence of the hip angle (a) + (c) and the ACL/MCL preloads (b)+(d) on ACL loads. Each bar represents the mean and the standard deviation of all measurement points of all muscle set-ups in the given knee flexion range.	3-49
Figure 3-11 Structure of the coupled simulation between Matlab Simulink and Simpack.	3-53
Figure 3-12 Picture of the MBS-model (left) and shema of the kinematics (degrees of freedom- DOF) of the model (right).	3-54
Figure 3-13 MBS-model of the knee. (1) Patella; (2) Femur head; (3) Tibia head; (4) medial femur condyle (prosthetic implant); (5) lateral femur condyle (prosthetic implant); (6) medial tibia plateau (prosthetic implant); (7) lateral tibia plateau (prosthetic implant); (a) dummy bodies quadriceps tendon; (b) dummy body medial collateral ligament; (c) dummy bodies hamstring muscles. The femoro-tibial joint and the patellofemoral joint are described by polygon contacts between (1)-(2), (4)-(6), (5)-(7), (a)-(2), (b)-(3); between (c)-(2) a point-surface contact is modelled.	3-55
Figure 3-14 The two implementations of the collateral ligaments in the digital model: As a double bundle and anatomically correct (left) and as a single bundle mirroring the implementation in the surrogate. The	

latter is used for the following tests. See also the results of a comparative simulation in Figure 3-2. 3-57

Figure 3-15 In the extended position, the dummy bodies of the hamstrings have bone contact (left). In the flexed knee, the quadriceps wrap around the femur, which is made possible by dummy bodies, the hamstring dummy bodies lose contact with the bone. 3-57

Figure 3-16 To model a continuous flexion movement a dummy body (green) is used, which rotates about the idealised pivot point (black cross) and is fixed to the tibia in the ankle joint, thus dragging the tibia with it (black arrow). 3-58

Figure 3-17 Definition of the effective direction of the external loads. The picture shows an internal rotation of the knee. 3-58

Figure 3-18 Comparison of the results of the surrogate study and its replication with the digital model. 3-60

Figure 3-19 Simulation results of ACL loads resulting due to different external loads and load combinations which were also studied by Markolf et al. (1990; 2004), see chapter 2.4. 3-61

Figure 3-20 ACL load for different combinations of valgus loadings and internal torque acting on the knee for different muscle activation patterns (Table 3-10). No anterior force and 10N axial compression is acting on the knee. 3-70

Figure 3-21 ACL load for different combinations of valgus loadings and internal torque acting on the knee for different muscle activation patterns (Table 3-10). 100 N anterior force and 10 N axial compression is acting on the knee. 3-71

Figure 3-22 ACL load for different combinations of valgus loadings and internal torque acting on the knee for different muscle activation patterns (Table 3-10). No anterior force and 100 N axial compression are acting on the knee. 3-72

Figure 3-23 ACL load for different combinations of valgus loadings and internal torque acting on the knee for different muscle activation patterns (Table 3-10). 100 N anterior force and 100 N axial compression are acting on the knee. 3-73

Figure 3-24 ACL load for different combinations of varus loadings and internal torque acting on the knee for different muscle activation patterns (Table 3-10). No anterior force and 10 N axial compression are acting on the knee. 3-76

Figure 3-25 ACL load for different combinations of varus loadings and internal torque acting on the knee for different muscle activation patterns (Table 3-10). 100 N anterior force and 10 N axial compression are acting on the knee. 3-77

Figure 3-26 ACL load for different combinations of varus loadings and internal torque acting on the knee for different muscle activation patterns (Table 3-10). No anterior force and 100 N axial compression are acting on the knee. 3-78

Figure 3-27 ACL load for different combinations of varus loadings and internal torque acting on the knee for different muscle activation patterns (Table 3-10). 100 N anterior force and 100 N axial compression are acting on the knee. 3-79

Figure 3-28 Generalized schema of the effect of various parameters on the ACL loading over the knee flexion range. Red: negative effect; Green: positive effect; light to dark coloring: weak to strong effect. Due to the multitude of possible loading scenarios, the schema is not comprehensive and is only based on the investigations of this work. Investigations of higher loads (>5Nm) for external torques are missing (see chapter 3.2). 3-82

Figure 4-1 Categories of ski bindings. Originally from Senner et al. (2014) and modified by Hermann and Senner (2020b). © Elsevier 2020, reprinted with permission. 4-87

Figure 4-2 Atomic Neox EBM Manual, 2004 (Atomic Austria GmbH 2004); Patent released 2006 (Holzer 2006). 4-88

Figure 4-3 Examples of Category V binding concepts: (A) Binding with force sensor and programmable release by Wunderly et al. (1988)¹ and Wunderly and Hull (1989), (B) Knee angle controlled release; US Patent 5,295,704-1994 (Flock 1992), (C) Shear loading controlled release; patent WO 2008/021813 A3 (Ettlinger and Dodge 2007), (D)

	Bio adaptive binding; US Patent 3,776566-1973 (Smolka 1971), (E) measured force triggered binding; US patent 5,064,215 .1991 (Platter and Rosenich 1989). ¹ ©Elsevier; reprinted with permission.....	4-89
Figure 4-4	Category VI binding concepts: (A) EMG controlled binding by Lieu and Mote, JR. (1980) ¹ , (B) Force and EMG controlled binding by Neptune and Hull (1992) ² , (C) Force controlled binding concept of Salomon SAS (Merino et al. 2009; Laurent et al. 2007). ¹ ©ASME, ² ©ASTM; reprinted with permission of the respective copyright holder.....	4-90
Figure 4-5	Four sensor systems are the basis for an algorithm for a mechatronic ski binding. The algorithm also includes information of the individual skier, for example age, fitness, gender, and more.....	4-91
Figure 4-6	(a) relationship between elongation and RS-values; (b) RS-fibre and measurement setup; (c) relationship between elongation and CS values; (d) CS-sensor and measurement setup, data logger not shown.	4-95
Figure 4-7	(a) frontal knee part of the knee flexion test rig; wires (4) running in tubes (3) bridge the gap between the silicon thigh (1) and shank (2), (b) hinge joint (5) of the knee flexion test rig, (c) thin tights covered the silicon so the prototypes did not catch the knee gap or the wires, (d) prototype of RS-pants (6) in test rig; knee part (7) include the RS-fibres, (e) prototype of CS-pants (8) in test rig; CS (9) stretched over the knee part, (f) knee flexion test rig with the leg in 0° flexion and (g) 60° flexion, (h) participant wearing RS-pants, (i) participant wearing CS-pants.....	4-97
Figure 4-8	(a)+(c) Results for the RS and CS-system on the knee flexion test rig for three different speed settings (slow, medium, fast). The setting 'slow' was repeated at the end to test for repeatability. RS/CS-values calibrated with the min. and max. values of the first flexion (red markers in graph (a) and (c)). Mean and maximal angular velocities for the three speed settings are given below the graphs. The top graph shows the dependence on the flexion/extension velocity. The bottom graph shows a comparison of KFA and RS-values (a) and	

CS-values (c). The black line shows the true KFA measured by a hall-sensor goniometer: the red line shows the respective RS/CS-values. (b) long time drift of the sensor signal of the RS in a constant flexion-extension of the KFA between 0°-60° for 3 hours. (d) long time behaviour of CS.....	4-100
Figure 4-9 Exemplary results for a male participant: Measurements (a) with the RS and (b) with the CS vs. the knee angle recorded by the camera-based MTS, Bland Altman diagram (c) of the results of the RS, and (d) of the CS after knee angle calculation using a two-point calibration, (e) participant wearing the RS-System (1), (f) participant wearing the CS-system (2). Participants wore ski boots in a ski binding (3), which was fixed on a platform (4) with a 15° inclination. The three coloured LED-markers (green, red, blue) are used by the MTS to determine the KFA.	4-102
Figure 4-10 Commercially available sports garments for tracking muscle activity of the tights by Myontec (left) and Athos (right). Pictures taken from the websites www.myontec.com and shop.liveathos.com on the 21.03.2020.....	4-108
Figure 4-11 MG-pants prototype using stainless steel electrodes (top-left). The electrodes are connected via buttons on the outside of the pants (bottom-left) to a sensor module (top-right) by Myon (Myon EMG Mobile System: amplifier, wireless transmission). Standard compression pants were used as a second layer (bottom-right) to improve electrode-skin-contact.....	4-110
Figure 4-12 Left: SENIAM recommended application for the quadriceps. Middle: row-application; electrodes applied to the quadriceps corresponding to the electrode layout of the measuring pants. Right: hamstring application (SENIAM).	4-111
Figure 4-13 Isomed 2000 (D&R Festl GmbH, Germany).....	4-112
Figure 4-14 Myon EMG Mobil System (1)+(2) and Ambu BlueSensor P Electrodes (3)	4-112

Figure 4-15 Typical test record, starting with 100% maximum voluntary performance, followed by stepwise 20% decreases and a second maximum voluntary performance with two decreases. 4-112

Figure 4-16 Selected angles between femur-tibia for the measurements. Left: 60° for quadriceps activation; Right: 90° for hamstrings activation. 180° would be a straight leg. 4-113

Figure 4-17 Hamstrings: regression of non-normalized values of EMG and flexion moment. Orange: standard electrodes (SENIAM). Blue: Pants 4-115

Figure 4-18 Hamstrings: regression of normalized values of EMG and flexion moment. Orange: standard electrodes (SENIAM). Blue: Pants 4-115

Figure 4-19 Quadriceps: regression of non-normalized values of EMG and flexion moment. Orange: standard electrodes (SENIAM). Green: standard electrodes applied in a row. Blue: Pants 4-115

Figure 4-20 Quadriceps: regression of normalized values of EMG and flexion moment. Orange: standard electrodes (SENIAM). Green: standard electrodes applied in a row. Blue: Pants 4-115

Figure 4-21 Bland-Altman-Plot of rectified, average EMG of each participant; dots: Hamstrings; squares: quadriceps..... 4-116

Figure 4-22 Bland-Altman-Plot of ratio (EMG/applied moment) of each participant; dots: hamstrings; squares: quadriceps..... 4-116

Figure 4-23 Selection of measurement systems to record skiing loads. Systems recording loads on the two binding components separately: (A) Schwameder et al. (2001), (B) Falda-Buscaiot (2017), (C) Saito et al. (2015), (D) Stricker et al. (2010)¹; Systems recording absolute loads for the whole binding: (E) system of the Technical University of Munich first published in Kiefmann et al. (2006), (F) system of MARKER Deutschland GmbH, Penzberg, Germany (unpublished), (G) Hirose et al. (2015), (H) Meyer et al. (2019) and Meyer (2012).
¹©Taylor & Francis; all figures reprinted with permission of the respective copyright holder..... 4-120

Figure 4-24 Force and pressure sensor systems to measure vertical loads in skiing and pressure distribution in the ski boot. Systems based on

force sensors: (A) Rađenović et al. (2001), (B) ski boot integrated force measurement plates (right) presented by Wimmer and Holzner (1997) and PAROTEC pressure insoles with 16 sensors (see D) - picture taken from Senner (2001); Systems based on pressure sensors: (C) PEDAR sensor insole by Novel GmbH, Munich, Germany used by (Raschner 1997), (D) PAROTEC sensor Insole by Paromed, Neubeuern, Germany (Senner 2001), (E) MOTICON sensor insole and mobile app by Moticon ReGo AG, (F) single pressure sensors around the leg and foot to measure pressure in the ski boot (Senner 2001), (G) Sensor “sock” for measuring pressure in a ski boot presented by Schaff et al. (1997). 4-122

Figure 4-25 Shema of the pressure sensor (left) and steps of manufacturing: centre left: foils with conductive tracks; centre right: wired sensor foils; right: finished sensor with pressure sensitive conductive material layer over the foils with the conductive tracks and protective, non-conductive foils laminated on both sides of the sensor..... 4-125

Figure 4-26 Sensor characteristic of the large sensor type derived of 5 of the self-made pressure sensors..... 4-126

Figure 4-27 Placement of the 17 pressure sensors of ski boot prototype ‘PTBoot’ (placed on the inner side of the hard shell of the boot). At the same positions, sensors of the two other prototypes were placed (outside the ski sock and at the skin of the foot; see Figure 4-28)..... 4-127

Figure 4-28 Placement of 17 pressure sensors in the sock prototype ‘PTSock’ and the placement of the sensors directly on the skin of the foot ‘PTFoot’. Sensors 6, and 10 are of a smaller diameter (20 mm). All other sensors have a diameter of 30 mm. Positions of sensors 1-17 correspond to positions of the sensors of the ski boot prototype (Figure 4-27). 4-127

Figure 4-29 Coordinate system of the measurement binding according to DIN:ISO 9462:2017 picture taken from (DIN ISO). 4-128

Figure 4-30 Set up of the data logger showing a system with 17 sensors. 4-129

Figure 4-31 The three sensor prototypes and the test set up with the participant wearing all prototypes and standing in the measurement binding. (A)

sensors attached to the skin of the foot; (B) measurement sock; (C) view in the outer shell of the measurement boot. The sensors are visible; (D) test set up with measurement binding.....	4-130
Figure 4-32 Simulation of ski-typical body postures to test the sensors. (A) backward-leaning; (B) forward-leaning; (C) left curve / edge force (respective movement for right curve); (D) simulation of internal/external rotation.	4-130
Figure 4-33 Comparison of the pressure sensor values of the three prototypes. The grey areas and a respective annotation indicate the six skiing positions.	4-132
Figure 4-34 Pearson correlations between all sensors of each of the three prototypes and the measurements of the measurement bindings.	4-133
Figure 4-35 Low-cost GPS-IMU prototype.....	4-141
Figure 4-36 from left to right: reference station, rover and low-cost prototype in the backpack carried by the test skier, test skier	4-142
Figure 4-37 Overview of a linear Kalman filter, based on a loosely coupled integration of IMU and GPS. The barometer was not used in the Kalman filter.....	4-143
Figure 4-38 Section of the pist map of the ski area showing slope Kälbersalvenabfahrt Nr. 2b (https://www.bergfex.at/brixen/panorama/ , September 18th 2020).....	4-146
Figure 4-39 Kälbersalvenabfahrt. Green Pin: start of recorded run, blue pin: location of the reference station, red pin: end of the recorded runs. Red circles mark areas with potential GPS loss due to buildings or forests (picture modified from Google Earth. Snow situation not necessarily representing the situation on the test days)	4-146
Figure 4-40 Profiles and speed ranges of the ski runs for the different skiing styles (a) plow, (b) short turn, (c) long turn, (d) speed run on the slope shown in Figure 4-39.	4-147
Figure 4-41 Bland Altman plot for eight runs in four different skiing styles (two runs each).....	4-147
Figure 4-42 Speed, number of satellites seen by the prototype, horizontal deviation, and absolute error of the speed of one run 1.....	4-149

Figure 4-43 Speed, number of satellites seen by the prototype, horizontal deviation, and absolute error of the speed of one run 2..... 4-149

Figure 4-44 Speed, number of satellites seen by the prototype, horizontal deviation, and absolute error of the speed of one run 3..... 4-150

Figure 4-45 Speed, number of satellites seen by the prototype, horizontal deviation, and absolute error of the speed of one run 4 (speed run). . 4-150

Figure 4-46 Example of the decreasing number of satellites likely due to the descend on the slope Talabfahrt Scheffau (see map in the appendix 7.9.1, Figure 7-41). 4-151

Figure 4-47 Exemplary investigation of the performance of the Kalman filter after a simulated GPS loss at three different speed levels. Left: GPS is lost at the time the skier starts skiing; Middle: GPS is lost at a higher speed while still accelerating; Right: GPS is lost at a higher speed with a slightly unstable speed estimation of the Kalman filter. 4-152

Figure 4-48 Relative altitude loss during a ski run measured by GPS (grey line), differential GPS (dotted line), and a barometer (blue line). 4-152

Figure 4-49 Relation between the speed (dotted line) and the errors in altitude measured with the barometer (blue line) and the GPS (grey line). 4-152

Figure 4-50 Concept of a mechatronic ski binding algorithm and the input variables. For input variables (i–iii) pictures of self-designed sensor-systems are given. Taken and adapted from Hermann and Senner (2020b). © Elsevier 2020, Reprinted with permission. 4-156

Figure 4-51 Example of the Fuzzy membership functions for the knee flexion angle to the Fuzzy set “critical knee flexion”: The “membership degree” of a knee angle of 15° is about 0.5 in the Fuzzy set. 4-158

Figure 4-52 Example of a Mamdani Max-Min interference system for a Fuzzy logic with three rules for the two antecedents (input parameters) knee angle and tibia torque which are connected by an AND conjunction (meaning the minimum of the membership values of the two antecedents is used to define the consequent (output) membership value). The output of the fuzzy controller is an injury risk value between 0 and 30 and results from the centroid of the aggregated risk values for each individual rule. 4-159

Figure 4-53 Proposed structure of a Fuzzy controller algorithm for a mechatronic ski binding..... 4-160

Figure 4-54 Membership functions of the parameter Knee Angle; input values are the current knee angles in degree; membership functions are Hyperextension, Extension, NearExtension, Small Flexion, 90degFlexion, FullFlexion, Hyperflexion. 4-164

Figure 4-55 Membership functions of the parameter internal/external rotational torque; scaled input value of the moment M_z (for example measured by means of a measurement binding)..... 4-164

Figure 4-56 Membership functions of the parameter varus/valgus moment; scaled input value of the varus/valgus moment (for example calculated from moment M_x and force F_y measured by means of a measurement binding). 4-164

Figure 4-57 Membership functions of the parameter quadriceps/hamstrings activation; horizontal axis: scaled input value of the quadriceps/hamstrings ratio (measured by measuring pants (for example see chapter 4.2.2)). 4-165

Figure 4-58 Membership functions of the parameter negative moment M_y ; scaled input value of the moment M_y (for example measured by means of measurement binding). 4-165

Figure 4-59 Membership function of the parameter “speed”; input value is the speed of the skier (for example measured by means of a GPS-IMU-system). 4-165

Figure 4-60 Examples of outputs surfaces provided by Matlab illustrating the relationship of the input membership functions and the fuzzy rules. Top-left: output surface for the inputs “knee angle” and “varus/valgus” and the output parameter “risk”. Top-right: output surface for the inputs “knee angle” and “rotation” and the output parameter “risk”. Bottom-left: output surface for the inputs “knee angle” and “negative M_y ” and the output parameter “risk”. Bottom-right: output surface for the inputs “knee angle” and “Quadriceps/Hamstring activation” and the output parameter “risk”. 4-166

LIST OF FIGURES

Figure 7-1 Anatomical and mechanical axes of the right leg. Frontal view. Taken and supplemented from Schünke (2013) page 272. 7-238

Figure 7-2 Sagittal section of a knee joint. Taken and adapted from Faller and Schünke (2008), page 203. 7-239

Figure 7-3 Right knee joint. Front view. Taken and adapted from Schünke (2013), page 293. 7-239

Figure 7-4 Flexors (top) and extensors (bottom) of the knee joint. Taken and adapted from Kapandji and Koebke (2006), page 141 and 143. 7-242

Figure 7-5 The rotators of the knee joint. Taken from Kapandji and Koebke (2006) page 143. (*The function of the tensor fasciae latae muscle as rotator is not clearly recognized in the literature. Schünke (2013) emphasizes that only the M. biceps femoris is responsible for external rotation.)..... 7-243

Figure 7-6 Flexion and extension in the knee joint. a: Range of motion of flexion and extension of the human leg. b-d: Intersection points of the cruciate ligaments and the collateral ligaments for different joint angles (lateral view). e: During flexion, the axis of motion moves along a curve (involute). Here, the distance of the axis of motion to the instantaneous articular surface corresponds to the radius of curvature of the femoral condyle. Taken from Schünke (2013), page 303..... 7-244

Figure 7-7 Behaviour of the cruciate (left) and collateral (right) ligaments during internal and external rotation of the knee joint. The femur is drawn unnaturally far from the tibia for the purpose of illustration. Taken from Kapandji and Koebke (2006), page 127 and 129. 7-245

Figure 7-8 Qualitative progression of the moment to be applied for the internal and external rotation of the tibia. The stiffness of the knee increases with increasing rotation and can be divided into two approximately linear ranges (primary and secondary stiffness). The hysteresis that occurs when the leg is rotated back can also be seen. Taken and adapted from (Louie and Mote 1987), page 294..... 7-246

Figure 7-9 Relationship of applied torque on the tibia and the tibia rotation (rotation of tibia with respect to the femur). Each number is associated with a publication stated in Table 7-1..... 7-253

Figure 7-10 Buckle Transducer application to a ligament. Original source Gertel et al. (1993), taken with permission 7-255

Figure 7-11 DVRT Sensor applied to the ACL. Original source Beynnon and Fleming (1998), taken with permission. 7-255

Figure 7-12 Two Ω -transducers. One attached to each bundle of the ACL. Original source Dürselen et al. (1995), taken with permission..... 7-255

Figure 7-13 Exemplary measurement using the DVTS. Observable are local strain differences in the structures. Picture taken with permission from Lehner (2007) 7-256

Figure 7-14 Method Markolf and his group used to measure ACL loading. the load cell is firmly attached to the milled bone cylinder with the ACL attached to and then fixed to the tibia. Original source Markolf et al. (1990). 7-257

Figure 7-15 Left: Load cell of the surrogate, based on strain gauges to measure ACL loads. Right: showing the load cell in the tibia head with the ACL implemented. 7-257

Figure 7-16 Results for the test set up: Preload ACL 50N, preload MCL 45N, hip angle -20°. Each measurement was repeated five times..... 7-259

Figure 7-17 Results for the test set up: Preload ACL 50N, preload MCL 45N, hip angle +20°. Each measurement was repeated five times..... 7-260

Figure 7-18 Results for the test set up: Preload ACL 85N, preload MCL 75N, hip angle -20°. Each measurement was repeated five times..... 7-261

Figure 7-19 Results for the test set up: Preload ACL 85N, preload MCL 75N, hip angle +20°. Each measurement was repeated five times..... 7-262

Figure 7-20 Mean ACL loads for different knee flexion ranges for different muscle activation for the setting -20° hip flexion, pre-loads: ACL 50 N, MCL 45 N. Each mean value is calculated from the means of the five repetitions of each setup. For each knee flexion range, the muscle activation was tested with one-way-ANOVA and a post-hoc significance test. The p-values are given below each set of bars. Dark

grey fields are significant ($p < 0.05$). Left: results for the flexion movement. Right: results for the extension movement.	7-263
Figure 7-21 Mean ACL loads for different knee flexion ranges for different muscle activation for the setting $+20^\circ$ hip flexion, pre-loads: ACL 50 N, MCL 45 N. Each mean value is calculated from the means of the five repetitions of each setup. For each knee flexion range, the muscle activation was tested with one-way-ANOVA and a post-hoc significance test. The p-values are given below each set of bars. Dark grey fields are significant ($p < 0.05$). Left: results for the flexion movement. Right: results for the extension movement.	7-267
Figure 7-22 Mean ACL loads for different knee flexion ranges for different muscle activation for the setting -20° hip flexion, pre-loads: ACL 85 N, MCL 75 N. Each mean value is calculated from the means of the five repetitions of each setup. For each knee flexion range, the muscle activation was tested with one-way-ANOVA and a post-hoc significance test. The p-values are given below each set of bars. Dark grey fields are significant ($p < 0.05$). Left: results for the flexion movement. Right: results for the extension movement.	7-271
Figure 7-23 Kelvin Voigt Element used to model the visco-elastic behaviour of the ligaments off the digital model.	7-278
Figure 7-24 Exemplary force-strain curve of the ligaments, which is described by a non-linear part and a linear part separated by ϵl (Blankevoort and Huiskes 1991).....	7-279
Figure 7-25 Characteristic of the collateral and cruciate ligaments according to literature (Blankevoort and Huiskes 1991) (dashed line), the data sheet of the LARS Ligaments (dotted line) and modified characteristics for the use in the MBS-model representing the behaviour of the surrogate.....	7-280
Figure 7-26 Effect of a variation of the initial length of the ACL on the MCL, PCL, and LCL.	7-284
Figure 7-27 Effect of a variation of the initial length of the PCL on the MCL, ACL, and LCL.	7-284

Figure 7-28 Effect of a variation of the initial length of the MCL on the ACL, PCL, and LCL.	7-286
Figure 7-29 Effect of a variation of the initial length of the LCL on the MCL, PCL, and ACL.....	7-286
Figure 7-30 Effect of using different spring characteristics of the ligaments. Blue: characteristics reported by Blankevoort and Huiskes (1991); green: characteristics used in the digital model presented in this work; orange: characteristics of the LARS ligaments used in the surrogate presented in chapter 3.1.....	7-288
Figure 7-31 Commonly used principles for pressure measurement in thin film sensors. Image taken from (Zang et al. 2015) © Royal Society of Chemistry, reprinted with permission.....	7-290
Figure 7-32 Principle of a capacitive textile sensor (left) and prototype (right) presented by Meyer (2008). The conductive textiles are arranged in perpendicular stripes (1) forming the capacitor and are separated by a compressible spacer (2). The stripes are separated by non-conductive yarn (3).	7-292
Figure 7-33 Pressure dependant resistance by the formation of percolation networks. Image source: www.openmusiclabs.com/learning/sensors/fsr/ , visited on 2021, Jan 10.....	7-293
Figure 7-34 Schema of a data acquisition unit for recording six textile pressure sensors (Shu et al. 2010) © 2010 IEEE, reprinted and altered with permission.	7-294
Figure 7-35 Schematic visualisation of an ideal and true sensor characteristic... ..	7-295
Figure 7-36 Schematic visualisation of sensor hysteresis	7-296
Figure 7-37 Spearman correlations between all sensors of each of the three prototypes and the measurements of the measurement bindings.	7-297
Figure 7-38 Map of run (orange line) "Zinsberg (top) to Jochbahn (bottom).....	7-298
Figure 7-39 Map of run (orange line) "Jochbahn (bottom) to Südhangbahn (bottom)"	7-299
Figure 7-40 Map of run (orange line) "Südhangabfahrt 2"	7-299
Figure 7-41 Map of run (orange line) "Talabfahrt Scheffau"	7-300

LIST OF FIGURES

Figure 7-42 Map of run (orange line) "Gondel Scheffau (top) to Eiberbahn" 7-301

Figure 7-43 Map of run (orange line) "Aualmbahn (top) to Kälbersalvenbahn".... 7-301

Figure 7-44 Speed absolute and in the axes of the earth-frame assuming a low (left), medium (middle) and high (right) uncertainty of the GPS measurement..... 7-303

Figure 7-45 Behaviour of the absolute speed of the integrated navigation solution compared to the pure GPS measurement and the reference solution when skiing "long turns". 7-304

Figure 7-46 Examples of the behaviour of the absolute speed of the integrated navigation solution in the event of strong deviations of the GPS measurement from the reference solution when skiing "long turns". .. 7-304

Figure 7-47 Behaviour of the speed of the integrated navigation solution in comparison to the pure GPS measurement and the reference solution when skiing "long turns" shown in the three coordinate axes of the earth-fixed coordinate system..... 7-305

Figure 7-48 Behaviour of the speed of the integrated navigation solution compared to the reference solution when skiing "long turns" shown in the three coordinate axes of the earth-based coordinate system.... 7-306

List of Tables

Table 2-1 Muscles and their main function regarding the knee joint used in the knee surrogate studies and the multi-body simulations.	2-9
Table 2-2 Common characteristics of different in-vivo study designs	2-15
Table 2-3 Categorization of 17 injury mechanisms by Freudiger and Friedrich (2000).	2-26
Table 3-1 Applied muscle forces for quadriceps and hamstrings. Percentage value refers to peak muscle forces stated by Arnold et al. (2010). The peak force for M. vastus medialis is stated with 1444 N. As our surrogate is differentiating between M. vastus medialis longus and obliquus, the peak force was divided equally on both. The peak forces stated for the two heads of M. biceps femoris are summed up.	3-42
Table 3-2 List of controlled parameters and pre-settings. In total 24 different settings were each tested 5 times in a randomized order (120 tests in total).	3-43
Table 3-3 Maximal ACL loads for the flexion and extension movements.	3-47
Table 3-4 Limitations of the knee's degrees of freedom. Selection of limits is based on Jagodzinski et al. (2016).	3-55
Table 3-5 Parameters of the non-linear-elastic model of the ligaments as used in the MBS-model. The MCL is separated by a dummy body in a distal and proximal part.	3-56
Table 3-6 Scenarios and parameter settings of the surrogate studies replicated for the validation of the digital model.	3-59
Table 3-7 External loads used in the validation tests to replicate the studies of Markolf et al. (1990; 2004).	3-59
Table 3-8 Muscle setups with respective muscle forces used in the tests to replicate the studies of Markolf et al. (1990; 2004).	3-60
Table 3-9 Comparison of results of replicated loading simulations and the reported results in the literature: Effect of external forces applied on the knee on the ACL loads.	3-64

Table 3-10 Parameters varied in the simulations of ski typical loads of the knee.	3-68
Table 4-1 Results of comparison test; n=20 participants. RS: piezo-resistive sensor system; CS: capacitive sensor system. Reference system: Camera-based 2D tracking.....	4-103
Table 4-2 Number of days per week with sportive activity.....	4-110
Table 4-3 Advantages and disadvantages of resistive and capacitive pressure sensors.....	4-125
Table 4-4 Parameters for the sensor characteristic approximation for the four small sensors used. Parameters refer to equation 4-2.	4-126
Table 4-5 Recommendation of the placement of pressure sensors to determine skiing manoeuvres based on the results with the three prototypes. ...	4-134
Table 4-6 Self-perceived speed and binding release/non-release at moment of ACL injury. Data originally published in Ruedl et al. (2016).....	4-138
Table 4-7 Information stored according to the two possible GPS codes of the prototype as defined by the manufacturer (GlobalTop Technology Inc. 2011).....	4-142
Table 4-8 Different test scenarios.....	4-144
Table 4-9 Characteristics of the six runs performed during scenario D.	4-145
Table 4-10 RMSE of the speed [m/s] for different skiing styles.....	4-148
Table 4-11 Results of the application of the algorithm on a data set of six patients who have suffered an ACL injury while skiing as reported by Fischer et al. (1996). Information marked with * are provided by the case report. Only risk value 1 and risk value 2 are represented. The speed risk value is not used. Risk values >10 would lead to a reduction of the retention value.	4-167
Table 7-1 Studies investigating internal and external rotation of the tibia. Given are the maximal applied torques for the maximal rotation in different knee angles and hip angles. N states the number of samples/test subjects included in the study.....	7-248
Table 7-2 A selection of studies to investigate the dependence of the range of rotation of the tibia on the applied moment around the tibial longitudinal axis in different knee angle positions.	7-252

Table 7-3 Results of Turkey's honestly significant difference test (post-hoc) for the setting hip angle -20° , pre-loads: ACL 50N, MCL 45 N, flexion movement, testing for significant differences between the mean values of ACL loads in the pre-defined knee flexion ranges. The mean values again reflect the means of the five repetitions for each muscle setting. Dark grey fields are significant ($p < 0.05$). 7-263

Table 7-4 Results of Turkey's honestly significant difference test (post-hoc) for the setting hip angle -20° , pre-loads: ACL 50N, MCL 45 N, extension movement, testing for significant differences between the mean values of ACL loads in the pre-defined knee flexion ranges. The mean values again reflect the means of the five repetitions for each muscle setting. Dark grey fields are significant ($p < 0.05$). 7-265

Table 7-5 Results of Turkey's honestly significant difference test (post-hoc) for the setting hip angle $+20^{\circ}$, pre-loads: ACL 50N, MCL 45 N, flexion movement, testing for significant differences between the mean values of ACL loads in the pre-defined knee flexion ranges. The mean values again reflect the means of the five repetitions for each muscle setting. Dark grey fields are significant ($p < 0.05$). 7-267

Table 7-6 Results of Turkey's honestly significant difference test (post-hoc) for the setting hip angle $+20^{\circ}$, pre-loads: ACL 50N, MCL 45 N, extension movement, testing for significant differences between the mean values of ACL loads in the pre-defined knee flexion ranges. The mean values again reflect the means of the five repetitions for each muscle setting. Dark grey fields are significant ($p < 0.05$). 7-269

Table 7-7 Results of Turkey's honestly significant difference test (post-hoc) for the setting hip angle -20° , pre-loads: ACL 85N, MCL 75 N, flexion movement, testing for significant differences between the mean values of ACL loads in the pre-defined knee flexion ranges. The mean values again reflect the means of the five repetitions for each muscle setting. Dark grey fields are significant ($p < 0.05$). 7-271

Table 7-8 Results of Turkey's honestly significant difference test (post-hoc) for the setting hip angle -20° , pre-loads: ACL 85N, MCL 75 N, extension movement, testing for significant differences between the mean

values of ACL loads in the pre-defined knee flexion ranges. The mean values again reflect the means of the five repetitions for each muscle setting. Dark grey fields are significant ($p < 0.05$). 7-273

Table 7-9 Results of Turkey's honestly significant difference test (post-hoc) for the setting hip angle $+20^\circ$, pre-loads: ACL 85N, MCL 75 N, flexion movement, testing for significant differences between the mean values of ACL loads in the pre-defined knee flexion ranges. The mean values again reflect the means of the five repetitions for each muscle setting. Dark grey fields are significant ($p < 0.05$). 7-275

Table 7-10 Results of Turkey's honestly significant difference test (post-hoc) for the setting hip angle $+20^\circ$, pre-loads: ACL 85N, MCL 75 N, extension movement, testing for significant differences between the mean values of ACL loads in the pre-defined knee flexion ranges. The mean values again reflect the means of the five repetitions for each muscle setting. Dark grey fields are significant ($p < 0.05$). 7-276

Table 7-11 Parameters of the non-linear-elastic model of the ligaments by Blankevoort and Huiskes (1991), LARS Ligaments, and the modified parameters used for the present MBS-model. 7-281

Table 7-12 Initial length of the ligaments used in the MBS-model. 7-282

Table 7-13 Influence of the initial lengths of the ACL, PCL, MCL, LCL on ACL loads 7-287

Table 7-14 List of the risk values for the respective load cases: without external loads and pure individual loads. These single-load cases are not expected to occur in real-life skiing. Nevertheless, the values are the basis for comparison between loading scenarios. The reference for the derivation of the risk values is given in the last column. 7-309

Table 7-15 List of the risk values for the respective load cases: combination of two loads. 7-311

Table 7-16 List of the risk values for the respective load cases: combination of three loads. 7-313

Table 7-17 List of the risk values for the respective load cases: anterior tibial translation and combination of anterior tibial translation with muscle activation. 7-314

LIST OF TABLES

Table 7-18 Definition of ranges for the membership functions for the knee flexion
angles..... 7-315

Literature

- Ahmed, A. M., Burke, D. L., Duncan, N. A., and Chan, K. H. 1992. Ligament tension pattern in the flexed knee in combined passive anterior translation and axial rotation. *J. Orthop. Res.* 10(6):854-867. <https://doi.org/10.1002/jor.1100100615>.
- Alam, M., Bull, A. M. J., Thomas, R. d., and Amis, A. A. 2011. Measurement of rotational laxity of the knee: in vitro comparison of accuracy between the tibia, overlying skin, and foot. *The American journal of sports medicine* 39(12):2575-2581. <https://doi.org/10.1177/0363546511424872>.
- Alentorn-Geli, E., Myer, G. D., Silvers, H. J., Samitier, G., Romero, D., Lázaro-Haro, C., and Cugat, R. 2009. Prevention of non-contact anterior cruciate ligament injuries in soccer players. Part 1: Mechanisms of injury and underlying risk factors. *Knee surgery, sports traumatology, arthroscopy official journal of the ESSKA* 17(7):705-729. <https://doi.org/10.1007/s00167-009-0813-1>.
- Ali, A. A., Shalhoub, S. S., Cyr, A. J., Fitzpatrick, C. K., Maletsky, L. P., Rullkoetter, P. J., and Shelburne, K. B. 2016. Validation of predicted patellofemoral mechanics in a finite element model of the healthy and cruciate-deficient knee. *Journal of biomechanics* 49(2):302-309. <https://doi.org/10.1016/j.jbiomech.2015.12.020>.
- Alkner, B. A., Tesch, P. A., and Berg, H. E. 2000. Quadriceps EMG/force relationship in knee extension and leg press. *Medicine and Science in Sports and Exercise* 32(2):459-463.
- Almquist, P. O., Arnbjörnsson, A., Zätterström, R., Ryd, L., Ekdahl, C., and Fridén, T. 2002. Evaluation of an external device measuring knee joint rotation: an in vivo study with simultaneous Roentgen stereometric analysis. *J. Orthop. Res.* 20(3):427-432. [https://doi.org/10.1016/S0736-0266\(01\)00148-6](https://doi.org/10.1016/S0736-0266(01)00148-6).
- Almquist, P. O., Ekdahl, C., Isberg, P.-E., and Fridén, T. 2013. Knee rotation in healthy individuals related to age and gender. *Journal of orthopaedic research official publication of the Orthopaedic Research Society* 31(1):23-28. <https://doi.org/10.1002/jor.22184>.

- Arnold, E. M., Ward, S. R., Lieber, R. L., and Delp, S. L. 2010. A model of the lower limb for analysis of human movement. *Annals of biomedical engineering* 38(2):269-279. <https://doi.org/10.1007/s10439-009-9852-5>.
- Ashruf, C. 2002. Thin flexible pressure sensors. *SR* 22(4):322-327. <https://doi.org/10.1108/02602280210444636>.
- Asseln, M. 2019. Morphological and Functional Analysis of the Knee Joint for Implant Design Optimization: Aachener Beiträge zur Medizintechnik. Dissertation, Aachen.
- Atomic Austria GmbH. 2004. NEOX EBM: Instructions.
- Aumüller, G., Aust, G., Engele, J., Kirsch, J., Maio, G., Mayerhofer, A., Mense, S., and Reißig, D. 2017. Anatomie. 4., aktualisierte Auflage. Thieme Electronic Book Library. Georg Thieme Verlag, Stuttgart, New York, Delhi.
- Aune, A. K., Cawley, P. W., and Ekeland, A. 1997. Quadriceps muscle contraction protects the anterior cruciate ligament during anterior tibial translation. *The American journal of sports medicine* 25(2):187-190. <https://doi.org/10.1177/036354659702500208>.
- Aune, A. K., Schaff, P., and Nordsletten, L. 1995. Contraction of knee flexors and extensors in skiing related to the backward fall mechanism of injury to the anterior cruciate ligament. *Scandinavian journal of medicine & science in sports* 5(3):165-169. <https://doi.org/10.1111/j.1600-0838.1995.tb00031.x>.
- Awan, F., He, Y., Le, L., Tran, L.-L., Han, H.-D., and Nguyen, L. P. 2019. ElectroMyography Acquisition System Using Graphene-based e-Textiles. Pages 59–62 in: 2019 International Symposium on Electrical and Electronics Engineering: Proceedings October 10-12, 2019, Ho Chi Minh City, Vietnam, Ho Chi Minh, Vietnam, 10/10/2019 - 10/12/2019. IEEE, [Piscataway, New Jersey].
- Bally, A. 1996. Release level for backward release. ASTM Special Technical Publication(1266).
- Bancroft, J. B., and Lachapelle, G. 2011. Data fusion algorithms for multiple inertial measurement units. *Sensors* 11(7):6771-6798. <https://doi.org/10.3390/s110706771>.

- Barden, R. C., Goodapati, G., Fredricks, B. L., Wilson, G. J., and Herr, J. W. 2016. Remote Release Ski Binding (verified 19 Mar. 2021).
- Barone, M., Senner, V., and Schaff, P. 1999. ACL injury mechanism in alpine skiing: analysis of an accidental ACL rupture. *ASTM Special Technical Publication*(1345):63-81.
- Bates, N. A., Myer, G. D., Shearn, J. T., and Hewett, T. E. 2015. Anterior cruciate ligament biomechanics during robotic and mechanical simulations of physiologic and clinical motion tasks: a systematic review and meta-analysis. *Clinical biomechanics* (Bristol, Avon) 30(1):1-13.
<https://doi.org/10.1016/j.clinbiomech.2014.12.006>.
- Bauer+Kirch GmbH. 2015. Geschwindigkeitsanpassbare Skisicherheitsbindung: Offenlegungsschrift A63C 9/088 (2006.01) (verified 28 Nov. 2019).
- Baumeister, D. 2018. Konzeptionierung eines Fuzzy-Reglers für die Anwendung in einer mechatronischen Skibindung zur Bestimmung der Knieverletzungswahrscheinlichkeit. Master Thesis (unpublished), Munich.
- Beeby, S. 2004. MEMS mechanical sensors. Artech House microelectromechanical systems (MEMS) series. Artech House, Boston.
- Bendjaballah, M. Z., Shirazi-Adl, A., and Zukor, D. J. 1997. Finite element analysis of human knee joint in varus-valgus. *Clinical Biomechanics* 12(3):139-148.
[https://doi.org/10.1016/S0268-0033\(97\)00072-7](https://doi.org/10.1016/S0268-0033(97)00072-7).
- Bere, T., Flørenes, T. W., Krosshaug, T., Haugen, P., Svandal, I., Nordsletten, L., and Bahr, R. 2014. A systematic video analysis of 69 injury cases in World Cup alpine skiing. *Scandinavian journal of medicine & science in sports* 24(4):667-677.
<https://doi.org/10.1111/sms.12038>.
- Bere, T., Flørenes, T. W., Krosshaug, T., Koga, H., Nordsletten, L., Irving, C., Muller, E., Reid, R. C., Senner, V., and Bahr, R. 2011. Mechanisms of anterior cruciate ligament injury in World Cup alpine skiing: a systematic video analysis of 20 cases. *The American journal of sports medicine* 39(7):1421-1429.
<https://doi.org/10.1177/0363546511405147>.
- Bere, T., Mok, K.-M., Koga, H., Krosshaug, T., Nordsletten, L., and Bahr, R. 2013. Kinematics of anterior cruciate ligament ruptures in World Cup alpine skiing: 2

- case reports of the slip-catch mechanism. *The American journal of sports medicine* 41(5):1067-1073. <https://doi.org/10.1177/0363546513479341>.
- Bergmann, J. H. M., Anastasova-Ivanova, S., Spulber, I., Gulati, V., Georgiou, P., and McGregor, A. 2013. An Attachable Clothing Sensor System for Measuring Knee Joint Angles. *IEEE Sensors J.* 13(10):4090-4097. <https://doi.org/10.1109/JSEN.2013.2277697>.
- Berns, G. S., Hull, M. L., and Patterson, H. A. 1992. Strain in the anteromedial bundle of the anterior cruciate ligament under combination loading. *J. Orthop. Res.* 10(2):167-176. <https://doi.org/10.1002/jor.1100100203>.
- Bertozzi, L., Stagni, R., Fantozzi, S., and Cappello, A. 2008. Evaluation of a cruciate ligament model: sensitivity to the parameters during drawer test simulation. *Journal of applied biomechanics* 24(3):234-243. <https://doi.org/10.1123/jab.24.3.234>.
- Beynon, B. D., and Fleming, B. C. 1998. Anterior cruciate ligament strain in-vivo: a review of previous work. *Journal of biomechanics* 31(6):519-525. [https://doi.org/10.1016/s0021-9290\(98\)00044-x](https://doi.org/10.1016/s0021-9290(98)00044-x).
- Beynon, B. D., Johnson, R. J., Fleming, B. C., Stankewich, C. J., Renström, P. A., and Nichols, C. E. 1997. The strain behavior of the anterior cruciate ligament during squatting and active flexion-extension. A comparison of an open and a closed kinetic chain exercise. *The American journal of sports medicine* 25(6):823-829. <https://doi.org/10.1177/036354659702500616>.
- Bianchi, G., and Brügger, O. 2016. Unfallgeschehen beim Ski- und Snowboardfahren in der Schweiz: Unfallausmass, Risikoabschätzung und Entwicklung. bfu – Beratungsstelle für Unfallverhütung. bfu Grundlagen. <https://doi.org/10.13100/bfu.2.286.01>.
- Bigland, B., and Lippold, O. C. J. 1954. The Relation Between Force, Velocity and Integrated Electrical Activity in Human Muscles. *The Journal of Physiology* 123(1):214-224.
- Binder, E., Lubert, M., and Schaff, P. 1997. Neue Bewertungsmöglichkeiten für Knieorthesen auf der Basis eines Kniesimulators. *Orthopädie-Technik*(9):754-757.

- Blackburn, J. T., and Padua, D. A. 2008. Influence of trunk flexion on hip and knee joint kinematics during a controlled drop landing. *Clinical Biomechanics* 23(3):313-319. <https://doi.org/10.1016/j.clinbiomech.2007.10.003>.
- Bland, J. M., and Altman, D. G. 1986. Statistical methods for assessing agreement between two methods of clinical measurement. *Lancet (London, England)* 1(8476):307-310.
- Blankevoort, L., and Huiskes, R. 1991. Ligament-bone interaction in a three-dimensional model of the knee. *Journal of biomechanical engineering* 113(3):263-269. <https://doi.org/10.1115/1.2894883>.
- Bloemker, K. H., Guess, T. M., Maletsky, L., and Dodd, K. 2012. Computational knee ligament modeling using experimentally determined zero-load lengths. *The open biomedical engineering journal* 6:33-41. <https://doi.org/10.2174/1874230001206010033>.
- Borgelt, C., Klawonn, F., Kruse, R., and Nauck, D. 2003. *Neuro-Fuzzy-Systeme*. Vieweg+Teubner Verlag, Wiesbaden.
- Branch, T. P., Browne, J. E., Campbell, J. D., Siebold, R., Freedberg, H. I., Arendt, E. A., Lavoie, F., Neyret, P., and Jacobs, C. A. 2010. Rotational laxity greater in patients with contralateral anterior cruciate ligament injury than healthy volunteers. *Knee surgery, sports traumatology, arthroscopy official journal of the ESSKA* 18(10):1379-1384. <https://doi.org/10.1007/s00167-009-1010-y>.
- Brodie, M., Walmsley, A., and Page, W. 2008. Fusion motion capture: a prototype system using inertial measurement units and GPS for the biomechanical analysis of ski racing. *Sports Technol.* 1(1):17-28. <https://doi.org/10.1002/jst.6>.
- Bronner, S., Agraharasamakulam, S., and Ojofeitimi, S. 2010. Reliability and validity of electrogoniometry measurement of lower extremity movement. *Journal of medical engineering & technology* 34(3):232-242. <https://doi.org/10.3109/03091900903580512>.
- Brown, T. D., van Hoeck, J. E., and Brand, R. A. 1990. Laboratory evaluation of prophylactic knee brace performance under dynamic valgus loading using a surrogate leg model. *Clinics in sports medicine* 9(4):751-762.

- Brucker, P. U., Katzmaier, P., Olvermann, M., Huber, A., Waibel, K., Imhoff, A. B., and Spitzenpfeil, P. 2014. Alpinen Skibreiten- und Skileistungssport. Typische Verletzungsmuster und Möglichkeiten der Prävention. *Der Unfallchirurg* 117(1):24-32. <https://doi.org/10.1007/s00113-013-2464-4>.
- Brucker, P. U., Spitzenpfeil, P., Huber, A., Waibel, K., and Maier, W. 2011. Belastungen und Verletzungen des Kniegelenkes im Alpinen Ski-Hochleistungssport – Eine Status-quo-Analyse unter spezieller Fokussierung auf das vordere Kreuzband. *Sport-Orthopädie - Sport-Traumatologie - Sports Orthopaedics and Traumatology* 27(4):247-254. <https://doi.org/10.1016/j.orthtr.2011.10.007>.
- Cassidy, K., Hangalur, G., Sabharwal, P., and Chandrashekar, N. 2013. Combined in Vivo/ in Vitro Method to Study Anteromedial Bundle Strain in the ACL Using a Dynamic Knee Simulator 135(3):035001-1 - 035001-8. <https://doi.org/10.1115/1.4023520>.
- Cawley, P. W., France, E. P., and Paulos, L. E. 1989. Comparison of rehabilitative knee braces. A biomechanical investigation. *The American journal of sports medicine* 17(2):141-146. <https://doi.org/10.1177/036354658901700201>.
- Cerulli, G., Benoit, D. L., Lamontagne, M., Caraffa, A., and Liti, A. 2003. In vivo anterior cruciate ligament strain behaviour during a rapid deceleration movement: case report. *Knee surgery, sports traumatology, arthroscopy official journal of the ESSKA* 11(5):307-311. <https://doi.org/10.1007/s00167-003-0403-6>.
- Charnley, J. 1960. The lubrication of animal joints in relation to surgical reconstruction by arthroplasty. *Annals of the Rheumatic Diseases* 19(1):10-19. <https://doi.org/10.1136/ard.19.1.10>.
- Clavert, P., Kempf, J.-F., Bonomet, F., Boutemy, P., Marcelin, L., and Kahn, J.-L. 2001. Effects of freezing/thawing on the biomechanical properties of human tendons. *Surgical and Radiologic Anatomy* 23(4):259-262.
- Colyer, S. L., and Mc Guigan, P. M. 2018. Textile Electrodes Embedded in Clothing: A Practical Alternative to Traditional Surface Electromyography when Assessing Muscle Excitation during Functional Movements. *Journal of Sports Science and Medicine* 17:101-109.

- Crowninshield, R., Pope, M. H., and Johnson, R. J. 1976. An analytical model of the knee. *Journal of biomechanics* 9(6):397-405. [https://doi.org/10.1016/0021-9290\(76\)90117-2](https://doi.org/10.1016/0021-9290(76)90117-2).
- Daley, B. J., Ralston, J. L., Brown, T. D., and Brand, R. A. 1993. A parametric design evaluation of lateral prophylactic knee braces. *Journal of biomechanical engineering* 115(2):131-136. <https://doi.org/10.1115/1.2894112>.
- D'Antonio, N. F., Polt, D., and Eibl, V. 1980. Battery-Charging Generator for Electronic Ski Binding: US Patent (verified 19 Mar. 2021).
- Delp, S. L., Hess, W. E., Hungerford, D. S., and Jones, L. C. 1999. Variation of rotation moment arms with hip flexion. *Journal of biomechanics* 32(5):493-501. [https://doi.org/10.1016/S0021-9290\(99\)00032-9](https://doi.org/10.1016/S0021-9290(99)00032-9).
- DeMorat, G., Weinhold, P., Blackburn, T., Chudik, S., and Garrett, W. 2004. Aggressive quadriceps loading can induce noncontact anterior cruciate ligament injury. *The American journal of sports medicine* 32(2):477-483. <https://doi.org/10.1177/0363546503258928>.
- DIN ISO. Skibindungen für den alpinen Skilauf – Anforderungen und Prüfverfahren, Berlin. Beuth Verlag GmbH 97.220.20 (verified 20 Aug. 2020).
- Draganich, L. F., and Vahey, J. W. 1990. An in vitro study of anterior cruciate ligament strain induced by quadriceps and hamstrings forces. *J. Orthop. Res.* 8(1):57-63. <https://doi.org/10.1002/jor.1100080107>.
- Drillis, R., Contini, R., and Bluestein, M. 1966. *Body Segment Parameters: A Survey of Measurement Techniques*, Report 1163-03, New York.
- Dürselen, L., Claes, L., and Kiefer, H. 1995. The influence of muscle forces and external loads on cruciate ligament strain. *The American journal of sports medicine* 23(1):129-136. <https://doi.org/10.1177/036354659502300122>.
- Eberle, R., Heinrich, D., van den Bogert, A. J., Oberguggenberger, M., and Nachbauer, W. 2019. An approach to generate noncontact ACL-injury prone situations on a computer using kinematic data of non-injury situations and Monte Carlo simulation. *Computer methods in biomechanics and biomedical engineering* 22(1):3-10. <https://doi.org/10.1080/10255842.2018.1522534>.

- Eiba, M. 2014. Eruierung des Bewegungsablaufes eines Kniesimulators mittels einer 3D-Videoanalyse. Zusammenhang zwischen am Ski eingeleiteten Kräften und diversen Rotationswinkeln bei unterschiedlichen Knie- und Hüftwinkeln. Master Thesis, Munich.
- Ekeland, A., Rødven, A., and Heir, S. 2017. Injury Trends in Recreational Skiers and Boarders in the 16-Year Period 1996–2012. Pages 3–16 in: *Snow Sports Trauma and Safety*. I. S. Scher, R. M. Greenwald, and N. Petrone, eds. Springer International Publishing, Cham.
- Ekeland, A., Rødven, A., and Heir, S. 2019. Injuries among children and adults in alpine skiing and snowboarding. *Journal of science and medicine in sport* 22 Suppl 1:S3-S6. <https://doi.org/10.1016/j.jsams.2018.07.011>.
- Erickson, A. R., Yasuda, K., Beynnon, B., Johnson, r., and Pope, M. 1993. An in vitro dynamic evaluation of prophylactic knee braces during lateral impact loading. *The American journal of sports medicine* 21(1):26-35.
- Ettlinger, C. F., Dodge, D., Johnson, R. J., Shealy, J. E., Sargent, M., Johnson, R. J., Stealy, J., Senner, V., and Dean, S. W. 2010. Retention Requirements for Alpine Ski Bindings. *J. ASTM Int.* 7(6):102978. <https://doi.org/10.1520/JAI102978>.
- Ettlinger, C. F., and Dodge, D. J. 2007. Alpine Ski Binding System having Release Logic for Inhibiting Anterior Cruciate Ligament Injury (verified 07 Nov. 2019).
- Ettlinger, C. F., Johnson, R. J., and Shealy, J. E. 1995. A Method to Help Reduce the Risk of Serious Knee Sprains Incurred in Alpine Skiing. *The American journal of sports medicine* 23(5):531-537.
- Falda-Buscaiot, T. 2017. Analyse biomécanique en ski alpin conception et validation d'un nouveau capteur d'efforts 3D à l'interface skieur-environnement. Docteur de la Communauté, Grenoble Alpes.
- Falda-Buscaiot, T., Hintzy, F., Rougier, P., Lacouture, P., and Coulmy, N. 2017. Influence of slope steepness, foot position and turn phase on plantar pressure distribution during giant slalom alpine ski racing. *PloS one* 12(5):e0176975. <https://doi.org/10.1371/journal.pone.0176975>.

- Faller, A., and Schünke, M. 2008. *Der Körper des Menschen: Einführung in Bau und Funktion ; [mit 4 Tafeln zum Herausnehmen].* 15., komplett überarb. Aufl. Thieme, Stuttgart, New York.
- Farina, D. 2006. Interpretation of the Surface Electromyogram in Dynamic Contractions. *Exercise and Sport Sciences Reviews* 34(3):121-127.
- Fasel, B. 2017. Drift reduction for inertial sensor based orientation and position estimation in the presence of high dynamic variability during competitive skiing and daily-life walking. PhD Thesis, Lausanne.
- Fasel, B., Spörri, J., Schütz, P., Lorenzetti, S., and Aminian, K. 2017a. An Inertial Sensor-Based Method for Estimating the Athlete's Relative Joint Center Positions and Center of Mass Kinematics in Alpine Ski Racing. *Frontiers in physiology* 8:850. <https://doi.org/10.3389/fphys.2017.00850>.
- Fasel, B., Spörri, J., Schütz, P., Lorenzetti, S., and Aminian, K. 2017b. Validation of functional calibration and strap-down joint drift correction for computing 3D joint angles of knee, hip, and trunk in alpine skiing. *PloS one* 12(7):e0181446. <https://doi.org/10.1371/journal.pone.0181446>.
- Finni, T., Hu, M., Kettunen, P., Vilavuo, T., and Cheng, S. 2007. Measurement of EMG activity with textile electrodes embedded into clothing. *Physiological measurement* 28(11):1405-1419. <https://doi.org/10.1088/0967-3334/28/11/007>.
- Fischer, J. F., Loureiro, O., Leyvraz, P. F., and Bally, A. 1996. Injury mechanism of the anterior cruciate ligament in alpine skiing: Case studies. *ASTM Special Technical Publication* 1266.
- Fleming, B. C., Renstrom, P. A., Beynnon, B. D., Engstrom, B., Peura, G. D., Badger, G. J., and Johnson, R. J. 2001. The effect of weightbearing and external loading on anterior cruciate ligament strain. *Journal of biomechanics* 34(2):163-170. [https://doi.org/10.1016/S0021-9290\(00\)00154-8](https://doi.org/10.1016/S0021-9290(00)00154-8).
- Flock, T. P. 1992. Ski Binding with Knee Flex Sensor (verified 07 Nov. 2019).
- France, E. P., and Cawley, P. 2005. Mechanical Testing of Functional Knee Braces: An Evaluation of the BREG FUSION XT versus Selected Custom and Off-The-Shelf Functional Knee Braces.

- France, E. P., Paulos, L. E., Jayaraman, G., and Rosenberg, T. D. 1987. The biomechanics of lateral knee bracing. Part II: Impact response of the braced knee. *The American journal of sports medicine* 15(5):430-438.
<https://doi.org/10.1177/036354658701500502>.
- Freriks, B., and Hermens, H. J. 2000. SENIAM: European recommendations for surface electromyography results of the SENIAM project. 2nd ed. Roessingh Research and Development, [Pays-Bas].
- Freudiger, S., and Friedrich, N. F. 2000. Critical load cases for knee ligaments at skiing - an engineering approach. *ASTM Special Technical Publication(1397)*:160-174.
- Gabriel, M. T., Wong, E. K., Woo, S. L.-Y., Yagi, M., and Debski, R. E. 2004. Distribution of in situ forces in the anterior cruciate ligament in response to rotatory loads. *Journal of Orthopaedic Research* 22(1):85-89.
[https://doi.org/10.1016/S0736-0266\(03\)00133-5](https://doi.org/10.1016/S0736-0266(03)00133-5).
- Ganapathy, P. K., Collins, A. T., and Garrett, W. E. 2018. Mechanisms of Noncontact Anterior Cruciate Ligament Injuries. *The anterior cruciate ligament: Reconstruction and basic science: Second edition*:16-19.e2.
<https://doi.org/10.1016/B978-0-323-38962-4.00004-7>.
- Gehrke, I., Lutz, V., Schmelzeisen, D., Tenner, V., and Gries, T. 2019. Smart Textiles Production. *MDPI*.
- Gertel, T. H., Lew, W. D., Lewis, J. L., Stewart, N. J., and Hunter, R. E. 1993. Effect of anterior cruciate ligament graft tensioning direction, magnitude, and flexion angle on knee biomechanics. *The American journal of sports medicine* 21(4):572-581. <https://doi.org/10.1177/036354659302100415>.
- Gianotti, S. M., Marshall, S. W., Hume, P. A., and Bunt, L. 2009. Incidence of anterior cruciate ligament injury and other knee ligament injuries: a national population-based study. *Journal of science and medicine in sport* 12(6):622-627.
<https://doi.org/10.1016/j.jsams.2008.07.005>.
- Gioberto, G., Compton, C., and Dunne, L. 2016. Machine-Stitched E-textile Stretch Sensors. *Sensors & Transducers* 202(7):25-37.

- GlobalTop Technology Inc. 2011. FGPMOPA6H GPS Standalone Module Data Sheet, Tainan, Taiwan.
- Glynn, D. W., Kennedy, F. E., Hood, M. O., and Greenwald, R. M. 2002. A Comparative Evaluation of New and Conventional Knee Orthoses for Control of Anterior Tibial Displacement. *Journal of Prosthetics and Orthotics*(14):113-120.
- Gruber, M. 2001. Die neuromuskuläre Kontrolle des Kniegelenks vor und nach einem spezifischen sensomotorischen Training beim unverletzten Sportler. Dissertation, Stuttgart.
- Guex, K., Gojanovic, B., and Millet, G. P. 2012. Influence of hip-flexion angle on hamstrings isokinetic activity in sprinters. *Journal of athletic training* 47(4):390-395. <https://doi.org/10.4085/1062-6050-47.4.04>.
- Guo, L., Sandsjö, L., Ortiz-Catalan, M., and Skrifvars, M. 2020. Systematic review of textile-based electrodes for long-term and continuous surface electromyography recording. *Textile Research Journal* 90(2):227-244. <https://doi.org/10.1177/0040517519858768>.
- Gyi, D. E., Porter, J. M., and Robertson, N. K. 1998. Seat pressure measurement technologies: considerations for their evaluation. *Applied Ergonomics* 29(2):85-91. [https://doi.org/10.1016/S0003-6870\(97\)00036-7](https://doi.org/10.1016/S0003-6870(97)00036-7).
- Hame, S. L., Oakes, D. A., and Markolf, K. L. 2002. Injury to the anterior cruciate ligament during alpine skiing: a biomechanical analysis of tibial torque and knee flexion angle. *The American journal of sports medicine* 30(4):537-540. <https://doi.org/10.1177/03635465020300041301>.
- Hangalur, G., Brenneman, E., Nicholls, M., Bakker, R., Laing, A., and Chandrashekar, N. 2016. Can a knee brace reduce the strain in the anterior cruciate ligament? A study using combined in vivo/in vitro method. *Prosthetics and orthotics international* 40(3):394-399. <https://doi.org/10.1177/0309364615574167>.
- Harfe, D. T., Chuinard, C. R., Espinoza, L. M., Thomas, K. A., and Solomonow, M. 1998. Elongation patterns of the collateral ligaments of the human knee. *Clinical Biomechanics* 13(3):163-175. [https://doi.org/10.1016/S0268-0033\(97\)00043-0](https://doi.org/10.1016/S0268-0033(97)00043-0).

- Harms, H., Amft, O., and Tr Ster, G. 2010. Estimating posture-recognition performance in sensing garments using geometric wrinkle modeling. *IEEE transactions on information technology in biomedicine a publication of the IEEE Engineering in Medicine and Biology Society* 14(6):1436-1445. <https://doi.org/10.1109/TITB.2010.2076822>.
- Haughom, B. D., Souza, R., Schairer, W. W., Li, X., and Ma, C. B. 2012. Evaluating rotational kinematics of the knee in ACL-ruptured and healthy patients using 3.0 Tesla magnetic resonance imaging. *Knee surgery, sports traumatology, arthroscopy official journal of the ESSKA* 20(4):663-670. <https://doi.org/10.1007/s00167-011-1809-1>.
- Heinrich, D., van den Bogert, A. J., and Nachbauer, W. 2014. Relationship between jump landing kinematics and peak ACL force during a jump in downhill skiing: a simulation study. *Scandinavian journal of medicine & science in sports* 24(3):e180-7. <https://doi.org/10.1111/sms.12120>.
- Hermann, A., Baumeister, D., Carqueville, P., and Senner, V. 2022a. A Fuzzy Controller Design for a Mechatronic Ski Binding. *Conference Proceedings ISEA2022; Engineering of Sport 14th Conference, Perdue Lafayette*.
- Hermann, A., Carqueville, P., Baldinger, M., and Senner, V. 2021. Measuring Pressure in Different Layers of the Ski Boot to Estimate Skiing Movements. *Proceedings of the 9th International Conference on Sport Sciences Research and Technology Support. 9th International Conference on Sport Sciences Research and Technology Support. SCITEPRESS - Science and Technology:28-35*. <https://doi.org/10.5220/0010650700003059>.
- Hermann, A., Jung, A., Gruen, A., Brucker, P. U., and Senner, V. 2022b. A lower leg surrogate study to investigate the effect of quadriceps-hamstrings activation ratio on ACL tensile force. *Journal of science and medicine in sport* 25(9):770-775. <https://doi.org/10.1016/j.jsams.2022.05.006>.
- Hermann, A., Ostarhild, J., Mirabito, Y., Bauer, N., and Senner, V. 2020. Stretchable piezoresistive vs. capacitive silicon sensors integrated into ski base layer pants for measuring the knee flexion angle. *Sports Eng* 23(1). <https://doi.org/10.1007/s12283-020-00336-9>.

- Hermann, A., and Senner, V. 2020a. EMG-pants in Sports: Concept Validation of Textile-integrated EMG Measurements. Pages 197–204 in: Proceedings of the 8th International Conference on Sport Sciences Research and Technology Support, Budapest, Hungary. P. Pezarat-Correia, J. Vilas-Boas, and J. Capri, eds. SCITEPRESS - Science and Technology Publications.
- Hermann, A., and Senner, V. 2020b. Knee injury prevention in alpine skiing. A technological paradigm shift towards a mechatronic ski binding. *Journal of science and medicine in sport*(22). <https://doi.org/10.1016/j.jsams.2020.06.009>.
- Hermann, L. 2021. Entstehung von Kreuzbandverletzungen im alpinen Skilauf. Master Thesis (unpublished), Munich.
- Hewett, T. E., Myer, G. D., and Ford, K. R. 2006. Anterior cruciate ligament injuries in female athletes: Part 1, mechanisms and risk factors. *The American journal of sports medicine* 34(2):299-311. <https://doi.org/10.1177/0363546505284183>.
- Hirokawa, S., and Tsuruno, R. 2000. Three-dimensional deformation and stress distribution in an analytical/computational model of the anterior cruciate ligament. *Journal of biomechanics* 33(9):1069-1077. [https://doi.org/10.1016/S0021-9290\(00\)00073-7](https://doi.org/10.1016/S0021-9290(00)00073-7).
- Hirose, K., Kondo, A., and Doki, H. 2015. Comparison of Carving and Skidding Turns by Joint Torque of Skier and Gliding Velocities in Ski Running on Alpine Ski Slope. *Procedia Engineering* 112:338-343. <https://doi.org/10.1016/j.proeng.2015.07.259>.
- Hochmann, D. 2012. Prüf- und Bewertungsmethoden für Knieorthesen. 1. Aufl. Forschung für die Rehabilitationstechnik. Walter de Gruyter GmbH Co.KG, s.I.
- Höher, J., Vogrin, T. M., Woo, S. L., Carlin, G. J., Arøen, A., and Harner, C. D. 1999. In situ forces in the human posterior cruciate ligament in response to muscle loads: a cadaveric study. *J. Orthop. Res.* 17(5):763-768. <https://doi.org/10.1002/jor.1100170522>.
- Holden, J. P., Grood, E. S., Korvick, D. L., Cummings, J. F., Butler, D. L., and Bylski-Austrow, D. I. 1994. In vivo forces in the anterior cruciate ligament: Direct measurements during walking and trotting in a quadruped. *Journal of biomechanics* 27(5):517-526. [https://doi.org/10.1016/0021-9290\(94\)90063-9](https://doi.org/10.1016/0021-9290(94)90063-9).

- Holleczek, T., Ru, A., Harms, H., and Tro, G. 2010. Textile pressure sensors for sports applications. Pages 732–737 in: 2010 IEEE sensors: Waikoloa, Hawaii, USA, 1 - 4 November 2010 ; [the Ninth IEEE Sensors Conference 2010, Kona, HI, 11/1/2010 - 11/4/2010. IEEE, Piscataway, NJ.
- Holleczek, T., Zysset, C., Arnrich, B., Roggen, D., and Troster, G. 2009. Towards an Interactive Snowboarding Assistance System. Pages 147–148 in: Proceedings / 2009 International Symposium on Wearable Computers: ISWC 2009 ; 4 - 7 September 2009, Linz, Austria, Linz, Austria, 9/4/2009 - 9/7/2009. IEEE Computer Society, Los Alamitos, Calif.
- Holzer, H. 2006. Safety Ski Binding incorporating a Toe and a Heel Binding and an Electronic Circuit Arrangement (verified 19 Jan. 2021).
- Hosseini, A., Qi, W., Tsai, T.-Y., Liu, Y., Rubash, H., and Li, G. 2015. In vivo length change patterns of the medial and lateral collateral ligaments along the flexion path of the knee. *Knee surgery, sports traumatology, arthroscopy official journal of the ESSKA* 23(10):3055-3061. <https://doi.org/10.1007/s00167-014-3306-9>.
- Hsu, W.-H., Fisk, J. A., Yamamoto, Y., Debski, R. E., and Woo, S. L.-Y. 2006. Differences in torsional joint stiffness of the knee between genders: a human cadaveric study. *The American journal of sports medicine* 34(5):765-770. <https://doi.org/10.1177/0363546505282623>.
- Hull, M. L., Gregory, G. S., Varma, H., and Patterson, H. A. 1996. Erratum. *Journal of biomechanics* 29(8):1115. [https://doi.org/10.1016/0021-9290\(96\)88450-8](https://doi.org/10.1016/0021-9290(96)88450-8).
- Hull, M. L., and Johnson, C. 1989. Axial Rotation of the Lower Limb Under Torsional Loading: I. Static and Dynamic Measurements in Vivo. 277-277-14 in: *Skiing Trauma and Safety: Seventh International Symposium*. R. J. Johnson, C. D. Mote, and M.-H. Binet, eds. ASTM International, 100 Barr Harbor Drive, PO Box C700, West Conshohocken, PA 19428-2959.
- Hume, P. A., Lorimer, A. V., Griffiths, P. C., Carlson, I., and Lamont, M. 2015. Recreational Snow-Sports Injury Risk Factors and Countermeasures: A Meta-Analysis Review and Haddon Matrix Evaluation. *Sports Med* 45(8):1175-1190. <https://doi.org/10.1007/s40279-015-0334-7>.

- Hunston, M. 2002. Innovative thin-film pressure mapping sensors. *SR* 22(4):319-321. <https://doi.org/10.1108/02602280210697852>.
- Imhoff, A. B. 2000. *Knie: Mit 10 Tabellen. Fortbildung Orthopädie 3*. Steinkopff, Darmstadt.
- Jagodzinski, M., Müller, W., and Friederich, N. 2016. Anatomie. Pages 1–14 in: *Das Knie: Form, Funktion und ligamentäre Wiederherstellungschirurgie ; [Extras online*. M. Jagodzinski, N. F. Friederich, and W. Müller, eds. Springer, Berlin.
- Järvinen, M., Natri, A., Laurila, S., and Kannus, P. 1994. Mechanisms of anterior cruciate ligament ruptures in skiing. *Knee Surgery, Sports Traumatology, Arthroscopy* 2(4):224-228.
- Johnson, R. J., Ettliger, C. F., and Shealy, J. E. 2009. Update on Injury Trends in Alpine Skiing. Pages 11–22 in: *Skiing trauma and safety: seventeenth volume*. R. J. Johnson, ed. American Society for Testing and Materials, West Conshohocken, Pa.
- Jonsson, H., Kärrholm, J., and Elmqvist, L. G. 1989. Kinematics of active knee extension after tear of the anterior cruciate ligament. *The American journal of sports medicine* 17(6):796-802. <https://doi.org/10.1177/036354658901700613>.
- Jung, H.-J., Vangipuram, G., Fisher, M. B., Yang, G., Hsu, S., Bianchi, J., Ronholdt, C., and Woo, S. L.-Y. 2011. The effects of multiple freeze-thaw cycles on the biomechanical properties of the human bone-patellar tendon-bone allograft. *Journal of orthopaedic research official publication of the Orthopaedic Research Society* 29(8):1193-1198. <https://doi.org/10.1002/jor.21373>.
- Kanamori, A., Woo, S. L., Ma, C. B., Zeminski, J., Rudy, T. W., Li, G., and Livesay, G. A. 2000. The forces in the anterior cruciate ligament and knee kinematics during a simulated pivot shift test: A human cadaveric study using robotic technology. *Arthroscopy the journal of arthroscopic & related surgery official publication of the Arthroscopy Association of North America and the International Arthroscopy Association* 16(6):633-639. <https://doi.org/10.1053/jars.2000.7682>.
- Kanamori, A., Zeminski, J., Rudy, T. W., Li, G., Fu, F. H., and Woo, S. L.-Y. 2002. The effect of axial tibial torque on the function of the anterior cruciate ligament: a biomechanical study of a simulated pivot shift test. *Arthroscopy the journal of*

arthroscopic & related surgery official publication of the Arthroscopy Association of North America and the International Arthroscopy Association 18(4):394-398. <https://doi.org/10.1053/jars.2002.30638>.

Kapandji, A. I., and Koebke, J. 2006. Funktionelle Anatomie der Gelenke: Schematisierte und kommentierte Zeichnungen zur menschlichen Biomechanik ; [obere Extremität, untere Extremität, Rumpf und Wirbelsäule. 4., unveränd. Aufl; einbd. Ausg. Thieme, Stuttgart.

Kazemi, M., Dabiri, Y., and Li, L. P. 2013. Recent advances in computational mechanics of the human knee joint. *Computational and mathematical methods in medicine* 2013:718423. <https://doi.org/10.1155/2013/718423>.

Keays, S. L., Sayers, M., Mellifont, D. B., and Richardson, C. 2013. Tibial displacement and rotation during seated knee extension and wall squatting: a comparative study of tibiofemoral kinematics between chronic unilateral anterior cruciate ligament deficient and healthy knees. *The Knee* 20(5):346-353. <https://doi.org/10.1016/j.knee.2012.07.005>.

Kiapour, A. M., Kiapour, A., Goel, V. K., Quatman, C. E., Wordeman, S. C., Hewett, T. E., and Demetropoulos, C. K. 2015. Uni-directional coupling between tibiofemoral frontal and axial plane rotation supports valgus collapse mechanism of ACL injury. *Journal of biomechanics* 48(10):1745-1751. <https://doi.org/10.1016/j.jbiomech.2015.05.017>.

Kiefmann, A., Krinninger, M., Lindemann, U., Senner, V., and Spitzenpfeil, P. 2006. A New Six Component Dynamometer for Measuring Ground Reaction Forces in Alpine Skiing. Pages 87–92 in: *The Engineering of Sports 6*. Springer, New York, NY.

Kim, S., Lee, S., and Jeong, W. 2020. EMG Measurement with Textile-Based Electrodes in Different Electrode Sizes and Clothing Pressures for Smart Clothing Design Optimization. *Polymers* 12(10). <https://doi.org/10.3390/polym12102406>.

Kohn, D. 2005. Knie: 67 Tabellen. *Orthopädie und orthopädische Chirurgie / hrsg. von Carl Joachim Wirth*. Thieme, Stuttgart.

Konrad, P. 2011. EMG-FIBEL: Eine praxisorientierte Einführung in die kinesiologische Elektromyographie. Version 1.1.

- Kos, A., and Umek, A. 2018. Smart sport equipment: SmartSki prototype for biofeedback applications in skiing. *Pers Ubiquit Comput* 22(3):535-544. <https://doi.org/10.1007/s00779-018-1146-1>.
- Koyanagi, M., Shino, K., Yoshimoto, Y., Inoue, S., Sato, M., and Nakata, K. 2006. Effects of changes in skiing posture on the kinetics of the knee joint. *Knee surgery, sports traumatology, arthroscopy official journal of the ESSKA* 14(1):88-93. <https://doi.org/10.1007/s00167-004-0609-2>.
- Krosshaug, T., Andersen, T. E., Olsen, O.-E. O., Myklebust, G., and Bahr, R. 2005. Research approaches to describe the mechanisms of injuries in sport: limitations and possibilities. *British journal of sports medicine* 39(6):330-339. <https://doi.org/10.1136/bjsm.2005.018358>.
- Krosshaug, T., and Bahr, R. 2005. A model-based image-matching technique for three-dimensional reconstruction of human motion from uncalibrated video sequences. *Journal of biomechanics* 38(4):919-929. <https://doi.org/10.1016/j.jbiomech.2004.04.033>.
- Krueger, A., Edelmann-Nusser, J., Spitzenpfeil, P., Huber, A., Waibel, K.-H., and Witte, K. 2006. A measuring method for combined determination of the edging angle and the ground reaction force in alpine skiing in: 24 International Symposium on Biomechanics in Sports, Salzburg, July 14-16, 2006. E. Müller, ed.
- Lafontaine, D., Lamontagne, M., Dupuis, D., and Diallo, B. 1998. Analysis of the distribution of pressures under the feet of elite alpine ski instructors. in: 16 International Symposium on Biomechanics in Sports, Konstanz, July 21-25, 1998. H. J. Riehle, and M. M. Vieten, eds.
- Laporte, J.-D., Binet, M. H., and Constans, D. 2000. Evolution of ACL Ruptures in French Ski Resorts 1992-1999. Pages 95–107 in: *Skiing Trauma and Safety: Thirteenth Volume*. R. J. Johnson, J. E. Shealy, and P. Zucco, eds. ASTM International, West Conshohocken, Pa.
- Laurent, D., Merino, J. F., Miette, P., and Desarmaux, P. 2007. Fixation de sécurité d'une chaussure sur un ski (verified 19 Mar. 2021).
- Lee, J., Llerena Zambrano, B., Woo, J., Yoon, K., and Lee, T. 2020. Recent Advances in 1D Stretchable Electrodes and Devices for Textile and Wearable

- Electronics: Materials, Fabrications, and Applications. *Advanced materials* (Deerfield Beach, Fla.) 32(5):e1902532. <https://doi.org/10.1002/adma.201902532>.
- Lehner, S. 2007. Entwicklung und Validerung biomechanischer Computermodelle und deren Einsatz in der Sportwissenschaft. Dissertation, Koblenz-Landau.
- Li, G., Geng, Y., Tao, D., and Zhou, P. 2011. Performance of electromyography recorded using textile electrodes in classifying arm movements. *Conference proceedings: Annual International Conference of the IEEE Engineering in Medicine and Biology Society. IEEE Engineering in Medicine and Biology Society. Annual Conference 2011*:4243-4246. <https://doi.org/10.1109/IEMBS.2011.6091053>.
- Li, G., Gill, T. J., DeFrate, L. E., Zayontz, S., Glatt, V., and Zarins, B. 2002. Biomechanical consequences of PCL deficiency in the knee under simulated muscle loads—an in vitro experimental study. *Journal of Orthopaedic Research* 20(4):887-892. [https://doi.org/10.1016/S0736-0266\(01\)00184-X](https://doi.org/10.1016/S0736-0266(01)00184-X).
- Li, G., Rudy, T. W., Sakane, M., Kanamori, A., Ma, C. B., and Woo, S. L.-Y. 1999. The importance of quadriceps and hamstring muscle loading on knee kinematics and in-situ forces in the ACL. *Journal of biomechanics* 32(4):395-400. [https://doi.org/10.1016/S0021-9290\(98\)00181-X](https://doi.org/10.1016/S0021-9290(98)00181-X).
- Li, G., van de Velde, S. K., and Bingham, J. T. 2008. Validation of a non-invasive fluoroscopic imaging technique for the measurement of dynamic knee joint motion. *Journal of biomechanics* 41(7):1616-1622. <https://doi.org/10.1016/j.jbiomech.2008.01.034>.
- Li, M., Assadian, M., Ramezani, M., and Aw, K. C. 2019. Printed soft angular/torque sensors using carbon black-silicone composite. *SR* 39(4):598-603. <https://doi.org/10.1108/SR-11-2018-0290>.
- Li, Y., He, T., Shi, L., Wang, R., and Sun, J. 2020. Strain Sensor with Both a Wide Sensing Range and High Sensitivity Based on Braided Graphene Belts. *ACS applied materials & interfaces* 12(15):17691-17698. <https://doi.org/10.1021/acsami.9b21921>.
- Lieu, D. K., and Mote, C. D., JR. 1980. An Electronic Ski Binding Design with Biofeedback. *Journal of Mechanical Design* 102(4):677-682.

- Liggins, A. B., and Bowker, P. 1991. A quantitative assessment of orthoses for stabilization of the anterior cruciate ligament deficient knee. Proceedings of the Institution of Mechanical Engineers. Part H, Journal of engineering in medicine 205(2):81-87. https://doi.org/10.1243/PIME_PROC_1991_205_272_02.
- Liu, S., Lunsford, T., Gude, S., and Vangsness, C. 1994. Comparison of Functional Knee Braces for Control of Anterior Tibial Displacement. Clinical Orthopaedics & Related Research(303):203-210.
- Lohmander, L. S., Englund, P. M., Dahl, L. L., and Roos, E. M. 2007. The long-term consequence of anterior cruciate ligament and meniscus injuries: osteoarthritis. The American journal of sports medicine 35(10):1756-1769. <https://doi.org/10.1177/0363546507307396>.
- Lorbach, O., Wilmes, P., Maas, S., Zerbe, T., Busch, L., Kohn, D., and Seil, R. 2009a. A non-invasive device to objectively measure tibial rotation: verification of the device. Knee surgery, sports traumatology, arthroscopy official journal of the ESSKA 17(7):756-762. <https://doi.org/10.1007/s00167-009-0756-6>.
- Lorbach, O., Wilmes, P., Theisen, D., Brockmeyer, M., Maas, S., Kohn, D., and Seil, R. 2009b. Reliability testing of a new device to measure tibial rotation. Knee surgery, sports traumatology, arthroscopy official journal of the ESSKA 17(8):920-926. <https://doi.org/10.1007/s00167-009-0772-6>.
- Louie, J. K., and Mote, C. D. 1987. Contribution of the musculature to rotatory laxity and torsional stiffness at the knee. Journal of biomechanics 20(3):281-300. [https://doi.org/10.1016/0021-9290\(87\)90295-8](https://doi.org/10.1016/0021-9290(87)90295-8).
- Lund, M. E., Zee, M. de, Andersen, M. S., and Rasmussen, J. 2012. On validation of multibody musculoskeletal models. Proceedings of the Institution of Mechanical Engineers. Part H, Journal of engineering in medicine 226(2):82-94. <https://doi.org/10.1177/0954411911431516>.
- Lunsford, T. R., Lunsford, B. R., Greenfield, J., and Ross, S. E. 1990. Response of Eight Knee Orthoses to Valgus, Varus and Axial Rotation Loads. JPO: Journal of Prosthetics and Orthotics 2(4):274-288.
- Lynn, S. K., Watkins, C. M., Wong, M. A., Balfany, K., and Feeney, D. F. 2018. Validity and Reliability of Surface Electromyography Measurements from a

- Wearable Athlete Performance System. *Journal of Sports Science and Medicine* 17:205-2015.
- Markolf, K., Boguszewski, D., Yamaguchi, K., Lama, C., and McAllister, D. 2018. Prediction of ACL Force Produced by Tibiofemoral Compression During Controlled Knee Flexion: A New Robotic Testing Methodology. *Journal of biomechanical engineering*. <https://doi.org/10.1115/1.4040775>.
- Markolf, K. L., Bargar, W. L., Shoemaker, S. C., and Amstutz, H. C. 1981. The role of joint load in knee stability. *JBJS* 63(4):570-585.
- Markolf, K. L., Burchfield, D. M., Shapiro, M. M., Davis, B. R., Finerman, G. A. M., and Slauterbeck, J. L. 1996. Biomechanical Consequences of Replacement of the Anterior Cruciate Ligament with a Patellar Ligament Allograft. Part I: Insertion of the Graft and Anterior-Posterior Testing*. *JBJS* 78(11):1720.
- Markolf, K. L., Burchfield, D. M., Shapiro, M. M., Shepard, M. F., Finerman, G. A., and Slauterbeck, J. L. 1995. Combined knee loading states that generate high anterior cruciate ligament forces. *J. Orthop. Res.* 13(6):930-935. <https://doi.org/10.1002/jor.1100130618>.
- Markolf, K. L., Gorek, J. F., Kabo, J. M., and Shapiro, M. S. 1990. Direct measurement of resultant forces in the anterior cruciate ligament. An in vitro study performed with a new experimental technique. *The Journal of bone and joint surgery. American volume* 72(4):557-567.
- Markolf, K. L., Mensch, J. S., and Amstutz, H. C. 1976. Stiffness and laxity of the knee-the contributions of the supporting structures. A quantitative in vitro study. *The Journal of Bone & Joint Surgery* 58(5):583-594.
- Markolf, K. L., O'Neill, G., Jackson, S. R., and McAllister, D. R. 2004. Effects of applied quadriceps and hamstrings muscle loads on forces in the anterior and posterior cruciate ligaments. *The American journal of sports medicine* 32(5):1144-1149. <https://doi.org/10.1177/0363546503262198>.
- Markolf, K. L., Park, S., Jackson, S. R., and McAllister, D. R. 2008. Contributions of the posterolateral bundle of the anterior cruciate ligament to anterior-posterior knee laxity and ligament forces. *Arthroscopy the journal of arthroscopic & related surgery official publication of the Arthroscopy Association of North America and*

the International Arthroscopy Association 24(7):805-809.

<https://doi.org/10.1016/j.arthro.2008.02.012>.

Mathewson, P. R., and Greenwald, R. M. 2003. Reduction in Anterior Cruciate Ligament Load and Tibiofemoral Rotation under Applied Axial Rotation: A Surrogate Model Study of the Efficacy of a New Knee Derotation Brace Concept. *JPO: Journal of Prosthetics and Orthotics* 15(1):1-8.

Mattmann, C., Clemens, F., and Tröster, G. 2008. Sensor for Measuring Strain in Textile. *Sensors* 8(6):3719-3732. <https://doi.org/10.3390/s8063719>.

Mendes, J. J. A., Vieira, M. E. M., Pires, M. B., and Stevan, S. L. 2016. Sensor Fusion and Smart Sensor in Sports and Biomedical Applications. *Sensors* 16(10). <https://doi.org/10.3390/s16101569>.

Merino, J. F., Damiani, L., Bonnet, S., Francoise, H., Cado, G., and Mansuy, M. 2009. Three years on snow binding measurements in alpine skiing in: *ISSS 2009 Book of Abstracts*, München. V. Senner, V. Fastenbauer, and H. Böhm, eds.

Merino, J. F., Laporte JD, and Joubert, P. 2007. Lower leg injuries and fall mechanisms during alpine skiing practice, Aviemore, Scotland.

Meyer, F. 2012. Biomechanical analysis of alpine skiers performing giant slalom turns. Dissertation, Lausanne.

Meyer, F., Preneloup, A., and Schorderet, A. 2019. Development of a New Embedded Dynamometer for the Measurement of Forces and Torques at the Ski-Binding Interface. *Sensors* 19(19). <https://doi.org/10.3390/s19194324>.

Meyer, J. 2008. Textile pressure sensor: design, error modeling and evaluation. Dissertation.

Michels, K., Kruse, R., Klawonn, F., and Nürnberger, A. 2002. *Fuzzy-Regelung*. Springer Berlin Heidelberg, Berlin, Heidelberg.

Moon, D. K., Woo, S. L.-Y., Takakura, Y., Gabriel, M. T., and Abramowitch, S. D. 2006. The effects of refreezing on the viscoelastic and tensile properties of ligaments. *Journal of biomechanics* 39(6):1153-1157. <https://doi.org/10.1016/j.jbiomech.2005.02.012>.

- More, R. C., Karras, B. T., Neiman, R., Fritschy, D., Woo, S. L., and Daniel, D. M. 1993. Hamstrings--an anterior cruciate ligament protagonist. An in vitro study. *The American journal of sports medicine* 21(2):231-237. <https://doi.org/10.1177/036354659302100212>.
- Morère, C. S., Suraczyński, Ł., Pérez-Tabernerero, A. R., Vihriälä, E., and Myllylä, T. 2016. MEMS Technology Sensors as a More Advantageous Technique for Measuring Foot Plantar Pressure and Balance in Humans. *Journal of Sensors* 2016:1-9. <https://doi.org/10.1155/2016/6590252>.
- Mouton, C., Seil, R., Agostinis, H., Maas, S., and Theisen, D. 2012. Influence of individual characteristics on static rotational knee laxity using the Rotameter. *Knee surgery, sports traumatology, arthroscopy official journal of the ESSKA* 20(4):645-651. <https://doi.org/10.1007/s00167-011-1877-2>.
- Muhammad Sayem, A. S., Hon Teay, S., Shahariar, H., Fink, P. L., and Albarbar, A. 2020. Review on Smart Electro-Clothing Systems (SeCSs). *Sensors* 20(3). <https://doi.org/10.3390/s20030587>.
- Munro, B. J., Campbell, T. E., Wallace, G. G., and Steele, J. R. 2008. The intelligent knee sleeve: A wearable biofeedback device. *Sensors and Actuators B: Chemical* 131(2):541-547. <https://doi.org/10.1016/j.snb.2007.12.041>.
- Myer, G. D., Ford, K. R., Barber Foss, K. D., Liu, C., Nick, T. G., and Hewett, T. E. 2009. The relationship of hamstrings and quadriceps strength to anterior cruciate ligament injury in female athletes. *Clinical journal of sport medicine official journal of the Canadian Academy of Sport Medicine* 19(1):3-8. <https://doi.org/10.1097/JSM.0b013e318190bddb>.
- Naghibi Beidokhti, H., Janssen, D., van de Groes, S., Hazrati, J., van den Boogaard, T., and Verdonschot, N. 2017. The influence of ligament modelling strategies on the predictive capability of finite element models of the human knee joint. *Journal of biomechanics* 65:1-11. <https://doi.org/10.1016/j.jbiomech.2017.08.030>.
- Natri, A., Beynnon, B. D., Ettliger, C. F., Johnson, R. J., and Shealy, J. E. 1999. Alpine ski bindings and injuries. Current findings. *Sports medicine (Auckland, N.Z.)* 28(1):35-48. <https://doi.org/10.2165/00007256-199928010-00004>.

- Neptune, R. R., and Hull, M. L. 1992. A New Electromechanical Ski Binding with Release Sensitivity to Torsion and Bending Moments Transmitted by the Leg. *International Journal of Sport Biomechanics*(8):339-339-15.
<https://doi.org/10.1520/STP37942S>.
- Neuhofer, C., Pohlmann, M., and Sporer, L. 2014. Ermittlung kinematischer und kinetischer Größen der Knieinnen- und außenrotation im Skisport für ein Orthesenmodell. Hausarbeit, München.
- Neville, A., Morina, A., Liskiewicz, T., and Yan, Y. 2007. Synovial joint lubrication — does nature teach more effective engineering lubrication strategies? *Proceedings of the Institution of Mechanical Engineers, Part C: Journal of Mechanical Engineering Science* 221(10):1223-1230.
<https://doi.org/10.1243/09544062JMES724>.
- Nusser, M., Hermann, A., and Senner, V. 2016. Artificial Knee Joint and Ski Load Simulator for the Evaluation of Knee Braces and Ski Bindings. *Procedia Engineering* 147:220-227. <https://doi.org/10.1016/j.proeng.2016.06.217>.
- Nusser, M. M. 2016. Entwicklung, Evaluation und Anwendung eines Kniesimulators zur Ermittlung der auftretenden Kräfte im Knie unter skitypischen Belastungssituationen. Dissertation, München.
- Oberhofer, K., Hosseini Nasab, S. H., Schütz, P., Postolka, B., Snedeker, J. G., Taylor, W. R., and List, R. 2017. The influence of muscle-tendon forces on ACL loading during jump landing: a systematic review. *Muscles, ligaments and tendons journal* 7(1):125-135. <https://doi.org/10.11138/mltj/2017.7.1.125>.
- O'Brien, S., Searle, T., and Alici, G. 2019. Flexible Surface Electrodes Targeting Biopotential Signals from Forearm Muscles for Control of Prosthetic Hands: Part 1 – Characterisation of sEMG Electrodes. Pages 1019–1024 in: 2019 IEEE/ASME International Conference on Advanced Intelligent Mechatronics, AIM.
- Pandy, M. G., and Shelburne, K. B. 1997. Dependence of cruciate-ligament loading on muscle forces and external load. *Journal of biomechanics* 30(10):1015-1024.
[https://doi.org/10.1016/s0021-9290\(97\)00070-5](https://doi.org/10.1016/s0021-9290(97)00070-5).
- Pani, D., Achilli, A., Spanu, A., Bonfiglio, A., Gazzoni, M., and Botter, A. 2019. Validation of Polymer-Based Screen-Printed Textile Electrodes for Surface EMG

- Detection. *IEEE transactions on neural systems and rehabilitation engineering a publication of the IEEE Engineering in Medicine and Biology Society* 27(7):1370-1377. <https://doi.org/10.1109/TNSRE.2019.2916397>.
- Pantazelos, G., Lane, J. K., and Cameron, M. R. 2020. Processor-Controlled Snow Sport Boot Binding (verified 19 Mar. 2021).
- Papannagari, R., DeFrate, L. E., Nha, K. W., Moses, J. M., Moussa, M., Gill, T. J., and Li, G. 2007. Function of posterior cruciate ligament bundles during in vivo knee flexion. *The American journal of sports medicine* 35(9):1507-1512. <https://doi.org/10.1177/0363546507300061>.
- Park, H.-S., Wilson, N. A., and Zhang, L.-Q. 2008. Gender differences in passive knee biomechanical properties in tibial rotation. *Journal of orthopaedic research official publication of the Orthopaedic Research Society* 26(7):937-944. <https://doi.org/10.1002/jor.20576>.
- Paterno, M. V., Schmitt, L. C., Ford, K. R., Rauh, M. J., Myer, G. D., Huang, B., and Hewett, T. E. 2010. Biomechanical measures during landing and postural stability predict second anterior cruciate ligament injury after anterior cruciate ligament reconstruction and return to sport. *The American journal of sports medicine* 38(10):1968-1978. <https://doi.org/10.1177/0363546510376053>.
- Petersen, W., and Zantop, T. 2009. *Das vordere Kreuzband: Grundlagen und aktuelle Praxis der operativen Therapie; mit 29 Tabellen*. Deutscher Ärzteverlag.
- Petrone, N., Candioto, G., Marzella, E., Uriati, F., Carraro, G., Bäckström, M., and Koptuyug, A. 2019. Feasibility of using a novel instrumented human head surrogate to measure helmet, head and brain kinematics and intracranial pressure during multidirectional impact tests. *Journal of science and medicine in sport* 22 Suppl 1:S78-S84. <https://doi.org/10.1016/j.jsams.2019.05.015>.
- Petrone, N., Ceolin, F., and Morandin, T. 2010. Full scale impact testing of ski safety barriers using an instrumented anthropomorphic dummy. *Procedia Engineering* 2(2):2593-2598. <https://doi.org/10.1016/j.proeng.2010.04.037>.
- Petrone, N., Marcolin, G., and Panizzolo, F. A. 2013. The effect of boot stiffness on field and laboratory flexural behavior of alpine ski boots. *Sports Eng* 16(4):265-280. <https://doi.org/10.1007/s12283-013-0133-z>.

- Petrone, N., Panizzolo, F., and Marcolin, G. 2011. Behaviour of an instrumented anthropomorphic dummy during full scale drop tests. *Procedia Engineering* 13:304-309. <https://doi.org/10.1016/j.proeng.2011.05.089>.
- Pettys-Baker, R., Compton, C., Utset-Ward, S., Tompkins, M., Holschuh, B., and Dunne, L. E. 2017. Design and Development of Valgus-Sensing Leggings. *Frontiers in Biomedical Devices, BIOMED - 2017 Design of Medical Devices Conference, DMD 2017*. <https://doi.org/10.1115/DMD2017-3526>.
- Petushek, E., Richter, C., Donovan, D., Ebben, W. P., Watts, P. B., and Jensen, R. L. 2012. Comparison of 2D video and electrogoniometry measurements of knee flexion angle during a countermovement jump and landing task. *Sports Eng* 15(3):159-166. <https://doi.org/10.1007/s12283-012-0094-7>.
- Platter, F., and Rosenich, P. 1989. *Safety Ski Binding* (verified 07 Nov. 2019).
- Prodromos, C. C. 2018. *The Anterior Cruciate Ligament*. Elsevier.
- Putame, G., Terzini, M., Bignardi, C., Beale, B., Hulse, D., Zanetti, E., and Audenino, A. 2019. Surgical Treatments for Canine Anterior Cruciate Ligament Rupture: Assessing Functional Recovery Through Multibody Comparative Analysis. *Frontiers in bioengineering and biotechnology* 7:180. <https://doi.org/10.3389/fbioe.2019.00180>.
- Qiu, A., Li, P., Yang, Z., Yao, Y., Lee, I., and Ma, J. 2019. A Path Beyond Metal and Silicon: Polymer/Nanomaterial Composites for Stretchable Strain Sensors. *Adv. Funct. Mater.* 29(17):1806306. <https://doi.org/10.1002/adfm.201806306>.
- Rađenović, O., Nemec, B., and Medved, V. 2001. A New Biomechanical Measurement and Testing Method for Turns in Alpine Skiing.
- Raschner, C. 1997. *Kinematische und dynamische Technikanalyse im Slalom als Grundlage fuer die Entwicklung skispezifischer Krafttrainingsgeraete und Krafttrainingsmethoden.*, Salzburg.
- Raschner, C., Schiefermueller, C., Zallinger, G., Hofer, E., Müller, E., and Brunner, F. 2001. Carving turns versus traditional parallel turns - a comparative biomechanical analysis. Pages 56–57 in: *Science and skiing II: Tagungsband* ; St. Christoph a. Arlberg, Austria, January 9 - 15, 2000. E. Müller, ed. Kovač, Hamburg.

- Razak, A. H. A., Zayegh, A., Begg, R. K., and Wahab, Y. 2012. Foot plantar pressure measurement system: a review. *Sensors*:9884-9912.
<https://doi.org/10.3390/s120709884>.
- Regenfelder, F. G. 2008. Optimierung eines roboterbasierten Versuchsaufbaus zur Bestimmung biomechanischer Eigenschaften des Kniegelenks in 6 Freiheitsgraden. Dissertation, Munich.
- Reiter, A., Krumbeck, M., and Mangold, M. 2017. Elektronisch auslösbare Bindung für ein Gleitbrett (verified 19 Mar. 2021).
- Renström, P., Arms, S. W., Stanwyck, T. S., Johnson, R. J., and Pope, M. H. 1986. Strain within the anterior cruciate ligament during hamstring and quadriceps activity. *The American journal of sports medicine* 14(1):83-87.
<https://doi.org/10.1177/036354658601400114>.
- Ribas Manero, R. B., Shafti, A., Michael, B., Grewal, J., Ribas Fernandez, J. L., Althoefer, K., and Howard, M. J. 2016. Wearable embroidered muscle activity sensing device for the human upper leg. *Conference proceedings: Annual International Conference of the IEEE Engineering in Medicine and Biology Society. IEEE Engineering in Medicine and Biology Society. Annual Conference 2016*:6062-6065. <https://doi.org/10.1109/EMBC.2016.7592111>.
- Riedmayer, M. 1998. [DE] Vorrichtung zum Bestimmen und Weiterarbeiten von Fahr- und/oder Zustandsdaten für eine sich mittels an den Füßen befestigbaren Skiern oder eines Snowboards als Fahrvorrichtungen fortbewegende Person [EN] Drive or condition detection arrangement: Offenlegungsschrift A63C 11/00 (verified 11 Sep. 2020).
- Robinson, J. R., Bull, A. M. J., and Amis, A. A. 2005. Structural properties of the medial collateral ligament complex of the human knee. *Journal of biomechanics* 38(5):1067-1074. <https://doi.org/10.1016/j.jbiomech.2004.05.034>.
- Rohen, J. W., and Lütjen-Drecoll, E. 2006. Funktionelle Anatomie des Menschen: Lehrbuch der makroskopischen Anatomie nach funktionellen Gesichtspunkten ; mit 44 Tabellen. 11., überarb. und erw. Aufl. Schattauer, Stuttgart, New York.

- Rowe, P. J., Myles, C. M., Hillmann, S. J., and Hazlewood, M. E. 2001. Validation of Flexible Electrogoniometry as a Measure of Joint Kinematics. *Physiotherapy* 87(9):479-488. [https://doi.org/10.1016/S0031-9406\(05\)60695-5](https://doi.org/10.1016/S0031-9406(05)60695-5).
- Ruedl, G., and Burtscher, M. 2019. Why not consider a sex factor within the ISO 11088 ski binding setting standard? *British journal of sports medicine* 53(17):1127-1128. <https://doi.org/10.1136/bjsports-2017-098572>.
- Ruedl, G., Helle, K., Tecklenburg, K., Schranz, A., Fink, C., and Burtscher, M. 2016. Factors associated with self-reported failure of binding release among ACL injured male and female recreational skiers: a catalyst to change ISO binding standards? *British journal of sports medicine* 50(1):37-40. <https://doi.org/10.1136/bjsports-2015-095482>.
- Ruedl, G., Webhofer, M., Linortner, I., Schranz, A., Fink, C., Patterson, C., Nachbauer, W., and Burtscher, M. 2011. ACL injury mechanisms and related factors in male and female carving skiers: a retrospective study. *International journal of sports medicine* 32(10):801-806. <https://doi.org/10.1055/s-0031-1279719>.
- Saito, A., Doki, H., Kondo, A., and Hirose, K. 2015. An Attempt for Developing the Measurement System of Reaction Force from Snow Surface for Private Ski Boots by Compact Force Sensors. *Procedia Engineering* 112:326-331. <https://doi.org/10.1016/j.proeng.2015.07.257>.
- Schaff, P., Senner, V., and Kaiser, F. 1997. Pressure distribution measurements for the alpine skier - from the biomechanical high tech measurement to its application as Swingbeep-feedback system. Pages 159–172 in: *Science and skiing*. E. Müller, ed. E & FN Spon, London, New York.
- Scher, I. S., and Mote Jr., C. D. 2001. Minimum retention settings: Examining prediction methods. *ASTM Special Technical Publication*(1397).
- Schmitz, R. J., Ficklin, T. K., Shimokochi, Y., Nguyen, A.-D., Beynonn, B. D., Perrin, D. H., and Shultz, S. J. 2008. Varus/valgus and internal/external torsional knee joint stiffness differs between sexes. *The American journal of sports medicine* 36(7):1380-1388. <https://doi.org/10.1177/0363546508317411>.

- Schulz, D. 2019. Unfälle & Verletzungen im alpinen Skisport: Zahlen und Trends 2018/2019.
- Schünke, M. 2013. Funktionelle Anatomie Topographie und Funktion des Bewegungssystems. 2., Auflage. Thieme, Stuttgart.
- Schünke, M. 2014. Topografie und Funktion des Bewegungssystems: Funktionelle Anatomie. 2. Aufl. Georg Thieme Verlag KG, s.l.
- Schünke, M., Schulte, E., Schumacher, U., Voll, M., and Wesker, K. 2018. Prometheus - LernAtlas der Anatomie: Allgemeine Anatomie und Bewegungssystem. 5. überarbeitete und erweiterte Auflage. Georg Thieme Verlag, Stuttgart, New York.
- Schwameder, H., Nigg, B., Tschanner, V., and Stefanyshyn, D. 2001. The effect of binding position on kinetic variables in alpine skiing. Pages 43–54 in: Science and skiing II: Tagungsband ; St. Christoph a. Arlberg, Austria, January 9 - 15, 2000. E. Müller, ed. Kovač, Hamburg.
- Seering, W. P., Piziali, R. L., Nagel, D. A., and Schurman, D. J. 1980. The function of the primary ligaments of the knee in varus-valgus and axial rotation. *Journal of biomechanics* 13(9):785-794. [https://doi.org/10.1016/0021-9290\(80\)90240-7](https://doi.org/10.1016/0021-9290(80)90240-7).
- Senner, V. 2001. Biomechanische Methoden am Beispiel der Sportgeräteentwicklung. Dissertation, München.
- Senner, V., Lehner, S., Nusser, M., and Michel, F. I. 2014. Skiausrüstung und Knieverletzungen beim alpinen Skifahren um Freizeitsport: Eine Expertise zum gegenwärtigen Stand der Technik und deren Entwicklungspotential. *bfu Report* 69, Bern.
- Senner, V., Michel, F. I., Lehner, S., and Brügger, O. 2013. Technical possibilities for optimising the ski-binding-boot functional unit to reduce knee injuries in recreational alpine skiing. *Sports Eng* 16(4):211-228. <https://doi.org/10.1007/s12283-013-0138-7>.
- Senner, V., Schaff, P., and Hauser, W. 1996. Influences of Ski Boot Binding System on Load Reduction and Kinematics of Lower Leg During Backward Fall: Dynamic Simulation Using an Anthropometric Dummy. *Skiing Trauma and Safety: Tenth Volume*, ASTM STP 1266, West Conshohocken, Pa.

- Senner, V., and Schott, W. 2009. Emergency Release Device for Winter Sports Equipment (Notauslösevorrichtung für Wintersportgeräte) A63C 9/08 (verified 02 Jun. 2021).
- Senner, V., and Schott, W. 2017. A system for harvesting electrical energy during ski touring: EP A63C 9/088; A63C 11/22 (verified 02 Jun. 2021).
- Seon, J. K., Gadikota, H. R., Wu, J.-L., Sutton, K., Gill, T. J., and Li, G. 2010. Comparison of single- and double-bundle anterior cruciate ligament reconstructions in restoration of knee kinematics and anterior cruciate ligament forces. *The American journal of sports medicine* 38(7):1359-1367. <https://doi.org/10.1177/0363546510361494>.
- Shafti, A., Ribas Manero, R. B., Borg, A. M., Althoefer, K., and Howard, M. J. 2017. Embroidered Electromyography: A Systematic Design Guide. *IEEE transactions on neural systems and rehabilitation engineering a publication of the IEEE Engineering in Medicine and Biology Society* 25(9):1472-1480. <https://doi.org/10.1109/TNSRE.2016.2633506>.
- Shapiro, M. S., Markolf, K. L., Finerman, G. A., and Mitchell, P. W. 1991. The effect of section of the medial collateral ligament on force generated in the anterior cruciate ligament. *JBJS* 73(2):248-256.
- Sharkey, N. A., and Hamel, A. J. 1998. A dynamic cadaver model of the stance phase of gait: performance characteristics and kinetic validation. *Clinical Biomechanics* 13(6):420-433. [https://doi.org/10.1016/S0268-0033\(98\)00003-5](https://doi.org/10.1016/S0268-0033(98)00003-5).
- Shelburne, K. B., Pandy, M. G., Anderson, F. C., and Torry, M. R. 2004. Pattern of anterior cruciate ligament force in normal walking. *Journal of biomechanics* 37(6):797-805. <https://doi.org/10.1016/j.jbiomech.2003.10.010>.
- Shoemaker, S. C., and Markolf, K. L. 1982. In vivo rotatory knee stability. Ligamentous and muscular contributions. *JBJS* 64(2):208-216. <https://doi.org/10.2106/00004623-198264020-00010>.
- Shoemaker, S. C., Markolf, K. L., Dorey, F. J., Zager, S., and Namba, R. 1988. Tibial torque generation in a flexed weight-bearing stance. *Clinical orthopaedics and related research*(228):164-170.

- Shu, L., Hua, T., Wang, Y., Qiao Li, Q., Feng, D. D., and Tao, X. 2010. In-shoe plantar pressure measurement and analysis system based on fabric pressure sensing array. *IEEE transactions on information technology in biomedicine a publication of the IEEE Engineering in Medicine and Biology Society*:767-775. <https://doi.org/10.1109/TITB.2009.2038904>.
- Shultz, S. J., Schmitz, R. J., and Beynnon, B. D. 2011. Variations in varus/valgus and internal/external rotational knee laxity and stiffness across the menstrual cycle. *Journal of orthopaedic research official publication of the Orthopaedic Research Society* 29(3):318-325. <https://doi.org/10.1002/jor.21243>.
- Shultz, S. J., Shimokochi, Y., Nguyen, A.-D., Schmitz, R. J., Beynnon, B. D., and Perrin, D. H. 2007a. Measurement of varus-valgus and internal-external rotational knee laxities in vivo--Part I: assessment of measurement reliability and bilateral asymmetry. *J. Orthop. Res.* 25(8):981-988. <https://doi.org/10.1002/jor.20397>.
- Shultz, S. J., Shimokochi, Y., Nguyen, A.-D., Schmitz, R. J., Beynnon, B. D., and Perrin, D. H. 2007b. Measurement of varus-valgus and internal-external rotational knee laxities in vivo--Part II: relationship with anterior-posterior and general joint laxity in males and females. *J. Orthop. Res.* 25(8):989-996. <https://doi.org/10.1002/jor.20398>.
- Shyr, T.-W., Shie, J.-W., Jiang, C.-H., and Li, J.-J. 2014. A textile-based wearable sensing device designed for monitoring the flexion angle of elbow and knee movements. *Sensors (Basel, Switzerland)* 14(3):4050-4059. <https://doi.org/10.3390/s140304050>.
- Siebels, W. 1993. Optimierung von Werkstoffen für die Bandersatzchirurgie. Dissertation, Munich.
- Skaloud, J., and Limpach, P. 2003. Synergy of CP-DGPS, Accelerometry and Magnetic Sensors for precise Trajectory in Ski Racing. *Proceedings of the 16th International Technical Meeting of the Satellite Division of The Institute of Navigation (ION GPS/GNSS 2003)*:2173-2181.
2020. Skibindungen für den alpinen Skilauf - Auswahl von Auslösedrehmomentwerten (ISO 8061) 97.220.20.

2018. Skibindungen für den alpinen Skilauf - Auswahl von Auslösedrehmomentwerten mittels Tibia-Verfahren, Berlin. Beuth 97.220.20.
- Smolka, T. G. 1971. Safety Ski Binding (verified 07 Nov. 2019).
- Solomonow, M., Baratta, R., Zhou, B. H., Shoji, H., Bose, W., Beck, C., and D'Ambrosia, R. 1987. The synergistic action of the anterior cruciate ligament and thigh muscles in maintaining joint stability. *The American journal of sports medicine* 15(3):207-213. <https://doi.org/10.1177/036354658701500302>.
- Spitzenpfeil, P., Huber, A., and Waibel, K. 2006. Mechanical load and muscular expenditure in alpine ski racing in: 24 International Symposium on Biomechanics in Sports, Salzburg, July 14-16, 2006. E. Müller, ed.
- Spörri, J., Kröll, J., Gilgien, M., and Müller, E. 2017. How to Prevent Injuries in Alpine Ski Racing: What Do We Know and Where Do We Go from Here? *Sports medicine (Auckland, N.Z.)* 47(4):599-614. <https://doi.org/10.1007/s40279-016-0601-2>.
- Stoller, D. W. 2017. *Stoller's orthopaedics and sports medicine: The knee*. Buenos Aires; Wolters Kluwer, Philadelphia, Baltimore, New York, London, Hong Kong, Sydney, Tokyo.
- Stricker, G., Scheiber, P., Lindenhofer, E., and Müller, E. 2010. Determination of forces in alpine skiing and snowboarding: Validation of a mobile data acquisition system. *European Journal of Sport Science* 10(1):31-41. <https://doi.org/10.1080/17461390903108141>.
- Sumner, B., Mancuso, C., and Paradiso, R. 2013. Performances evaluation of textile electrodes for EMG remote measurements. *Proceedings of the Annual International Conference of the IEEE Engineering in Medicine and Biology Society, EMBS*:6510-6513. <https://doi.org/10.1109/EMBC.2013.6611046>.
- Supej, M. 2010. 3D measurements of alpine skiing with an inertial sensor motion capture suit and GNSS RTK system. *Journal of sports sciences* 28(7):759-769. <https://doi.org/10.1080/02640411003716934>.
- Tikkanen, O., Hu, M., Vilavuo, T., Tolvanen, P., Cheng, S., and Finni, T. 2012. Ventilatory threshold during incremental running can be estimated using EMG

- shorts. *Physiological measurement* 33(4):603-614. <https://doi.org/10.1088/0967-3334/33/4/603>.
- Tognetti, A., Bartalesi, R., Lorussi, F., and Rossi, D. de. 2007. Body segment position reconstruction and posture classification by smart textiles. *Transactions of the Institute of Measurement and Control* 29(3-4):215-253. <https://doi.org/10.1177/0142331207069487>.
- Tognetti, A., Lorussi, F., Mura, G. D., Carbonaro, N., Pacelli, M., Paradiso, R., and Rossi, D. D. 2014. New generation of wearable goniometers for motion capture systems. *Journal of neuroengineering and rehabilitation* 11:56. <https://doi.org/10.1186/1743-0003-11-56>.
- Turner, W. D., Vasseur, P., Gorek, J. E., Rodrigo, J. J., and Wedell, J. R. 1988. An in Vitro Study of the Structural Properties of Deep-Frozen Versus Freeze-dried, Ethylene Oxide-Sterilized Canine Anterior Cruciate Ligament Bone-Ligament-Bone Preparations. *Clinical orthopaedics and related research*.
- Uetz, H., and Wiedemeyer, J. 1984. *Tribologie der Polymere: Grundlagen und Anwendungen in der Technik; Reibung- Verschleiß- Schmierung mit 421 Bildern und 51 Tafeln* 37. Hanser, München.
- van Mechelen, W., Hlobil, H., and Kemper, H. C. 1992. Incidence, severity, aetiology and prevention of sports injuries. A review of concepts. *Sports medicine (Auckland, N.Z.)* 14(2):82-99. <https://doi.org/10.2165/00007256-199214020-00002>.
- Vanat, L. 2019. 2019 International Report on Snow & Mountain Tourism: Overview of the key industry figures for ski resorts.
- Visser, J. J., Hoogkamer, J. E., Bobbert, M. F., and Huijing, P. A. 1990. Length and moment arm of human leg muscles as a function of knee and hip-joint angles. *European journal of applied physiology and occupational physiology* 61(5-6):453-460. <https://doi.org/10.1007/BF00236067>.
- Wägli, A. 2009. *Trajectory Determination and Analysis in Sports by Satellite and Inertial Navigation*. These pour l'obtention du grade de docteur ès sciences, Lausanne.

- Wang, L., Fu, X., He, J., Shi, X., Chen, T., Chen, P., Wang, B., and Peng, H. 2020. Application Challenges in Fiber and Textile Electronics. *Advanced materials* (Deerfield Beach, Fla.) 32(5):e1901971. <https://doi.org/10.1002/adma.201901971>.
- Wascher, D. C., Markolf, K. L., Shapiro, M. S., and Finerman, G. A. 1993. Direct in Vitro Measurement of Forces in the Cruciate Ligaments: Part I: The Effect of Multiplane Loading in the Intact Knee. *The Journal of Bone and Joint Surgery* 75(3):377-386.
- Wijdicks, C. A., Griffith, C. J., LaPrade, R. F., Spiridonov, S. I., Johansen, S., Armitage, B. M., and Engebretsen, L. 2009. Medial Knee Injury: Part 2, Load Sharing Between the Posterior Oblique Ligament and Superficial Medial Collateral Ligament. *The American journal of sports medicine* 37(9):1771-1776.
- Wimmer, M. A., and Holzner, R. 1997. Constraint Forces may influence the measurement of vertical ground reaction forces during slalom skiing. Pages 208–215 in: *Science and skiing*. E. Müller, ed. E & FN Spon, London, New York.
- Withrow, T. J., Huston, L. J., Wojtys, E. M., and Ashton-Miller, J. A. 2008. Effect of varying hamstring tension on anterior cruciate ligament strain during in vitro impulsive knee flexion and compression loading. *The Journal of bone and joint surgery. American volume* 90(4):815-823. <https://doi.org/10.2106/JBJS.F.01352>.
- Wojtys, E. M., Huston, L. J., Lindenfeld, T. N., Hewett, T. E., and Greenfield, M. L. 1998. Association between the menstrual cycle and anterior cruciate ligament injuries in female athletes. *The American journal of sports medicine* 26(5):614-619. <https://doi.org/10.1177/03635465980260050301>.
- Woo, S. L., Hollis, J. M., Adams, D. J., Lyon, R. M., and Takai, S. 1991. Tensile properties of the human femur-anterior cruciate ligament-tibia complex. The effects of specimen age and orientation. *The American journal of sports medicine* 19(3):217-225. <https://doi.org/10.1177/036354659101900303>.
- Wunderly, G., and Hull, M. 1989. *A Mechanical Alpine Ski Binding with Programmable Release*, Philadelphia: ASTM International.
- Wunderly, S., Hull, M. L., and Maxwell, S. 1988. A Second Generation Microcomputer Controlled Binding System for Alpine Skiing Research. *Journal of biomechanics* 21(4):299-318.

- Yamada, T., Hayamizu, Y., Yamamoto, Y., Yomogida, Y., Izadi-Najafabadi, A., Futaba, D. N., and Hata, K. 2011. A stretchable carbon nanotube strain sensor for human-motion detection. *Nature nanotechnology* 6(5):296-301. <https://doi.org/10.1038/nnano.2011.36>.
- Yildirim, G., Walker, P. S., and Boyer, J. 2009. Total knees designed for normal kinematics evaluated in an up-and-down crouching machine. *Journal of orthopaedic research official publication of the Orthopaedic Research Society* 27(8):1022-1027. <https://doi.org/10.1002/jor.20839>.
- Yoneyama, T., Kagawa, H., Unemoto, M., Iizuka, T., and Scott, N. W. 2009. A ski robot system for qualitative modelling of the carved turn. *Sports Eng* 11(3):131-141. <https://doi.org/10.1007/s12283-009-0018-3>.
- Yoshioka, S., Fujita, Z., Hay, D. C., and Ishige, Y. 2018. Pose tracking with rate gyroscopes in alpine skiing. *Sports Eng* 21(3):177-188. <https://doi.org/10.1007/s12283-017-0261-y>.
- Yu, B., Lin, C.-F., and Garrett, W. E. 2006. Lower extremity biomechanics during the landing of a stop-jump task. *Clinical Biomechanics* 21(3):297-305. <https://doi.org/10.1016/j.clinbiomech.2005.11.003>.
- Zang, Y., Zhang, F., Di, C., and Zhu, D. 2015. Advances of flexible pressure sensors toward artificial intelligence and health care applications. *Mater. Horiz.* 2(2):140-156. <https://doi.org/10.1039/C4MH00147H>.
- Zavatsky, A. B. 1997. A kinematic-freedom analysis of a flexed-knee-stance testing rig. *Journal of biomechanics* 30(3):277-280. [https://doi.org/10.1016/S0021-9290\(96\)00142-X](https://doi.org/10.1016/S0021-9290(96)00142-X).
- Zhang, H., Li, W., Tao, X., Xu, P., and Liu, H. 2011. Textile-structured human body surface biopotential signal acquisition electrode. Pages 2792–2797 in: 4th International Congress on Image and Signal Processing (CISP), 2011: 15 - 17 Oct. 2011, Shanghai, China ; proceedings, Shanghai, China, 10/15/2011 - 10/17/2011. P. Qiu, ed. IEEE, Piscataway, NJ.
- Zihajehzadeh, S., Loh, D., Lee, T. J., Hoskinson, R., and Park, E. J. 2015. A cascaded Kalman filter-based GPS/MEMS-IMU integration for sports applications. *Measurement* 73:200-210. <https://doi.org/10.1016/j.measurement.2015.05.023>.

7 Appendix

7.1 The Human Knee

7.1.1 Axes of the Leg

Figure 7-1 shows a frontal view of a leg. Also shown are the bones consisting of the femur (thigh), patella (kneecap), tibia (lower leg), and fibula (fibula), as well as the anatomical and mechanical axes of the leg.

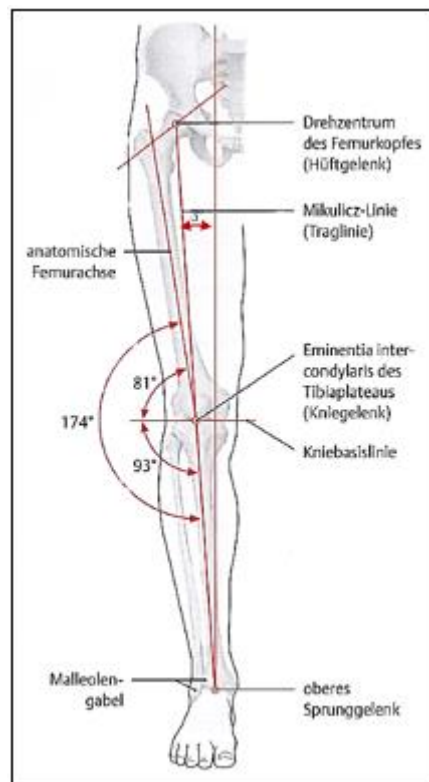


Figure 7-1 Anatomical and mechanical axes of the right leg. Frontal view. Taken and supplemented from Schünke (2013) page 272.

In a leg with normal axial conditions, the hip joint, the knee joint, and the ankle joint lie on a load-bearing line (Mikulicz line) (Schünke 2013) and thus form the mechanical axis of the leg. It has an angle of 3° to the vertical. On the lower leg, the mechanical and anatomical axes coincide. The longitudinal axis of the femur and the weight-bearing line takes an angle of 6° . Thus, there is an angle of 174° between the tibia and femur in the frontal plane, resulting in a natural valgus (outward facing) position. However, the angles given should not be considered absolute and may vary, especially depending on sex and age. (Kapandji and Koebke 2006)

7.1.2 Knee Joint

The knee joint is a compound joint consisting of the femoro-tibial joint, between the femur and tibia, and the femoro-patellar joint, between the femur and patella (see Figure 7-2). The fibula is not involved in the joint. The joints are enclosed by a joint capsule. (Schünke 2013)

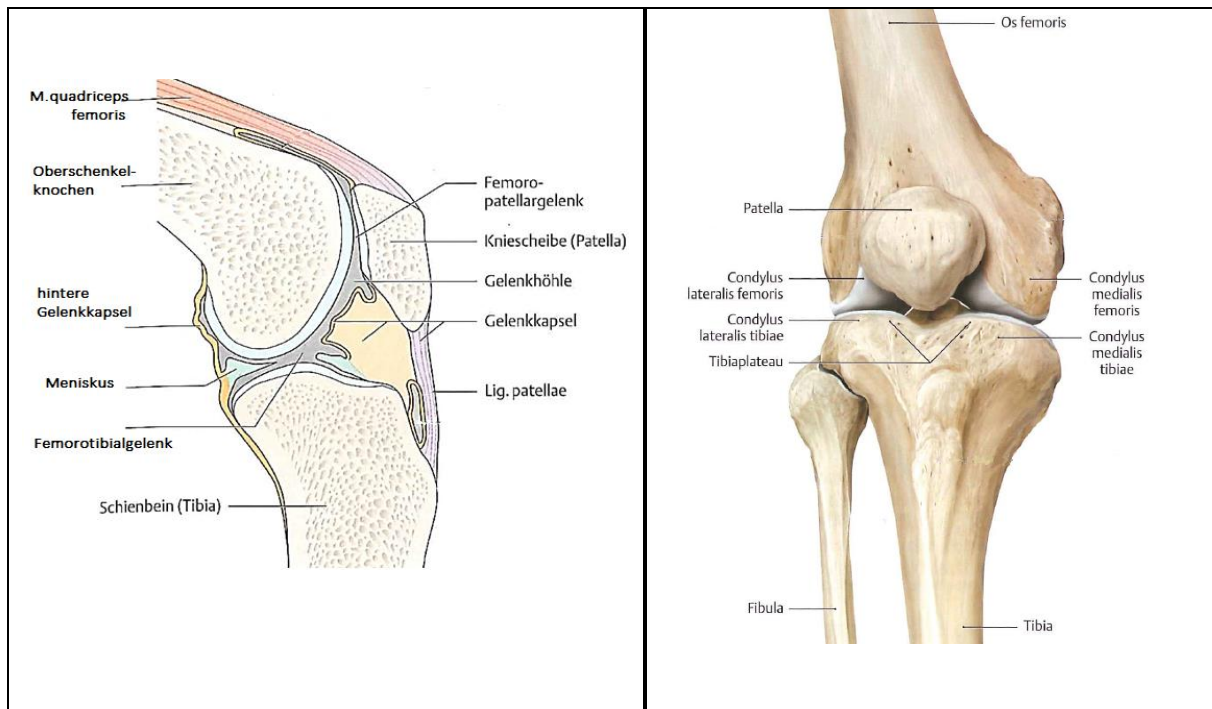


Figure 7-2 Sagittal section of a knee joint. Taken and adapted from Faller and Schünke (2008), page 203. *Figure 7-3 Right knee joint. Front view. Taken and adapted from Schünke (2013), page 293.*

Femoro-tibial joint

The femoro-tibial joint is formed by the two biconvex femoral condyles (condylus lateralis / medialis femoris) and the oval, slightly concave tibial condyles (condylus lateralis / medialis tibiae) (see Figure 7-3). The femoral condyles are not circular but have a spiral course with changing radii. The space between the joint partners is filled by the two menisci, which can move with the joint movement and absorb about one-third of the force transmitted in the joint. (Schünke 2013)

Femoro-patellar joint

The patella slides in the facies articularis patellae, which connects the two femoral condyles in the form of a depression. The contact force of the patella increases with increasing flexion and reaches over 1000 N at maximum flexion. (Schünke 2013)

Collateral ligaments

The external ligament (Lig. collaterale fibulare) and the internal ligament (Lig. collaterale tibiale) represent the two collateral ligaments of the knee. In the extended leg position, the two ligaments are taut and thus ensure the lateral stability of the knee. When the knee is flexed, the ligaments slacken, allowing increasing rotational and lateral movements. When viewed from the lateral side, the two collateral ligaments cross over each other. (Schünke 2013)

Cruciate Ligaments

The anterior and posterior cruciate ligaments (Lig. cruciata anterior / posterior) are located between the condyles of the femur and the tibia (Areae intercondylares). The cruciate ligaments have several tasks. They prevent the femur from slipping off the tibia in the anterior-posterior direction and play a major role in stabilising the joint in flexion. They also brake the external rotation of the knee (Schünke 2013). They are responsible, along with the musculature for the sliding motion between the tibia and femur (see also chapter 2.1.1). Not all fibre bundles of the cruciate ligaments have the same length and orientation, so not all bundles are tense at the same time during the knee movement. The anterior cruciate ligament also prevents excessive hyperextension (Kapandji and Koebke 2006).

Functionally, the anterior cruciate ligament can be divided into an anteromedial and a posterolateral bundle, and the posterior cruciate ligament into an anterolateral and a posteromedial bundle (Petersen and Zantop 2009). Histologically, this is not correct, as both ligaments are structured according to the principle of the scissors lattice and no bundles can be distinguished (Imhoff 2000).

7.1.3 Musculature

The knee joint allows flexion or extension and internal and external rotation of the tibia in relation to the femur. However, rotational movements are only possible in the flexed state, since in the extended leg the collateral ligaments, the cruciate ligaments, and a so-called final rotation prevent rotation of the tibia (Kapandji and Koebke 2006; Rohen and Lütjen-Drecoll 2006).

For this movement, the body has several muscles at its disposal, which are mainly the flexors (flexors) and extensors (extensors) of the thigh.

Flexors and extensors

An extension is caused solely by the muscles of the quadriceps femoris muscle (see Figure 7-4, extensors), which passes into the patella ligament, which attaches directly to the patella. In this process, the extensors are particularly powerful because they have to work against the body weight (Rohen and Lütjen-Drecoll 2006). Their work output is approximately three times what the flexors can collectively muster (Kapandji and Koebke 2006).

The ischiocrural muscles (see Figure 7-4) extend the hip joint and flex the knee joint. The two joints thus influence each other through the maximum length and extensor capacity of the muscles (Kapandji and Koebke 2006).

Other flexors include the sartorius and gracilis muscles. M. gastrocnemicus and M. popliteus do not take a significant role as flexors. However, the gastrocnemicus has an important function in stabilising the knee joint (Kapandji and Koebke 2006).

Rotators

The knee joint flexors are simultaneously responsible for rotation between the tibia and femur. The muscles involved in the internal rotation have their insertion at the medial tibial condyle. The biceps femoris muscle, which is responsible for external rotation, attaches to the caput fibulae (fibular head) (Rohen and Lütjen-Drecoll 2006). Rohen and Lütjen-Drecoll (2006) and Schünke (2013) emphasize that the biceps femoris muscle is the only external rotator. Kapandji and Koebke (2006) cite the fasciae latae muscle as an external rotator in addition to this one, but state that it can only generate rotational moment in the flexed knee. The internal rotators are more numerous and stronger than the external rotators. The rationale lies in the task of these to return the leg to the weight-bearing line and thus work against the body weight (Rohen and Lütjen-Drecoll 2006). In Figure 7-5, the rotators are shown. In addition, their points of action on the lower leg and their course are shown schematically.

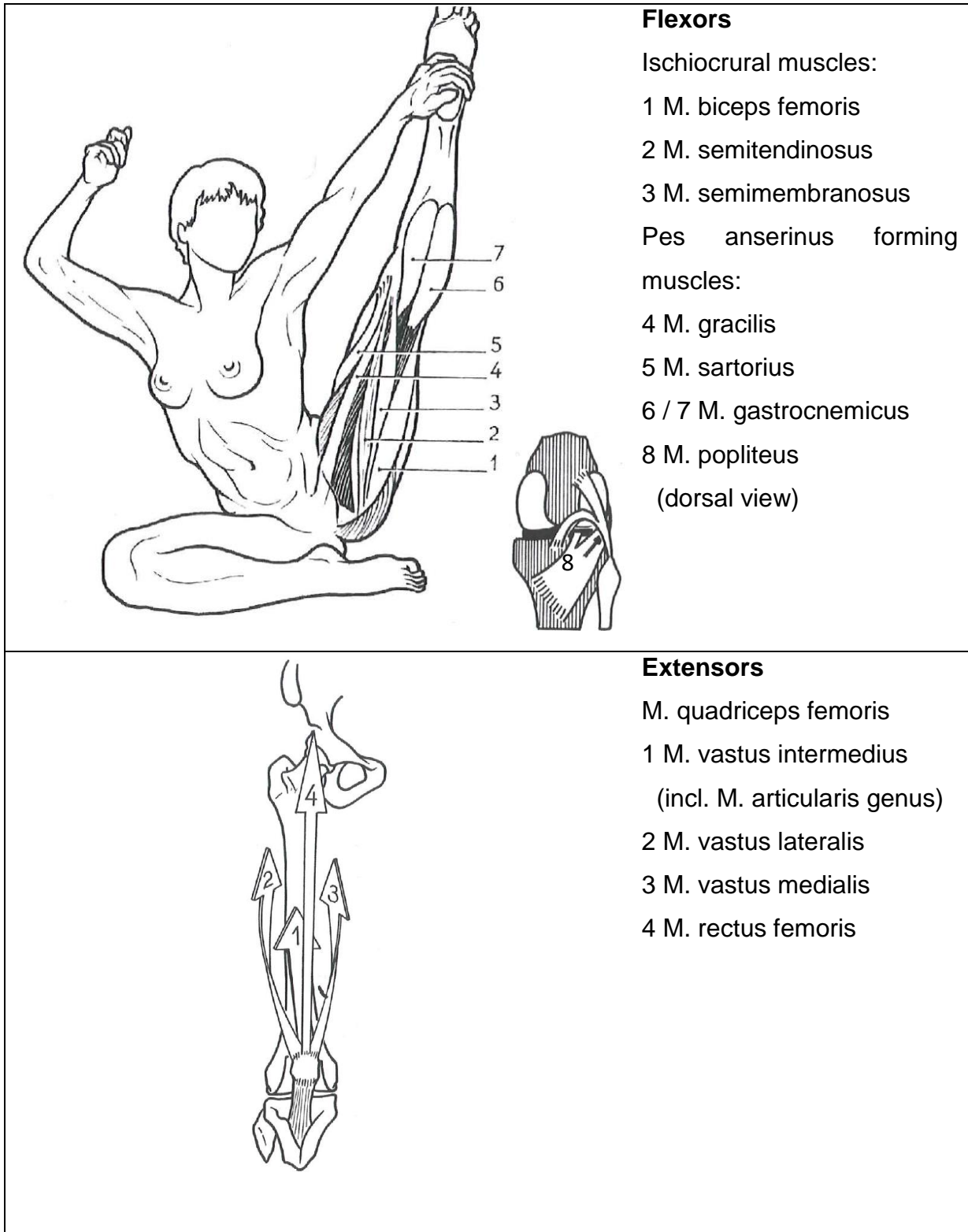
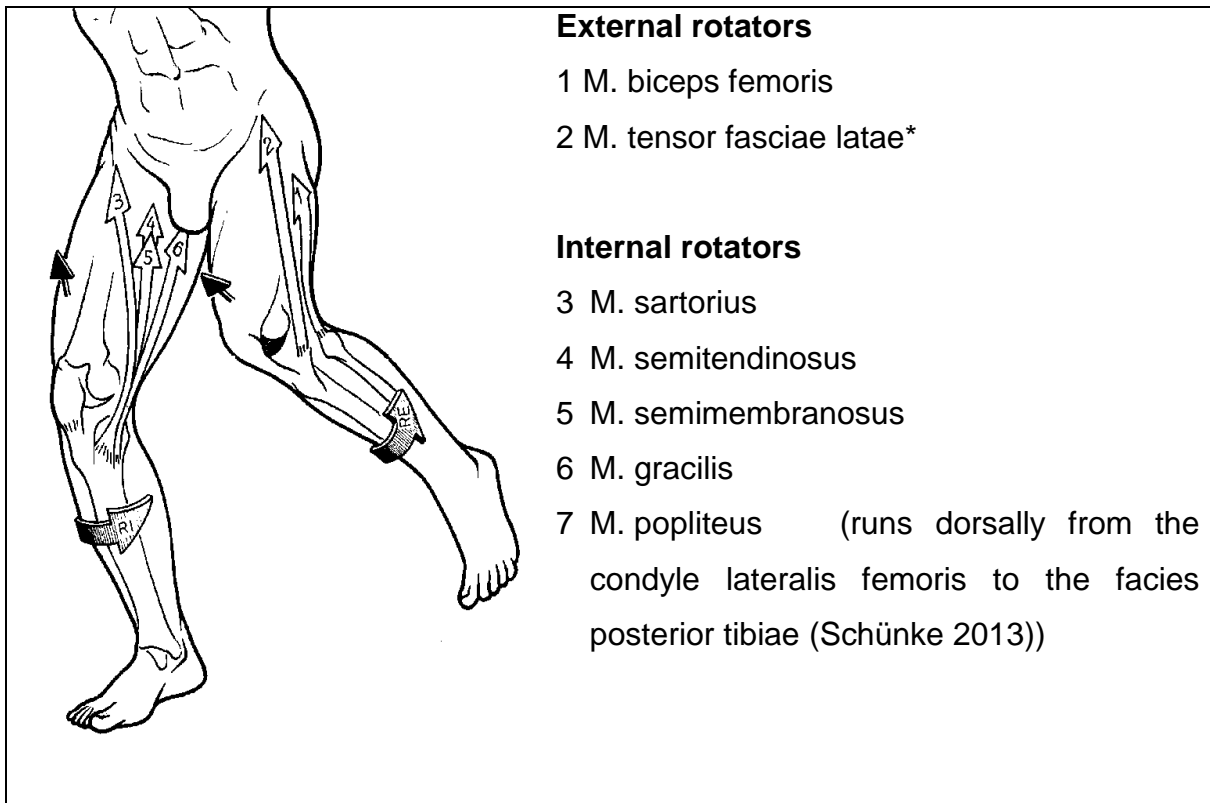


Figure 7-4 Flexors (top) and extensors (bottom) of the knee joint. Taken and adapted from Kapandji and Koebke (2006), page 141 and 143.

**External rotators**

- 1 M. biceps femoris
- 2 M. tensor fasciae latae*

Internal rotators

- 3 M. sartorius
- 4 M. semitendinosus
- 5 M. semimembranosus
- 6 M. gracilis
- 7 M. popliteus (runs dorsally from the condyle lateralis femoris to the facies posterior tibiae (Schünke 2013))

Figure 7-5 The rotators of the knee joint. Taken from Kapandji and Koebke (2006) page 143. (*The function of the tensor fasciae latae muscle as rotator is not clearly recognized in the literature. Schünke (2013) emphasizes that only the M. biceps femoris is responsible for external rotation.)

7.1.4 Kinematics

7.1.4.1 Flexion und Extension

In the knee joint, a distinction is made between active flexion, with which 120° to 140° can be achieved, depending on the hip angle, and passive flexion, with which 150° can be achieved, and 160° in kneeling sitting (Figure 7-6 a). Hyperextension beyond the straight extended leg is passively possible from 5° to 10°. Flexion in the femoro-tibial joint is a combination of rolling and sliding. Up to flexion of 15° medially and 20° laterally, the femoral condyles roll on the tibial plateau. With further flexion, the gliding motion increases more and more until the condyles rotate on the spot. The axis of rotation (axis of motion in Figure 7-6 e) moves with the joint position and describes an evolute. Both the intersection of the cruciate and collateral ligaments in the lateral view (Figure 7-6 b-d) lie on the axis of rotation (Schünke 2013; Kapandji and Koebke 2006).

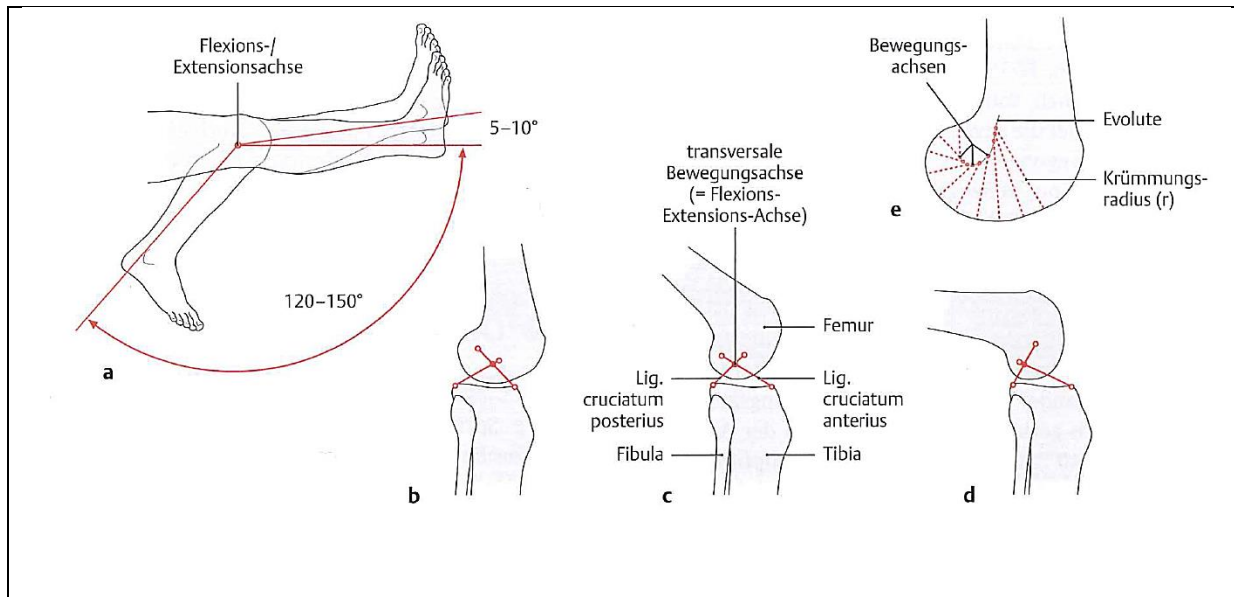


Figure 7-6 Flexion and extension in the knee joint. a: Range of motion of flexion and extension of the human leg. b-d: Intersection points of the cruciate ligaments and the collateral ligaments for different joint angles (lateral view). e: During flexion, the axis of motion moves along a curve (involute). Here, the distance of the axis of motion to the instantaneous articular surface corresponds to the radius of curvature of the femoral condyle. Taken from Schünke (2013), page 303.

7.1.4.2 Rotation

Rotation of the lower leg can only occur with a flexed leg position, whereby the maximum possible rotation increases with the angle of flexion. It is generally assumed in the literature that the greatest rotations can be achieved at a flexion of 90° (Almquist et al. 2002; Kapandji and Koebke 2006). Rohen and Lütjen-Drecoll (2006), however, claim that this is the case at a flexion of 50°. The maximum external rotation is greater than the maximum internal rotation (Seering et al. 1980). At 90° knee angle, maximal external rotation is 30-40° and maximal internal rotation is 10° (Schünke 2013). However, the literature does not agree on the exact figures. For example, Fick (in (Kapandji and Koebke 2006)) gives an internal rotation of 30° at 90° knee angle. In the study by (Neuhofer et al. 2014), the maximum rotation of the tibia was 18° (average 12.5°) inward and 17° (average 9.1°) outward. In addition to the degree of flexion of the knee, there are other factors that have an influence on the ability of the knee to rotate. The axis of rotation is not congruent with the central axis of the joint but is displaced medially. As a result, the lateral condyle has a path of motion almost twice as long as the medial condyle.

The collateral and cruciate ligaments play a significant role in limiting rotation.

During external rotation, the collateral ligaments wrap around the proximal end of the tibia, slowing rotation (Figure 7-7 right). The cruciate ligaments detach from each other during this process.

During internal rotation, the two cruciate ligaments become entangled, slowing the motion (Figure 7-7 left). (Kapandji and Koebke 2006)

A more detailed literature review on the relationship of tibial rotation as a function of moment about the tibia is provided in Table 7-1 (see page 7-248).

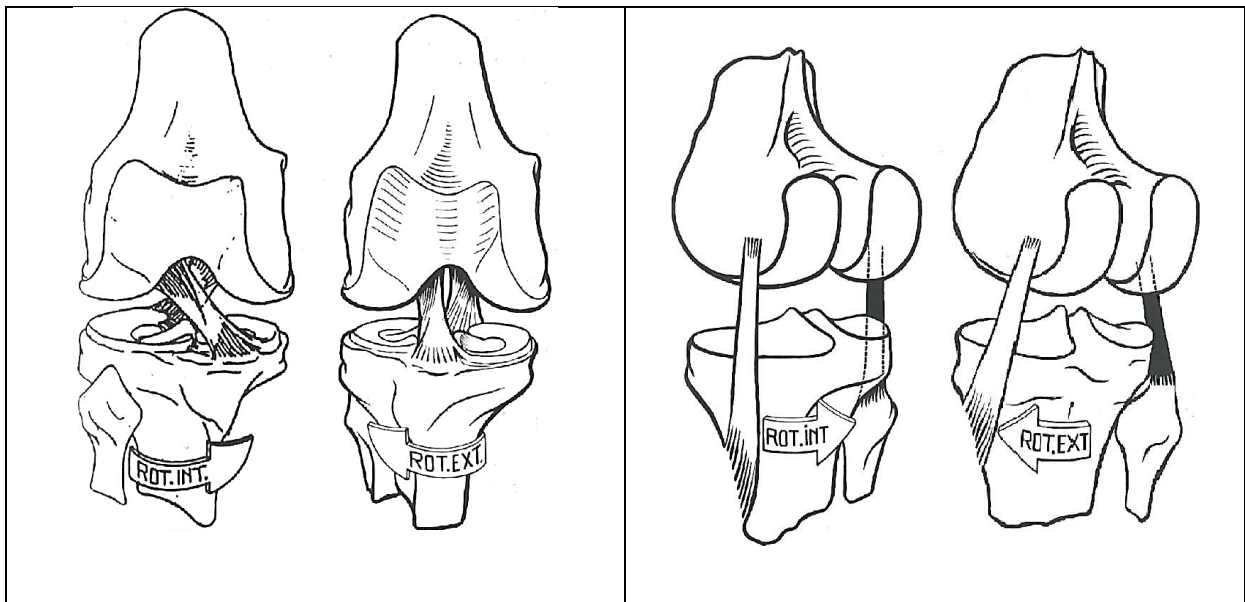


Figure 7-7 Behaviour of the cruciate (left) and collateral (right) ligaments during internal and external rotation of the knee joint. The femur is drawn unnaturally far from the tibia for the purpose of illustration. Taken from Kapandji and Koebke (2006), page 127 and 129.

Factors influencing knee rotation

Knee rotation depends on the following factors in addition to the flexion angle described in chapter 7.1.4.1:

Ligament structures

As described above, the cruciate and collateral ligaments limit the rotation of the knee. However, not only do their finite length and extensibility prevent further rotation but also twisting of the ligaments ensures that axial compression between the condyles and the menisci increases, resulting in an increase in stiffness to rotation (Kapandji and Koebke 2006).

Stiffness of the knee

The rotational range of motion of the knee is closely related to the stiffness of the knee with respect to tibial rotation. As mentioned earlier, stiffness of the knee is related to gender, among other factors. This is thought to be due to hormonal differences (Branch et al. 2010). This could be confirmed by Shultz et al. (2011) but only with negligible influence.

Louie and Mote (1987) were able to demonstrate the increase in stiffness due to muscle activations of individual thigh muscles.

In general, the stiffness of the knee increases with increasing rotation (see Figure 7-8). However, it can be roughly divided into two ranges. For small rotations it is 0.1-0.7 Nm/° (primary stiffness) (Markolf et al. 1976), for larger rotations, it is 2.2-2.8 Nm/° (secondary stiffness) (Louie and Mote 1987).

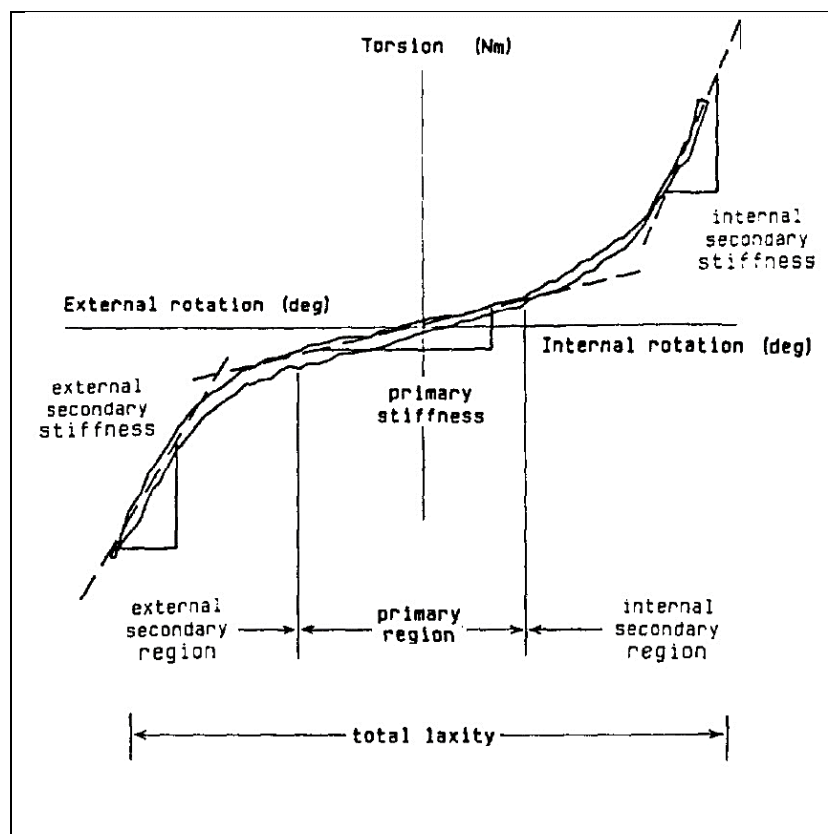


Figure 7-8 Qualitative progression of the moment to be applied for the internal and external rotation of the tibia. The stiffness of the knee increases with increasing rotation and can be divided into two approximately linear ranges (primary and secondary stiffness). The hysteresis that occurs when the leg is rotated back can also be seen. Taken and adapted from (Louie and Mote 1987), page 294.

Gender

Females can rotate the tibia 10-40% further than males (Mouton et al. 2012; Shultz et al. 2007b; Shultz et al. 2011; Park et al. 2008; Hsu et al. 2006; Branch et al. 2010; Almquist et al. 2013). This is likely due to lower stiffness of the female knee at lower moments (Schmitz et al. 2008).

Axial compression and body weight

As axial compression increases, rotational freedom decreases (Louie and Mote 1987; Shultz et al. 2007a; Markolf et al. 1981). Thus, higher body weight decreases rotational freedom (Mouton et al. 2012).

Musculature

Depending on which muscle of the thigh is tightened, at a knee angle of 90° the stiffness of the knee increases compared to the tibial rotation, by 25 - 361% (Louie and Mote 1987).

Cruciate Ligament Injuries

Branch et al. (2010) demonstrated in their study that patients with anterior cruciate ligament injury, compared to healthy individuals, have greater internal rotational freedom (20.6° versus 11.4°) and decreased external rotational freedom (16.7° versus 26.6°) in the knee.

7.2 Review of Studies Investigating Internal and External Rotation of the Tibia

Table 7-1 Studies investigating internal and external rotation of the tibia. Given are the maximal applied torques for the maximal rotation in different knee angles and hip angles. N states the number of samples/test subjects included in the study.

Nr.	Study	Knee angle [°]	Hip angle [°]	Torque applied at max internal rotation [Nm]	Max internal rotation [°]	Torque applied at max external rotation [Nm]	Max external rotation [°]	N	Notes
1	(Lorbach et al. 2009b)	--	--	5 10 15	22,1 ± 8,0 31,7 ± 9,8 39,2 ± 8,8	5 10 15	20,3 ± 6,9 30,9 ± 9,5 41,0 ± 12,1	20	Cadaver study (N=20) and use of the "Rotameters" (Device for clamping the foot)
2		--	--	5 10 15	18,9 ± 8,5 24,7 ± 9,4 27,9 ± 8,4	5 10 15	17,3 ± 6,9 22,5 ± 8,0 26,8 ± 8,8		Results of the "Knee-Nav" system (three infrared cameras tracking bone pins), which was simultaneously used with the Rotameter for verification (see no.1). Results are estimated to be more accurate than results from no.1.
3	(Almquist et al. 2002)	90	Not mentioned seating participants	3 6 9	11 ± 4 21 ± 6 30 ± 9	3 6 9	18 ± 6 27 ± 6 36 ± 7	5	Use of a device called „Rottometers“ (a chair which allows a fixation of the leg)
4		60		3 6 9	11 ± 5 15 ± 9 31 ± 3	3 6 9	16 ± 6 25 ± 5 34 ± 5		
5		90		3 6 9	6 ± 3 10 ± 3 13 ± 5	3 6 9	13 ± 7 16 ± 8 19 ± 8		
6		60		3 6 9	6 ± 5 10 ± 4 13 ± 4	3 6 9	6 ± 4 12 ± 4 15 ± 6		
7	(Louie and Mote 1987)	90	Not mentioned seating participants	17,1 *	17,2 *	18,7 *	25,4*	4	* each line corresponds to a test subject. Rotating the leg up to the comfort limit of the test subject. The values listed are for relaxed muscles . Experiments have also been carried out in which individual muscles in the leg were tensed. For active muscles, the maximum angles decreased and the tolerable moments increased. In addition, tests were carried out at a knee angle of 10 ° with the result of lower rotations and lower tolerable moments.
				21,5*	14,1*	26*	30,4*		
				19,6*	9,4*	22*	22,8*		
				24,9*	12,7*	24,6*	18,2*		
8		10		14,2*	12*	14,4*	13,1*		
				21,5*	13*	20,5*	13,3*		
				21*	4,9*	25,8*	6,3*		
		-*	-*	-*	-*				
9	(Mouton et al. 2012)	30	0 (laying on stomach)	5 10	23,2 ± 5,0 (f) 16,8 ± 3,7 (m)	5 10	35,6 ± 4,5 (f) 25,0 ± 5,9 (m)	60 (35 m / 25 f)	Use of a new version of the "Rotameters" (see no. 1/2). Results of this study: Larger rotations possible for woman compared to men. Influence of body weight.

APPENDIX

					39,4 ± 6,3 (f) 31,2 ± 4,8 (m)		53,0 ± 6,3 (f) 40,0 ± 7,8 (m)		
10				5	23,3 ± 4,7 (f) 18,4 ± 8,4 (m)	5	34,3 ± 6,4 (f) 23,9 ± 6,0 (m)	23 (19 m / 4 f)	Patients with non-contact-ACL-injuries. Results: No significant differences between injured and uninjured.
				10	41,6 ± 3,4 (f) 32,4 ± 6,3 (m)	10	52,5 ± 7,4 (f) 38,6 ± 7,6 (m)		
11	(Shultz et al. 2007a)	20	Not mentioned.	5	9,9 ± 4,5	5	13,6 ± 3,8	20 (10 m / 10 f)	Use of the "Vermont Knee Laxity Device" non-weight-bearing leg (NWB)
12			Laying on the back		4,0 ± 1,8		7,0 ± 3,5		Axial load on the foot = 40% of body weight (WB = weight bearing) Results: decrease of maximal rotation for WB-scenarios
13	(Shultz et al. 2007b)	20	Not mentioned.	5	11,8 ± 4,8 (f) 8,9 ± 2,5 (m)	5	15,7 ± 3,3 (f) 11,3 ± 3,5 (m)	10 m / 10 f	Use of the "Vermont Knee Laxity Device" non-weight-bearing (NWB)
14			Laying on the back		4,6 ± 1,9 (f) 3,0 ± 1,1 (m)		9,0 ± 2,8 (f) 4,5 ± 2,2 (m)		Axial load on the foot = 40% of body weight (WB = weight bearing) Results: significant differences for different genders with respect to internal-external rotation: f>m (50 – 60 % WB, 25 - 30% NWB)
15	(Shultz et al. 2011)	20	Not mentioned.	5	10.6±4.7 (f) 8.9±4.1 (m)	5	15.5±4.5 (f) 12.4±3.6 (m)	64 f / 43 m	Use of the "Vermont Knee Laxity Device" without axial load. (T1): During menstruation -estimated time with minimal anterior knee laxity
16			Laying on the back.		10.8±5.8 (f) 8.7±4.4 (m)		16.2±4.8 (f) 12.4±3.5 (m)		(T2): During the luteal phase of the menstrual cycle – estimated time with maximal anterior knee laxity. Results: - Influence of the gender: greater internal-external rotation for females. - negligible influence of the menstrual cycle. - menstrual cycle has influence on genu recurvatum, general joint laxity and anterior knee laxity.
17	(Hsu et al. 2006)	15	--	5	17.9 (f) 13.5 (m)	5	Ca. 22 (f)* Ca. 18 (m)*	38 f / 44 m	Cadaver study * value manually read from graph. - no value and no graph given
18		30		5	20.6 (f) 15.1 (m)	5	- -		Results: significant differences between the genders with respect to internal-external rotation: f>m (25 – 30 %). Lower joint stiffness for women.
19	(Park et al. 2008)	60	85	7	25,3 ± 6,4 (f) 19.3 ± 3,7 (m)	7	17,6 ± 3,9 (f) 16,4 ± 2,6 (m)	10 m / 10 f	Load applied by servo motor
20					18,5 ± 3,24 (m) 13,8 ± 4,17 (f)		22,2 ± 3,95 (m) 15,7 ± 3,71 (f)		Continuation of the experiment from no. 19. The moment at which the test person interrupted the rotation is give, unfortunately without specifying the rotational angle.
21	(Seering et al. 1980)	0	--	33 - 42	19	34 - 47	20	2	Cadaver study with two right legs.
22		30	--	13 - 16	19	42 - 44	20		
23	(Branch et al., 2010) (+ERRATUM)	--	Not mentioned.	5,65	11,4 ± 6,2	5,65	26,6 ± 4,9	14 (10 m / 4 f)	Use of an in-house developed "Custom Robotic Knee Testing System". Group without ACL-injury.

APPENDIX

24			Laying on the back	5,65	20,6 ± 5,7	5,65	16,7 ± 3,1	79 (51 m / 28 f)	Group with ACL-injury. Results: Larger internal rotation possible in comparison to uninjured. Less external rotation possible in comparison to uninjured.
25				5,65	16,8 ± 6,8 (m) 20,9 ± 6,9 (f)	5,65	13,4 ± 4,9 (m) 21,1 ± 7,0 (f)	93 (61 m / 32 f)	Differences between genders (ACL-injured and uninjured in the same group) Results: Larger rotations possible for woman compared to men.
26	(Eiba 2014)	0	-20	5 10 15 20	2,9 8,3 11,5 13	5 10 15 20	6,6 10 12,3 14,1	--	<p>Experiment on the leg surrogate of the Professorship of Sport Equipment and Materials (TUM) as part of a master's thesis. It enables external loads to be applied via a ski to an artificial leg with a knee that is instrumented with force and length change sensors. It is also possible to adjust muscle strength.</p> <p>Criticism of the study: It is not clear from the manuscript which muscle forces were set at the beginning of a test.</p> <p>Results related to tibial rotation: - the knee angle and the applied moment have an influence on the max. Rotations. - The ratio of the max. Internal rotation / max. External rotation depends on the knee angle. - The application of external loads also changes the muscular strength of the leg muscles. With individual muscles, the muscle strength increased, depending on the type of rotation and knee angle, by almost twice the original strength (which is unfortunately not mentioned).</p>
27		15		5 10 15 20	6,3 11,9 15,6 --	5 10 15 20	3,6 7,1 9,7 --		
28		30		5 10 15 20	8,5 14,5 -- --	5 10 15 20	6,3 10,1 12,7 15,3		
29		45		5 10 15 20	3,1 7,1 11 13,2	5 10 15 20	3,5 6,4 9,1 10,8		
30		60		5 10 15 20	1,7 4,1 5 6,9	5 10 15 20	1,9 6,1 8,6 11,4		
31		0	0	5 10 15 20	9,2 14,4 -- --	5 10 15 20	5 7,4 10,3 --		
32		15		5 10 15 20	0,7 6,6 10,2 11,4	5 10 15 20	3,6 7,2 9,5 11		
33		30		5 10 15 20	2,5 8,8 13,4 --	5 10 15 20	3,6 7,2 10,6 13,3		
34		45		5 10 15 20	5 9,9 13,2 --	5 10 15 20	3,2 6,4 9,1 11,6		
35		60		5 10 15 20	2,2 4,7 6,5 8,6	5 10 15 20	4 6,2 9 10,9		
36		0	20	5 10 15	3,8 9,1 12,1	5 10 15	4,8 8,3 10,5		

APPENDIX

				20	12,6	20	12,5		
37		15		5	8,5	5	3,1		
				10	14,1	10	7,1		
				15	--	15	10		
				20	--	20	11,7		
38		30		5	0,7	5	1,7		
				10	6,3	10	4,2		
				15	9,3	15	6,6		
				20	12,5	20	8,9		
39		45		5	0,4	5	3		
				10	5,8	10	4,8		
				15	9,9	15	7,5		
				20	12	20	9,7		
40		60		5	1,5	5	1,8		
				10	4,3	10	4,7		
				15	6,8	15	7,1		
				20	9,3	20	9,1		
41		90		5	0,8	5	8		
				10	0,2	10	9,2		
				15	4,0	15	10		
				20	--	20	11,5		
42	(Neuhofer et al. 2014)	90	Not mentioned. seating participants	End-Feel	32,2* 12,5**	End-Feel	37* 9,1**	14 (6 m / 8 f)	Interdisciplinary project work at the Professorship of Sports Equipment and Materials (TUM). Subjects sat on a chair suspended in the air. The foot was in a ski boot that was connected to a ski. A torque was applied via the ski to the leg, which had a knee angle of 90 °. The twisting of the ski boot and the tibia was evaluated using a marker camera system. Results: - Larger angles of rotation for women than for men (despite lower torques) - Results for internal rotation are too high, which the authors attribute to the freedom of movement of the foot in the ski boot. - Larger torques are possible during external rotation. * Rotational movements of the lower leg in relation to the thigh (ski boot rotation) ** Rotation in the knee joint

APPENDIX

Table 7-2 A selection of studies to investigate the dependence of the range of rotation of the tibia on the applied moment around the tibial longitudinal axis in different knee angle positions.

Nr.	Study	Knee angle [°]	Hip angle [°]	Torque [Nm]	Total tibia rotation [°]	n	Notes	
43	(Haughom et al. 2012)	15	No information. Person were laying on the back in the MRI	3,35	14,1 ± 4 (m)	16 (8 m/8 f)	Test in a MRI with 44 N axial load on the foot. Significant difference m/f: f>m	
					16,3 ± 5,7 (f)			
44					15,7 ± 5,1 (m)	11 (5 m/6 f)		Patients with previous ACL tear (complete). Significant difference to uninjured patients. Increased tibial rotation after ACL injury
					17,4 ± 4,2 (f)			
45	(Almquist et al. 2013)	90	No information. Seated test person	6	59 ± 11 (f)*	60 m / 60 f	Experiment using the "Rottameter" (compare no. 2-6). * Both the right and left knee were examined. No significant difference could be found. This table shows the values of the knee with the greater deflection. Results: - There was no significant influence of the knee angle with regard to the total internal external rotation at 6 Nm, 9 Nm and end-feel (deflection until the test subject thinks he has achieved the maximum painless rotation). - Distribution internal-external rotation: 40-44% to 56-60% (at all angles and moments) - No significant influence of age (male / female) on the rotation at all angles and moments - Significant difference between man and woman across all age groups, knee angles and moments (f> m: 10-20%)	
					52 ± 8 (m)*			
					77 ± 13 (f)*			
					68 ± 8 (m)*			
				9	73 ± 12 (f)*			
				End-Feel	65 ± 7 (m)*			
46		60		6	60 ± 13 (f)*			
				9	51 ± 9 (m)*			
				End-Feel	78 ± 14 (f)*			
					67 ± 8 (m)*			
					75 ± 13 (f)*			
					65 ± 9 (m)*			
47		30		6	57 ± 14 (f)*			
				9	44 ± 9 (m)*			
				End-Feel	78 ± 16 (f)*			
					63 ± 10 (m)*			
					77 ± 16 (f)*			
					62 ± 10 (m)*			
48		90		6	24 – 35 (f)		The author states that the "Rottameter" shows a linear, systematic error that is known. From this, the actual rotation between the tibia and femur can be calculated. The values listed here are calculated by the author for a knee angle of 90 °.	
				9	20 – 30 (m)			
				End-Feel	33 – 44 (f)			
					30 – 38 (m)			
					30 – 42 (f)			
					29 – 36 (m)			

APPENDIX

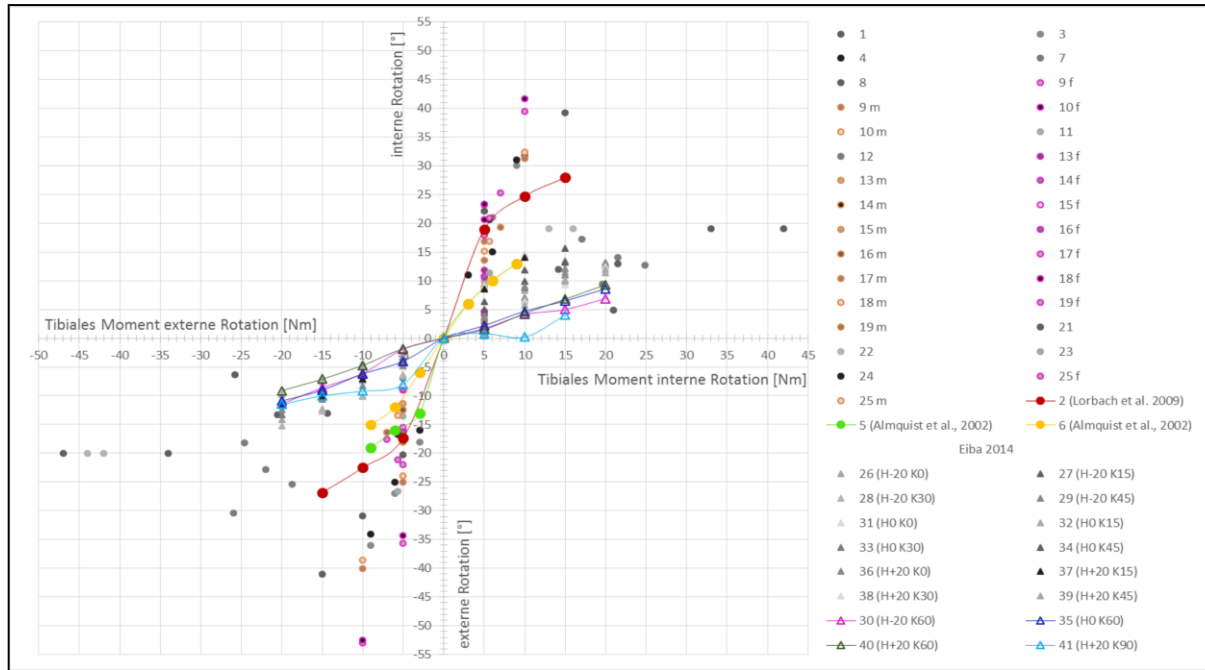


Figure 7-9 Relationship of applied torque on the tibia and the tibia rotation (rotation of tibia with respect to the femur). Each number is associated with a publication stated in Table 7-1.

7.3 Measuring ACL loads – An overview of methodologies

The injury mechanism studies reported in this dissertation mainly reference the publications of the group around Markolf and Washer (Markolf et al. 1981; Markolf et al. 1990; Wascher et al. 1993; Markolf et al. 2004; Markolf et al. 2008; Markolf et al. 2018). The results reported by this group are used to validate the surrogate (chapter 3.1) and the digital model (chapter 3.2). This deliberately ignores thousands of other publications about ACL and ACL loading and needs explanation. There are two main reasons:

1. **The methodology** used by Markolf, Washer, and group: The ACL and all other ligaments are internal structures of the knee and, therefore, are not observable from the outside. Moreover, instrumenting the ACL with any kind of sensor is a serious medical intervention and is not to be done with healthy persons. Any instrumentation of the ligament results in a cut or modification of the ligament and other structures in the preparation process, and therefore, in an alteration of the properties of the structure as well as the loss of internal “pre-tension” of the structures. The methodology used by Markolf, Washer, and group allows the measurement of ACL loading at the insertion site of the ACL with minimal damage to other structures of the knee. The following section will discuss in short the three main principles to measure ACL loading reported in the literature and in detail the methodology used by Markolf, Washer, and group.
2. **Number of publications using the same methodology:** The multiple publications of Markolf, Washer, and group allow the comparison of results for all relevant parameters such as muscle activation, knee angle, internal and external torque, varus and valgus moments and in a large range of the respective parameter values. This increases the internal validity (and as a result also the external validity) of the results of this dissertation, as the different scenarios are not validated against different methodologies.

Three main principles to measure ACL loading are reported in the literature:

- Principle of superposition
- Force and elongation measurement directly on the ligament
- Force measurement at the insertion site of the ligament

Principle of superposition

In superposition, a position-controlled robot executes a defined movement and at the same time registers the forces and moments needed for this (Höher et al. 1999; Li et al. 1999; Li et al. 2002; Seon et al. 2010). The first measurement is performed with an intact leg. In repeated measurements, selected structures are successively cut. Based on the difference in the results, conclusions can be drawn about the force distribution in the individual structures. This method, though often used, has serious limitations. It is unclear if the assumption is valid that the loss in loads represents the loads transmitted through the cut structure. More likely the knee settles into a new equilibrium and the remaining structures compensate for some of the loads previously transmitted through the cut structure.

Force and length recording directly on the ligament

Force or elongation sensors can be applied directly to the ligament by clamping or sewing or pins. Three different sensor types are reported in the literature - the "buckle transducer" (Gertel et al. 1993; Wijdicks et al. 2009; Ahmed et al. 1992) shown in Figure 7-10, the "reluctance transducer DVRTs" (Fleming et al. 2001; Harfe et al. 1998) shown in Figure 7-11 and the " Ω -transducer" (Dürselen et al. 1995) shown in Figure 7-12. Limitations are: In the process, surrounding ligaments or other knee structures are partially damaged. Depending on the sensor type and the location of the application, only a small region/section of the ligament is instrumented.

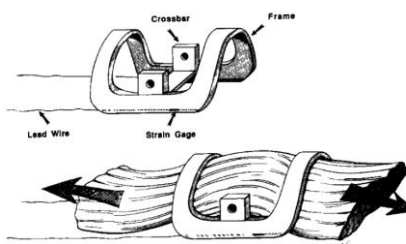


Figure 7-10 Buckle Transducer application to a ligament. Original source Gertel et al. (1993), taken with permission

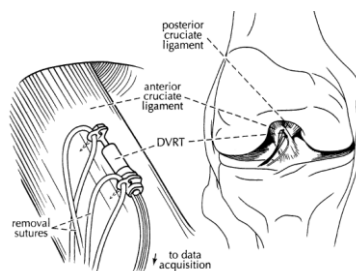


Figure 7-11 DVRT Sensor applied to the ACL. Original source Beynon and Fleming (1998), taken with permission.



Figure 7-12 Two Ω -transducers. One attached to each bundle of the ACL. Original source Dürselen et al. (1995), taken with permission.

As the ACL is not loaded homogenously the recording of an accurate loading condition for the whole structure is limited, especially for the DVRT Sensor (see example in Figure 7-13). Some of these sensors have been used in-vivo (Beynon and Fleming 1998; Holden et al. 1994).



Figure 7-13 Exemplary measurement using the DVTS. Observable are local strain differences in the structures. Picture taken with permission from Lehner (2007)

Force measurement at the insertion site of the ligament

This procedure includes the implementation of the load cell directly under the attachment point of the ligaments (Lehner 2007; Wascher et al. 1993; Markolf et al. 1995; Markolf et al. 2004; Markolf et al. 1990). This allows the registration of the tension of the entire ligament. Separate instrumentation of the individual ACL bundles has not been reported.

In 1990, Keith Markolf was the first to present results from an in-vitro study in which he attached a load cell on ACLs of human cadavers. In the preparation process, the bone base of the cruciate ligament on the tibia is isolated with a core drill and the resulting bone cylinder is attached to the load cell (Figure 7-14). Disadvantages of the measurement method become apparent when the knee joint is rotated. Forces not acting along the axis of the load cell can cause the isolated segment of bone to impact the surrounding bone wall and thus affect the measurement accuracy (Markolf et al. 1990). To circumvent this issue, Regenfelder (2008) copied the Markolf system but used a more rigid connection from the cruciate ligament to the sensor via a metal tube.

DIRECT MEASUREMENT OF RESULTANT FORCES IN THE ANTERIOR CRUCIATE LIGAMENT

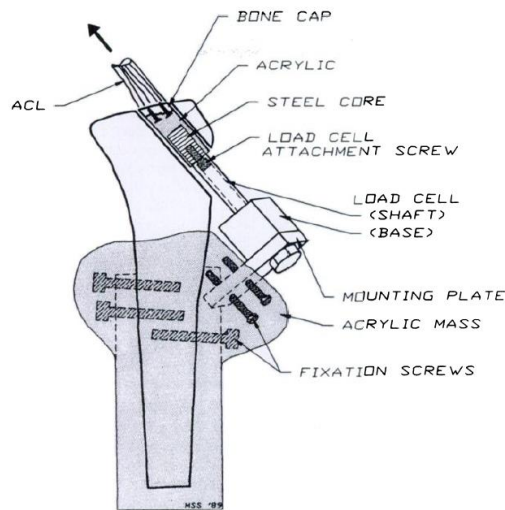


Figure 7-14 Method Markolf and his group used to measure ACL loading. the load cell is firmly attached to the milled bone cylinder with the ACL attached to and then fixed to the tibia. Original source Markolf et al. (1990).

Sensor principle used in the surrogate

The measurement principle of the surrogate uses a load cell at the insertion site of the ligaments (Figure 7-15). Therefore, the results are best comparable to the results of studies using the Markolf-system.



Figure 7-15 Left: Load cell of the surrogate, based on strain gauges to measure ACL loads. Right: showing the load cell in the tibia head with the ACL implemented.

7.4 RMSE and NRMSE

The root mean square error (RMSE) and the normalized root mean square error (NRMSE) are used to calculate the difference between two measurement series. Both are based on the mean square error (MSE). The RMSE weights larger errors stronger and weights smaller errors (< 1) less than the MSE. As smaller errors are often seen as results from measurement artefacts, the RMSE is established widely.

$$MSE = \frac{\sum(x_{1,i} - x_{2,i})}{n} \quad 7-1$$

$$RMSE = \sqrt{\frac{\sum(x_{1,i} - x_{2,i})^2}{n}} \quad 7-2$$

$$NRMSE = \frac{100}{x_{2,max} - x_{2,min}} * RMSE [\%] \quad 7-3$$

Where $x_{1,i}$ is the value of measurement 1 at measurement point i and $x_{2,i}$ is the value of measurement 2 at measurement point i . n is the total number of measurement points. Usually, measurement 2 represents the values of the reference system and measurement 1 the values of the system to be validated against the reference system. The unit of the RMSE is the same as the unit of the measured signal.

7.5 Surrogate Study – Complete Measurement Results

7.5.1 Results of Each Individual Measurement

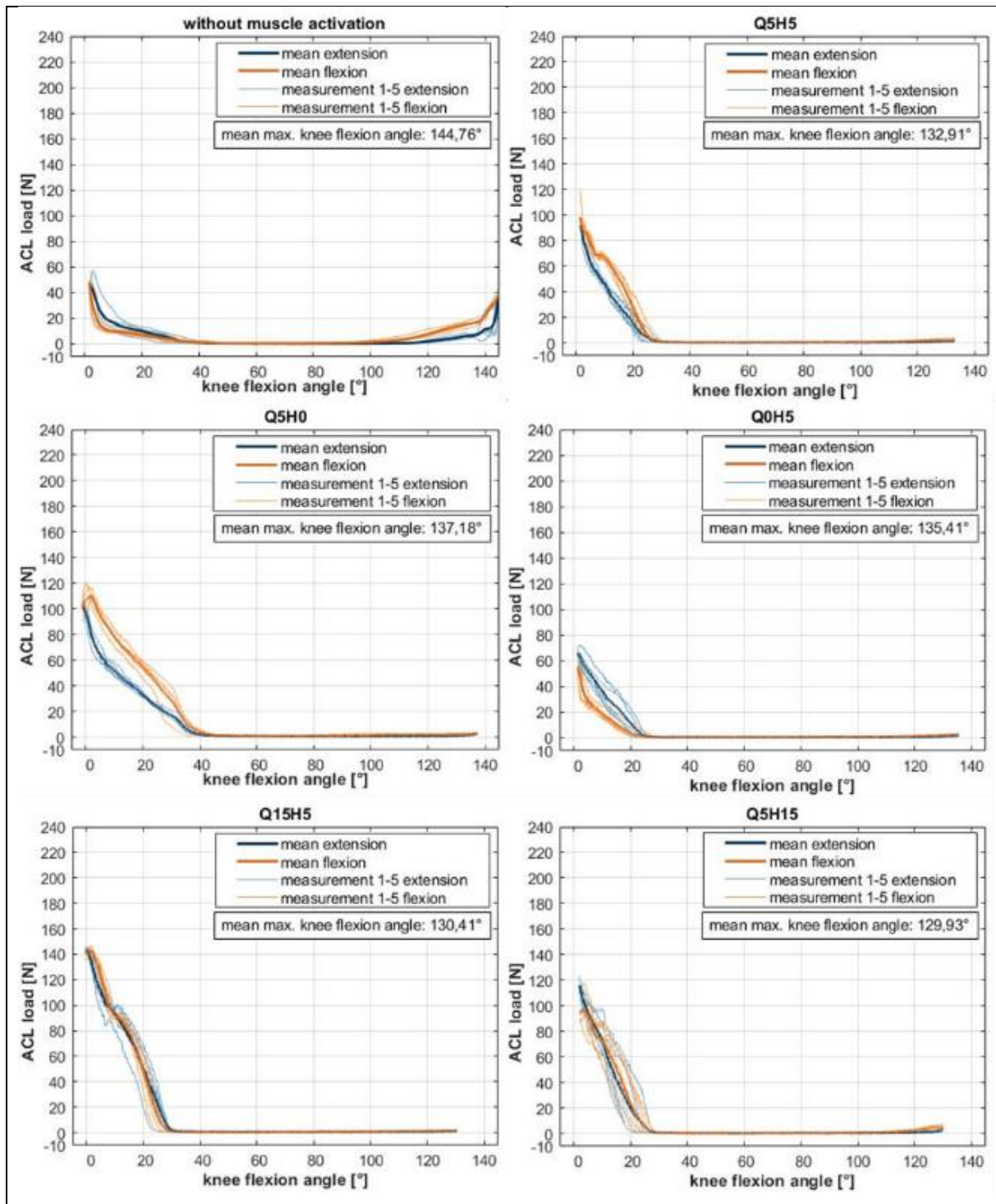


Figure 7-16 Results for the test set up: Preload ACL 50N, preload MCL 45N, hip angle -20°. Each measurement was repeated five times.

APPENDIX

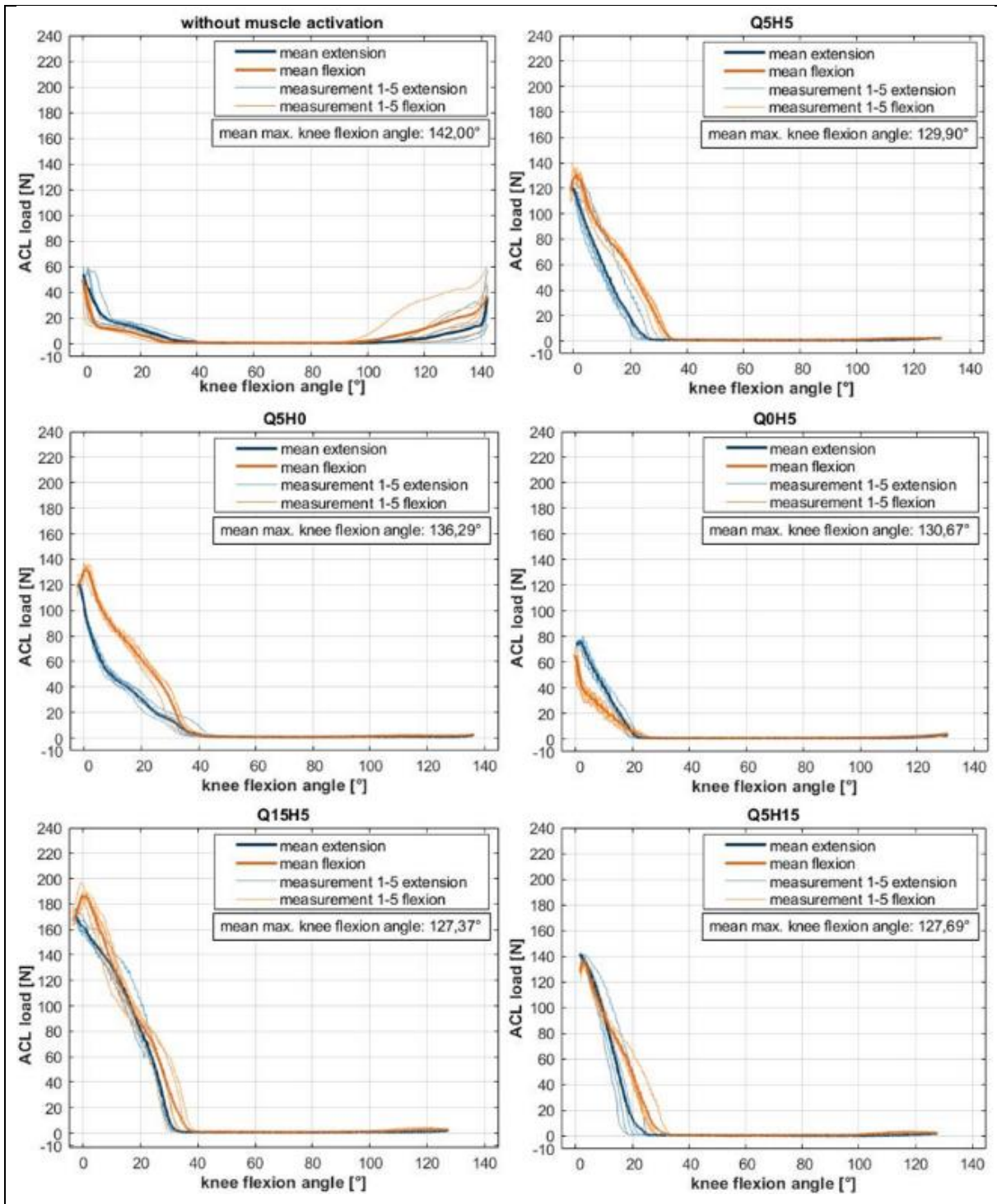


Figure 7-17 Results for the test set up: Preload ACL 50N, preload MCL 45N, hip angle +20°. Each measurement was repeated five times.

APPENDIX

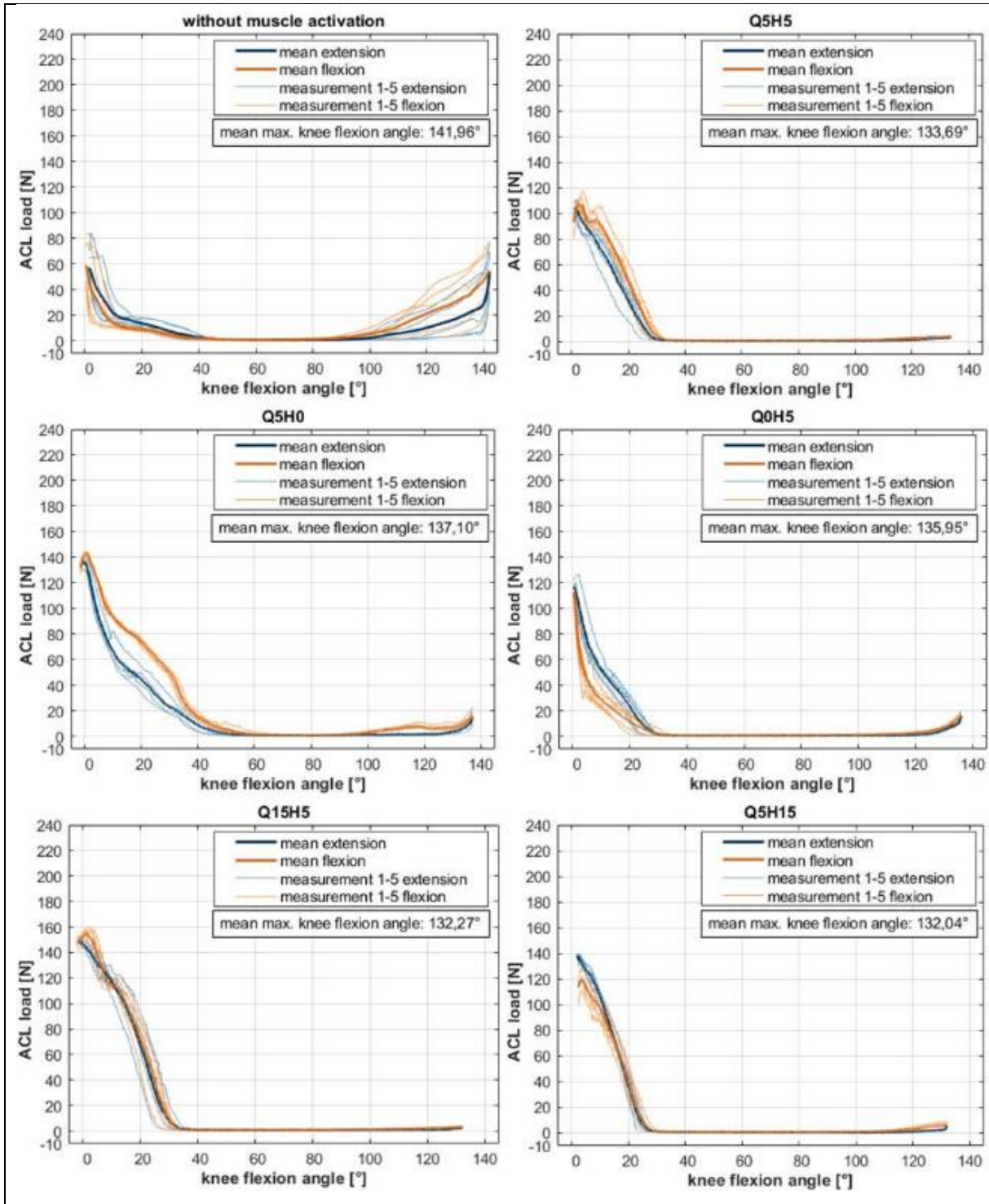


Figure 7-18 Results for the test set up: Preload ACL 85N, preload MCL 75N, hip angle -20°. Each measurement was repeated five times.

APPENDIX

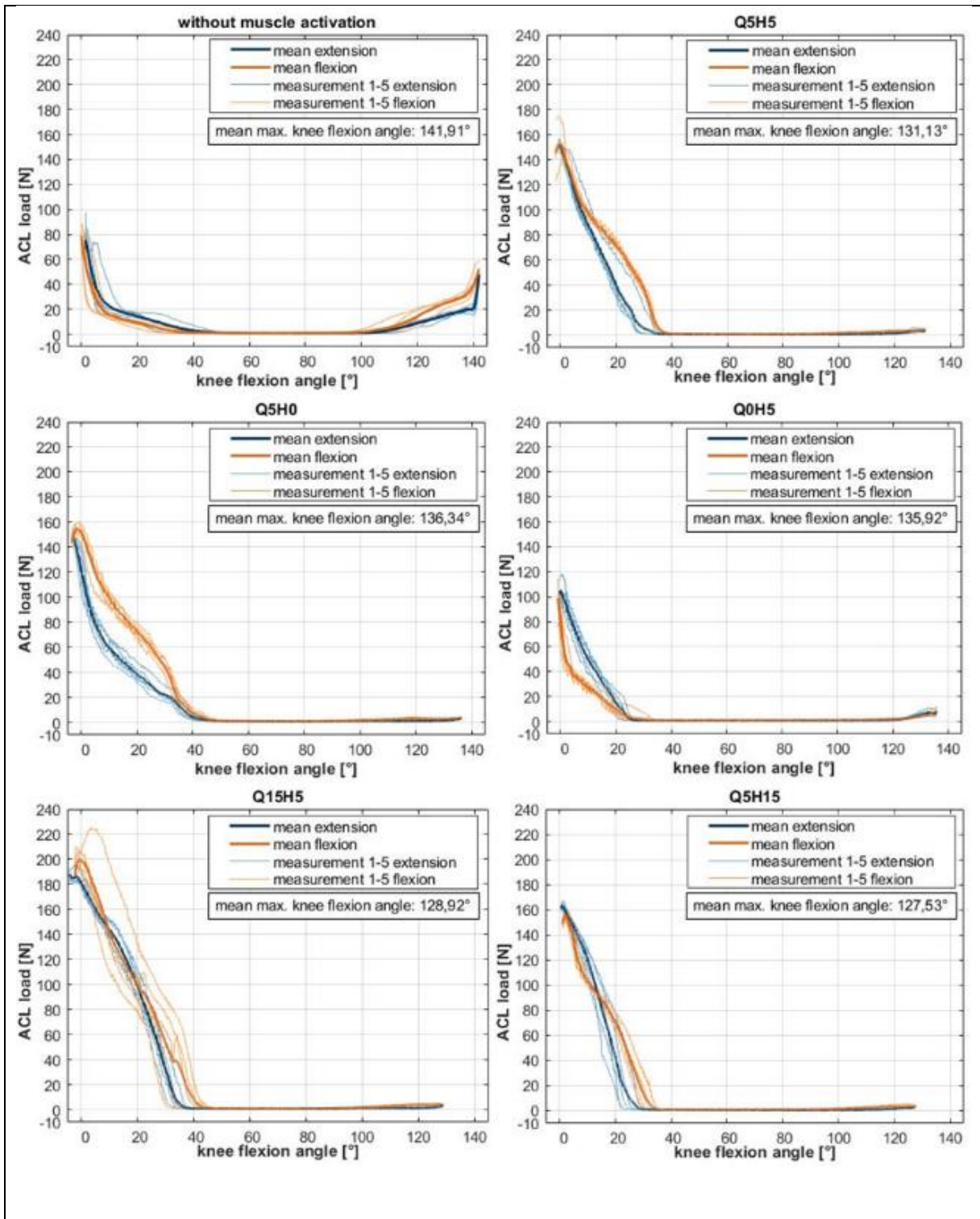


Figure 7-19 Results for the test set up: Preload ACL 85N, preload MCL 75N, hip angle +20°. Each measurement was repeated five times.

7.5.2 Further Results and Statistics of the Investigation

7.5.2.1 Setting: Hip Angle -20°; Preload ACL 50 N; Preload MCL 45 N

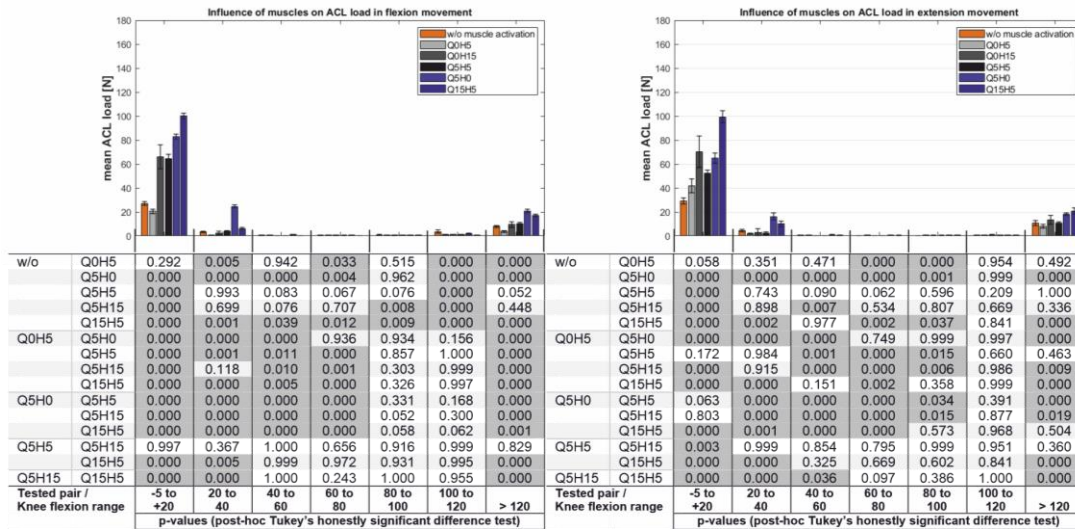


Figure 7-20 Mean ACL loads for different knee flexion ranges for different muscle activation for the setting -20° hip flexion, pre-loads: ACL 50 N, MCL 45 N. Each mean value is calculated from the means of the five repetitions of each setup. For each knee flexion range, the muscle activation was tested with one-way-ANOVA and a post-hoc significance test. The p-values are given below each set of bars. Dark grey fields are significant ($p < 0.05$). Left: results for the flexion movement. Right: results for the extension movement.

FLEXION MOVEMENT

Table 7-3 Results of Turkey's honestly significant difference test (post-hoc) for the setting hip angle -20°, pre-loads: ACL 50N, MCL 45 N, flexion movement, testing for significant differences between the mean values of ACL loads in the pre-defined knee flexion ranges. The mean values again reflect the means of the five repetitions for each muscle setting. Dark grey fields are significant ($p < 0.05$).

group 1	group 2	Flexion movement -5 to +20				Flexion movement +20 to +40			
		lower limit 95% CI	mean of groups difference	upper limit 95% CI	p	lower limit 95% CI	mean of groups difference	upper limit 95% CI	p
w/o	Q0H5	-7.8	0.0	7.8	1.000	-1.8	0.0	1.8	1.000
w/o	Q5H0	-70.3	-62.5	-54.7	0.000	-22.8	-21.0	-19.2	0.000
w/o	Q5H5	-45.7	-37.9	-30.1	0.000	-2.2	-0.4	1.4	0.981
w/o	Q5H15	-45.7	-38.0	-30.2	0.000	-1.0	0.9	2.7	0.679
w/o	Q15H5	-80.3	-72.5	-64.8	0.000	-4.8	-3.0	-1.2	0.000
Q0H5	Q5H0	-70.3	-62.5	-54.7	0.000	-22.8	-21.0	-19.2	0.000
Q0H5	Q5H5	-45.7	-37.9	-30.1	0.000	-2.2	-0.4	1.4	0.981
Q0H5	Q5H15	-45.7	-38.0	-30.2	0.000	-1.0	0.9	2.7	0.679
Q0H5	Q15H5	-80.3	-72.5	-64.8	0.000	-4.8	-3.0	-1.2	0.000
Q5H0	Q5H5	16.8	24.6	32.4	0.000	18.8	20.6	22.4	0.000
Q5H0	Q5H15	16.7	24.5	32.3	0.000	20.0	21.9	23.7	0.000
Q5H0	Q15H5	-17.9	-10.1	-2.3	0.006	16.1	18.0	19.8	0.000
Q5H5	Q5H15	-7.9	-0.1	7.7	1.000	-0.5	1.3	3.1	0.288
Q5H5	Q15H5	-42.4	-34.7	-26.9	0.000	-4.4	-2.6	-0.8	0.002
Q5H15	Q15H5	-42.4	-34.6	-26.8	0.000	-5.7	-3.9	-2.1	0.000

APPENDIX

Table 7-3 continued

group 1	group 2	Flexion movement +40 to +60				Flexion movement +60 to +80			
		lower limit 95% CI	mean of groups difference	upper limit 95% CI	p	lower limit 95% CI	mean of groups difference	upper limit 95% CI	p
w/o	Q0H5	-0.1	0.0	0.1	1.000	-0.1	0.0	0.1	1.000
w/o	Q5H0	-0.6	-0.5	-0.4	0.000	-0.3	-0.2	-0.1	0.000
w/o	Q5H5	-0.1	0.1	0.2	0.818	-0.1	0.0	0.1	0.992
w/o	Q5H15	-0.1	0.0	0.2	0.891	-0.1	0.0	0.1	0.993
w/o	Q15H5	-0.1	0.1	0.2	0.669	0.0	0.0	0.1	0.632
Q0H5	Q5H0	-0.6	-0.5	-0.4	0.000	-0.3	-0.2	-0.1	0.000
Q0H5	Q5H5	-0.1	0.1	0.2	0.818	-0.1	0.0	0.1	0.992
Q0H5	Q5H15	-0.1	0.0	0.2	0.891	-0.1	0.0	0.1	0.993
Q0H5	Q15H5	-0.1	0.1	0.2	0.669	0.0	0.0	0.1	0.632
Q5H0	Q5H5	0.4	0.5	0.7	0.000	0.1	0.2	0.3	0.000
Q5H0	Q5H15	0.4	0.5	0.7	0.000	0.1	0.1	0.2	0.001
Q5H0	Q15H5	0.4	0.5	0.7	0.000	0.1	0.2	0.3	0.000
Q5H5	Q5H15	-0.1	0.0	0.1	1.000	-0.1	0.0	0.1	0.865
Q5H5	Q15H5	-0.1	0.0	0.1	1.000	-0.1	0.0	0.1	0.919
Q5H15	Q15H5	-0.1	0.0	0.2	0.998	0.0	0.1	0.2	0.316

group 1	group 2	Flexion movement +80 to +100				Flexion movement +100 to +120			
		lower limit 95% CI	mean of groups difference	upper limit 95% CI	p	lower limit 95% CI	mean of groups difference	upper limit 95% CI	p
w/o	Q0H5	-0.3	0.0	0.3	1.000	-1.3	0.0	1.3	1.000
w/o	Q5H0	-0.3	0.0	0.3	0.999	0.2	1.5	2.9	0.018
w/o	Q5H5	-0.1	0.1	0.4	0.609	1.0	2.4	3.7	0.000
w/o	Q5H15	-0.1	0.2	0.5	0.198	0.9	2.2	3.5	0.000
w/o	Q15H5	-0.1	0.2	0.5	0.248	1.2	2.5	3.9	0.000
Q0H5	Q5H0	-0.3	0.0	0.3	0.999	0.2	1.5	2.9	0.018
Q0H5	Q5H5	-0.1	0.1	0.4	0.609	1.0	2.4	3.7	0.000
Q0H5	Q5H15	-0.1	0.2	0.5	0.198	0.9	2.2	3.5	0.000
Q0H5	Q15H5	-0.1	0.2	0.5	0.248	1.2	2.5	3.9	0.000
Q5H0	Q5H5	-0.1	0.2	0.5	0.377	-0.5	0.8	2.2	0.436
Q5H0	Q5H15	0.0	0.3	0.6	0.094	-0.7	0.7	2.0	0.653
Q5H0	Q15H5	0.0	0.2	0.5	0.123	-0.3	1.0	2.3	0.229
Q5H5	Q5H15	-0.2	0.1	0.4	0.965	-1.5	-0.2	1.2	0.999
Q5H5	Q15H5	-0.2	0.1	0.4	0.984	-1.2	0.2	1.5	0.998
Q5H15	Q15H5	-0.3	0.0	0.3	1.000	-1.0	0.3	1.7	0.967

group 1	group 2	Flexion movement from +120 and plus			
		lower limit 95% CI	mean of groups difference	upper limit 95% CI	p
w/o	Q0H5	-4.2	0.0	4.2	1.000
w/o	Q5H0	6.9	11.1	15.4	0.000
w/o	Q5H5	6.8	11.0	15.3	0.000
w/o	Q5H15	3.3	7.5	11.7	0.000
w/o	Q15H5	7.4	11.6	15.9	0.000
Q0H5	Q5H0	6.9	11.1	15.4	0.000
Q0H5	Q5H5	6.8	11.0	15.3	0.000
Q0H5	Q5H15	3.3	7.5	11.7	0.000
Q0H5	Q15H5	7.4	11.6	15.9	0.000
Q5H0	Q5H5	-4.3	-0.1	4.2	1.000
Q5H0	Q5H15	-7.9	-3.6	0.6	0.125
Q5H0	Q15H5	-3.7	0.5	4.8	0.999
Q5H5	Q5H15	-7.8	-3.5	0.7	0.140
Q5H5	Q15H5	-3.6	0.6	4.8	0.997
Q5H15	Q15H5	-0.1	4.2	8.4	0.057

APPENDIX

EXTENSION MOVEMENT

Table 7-4 Results of Turkey's honestly significant difference test (post-hoc) for the setting hip angle -20°, pre-loads: ACL 50N, MCL 45 N, extension movement, testing for significant differences between the mean values of ACL loads in the pre-defined knee flexion ranges. The mean values again reflect the means of the five repetitions for each muscle setting. Dark grey fields are significant ($p < 0.05$).

group 1	group 2	Extension movement -5 to +20				Extension movement +20 to +40			
		lower limit 95% CI	mean of groups difference	upper limit 95% CI	p	lower limit 95% CI	mean of groups difference	upper limit 95% CI	p
w/o	Q0H5	-10.1	0.0	10.1	1.000	-3.3	0.0	3.3	1.000
w/o	Q5H0	-43.7	-33.6	-23.5	0.000	-14.2	-10.9	-7.6	0.000
w/o	Q5H5	-30.8	-20.7	-10.6	0.000	-1.6	1.7	5.0	0.598
w/o	Q5H15	-45.0	-34.9	-24.8	0.000	-1.3	2.0	5.3	0.453
w/o	Q15H5	-74.5	-64.4	-54.3	0.000	-8.0	-4.7	-1.4	0.003
Q0H5	Q5H0	-43.7	-33.6	-23.5	0.000	-14.2	-10.9	-7.6	0.000
Q0H5	Q5H5	-30.8	-20.7	-10.6	0.000	-1.6	1.7	5.0	0.598
Q0H5	Q5H15	-45.0	-34.9	-24.8	0.000	-1.3	2.0	5.3	0.453
Q0H5	Q15H5	-74.5	-64.4	-54.3	0.000	-8.0	-4.7	-1.4	0.003
Q5H0	Q5H5	2.8	12.9	23.0	0.007	9.3	12.6	15.9	0.000
Q5H0	Q5H15	-11.4	-1.3	8.8	0.998	9.5	12.8	16.1	0.000
Q5H0	Q15H5	-40.9	-30.8	-20.7	0.000	2.9	6.2	9.5	0.000
Q5H5	Q5H15	-24.3	-14.2	-4.1	0.003	-3.0	0.3	3.6	1.000
Q5H5	Q15H5	-53.9	-43.8	-33.7	0.000	-9.7	-6.4	-3.1	0.000
Q5H15	Q15H5	-39.6	-29.5	-19.4	0.000	-9.9	-6.6	-3.3	0.000

group 1	group 2	Extension movement +40 to +60				Extension movement +60 to +80			
		lower limit 95% CI	mean of groups difference	upper limit 95% CI	p	lower limit 95% CI	mean of groups difference	upper limit 95% CI	p
w/o	Q0H5	-0.1	0.0	0.1	1.000	-0.1	0.0	0.1	1.000
w/o	Q5H0	-0.6	-0.4	-0.3	0.000	-0.4	-0.3	-0.2	0.000
w/o	Q5H5	0.0	0.1	0.2	0.452	-0.2	-0.1	0.0	0.014
w/o	Q5H15	0.0	0.1	0.2	0.058	-0.2	-0.1	0.0	0.114
w/o	Q15H5	-0.1	0.0	0.1	1.000	-0.3	-0.2	-0.1	0.000
Q0H5	Q5H0	-0.6	-0.4	-0.3	0.000	-0.4	-0.3	-0.2	0.000
Q0H5	Q5H5	0.0	0.1	0.2	0.452	-0.2	-0.1	0.0	0.014
Q0H5	Q5H15	0.0	0.1	0.2	0.058	-0.2	-0.1	0.0	0.114
Q0H5	Q15H5	-0.1	0.0	0.1	1.000	-0.3	-0.2	-0.1	0.000
Q5H0	Q5H5	0.4	0.5	0.6	0.000	0.1	0.2	0.3	0.000
Q5H0	Q5H15	0.4	0.6	0.7	0.000	0.1	0.2	0.3	0.000
Q5H0	Q15H5	0.3	0.4	0.6	0.000	0.1	0.2	0.3	0.001
Q5H5	Q5H15	-0.1	0.0	0.2	0.849	-0.1	0.0	0.1	0.923
Q5H5	Q15H5	-0.2	-0.1	0.0	0.287	-0.2	-0.1	0.0	0.514
Q5H15	Q15H5	-0.3	-0.1	0.0	0.029	-0.2	-0.1	0.0	0.108

group 1	group 2	Extension movement +80 to +100				Extension movement +100 to +120			
		lower limit 95% CI	mean of groups difference	upper limit 95% CI	p	lower limit 95% CI	mean of groups difference	upper limit 95% CI	p
w/o	Q0H5	-0.1	0.0	0.1	1.000	-0.4	0.0	0.4	1.000
w/o	Q5H0	-0.4	-0.2	-0.1	0.000	-0.3	0.1	0.5	0.992
w/o	Q5H5	-0.2	-0.1	0.0	0.275	-0.1	0.3	0.7	0.259
w/o	Q5H15	-0.2	-0.1	0.1	0.505	-0.2	0.2	0.6	0.743
w/o	Q15H5	-0.3	-0.2	0.0	0.011	-0.3	0.2	0.6	0.833
Q0H5	Q5H0	-0.4	-0.2	-0.1	0.000	-0.3	0.1	0.5	0.978
Q0H5	Q5H5	-0.2	-0.1	0.0	0.275	-0.1	0.3	0.7	0.205
Q0H5	Q5H15	-0.2	-0.1	0.1	0.505	-0.2	0.2	0.6	0.661
Q0H5	Q15H5	-0.3	-0.2	0.0	0.011	-0.2	0.2	0.6	0.762
Q5H0	Q5H5	0.0	0.1	0.3	0.028	-0.2	0.2	0.6	0.570
Q5H0	Q5H15	0.0	0.2	0.3	0.010	-0.3	0.1	0.5	0.966
Q5H0	Q15H5	-0.1	0.1	0.2	0.485	-0.3	0.1	0.5	0.988
Q5H5	Q5H15	-0.1	0.0	0.2	0.998	-0.5	-0.1	0.3	0.951
Q5H5	Q15H5	-0.2	-0.1	0.1	0.637	-0.6	-0.1	0.3	0.901
Q5H15	Q15H5	-0.2	-0.1	0.0	0.380	-0.4	0.0	0.4	1.000

EXTENSION MOVEMENTTable 7-4 *continued*

group 1	group 2	Extension movement from +120 plus			
		lower limit 95% CI	mean of groups difference	upper limit 95% CI	p
w/o	Q0H5	-4.0	0.0	4.0	1.000
w/o	Q5H0	-0.2	3.7	7.7	0.075
w/o	Q5H5	-0.2	3.8	7.8	0.067
w/o	Q5H15	-2.3	1.7	5.6	0.779
w/o	Q15H5	-0.1	3.9	7.9	0.056
Q0H5	Q5H0	-0.2	3.7	7.7	0.075
Q0H5	Q5H5	-0.2	3.8	7.8	0.067
Q0H5	Q5H15	-2.3	1.7	5.6	0.779
Q0H5	Q15H5	-0.1	3.9	7.9	0.056
Q5H0	Q5H5	-3.9	0.1	4.0	1.000
Q5H0	Q5H15	-6.0	-2.0	1.9	0.610
Q5H0	Q15H5	-3.8	0.2	4.1	1.000
Q5H5	Q5H15	-6.1	-2.1	1.8	0.575
Q5H5	Q15H5	-3.9	0.1	4.1	1.000
Q5H15	Q15H5	-1.7	2.2	6.2	0.525

7.5.2.2 Setting: Hip Angle +20°; Preload ACL 50 N; Preload MCL 45 N

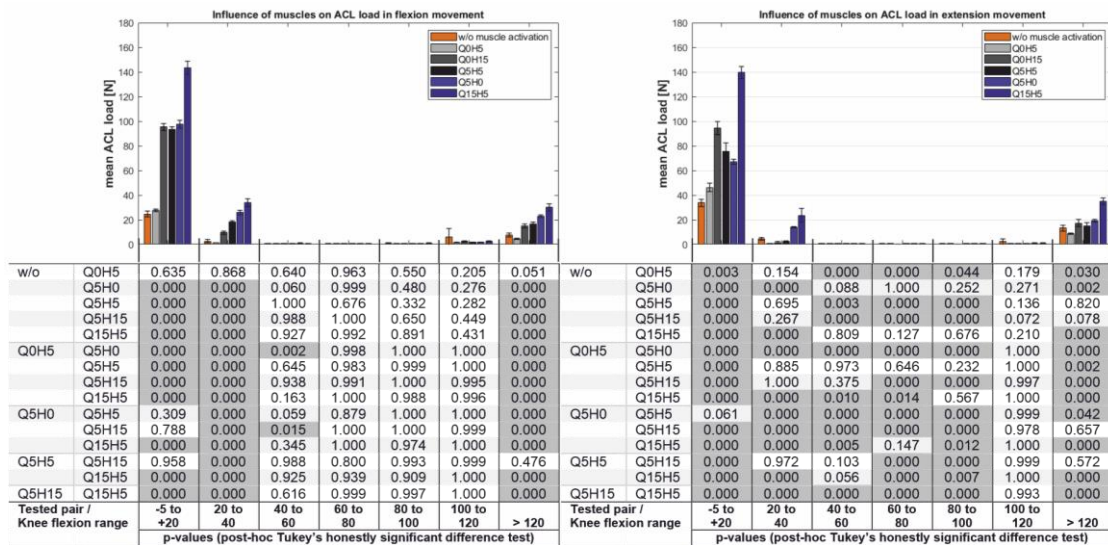


Figure 7-21 Mean ACL loads for different knee flexion ranges for different muscle activation for the setting +20° hip flexion, pre-loads: ACL 50 N, MCL 45 N. Each mean value is calculated from the means of the five repetitions of each setup. For each knee flexion range, the muscle activation was tested with one-way-ANOVA and a post-hoc significance test. The p-values are given below each set of bars. Dark grey fields are significant ($p < 0.05$). Left: results for the flexion movement. Right: results for the extension movement.

FLEXION MOVEMENT

Table 7-5 Results of Turkey's honestly significant difference test (post-hoc) for the setting hip angle +20°, pre-loads: ACL 50N, MCL 45 N, flexion movement, testing for significant differences between the mean values of ACL loads in the pre-defined knee flexion ranges. The mean values again reflect the means of the five repetitions for each muscle setting. Dark grey fields are significant ($p < 0.05$).

group 1	group 2	Flexion movement -5 to +20				Flexion movement +20 to +40			
		lower limit 95% CI	mean of groups difference	upper limit 95% CI	p	lower limit 95% CI	mean of groups difference	upper limit 95% CI	p
w/o	Q0H5	-15.7	-9.1	-2.5	0.003	-2.0	1.1	4.1	0.882
w/o	Q5H0	-81.2	-74.7	-68.1	0.000	-26.7	-23.7	-20.7	0.000
w/o	Q5H5	-74.3	-67.7	-61.2	0.000	-18.3	-15.3	-12.2	0.000
w/o	Q5H15	-65.0	-58.4	-51.9	0.000	-9.7	-6.7	-3.6	0.000
w/o	Q15H5	-129.4	-122.9	-116.3	0.000	-33.2	-30.2	-27.2	0.000
Q0H5	Q5H0	-72.1	-65.5	-59.0	0.000	-27.8	-24.8	-21.7	0.000
Q0H5	Q5H5	-65.2	-58.6	-52.0	0.000	-19.3	-16.3	-13.3	0.000
Q0H5	Q5H15	-55.9	-49.3	-42.8	0.000	-10.7	-7.7	-4.7	0.000
Q0H5	Q15H5	-120.3	-113.8	-107.2	0.000	-34.3	-31.3	-28.2	0.000
Q5H0	Q5H5	0.4	6.9	13.5	0.035	5.4	8.4	11.5	0.000
Q5H0	Q5H15	9.6	16.2	22.8	0.000	14.0	17.0	20.1	0.000
Q5H0	Q15H5	-54.8	-48.2	-41.6	0.000	-9.6	-6.5	-3.5	0.000
Q5H5	Q5H15	2.7	9.3	15.9	0.003	5.6	8.6	11.6	0.000
Q5H5	Q15H5	-61.7	-55.1	-48.6	0.000	-18.0	-15.0	-11.9	0.000
Q5H15	Q15H5	-71.0	-64.4	-57.8	0.000	-26.6	-23.6	-20.5	0.000

APPENDIX

Table 7-5 continued

group 1	group 2	Flexion movement +40 to +60				Flexion movement +60 to +80			
		lower limit 95% CI	mean of groups difference	upper limit 95% CI	p	lower limit 95% CI	mean of groups difference	upper limit 95% CI	p
w/o	Q0H5	-0.1	0.1	0.3	0.916	-0.2	0.0	0.1	0.975
w/o	Q5H0	-0.4	-0.2	0.0	0.010	-0.2	0.0	0.1	0.940
w/o	Q5H5	-0.2	0.0	0.2	0.984	-0.1	0.0	0.1	1.000
w/o	Q5H15	-0.2	0.0	0.2	1.000	-0.2	-0.1	0.1	0.593
w/o	Q15H5	-0.3	-0.1	0.1	0.394	-0.2	0.0	0.1	0.903
Q0H5	Q5H0	-0.5	-0.3	-0.1	0.001	-0.1	0.0	0.1	1.000
Q0H5	Q5H5	-0.3	-0.1	0.1	0.569	-0.1	0.0	0.1	0.983
Q0H5	Q5H15	-0.3	-0.1	0.1	0.889	-0.2	0.0	0.1	0.946
Q0H5	Q15H5	-0.4	-0.2	0.0	0.068	-0.1	0.0	0.1	1.000
Q5H0	Q5H5	0.0	0.2	0.4	0.048	-0.1	0.0	0.2	0.955
Q5H0	Q5H15	0.0	0.2	0.4	0.012	-0.2	0.0	0.1	0.979
Q5H0	Q15H5	-0.1	0.1	0.3	0.469	-0.1	0.0	0.1	1.000
Q5H5	Q5H15	-0.2	0.0	0.2	0.991	-0.2	-0.1	0.1	0.632
Q5H5	Q15H5	-0.3	-0.1	0.1	0.788	-0.2	0.0	0.1	0.924
Q5H15	Q15H5	-0.3	-0.1	0.1	0.437	-0.1	0.0	0.1	0.991

group 1	group 2	Flexion movement +80 to +100				Flexion movement +100 to +120			
		lower limit 95% CI	mean of groups difference	upper limit 95% CI	p	lower limit 95% CI	mean of groups difference	upper limit 95% CI	p
w/o	Q0H5	-0.2	0.1	0.5	0.849	-1.2	4.0	9.3	0.199
w/o	Q5H0	-0.2	0.2	0.6	0.801	-1.5	3.7	8.9	0.278
w/o	Q5H5	-0.2	0.2	0.6	0.727	-1.5	3.7	8.9	0.280
w/o	Q5H15	-0.3	0.1	0.5	0.922	-2.1	3.1	8.3	0.463
w/o	Q15H5	-0.3	0.1	0.5	0.994	-2.0	3.2	8.4	0.422
Q0H5	Q5H0	-0.4	0.0	0.4	1.000	-5.6	-0.3	4.9	1.000
Q0H5	Q5H5	-0.4	0.0	0.4	1.000	-5.6	-0.3	4.9	1.000
Q0H5	Q5H15	-0.4	0.0	0.4	1.000	-6.2	-0.9	4.3	0.993
Q0H5	Q15H5	-0.5	-0.1	0.3	0.988	-6.0	-0.8	4.4	0.996
Q5H0	Q5H5	-0.4	0.0	0.4	1.000	-5.2	0.0	5.2	1.000
Q5H0	Q5H15	-0.4	0.0	0.4	1.000	-5.8	-0.6	4.6	0.999
Q5H0	Q15H5	-0.5	-0.1	0.3	0.977	-5.7	-0.5	4.7	1.000
Q5H5	Q5H15	-0.4	-0.1	0.3	0.998	-5.8	-0.6	4.6	0.999
Q5H5	Q15H5	-0.5	-0.1	0.3	0.953	-5.7	-0.5	4.8	1.000
Q5H15	Q15H5	-0.4	-0.1	0.3	0.998	-5.1	0.1	5.3	1.000

group 1	group 2	Flexion movement from +120 and plus			
		lower limit 95% CI	mean of groups difference	upper limit 95% CI	p
w/o	Q0H5	5.9	16.1	26.3	0.001
w/o	Q5H0	6.7	16.9	27.1	0.000
w/o	Q5H5	6.7	16.8	27.0	0.000
w/o	Q5H15	6.0	16.2	26.3	0.001
w/o	Q15H5	5.8	16.0	26.1	0.001
Q0H5	Q5H0	-9.4	0.8	11.0	1.000
Q0H5	Q5H5	-9.4	0.7	10.9	1.000
Q0H5	Q5H15	-10.1	0.1	10.2	1.000
Q0H5	Q15H5	-10.3	-0.1	10.0	1.000
Q5H0	Q5H5	-10.2	-0.1	10.1	1.000
Q5H0	Q5H15	-10.9	-0.7	9.4	1.000
Q5H0	Q15H5	-11.1	-0.9	9.2	1.000
Q5H5	Q5H15	-10.8	-0.7	9.5	1.000
Q5H5	Q15H5	-11.0	-0.8	9.3	1.000
Q5H15	Q15H5	-10.3	-0.2	10.0	1.000

APPENDIX

EXTENSION MOVEMENT

Table 7-6 Results of Turkey's honestly significant difference test (post-hoc) for the setting hip angle +20°, pre-loads: ACL 50N, MCL 45 N, extension movement, testing for significant differences between the mean values of ACL loads in the pre-defined knee flexion ranges. The mean values again reflect the means of the five repetitions for each muscle setting. Dark grey fields are significant ($p < 0.05$).

group 1	group 2	Extension movement -5 to +20				Extension movement +20 to +40			
		lower limit 95% CI	mean of groups difference	upper limit 95% CI	p	lower limit 95% CI	mean of groups difference	upper limit 95% CI	p
w/o	Q0H5	-20.8	-14.4	-7.9	0.000	-1.0	3.2	7.4	0.206
w/o	Q5H0	-40.4	-34.0	-27.5	0.000	-12.3	-8.1	-3.9	0.000
w/o	Q5H5	-41.4	-34.9	-28.5	0.000	-2.1	2.1	6.3	0.624
w/o	Q5H15	-51.8	-45.4	-39.0	0.000	-1.2	3.0	7.2	0.258
w/o	Q15H5	-110.7	-104.3	-97.8	0.000	-22.2	-18.0	-13.8	0.000
Q0H5	Q5H0	-26.0	-19.6	-13.2	0.000	-15.6	-11.4	-7.2	0.000
Q0H5	Q5H5	-27.0	-20.6	-14.1	0.000	-5.3	-1.1	3.1	0.965
Q0H5	Q5H15	-37.5	-31.0	-24.6	0.000	-4.4	-0.2	4.0	1.000
Q0H5	Q15H5	-96.3	-89.9	-83.5	0.000	-25.4	-21.2	-17.0	0.000
Q5H0	Q5H5	-7.4	-1.0	5.5	0.997	6.1	10.3	14.5	0.000
Q5H0	Q5H15	-17.9	-11.4	-5.0	0.000	7.0	11.2	15.4	0.000
Q5H0	Q15H5	-76.7	-70.3	-63.9	0.000	-14.0	-9.8	-5.6	0.000
Q5H5	Q5H15	-16.9	-10.5	-4.1	0.000	-3.3	0.9	5.1	0.984
Q5H5	Q15H5	-75.8	-69.3	-62.9	0.000	-24.3	-20.1	-15.9	0.000
Q5H15	Q15H5	-65.3	-58.8	-52.4	0.000	-25.2	-21.0	-16.8	0.000

group 1	group 2	Extension movement +40 to +60				Extension movement +60 to +80			
		lower limit 95% CI	mean of groups difference	upper limit 95% CI	p	lower limit 95% CI	mean of groups difference	upper limit 95% CI	p
w/o	Q0H5	0.0	0.1	0.2	0.010	0.0	0.1	0.1	0.033
w/o	Q5H0	-0.2	-0.1	0.0	0.015	-0.1	0.0	0.0	0.200
w/o	Q5H5	0.0	0.1	0.2	0.055	0.0	0.1	0.2	0.000
w/o	Q5H15	0.1	0.2	0.3	0.000	0.2	0.3	0.3	0.000
w/o	Q15H5	-0.1	0.0	0.1	1.000	-0.1	0.0	0.1	1.000
Q0H5	Q5H0	-0.4	-0.3	-0.1	0.000	-0.2	-0.1	-0.1	0.000
Q0H5	Q5H5	-0.1	0.0	0.1	0.976	0.0	0.0	0.1	0.473
Q0H5	Q5H15	0.0	0.1	0.2	0.104	0.1	0.2	0.2	0.000
Q0H5	Q15H5	-0.2	-0.1	0.0	0.008	-0.1	-0.1	0.0	0.018
Q5H0	Q5H5	0.1	0.2	0.3	0.000	0.1	0.1	0.2	0.000
Q5H0	Q5H15	0.2	0.3	0.5	0.000	0.2	0.3	0.4	0.000
Q5H0	Q15H5	0.0	0.1	0.2	0.020	0.0	0.0	0.1	0.305
Q5H5	Q5H15	0.0	0.1	0.2	0.022	0.1	0.2	0.2	0.000
Q5H5	Q15H5	-0.2	-0.1	0.0	0.042	-0.2	-0.1	0.0	0.000
Q5H15	Q15H5	-0.3	-0.2	-0.1	0.000	-0.3	-0.3	-0.2	0.000

group 1	group 2	Extension movement +80 to +100				Extension movement +100 to +120			
		lower limit 95% CI	mean of groups difference	upper limit 95% CI	p	lower limit 95% CI	mean of groups difference	upper limit 95% CI	p
w/o	Q0H5	-0.1	0.1	0.2	0.462	-0.5	1.3	3.2	0.245
w/o	Q5H0	-0.3	-0.1	0.0	0.016	-0.6	1.3	3.1	0.300
w/o	Q5H5	0.0	0.2	0.3	0.006	-0.4	1.4	3.3	0.187
w/o	Q5H15	0.3	0.4	0.6	0.000	-0.2	1.6	3.5	0.107
w/o	Q15H5	-0.1	0.0	0.1	1.000	-0.5	1.3	3.2	0.257
Q0H5	Q5H0	-0.3	-0.2	-0.1	0.000	-1.9	-0.1	1.8	1.000
Q0H5	Q5H5	0.0	0.1	0.2	0.288	-1.7	0.1	1.9	1.000
Q0H5	Q5H15	0.2	0.4	0.5	0.000	-1.6	0.3	2.1	0.997
Q0H5	Q15H5	-0.2	-0.1	0.1	0.459	-1.9	0.0	1.8	1.000
Q5H0	Q5H5	0.2	0.3	0.4	0.000	-1.7	0.2	2.0	1.000
Q5H0	Q5H15	0.5	0.6	0.7	0.000	-1.5	0.3	2.2	0.991
Q5H0	Q15H5	0.0	0.1	0.3	0.016	-1.8	0.1	1.9	1.000
Q5H5	Q5H15	0.1	0.3	0.4	0.000	-1.7	0.2	2.0	1.000
Q5H5	Q15H5	-0.3	-0.2	0.0	0.006	-1.9	-0.1	1.7	1.000
Q5H15	Q15H5	-0.6	-0.4	-0.3	0.000	-2.1	-0.3	1.5	0.996

Table 7-6 continued

group 1	group 2	Extension movement from +120 plus			p
		lower limit 95% CI	mean of groups difference	upper limit 95% CI	
w/o	Q0H5	0.3	6.5	12.8	0.035
w/o	Q5H0	1.5	7.7	13.9	0.009
w/o	Q5H5	1.0	7.2	13.4	0.017
w/o	Q5H15	1.2	7.4	13.6	0.014
w/o	Q15H5	1.4	7.6	13.8	0.011
Q0H5	Q5H0	-5.0	1.2	7.4	0.991
Q0H5	Q5H5	-5.6	0.7	6.9	0.999
Q0H5	Q5H15	-5.4	0.8	7.0	0.998
Q0H5	Q15H5	-5.2	1.0	7.2	0.995
Q5H0	Q5H5	-6.7	-0.5	5.7	1.000
Q5H0	Q5H15	-6.6	-0.3	5.9	1.000
Q5H0	Q15H5	-6.4	-0.2	6.1	1.000
Q5H5	Q5H15	-6.1	0.2	6.4	1.000
Q5H5	Q15H5	-5.9	0.4	6.6	1.000
Q5H15	Q15H5	-6.0	0.2	6.4	1.000

7.5.2.3 Setting: Hip Angle -20°; Preload ACL 85 N; Preload MCL 75 N

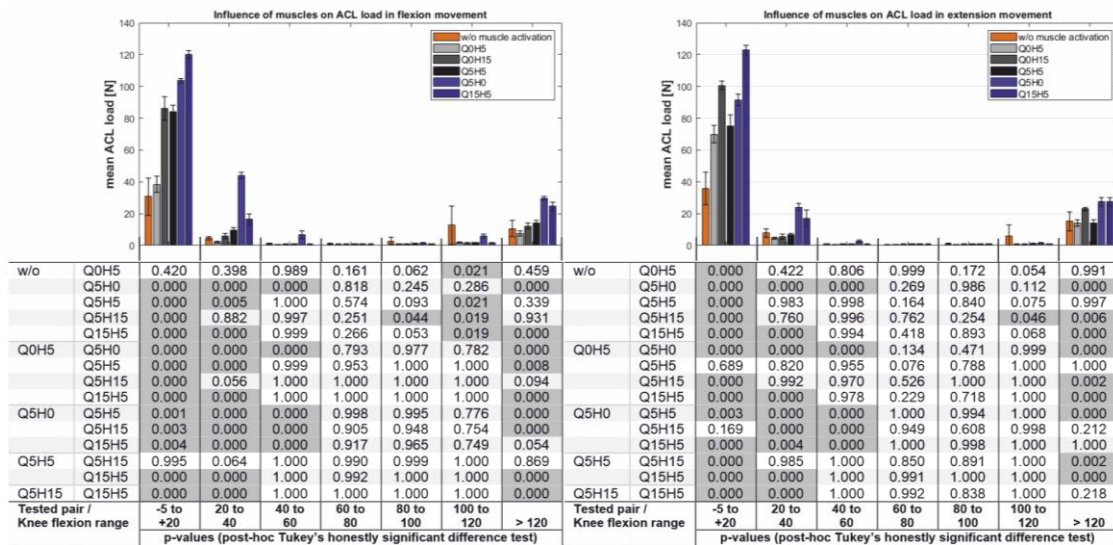


Figure 7-22 Mean ACL loads for different knee flexion ranges for different muscle activation for the setting -20° hip flexion, pre-loads: ACL 85 N, MCL 75 N. Each mean value is calculated from the means of the five repetitions of each setup. For each knee flexion range, the muscle activation was tested with one-way-ANOVA and a post-hoc significance test. The p-values are given below each set of bars. Dark grey fields are significant (p<0.05). Left: results for the flexion movement. Right: results for the extension movement.

FLEXION MOVEMENT

Table 7-7 Results of Turkey's honestly significant difference test (post-hoc) for the setting hip angle -20°, pre-loads: ACL 85N, MCL 75 N, flexion movement, testing for significant differences between the mean values of ACL loads in the pre-defined knee flexion ranges. The mean values again reflect the means of the five repetitions for each muscle setting. Dark grey fields are significant (p<0.05).

group 1	group 2	Flexion movement -5 to +20				Flexion movement +20 to +40			
		lower limit 95% CI	mean of groups difference	upper limit 95% CI	p	lower limit 95% CI	mean of groups difference	upper limit 95% CI	p
w/o	Q0H5	-21.0	-14.6	-8.1	0.000	-0.6	2.2	5.1	0.184
w/o	Q5H0	-83.1	-76.7	-70.2	0.000	-40.9	-38.1	-35.2	0.000
w/o	Q5H5	-60.3	-53.8	-47.4	0.000	-8.4	-5.5	-2.7	0.000
w/o	Q5H15	-54.5	-48.1	-41.6	0.000	-3.7	-0.9	2.0	0.930
w/o	Q15H5	-54.5	-48.1	-41.6	0.000	-3.7	-0.9	2.0	0.930
Q0H5	Q5H0	-68.6	-62.1	-55.7	0.000	-43.2	-40.3	-37.5	0.000
Q0H5	Q5H5	-45.7	-39.2	-32.8	0.000	-10.6	-7.7	-4.9	0.000
Q0H5	Q5H15	-40.0	-33.5	-27.1	0.000	-6.0	-3.1	-0.3	0.026
Q0H5	Q15H5	-40.0	-33.5	-27.1	0.000	-6.0	-3.1	-0.3	0.026
Q5H0	Q5H5	16.4	22.9	29.3	0.000	29.7	32.6	35.4	0.000
Q5H0	Q5H15	22.2	28.6	35.0	0.000	34.4	37.2	40.1	0.000
Q5H0	Q15H5	22.2	28.6	35.0	0.000	34.4	37.2	40.1	0.000
Q5H5	Q5H15	-0.7	5.7	12.2	0.102	1.8	4.6	7.5	0.000
Q5H5	Q15H5	-0.7	5.7	12.2	0.102	1.8	4.6	7.5	0.000
Q5H15	Q15H5	-6.4	0.0	6.4	1.000	-2.8	0.0	2.8	1.000

APPENDIX

Table 7-7 continued

group 1	group 2	Flexion movement +40 to +60				Flexion movement +60 to +80			
		lower limit 95% CI	mean of groups difference	upper limit 95% CI	p	lower limit 95% CI	mean of groups difference	upper limit 95% CI	p
w/o	Q0H5	-1.6	0.2	2.0	0.999	-0.1	0.3	0.7	0.287
w/o	Q5H0	-6.6	-4.8	-3.0	0.000	-0.2	0.2	0.6	0.741
w/o	Q5H5	-1.8	0.0	1.8	1.000	-0.2	0.2	0.6	0.818
w/o	Q5H15	-1.7	0.1	1.9	1.000	-0.1	0.3	0.7	0.390
w/o	Q15H5	-1.7	0.1	1.9	1.000	-0.1	0.3	0.7	0.390
Q0H5	Q5H0	-6.8	-5.0	-3.2	0.000	-0.5	-0.1	0.3	0.965
Q0H5	Q5H5	-2.0	-0.2	1.6	0.999	-0.5	-0.1	0.3	0.932
Q0H5	Q5H15	-1.9	-0.1	1.7	1.000	-0.4	0.0	0.4	1.000
Q0H5	Q15H5	-1.9	-0.1	1.7	1.000	-0.4	0.0	0.4	1.000
Q5H0	Q5H5	3.0	4.8	6.6	0.000	-0.4	0.0	0.4	1.000
Q5H0	Q5H15	3.1	4.9	6.7	0.000	-0.3	0.1	0.5	0.991
Q5H0	Q15H5	3.1	4.9	6.7	0.000	-0.3	0.1	0.5	0.991
Q5H5	Q5H15	-1.7	0.1	1.9	1.000	-0.3	0.1	0.5	0.976
Q5H5	Q15H5	-1.7	0.1	1.9	1.000	-0.3	0.1	0.5	0.976
Q5H15	Q15H5	-1.8	0.0	1.8	1.000	-0.4	0.0	0.4	1.000

group 1	group 2	Flexion movement +80 to +100				Flexion movement +100 to +120			
		lower limit 95% CI	mean of groups difference	upper limit 95% CI	p	lower limit 95% CI	mean of groups difference	upper limit 95% CI	p
w/o	Q0H5	-0.2	1.8	3.7	0.093	1.1	10.3	19.5	0.022
w/o	Q5H0	-0.7	1.2	3.2	0.403	-3.2	6.0	15.2	0.357
w/o	Q5H5	-0.3	1.6	3.6	0.137	1.1	10.3	19.6	0.021
w/o	Q5H15	-0.1	1.9	3.8	0.067	1.2	10.4	19.6	0.020
w/o	Q15H5	-0.1	1.9	3.8	0.067	1.2	10.4	19.6	0.020
Q0H5	Q5H0	-2.5	-0.5	1.4	0.954	-13.5	-4.3	4.9	0.709
Q0H5	Q5H5	-2.1	-0.1	1.8	1.000	-9.2	0.1	9.3	1.000
Q0H5	Q5H15	-1.8	0.1	2.0	1.000	-9.1	0.1	9.3	1.000
Q0H5	Q15H5	-1.8	0.1	2.0	1.000	-9.1	0.1	9.3	1.000
Q5H0	Q5H5	-1.5	0.4	2.4	0.985	-4.9	4.3	13.5	0.699
Q5H0	Q5H15	-1.3	0.6	2.6	0.908	-4.8	4.4	13.6	0.684
Q5H0	Q15H5	-1.3	0.6	2.6	0.908	-4.8	4.4	13.6	0.684
Q5H5	Q5H15	-1.7	0.2	2.2	0.999	-9.1	0.1	9.3	1.000
Q5H5	Q15H5	-1.7	0.2	2.2	0.999	-9.1	0.1	9.3	1.000
Q5H15	Q15H5	-1.9	0.0	1.9	1.000	-9.2	0.0	9.2	1.000

group 1	group 2	Flexion movement from +120 and plus			
		lower limit 95% CI	mean of groups difference	upper limit 95% CI	p
w/o	Q0H5	5.9	23.3	40.7	0.004
w/o	Q5H0	4.8	22.2	39.5	0.007
w/o	Q5H5	9.4	26.8	44.2	0.001
w/o	Q5H15	7.9	25.3	42.6	0.002
w/o	Q15H5	7.9	25.3	42.6	0.002
Q0H5	Q5H0	-18.5	-1.1	16.3	1.000
Q0H5	Q5H5	-13.9	3.5	20.9	0.988
Q0H5	Q5H15	-15.4	2.0	19.4	0.999
Q0H5	Q15H5	-15.4	2.0	19.4	0.999
Q5H0	Q5H5	-12.7	4.6	22.0	0.960
Q5H0	Q5H15	-14.3	3.1	20.5	0.993
Q5H0	Q15H5	-14.3	3.1	20.5	0.993
Q5H5	Q5H15	-18.9	-1.5	15.8	1.000
Q5H5	Q15H5	-18.9	-1.5	15.8	1.000
Q5H15	Q15H5	-17.4	0.0	17.4	1.000

APPENDIX

EXTENSION MOVEMENT

Table 7-8 Results of Turkey's honestly significant difference test (post-hoc) for the setting hip angle -20°, pre-loads: ACL 85N, MCL 75 N, extension movement, testing for significant differences between the mean values of ACL loads in the pre-defined knee flexion ranges. The mean values again reflect the means of the five repetitions for each muscle setting. Dark grey fields are significant ($p < 0.05$).

group 1	group 2	Extension movement -5 to +20				Extension movement +20 to +40			
		lower limit 95% CI	mean of groups difference	upper limit 95% CI	p	lower limit 95% CI	mean of groups difference	upper limit 95% CI	p
w/o	Q0H5	-35.5	-27.9	-20.4	0.000	0.0	2.7	5.4	0.047
w/o	Q5H0	-54.1	-46.6	-39.1	0.000	-18.3	-15.6	-12.9	0.000
w/o	Q5H5	-43.4	-35.9	-28.4	0.000	-1.9	0.8	3.5	0.952
w/o	Q5H15	-55.9	-48.4	-40.9	0.000	-0.4	2.3	5.0	0.125
w/o	Q15H5	-55.9	-48.4	-40.9	0.000	-0.4	2.3	5.0	0.125
Q0H5	Q5H0	-26.2	-18.7	-11.1	0.000	-21.1	-18.4	-15.7	0.000
Q0H5	Q5H5	-15.5	-8.0	-0.4	0.034	-4.7	-2.0	0.7	0.249
Q0H5	Q5H15	-28.0	-20.5	-12.9	0.000	-3.1	-0.4	2.3	0.997
Q0H5	Q15H5	-28.0	-20.5	-12.9	0.000	-3.1	-0.4	2.3	0.997
Q5H0	Q5H5	3.2	10.7	18.2	0.002	13.7	16.4	19.1	0.000
Q5H0	Q5H15	-9.3	-1.8	5.7	0.975	15.2	17.9	20.6	0.000
Q5H0	Q15H5	-9.3	-1.8	5.7	0.975	15.2	17.9	20.6	0.000
Q5H5	Q5H15	-20.0	-12.5	-5.0	0.000	-1.1	1.6	4.3	0.495
Q5H5	Q15H5	-20.0	-12.5	-5.0	0.000	-1.1	1.6	4.3	0.495
Q5H15	Q15H5	-7.5	0.0	7.5	1.000	-2.7	0.0	2.7	1.000

group 1	group 2	Extension movement +40 to +60				Extension movement +60 to +80			
		lower limit 95% CI	mean of groups difference	upper limit 95% CI	p	lower limit 95% CI	mean of groups difference	upper limit 95% CI	p
w/o	Q0H5	-0.4	0.2	0.7	0.955	-0.3	0.0	0.3	1.000
w/o	Q5H0	-2.0	-1.4	-0.9	0.000	-0.6	-0.2	0.1	0.298
w/o	Q5H5	-0.6	0.0	0.5	1.000	-0.6	-0.3	0.1	0.131
w/o	Q5H15	-0.6	0.0	0.5	1.000	-0.5	-0.2	0.2	0.677
w/o	Q15H5	-0.6	0.0	0.5	1.000	-0.5	-0.2	0.2	0.677
Q0H5	Q5H0	-2.1	-1.6	-1.0	0.000	-0.6	-0.2	0.1	0.304
Q0H5	Q5H5	-0.8	-0.2	0.4	0.874	-0.6	-0.3	0.1	0.135
Q0H5	Q5H15	-0.8	-0.2	0.4	0.902	-0.5	-0.2	0.2	0.685
Q0H5	Q15H5	-0.8	-0.2	0.4	0.902	-0.5	-0.2	0.2	0.685
Q5H0	Q5H5	0.8	1.4	1.9	0.000	-0.4	-0.1	0.3	0.997
Q5H0	Q5H15	0.8	1.4	1.9	0.000	-0.3	0.1	0.4	0.984
Q5H0	Q15H5	0.8	1.4	1.9	0.000	-0.3	0.1	0.4	0.984
Q5H5	Q5H15	-0.6	0.0	0.6	1.000	-0.2	0.1	0.5	0.862
Q5H5	Q15H5	-0.6	0.0	0.6	1.000	-0.2	0.1	0.5	0.862
Q5H15	Q15H5	-0.6	0.0	0.6	1.000	-0.3	0.0	0.3	1.000

group 1	group 2	Extension movement +80 to +100				Extension movement +100 to +120			
		lower limit 95% CI	mean of groups difference	upper limit 95% CI	p	lower limit 95% CI	mean of groups difference	upper limit 95% CI	p
w/o	Q0H5	-0.2	0.4	1.0	0.268	-0.1	5.2	10.5	0.055
w/o	Q5H0	-0.5	0.1	0.7	0.998	-0.7	4.6	9.9	0.110
w/o	Q5H5	-0.4	0.2	0.8	0.889	-0.3	5.0	10.3	0.075
w/o	Q5H15	-0.2	0.4	1.0	0.338	0.1	5.4	10.7	0.046
w/o	Q15H5	-0.2	0.4	1.0	0.338	0.1	5.4	10.7	0.046
Q0H5	Q5H0	-0.9	-0.3	0.2	0.482	-5.9	-0.6	4.7	0.999
Q0H5	Q5H5	-0.8	-0.2	0.4	0.858	-5.6	-0.3	5.0	1.000
Q0H5	Q5H15	-0.6	0.0	0.5	1.000	-5.2	0.1	5.4	1.000
Q0H5	Q15H5	-0.6	0.0	0.5	1.000	-5.2	0.1	5.4	1.000
Q5H0	Q5H5	-0.5	0.1	0.7	0.985	-5.0	0.3	5.6	1.000
Q5H0	Q5H15	-0.3	0.3	0.9	0.573	-4.6	0.7	6.0	0.998
Q5H0	Q15H5	-0.3	0.3	0.9	0.573	-4.6	0.7	6.0	0.998
Q5H5	Q5H15	-0.4	0.2	0.8	0.915	-4.9	0.4	5.7	1.000
Q5H5	Q15H5	-0.4	0.2	0.8	0.915	-4.9	0.4	5.7	1.000
Q5H15	Q15H5	-0.6	0.0	0.6	1.000	-5.3	0.0	5.3	1.000

Table 7-8 continued

group 1	group 2	Extension movement from +120 plus			
		lower limit 95% CI	mean of groups difference	upper limit 95% CI	p
w/o	Q0H5	-0.1	12.9	25.8	0.053
w/o	Q5H0	0.7	13.6	26.6	0.035
w/o	Q5H5	1.8	14.8	27.8	0.019
w/o	Q5H15	2.5	15.5	28.4	0.013
w/o	Q15H5	2.5	15.5	28.4	0.013
Q0H5	Q5H0	-12.2	0.8	13.7	1.000
Q0H5	Q5H5	-11.0	1.9	14.9	0.997
Q0H5	Q5H15	-10.4	2.6	15.6	0.988
Q0H5	Q15H5	-10.4	2.6	15.6	0.988
Q5H0	Q5H5	-11.8	1.2	14.1	1.000
Q5H0	Q5H15	-11.1	1.8	14.8	0.998
Q5H0	Q15H5	-11.1	1.8	14.8	0.998
Q5H5	Q5H15	-12.3	0.7	13.6	1.000
Q5H5	Q15H5	-12.3	0.7	13.6	1.000
Q5H15	Q15H5	-13.0	0.0	13.0	1.000

7.5.2.4 Setting: Hip Angle +20°; Preload ACL 85 N; Preload MCL 75 N

The following tables refer to Figure 3-9 (chapter 3.1.3 on page 3-48).

FLEXION MOVEMENT

Table 7-9 Results of Turkey's honestly significant difference test (post-hoc) for the setting hip angle +20°, pre-loads: ACL 85N, MCL 75 N, flexion movement, testing for significant differences between the mean values of ACL loads in the pre-defined knee flexion ranges. The mean values again reflect the means of the five repetitions for each muscle setting. Dark grey fields are significant (p<0.05).

group 1	group 2	Flexion movement -5 to +20				Flexion movement +20 to +40			
		lower limit 95% CI	mean of groups difference	upper limit 95% CI	p	lower limit 95% CI	mean of groups difference	upper limit 95% CI	p
w/o	Q0H5	-26.7	-9.9	6.9	0.468	-1.9	1.5	5.0	0.750
w/o	Q5H0	-102.0	-85.3	-68.5	0.000	-37.2	-33.8	-30.3	0.000
w/o	Q5H5	-92.4	-75.6	-58.8	0.000	-29.8	-26.3	-22.8	0.000
w/o	Q5H15	-82.7	-65.9	-49.1	0.000	-19.2	-15.7	-12.3	0.000
w/o	Q15H5	-133.4	-116.6	-99.8	0.000	-47.7	-44.2	-40.8	0.000
Q0H5	Q5H0	-92.1	-75.4	-58.6	0.000	-38.8	-35.3	-31.8	0.000
Q0H5	Q5H5	-82.5	-65.7	-48.9	0.000	-31.3	-27.8	-24.3	0.000
Q0H5	Q5H15	-72.8	-56.0	-39.2	0.000	-20.7	-17.3	-13.8	0.000
Q0H5	Q15H5	-123.5	-106.7	-89.9	0.000	-49.2	-45.8	-42.3	0.000
Q5H0	Q5H5	-7.1	9.7	26.4	0.496	4.0	7.5	11.0	0.000
Q5H0	Q5H15	2.6	19.4	36.1	0.017	14.6	18.0	21.5	0.000
Q5H0	Q15H5	-48.1	-31.3	-14.6	0.000	-13.9	-10.5	-7.0	0.000
Q5H5	Q5H15	-7.1	9.7	26.5	0.490	7.1	10.6	14.0	0.000
Q5H5	Q15H5	-57.8	-41.0	-24.2	0.000	-21.4	-18.0	-14.5	0.000
Q5H15	Q15H5	-67.5	-50.7	-33.9	0.000	-32.0	-28.5	-25.0	0.000

group 1	group 2	Flexion movement +40 to +60				Flexion movement +60 to +80			
		lower limit 95% CI	mean of groups difference	upper limit 95% CI	p	lower limit 95% CI	mean of groups difference	upper limit 95% CI	p
w/o	Q0H5	-0.4	0.0	0.3	1.000	-0.2	-0.1	0.0	0.044
w/o	Q5H0	-1.4	-1.0	-0.7	0.000	-0.2	-0.1	0.0	0.006
w/o	Q5H5	-0.5	-0.1	0.2	0.870	-0.1	0.0	0.1	0.889
w/o	Q5H15	-0.4	0.0	0.3	1.000	-0.2	-0.1	0.0	0.004
w/o	Q15H5	-0.5	-0.1	0.2	0.827	-0.2	-0.1	0.0	0.206
Q0H5	Q5H0	-1.4	-1.0	-0.7	0.000	-0.1	0.0	0.1	0.950
Q0H5	Q5H5	-0.5	-0.1	0.2	0.902	0.0	0.1	0.2	0.329
Q0H5	Q5H15	-0.4	0.0	0.3	1.000	-0.1	0.0	0.1	0.915
Q0H5	Q15H5	-0.5	-0.1	0.2	0.864	-0.1	0.0	0.1	0.968
Q5H0	Q5H5	0.5	0.9	1.2	0.000	0.0	0.1	0.2	0.067
Q5H0	Q5H15	0.7	1.0	1.4	0.000	-0.1	0.0	0.1	1.000
Q5H0	Q15H5	0.5	0.9	1.2	0.000	0.0	0.1	0.2	0.576
Q5H5	Q5H15	-0.2	0.1	0.5	0.929	-0.2	-0.1	0.0	0.052
Q5H5	Q15H5	-0.4	0.0	0.3	1.000	-0.2	0.0	0.1	0.781
Q5H15	Q15H5	-0.5	-0.1	0.2	0.897	0.0	0.1	0.2	0.500

APPENDIX

Table 7-9 continued

group 1	group 2	Flexion movement +80 to +100				Flexion movement +100 to +120			
		lower limit 95% CI	mean of groups difference	upper limit 95% CI	p	lower limit 95% CI	mean of groups difference	upper limit 95% CI	p
w/o	Q0H5	-0.3	0.0	0.2	0.998	2.2	4.2	6.1	0.000
w/o	Q5H0	-0.5	-0.3	-0.1	0.009	1.1	3.1	5.0	0.001
w/o	Q5H5	-0.4	-0.1	0.1	0.511	1.1	3.1	5.0	0.001
w/o	Q5H15	-0.3	-0.1	0.1	0.538	1.0	2.9	4.8	0.001
w/o	Q15H5	-0.4	-0.2	0.0	0.184	0.8	2.7	4.7	0.003
Q0H5	Q5H0	-0.5	-0.2	0.0	0.025	-3.1	-1.1	0.8	0.503
Q0H5	Q5H5	-0.3	-0.1	0.1	0.764	-3.0	-1.1	0.9	0.525
Q0H5	Q5H15	-0.3	-0.1	0.1	0.788	-3.2	-1.3	0.7	0.351
Q0H5	Q15H5	-0.4	-0.1	0.1	0.365	-3.4	-1.5	0.5	0.220
Q5H0	Q5H5	-0.1	0.2	0.4	0.336	-1.9	0.0	2.0	1.000
Q5H0	Q5H15	-0.1	0.2	0.4	0.314	-2.1	-0.2	1.8	1.000
Q5H0	Q15H5	-0.1	0.1	0.3	0.732	-2.3	-0.4	1.6	0.993
Q5H5	Q5H15	-0.2	0.0	0.2	1.000	-2.1	-0.2	1.8	1.000
Q5H5	Q15H5	-0.3	0.0	0.2	0.983	-2.3	-0.4	1.6	0.990
Q5H15	Q15H5	-0.3	-0.1	0.2	0.977	-2.1	-0.2	1.8	1.000

group 1	group 2	Flexion movement from +120 and plus			
		lower limit 95% CI	mean of groups difference	upper limit 95% CI	p
w/o	Q0H5	18.5	20.6	22.7	0.000
w/o	Q5H0	19.5	21.6	23.6	0.000
w/o	Q5H5	19.2	21.2	23.3	0.000
w/o	Q5H15	18.9	21.0	23.1	0.000
w/o	Q15H5	18.1	20.3	22.5	0.000
Q0H5	Q5H0	-1.1	1.0	3.1	0.708
Q0H5	Q5H5	-1.4	0.6	2.7	0.924
Q0H5	Q5H15	-1.7	0.4	2.5	0.986
Q0H5	Q15H5	-2.5	-0.3	1.9	0.999
Q5H0	Q5H5	-2.4	-0.3	1.8	0.997
Q5H0	Q5H15	-2.6	-0.5	1.6	0.967
Q5H0	Q15H5	-3.5	-1.2	1.0	0.526
Q5H5	Q5H15	-2.3	-0.2	1.9	0.999
Q5H5	Q15H5	-3.1	-0.9	1.3	0.786
Q5H15	Q15H5	-2.9	-0.7	1.5	0.917

EXTENSION MOVEMENT

Table 7-10 Results of Turkey's honestly significant difference test (post-hoc) for the setting hip angle +20°, pre-loads: ACL 85N, MCL 75 N, extension movement, testing for significant differences between the mean values of ACL loads in the pre-defined knee flexion ranges. The mean values again reflect the means of the five repetitions for each muscle setting. Dark grey fields are significant (p<0.05).

group 1	group 2	Extension movement -5 to +20				Extension movement +20 to +40			
		lower limit 95% CI	mean of groups difference	upper limit 95% CI	p	lower limit 95% CI	mean of groups difference	upper limit 95% CI	p
w/o	Q0H5	-32.0	-25.1	-18.1	0.000	0.2	5.0	9.8	0.039
w/o	Q5H0	-58.7	-51.8	-44.8	0.000	-17.4	-12.6	-7.7	0.000
w/o	Q5H5	-64.9	-57.9	-51.0	0.000	-6.5	-1.7	3.1	0.882
w/o	Q5H15	-74.9	-67.9	-61.0	0.000	-2.5	2.3	7.2	0.673
w/o	Q15H5	-132.9	-126.0	-119.1	0.000	-30.3	-25.4	-20.6	0.000
Q0H5	Q5H0	-33.6	-26.7	-19.8	0.000	-22.4	-17.6	-12.7	0.000
Q0H5	Q5H5	-39.8	-32.9	-26.0	0.000	-11.5	-6.7	-1.9	0.003
Q0H5	Q5H15	-49.8	-42.9	-36.0	0.000	-7.5	-2.7	2.1	0.534
Q0H5	Q15H5	-107.9	-100.9	-94.0	0.000	-35.3	-30.4	-25.6	0.000
Q5H0	Q5H5	-13.1	-6.2	0.7	0.099	6.0	10.9	15.7	0.000
Q5H0	Q5H15	-23.1	-16.2	-9.3	0.000	10.1	14.9	19.7	0.000
Q5H0	Q15H5	-81.2	-74.2	-67.3	0.000	-17.7	-12.9	-8.0	0.000
Q5H5	Q5H15	-16.9	-10.0	-3.1	0.002	-0.8	4.0	8.9	0.142
Q5H5	Q15H5	-75.0	-68.0	-61.1	0.000	-28.6	-23.7	-18.9	0.000
Q5H15	Q15H5	-65.0	-58.1	-51.1	0.000	-32.6	-27.8	-22.9	0.000

APPENDIX

Table 7-10 continued

group 1	group 2	Extension movement +40 to +60				Extension movement +60 to +80			
		lower limit 95% CI	mean of groups difference	upper limit 95% CI	p	lower limit 95% CI	mean of groups difference	upper limit 95% CI	p
w/o	Q0H5	0.0	0.2	0.5	0.106	-0.2	-0.1	0.0	0.395
w/o	Q5H0	-0.5	-0.3	0.0	0.050	-0.3	-0.2	-0.1	0.001
w/o	Q5H5	0.0	0.3	0.6	0.017	0.0	0.1	0.2	0.076
w/o	Q5H15	0.0	0.3	0.6	0.014	0.0	0.1	0.2	0.019
w/o	Q15H5	-0.1	0.2	0.4	0.452	-0.2	-0.1	0.0	0.026
Q0H5	Q5H0	-0.8	-0.5	-0.2	0.000	-0.2	-0.1	0.0	0.125
Q0H5	Q5H5	-0.2	0.1	0.3	0.957	0.1	0.2	0.3	0.001
Q0H5	Q5H15	-0.2	0.1	0.3	0.935	0.1	0.2	0.3	0.000
Q0H5	Q15H5	-0.3	-0.1	0.2	0.949	-0.2	0.0	0.1	0.711
Q5H0	Q5H5	0.3	0.6	0.8	0.000	0.1	0.3	0.4	0.000
Q5H0	Q5H15	0.3	0.6	0.9	0.000	0.2	0.3	0.4	0.000
Q5H0	Q15H5	0.2	0.4	0.7	0.001	-0.1	0.0	0.1	0.825
Q5H5	Q5H15	-0.3	0.0	0.3	1.000	-0.1	0.0	0.1	0.987
Q5H5	Q15H5	-0.4	-0.1	0.1	0.537	-0.3	-0.2	-0.1	0.000
Q5H15	Q15H5	-0.4	-0.2	0.1	0.483	-0.3	-0.2	-0.1	0.000

group 1	group 2	Extension movement +80 to +100				Extension movement +100 to +120			
		lower limit 95% CI	mean of groups difference	upper limit 95% CI	p	lower limit 95% CI	mean of groups difference	upper limit 95% CI	p
w/o	Q0H5	-0.1	0.0	0.2	1.000	1.4	2.8	4.2	0.000
w/o	Q5H0	-0.4	-0.2	-0.1	0.003	1.2	2.6	4.0	0.000
w/o	Q5H5	0.0	0.1	0.3	0.216	1.4	2.8	4.2	0.000
w/o	Q5H15	0.1	0.3	0.4	0.000	1.4	2.9	4.3	0.000
w/o	Q15H5	-0.3	-0.2	0.0	0.024	1.0	2.4	3.8	0.000
Q0H5	Q5H0	-0.4	-0.2	-0.1	0.001	-1.7	-0.3	1.1	0.991
Q0H5	Q5H5	-0.1	0.1	0.3	0.355	-1.5	-0.1	1.4	1.000
Q0H5	Q5H15	0.1	0.3	0.4	0.001	-1.4	0.0	1.4	1.000
Q0H5	Q15H5	-0.4	-0.2	0.0	0.012	-1.8	-0.4	1.0	0.926
Q5H0	Q5H5	0.2	0.4	0.5	0.000	-1.2	0.2	1.6	0.997
Q5H0	Q5H15	0.3	0.5	0.7	0.000	-1.1	0.3	1.7	0.988
Q5H0	Q15H5	-0.1	0.0	0.2	0.945	-1.6	-0.2	1.2	0.999
Q5H5	Q5H15	0.0	0.1	0.3	0.095	-1.3	0.1	1.5	1.000
Q5H5	Q15H5	-0.5	-0.3	-0.1	0.000	-1.8	-0.4	1.0	0.957
Q5H15	Q15H5	-0.6	-0.5	-0.3	0.000	-1.9	-0.5	1.0	0.914

group 1	group 2	Extension movement from +120 plus			
		lower limit 95% CI	mean of groups difference	upper limit 95% CI	p
w/o	Q0H5	8.1	9.6	11.1	0.000
w/o	Q5H0	10.8	12.3	13.8	0.000
w/o	Q5H5	9.7	11.2	12.7	0.000
w/o	Q5H15	10.2	11.7	13.2	0.000
w/o	Q15H5	10.7	12.3	13.8	0.000
Q0H5	Q5H0	1.3	2.8	4.2	0.000
Q0H5	Q5H5	0.1	1.6	3.1	0.025
Q0H5	Q5H15	0.7	2.2	3.6	0.002
Q0H5	Q15H5	1.1	2.7	4.3	0.000
Q5H0	Q5H5	-2.6	-1.1	0.4	0.221
Q5H0	Q5H15	-2.1	-0.6	0.9	0.810
Q5H0	Q15H5	-1.6	-0.1	1.5	1.000
Q5H5	Q5H15	-1.0	0.5	2.0	0.881
Q5H5	Q15H5	-0.5	1.1	2.6	0.338
Q5H15	Q15H5	-1.0	0.5	2.1	0.899

7.6 Study with the Digital Model

7.6.1 Mathematical Description of the Visco-Elastic Behaviour of the Ligaments

The visco-elastic behaviour of the ligaments is depicted by Kelvin-Voigt element, which consists of a parallel arrangement of an elastic spring element and a viscous damper element (Figure 7-23).

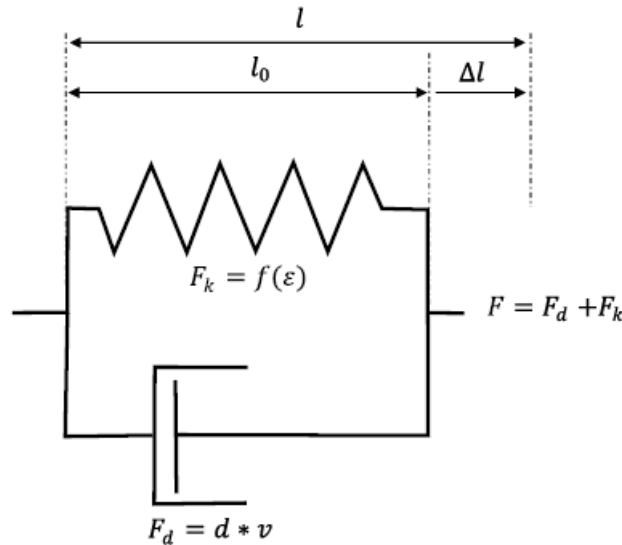


Figure 7-23 Kelvin Voigt Element used to model the visco-elastic behaviour of the ligaments off the digital model.

The resultant force is calculated using equation 7-4, with the elastic part $F_k(\varepsilon)$ and the viscose part $F_d(v)$.

$$F = F_k(\varepsilon) + F_d(v) \quad 7-4$$

The viscose part is dependent on the velocity v as given in equation 7-5.

$$F_d(v) = d * v \quad 7-5$$

The viscose part dampens the system, reducing the energy and oscillations of the system. The digital model is used for quasi-static experiments. Therefore, velocities are small, and the effect of the viscose element is neglectable. If the model is used for

dynamic tests in the future, the viscose part should be looked at more closely and optimized.

The elastic part of the ligaments in the used MBS-model is modelled by the non-linear-elastic model by Blankevoort and Huiskes (1991), which is a development of the model by Crowninshield et al. (1976). The force F_k represents the elastic part of the ligament and is dependent on the strain ε , which is separated in a non-linear and a linear part by ε_l as demonstrated in Figure 7-24 and described by a continuous function defined in sections according to equations 7-6 to 7-9, with l_0 as the initial length and l the actual length of the ligament, and the stiffness k .

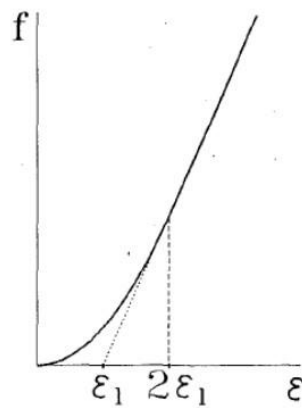


Figure 7-24 Exemplary force-strain curve of the ligaments, which is described by a non-linear part and a linear part separated by ε_l (Blankevoort and Huiskes 1991).

$$F_k = 0 \quad \varepsilon < 0 \quad 7-6$$

$$F_k = \frac{k\varepsilon^2}{4\varepsilon_l} \quad 0 < \varepsilon < \varepsilon_l \quad 7-7$$

$$F_k = k(\varepsilon - \varepsilon_l) \quad \varepsilon > \varepsilon_l \quad 7-8$$

$$\varepsilon = \frac{l - l_0}{l_0} \quad 7-9$$

7.6.2 Determination of the Stiffness k and Parameter ε_l

Determining the stress-strain characteristics of the ligaments is not easy. The characteristics of the LARS ligaments and given characteristics for knee models in literature differ greatly from each other (see Figure 7-25).

The stiffness k and the parameter ε_l of the LARS ligaments used in the surrogate can be extracted from the force-strain diagrams in the data sheets of the ACL (60 fibres), PCL (80 fibres) and LCL (100 fibres) and extrapolated for the MCL (32 fibres).

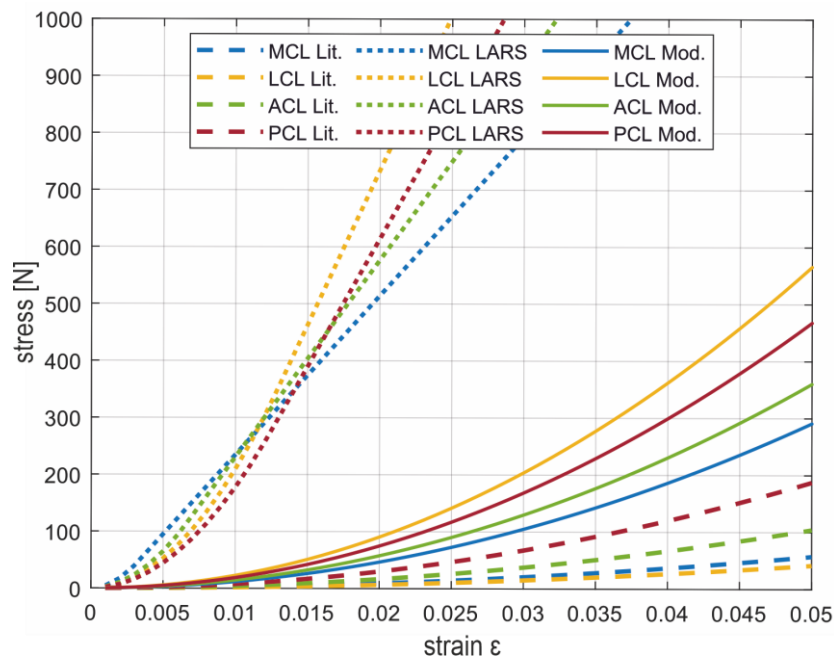


Figure 7-25 Characteristic of the collateral and cruciate ligaments according to literature (Blankevoort and Huiskes 1991) (dashed line), the data sheet of the LARS Ligaments (dotted line) and modified characteristics for the use in the MBS-model representing the behaviour of the surrogate.

In the used surrogate, the ligaments are effectively much longer than in the MBS-model since the ligaments are not implemented directly to the insertion site but through holes in the bones to the insertion and are fixed at the outer side of the bone. To be able to map this influence on the stiffness, the parameter k must be adapted. To obtain a realistic stress-strain behaviour, equations 7-10 and 7-11 must apply. It is assumed that the ligaments in the model are half as long as in the surrogate. Thus, according to equation 7-12, if the initial length l_0 is half, the stiffness k must be halved.

$$F_{Model} = F_{Surrogate} \quad 7-10$$

$$\Delta l_{Model} = \Delta l_{Surrogate} \quad 7-11$$

$$k_{Model} = k_{Surrogate} \frac{l_{0,Model}}{l_{0,Surrogate}} \quad 7-12$$

The characteristics of the LARS Ligaments show only a very small non-linear range. This behavior is not realistic for use in the surrogate. In the surrogate, the open fiber bundles are wrapped around the edges of the holes through which the ligaments are guided. This can lead to significant changes in the cross-section of the open fiber bundles and thus increases the non-linear part significantly. Especially because there is also a settlement behavior of the fixation of the ligaments. For these reasons, it must be assumed that the non-linear part is significantly larger in the present application. A value of $\varepsilon_l = 0.03$ presumed. This value is also used in the literature to model all ligamentous structures of the knee joint (Blankevoort and Huiskes 1991; Putame et al. 2019). The parameters of all characteristics are given in Table 7-11.

Table 7-11 Parameters of the non-linear-elastic model of the ligaments by Blankevoort and Huiskes (1991), LARS Ligaments, and the modified parameters used for the present MBS-model.

Ligament	Literature		LARS Ligaments		modified (used in the MBS-model)	
	k [N]	ε_l	k [N]	ε_l	k [N]	ε_l
MCL	2750	0.03	29739	0.0016	13967	0.03
ACL	5000	0.03	34591	0.0033	17296	0.03
PCL	9000	0.03	44897	0.0063	22449	0.03
LCL	2000	0.03	54320	0.0064	27160	0.03

7.6.3 Determination of the Initial Length l_0

The initial length of a ligament is a critical and not easy-to-determine parameter (Bloemker et al. 2012). The following method was applied to determine the initial length of the ligaments in the surrogate.

- (1) The internal and external rotation of the knee joint was blocked.

- (2) Tibia and Femur are in full extension.
- (3) Medio-lateral and anteroposterior translation of the tibia was blocked.
- (4) Application of 10 N axial force resulting in a compression of the knee joint to achieve an adjusting of the position of the tibia towards the femur.
- (5) Measuring the reference length of the ligaments l_r .
- (6) Calculation of l_0 for the PCL and LCL using formula 7-13 and the parameter ε_r of -0.27 for the PCL and 0.008 for the LCL as given by Blankevoort and Huiskes (1991).

$$l_0 = \frac{l_r}{(1 + \varepsilon_r)} \quad 7-13$$

- (7) Release the medio-lateral and anteroposterior translational degrees of freedom.
- (8) Apply reference forces for the ACL $F_{r,ACL} = 50N$ and MCL $F_{r,MCL} = 45N$ as applied in the studies using the surrogate (chapter 2.2.3).
- (9) Measure reference length l_r for the ACL and MCL.
- (10) Calculate l_0 for ACL and MCL using the assumption 7-14 and formula 7-15.

$$0 \leq \varepsilon_r \leq \varepsilon_l \quad 7-14$$

$$l_0 = \frac{l_r}{2\sqrt{\frac{F_r \varepsilon_l}{k} + 1}} \quad 7-15$$

The resulting initial length of the ligaments are listed in Table 7-12.

Table 7-12 Initial length of the ligaments used in the MBS-model.

Ligament	l_0 [mm]
MCL	51.6 + 43.5
ACL	29.8
PCL	30.6
LCL	71.7

7.6.4 Parameter Sensitivity Study

While performing studies with the surrogate, certain parameters, such as the initial length of the ligaments and pre-loads of the PCL and LCL, are not known. The pre-loads of the PCL and LCL are set once to achieve a correct alignment of the femur and tibia and are not changed or controlled afterward. The results of different implementations of ACL and PCL, either as double bundle or as single bundle, were already shown in chapter 3.1.2

A sensitivity study is performed to determine the influence of these unknown parameters of the surrogate. The simulated knee flexion ranges from -5° to 135° .

7.6.4.1 Test Scenarios

Variation of the initial ligament length

The initial length l_0 of ACL, PCL, LCL and MCL is shortened and lengthened by $\pm 5\%$ and compared with the initial state (Table 3-5). In each test, only one ligament is modified and the effect on all ligaments is observed. A variation of the initial length is equal to a variation of the pre-tension.

Variation of the spring characteristics

The determination of the parameters k and ε_l given in Table 3-5 can be found in the appendix 7.6.2. As different values can be found in literature (Blankevoort and Huiskes 1991) and also the LARS-Ligaments of the surrogate have different parameters, the effect of using the parameters reported in literature and of LARS on the results of the modelling are tested.

7.6.4.2 Results

Variation of the initial ligament length of the ACL (Figure 7-26)

As the ACL is only loaded in hyperextension, and smaller and larger flexion angles, changing the initial length of the ACL does affect ACL loads in these ranges of knee flexion. These knee flexion ranges of a loaded ACL increase (meaning a shift of flexion angle, where the ACL is unloaded) by shortening the length of the ligament, having a more pronounced effect for larger flexion. A reduced initial length increases ACL loads, and an increased initial length reduces ACL loads. A shortened or lengthened ACL does effect PCL loads for flexion angles above 90° , with the effect synchronous to the affect the ACL experiences itself. For small flexion angles, the loads of the collateral

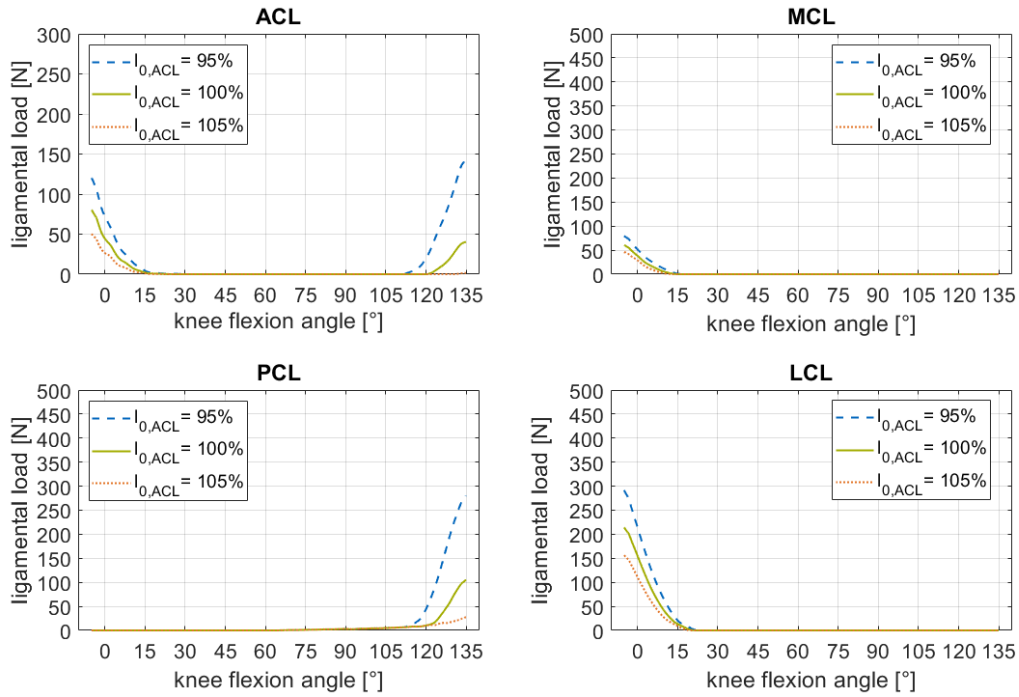


Figure 7-26 Effect of a variation of the initial length of the ACL on the MCL, PCL, and LCL.

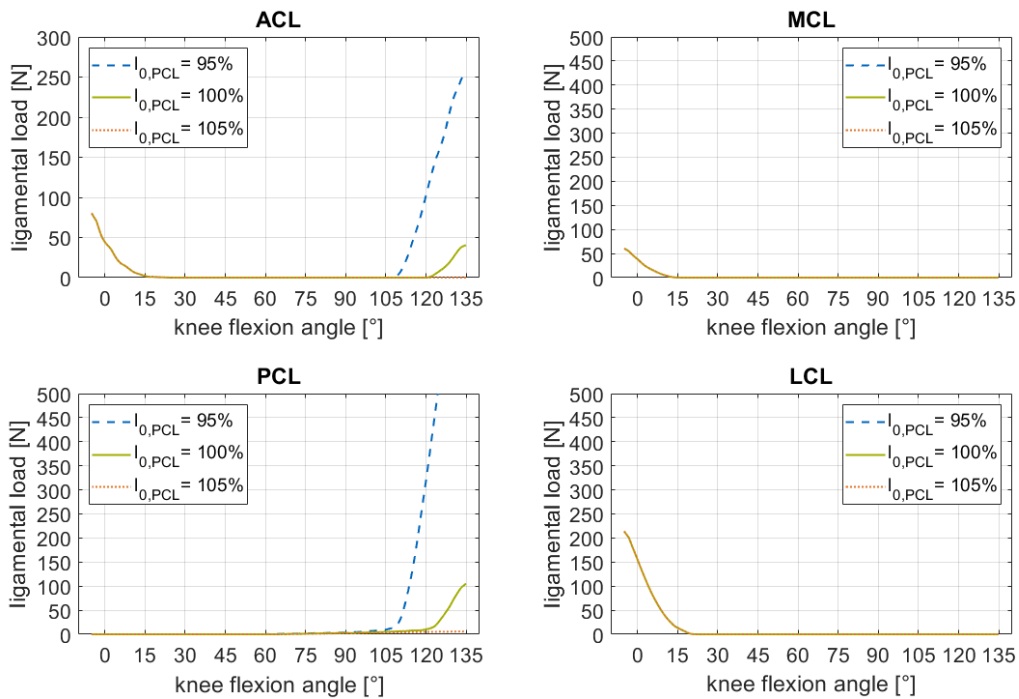


Figure 7-27 Effect of a variation of the initial length of the PCL on the MCL, ACL, and LCL.

ligaments are increased by a reduced and reduced by an increased initial length of the ACL. The flexion angle of an unloaded MCL and LCL does not shift noticeably due to a changed initial length of the ACL.

Variation of the initial ligament length of the PCL (Figure 7-27)

Changing the initial length of the PCL only affects ACL loads for large flexion angles (>105°). Shortening the PCL increases ACL loads and shifts the flexion angle of an unloaded ACL to a smaller flexion angle. Lengthening the PCL as the contrary effect. The effect is synchronous on the PCL itself. No effect of a varied initial length of the PCL can be observed on the MCL or LCL.

Variation of the initial ligament length of the MCL (Figure 7-28)

The initial length of the MCL does strongly affect the load of the MCL itself. In hyperextension, reducing the initial length by 5% does increase the MCL load above the strength of the ligament (Robinson et al. 2005) and leads to (high) loading of the MCL from hyperextension to 120° knee flexion. A lengthening of the MCL does reduce MCL loads, but only to a smaller effect. For flexion angles smaller than 30°, a reduced initial MCL length increases ACL loads, an increased initial MCL length reduces ACL loads. Also, the flexion angle of an unloaded ACL is affected in the same manner. PCL loads are not or are minimally affected by the initial length of the MCL. LCL loads decrease with an increased MCL length for flexion angles smaller than 20° and increase with a decreased MCL length for flexion angles between 15° to 90°.

Variation of the initial ligament length of the LCL (Figure 7-29)

Reducing the initial length of the LCL by 5% does strongly increase ACL, MCL and LCL loads for flexion angles from hyperextension to 30° for the ACL, 45° for the MCL, and 60° for the LCL and shifts the respective flexion angle of an unloaded ligament to higher values. A lengthening of the LCL does only affect the ACL and LCL, decreasing the ligament loads for flexion angles smaller than 15°. The PCL is not affected by the variation of the initial length of the LCL.

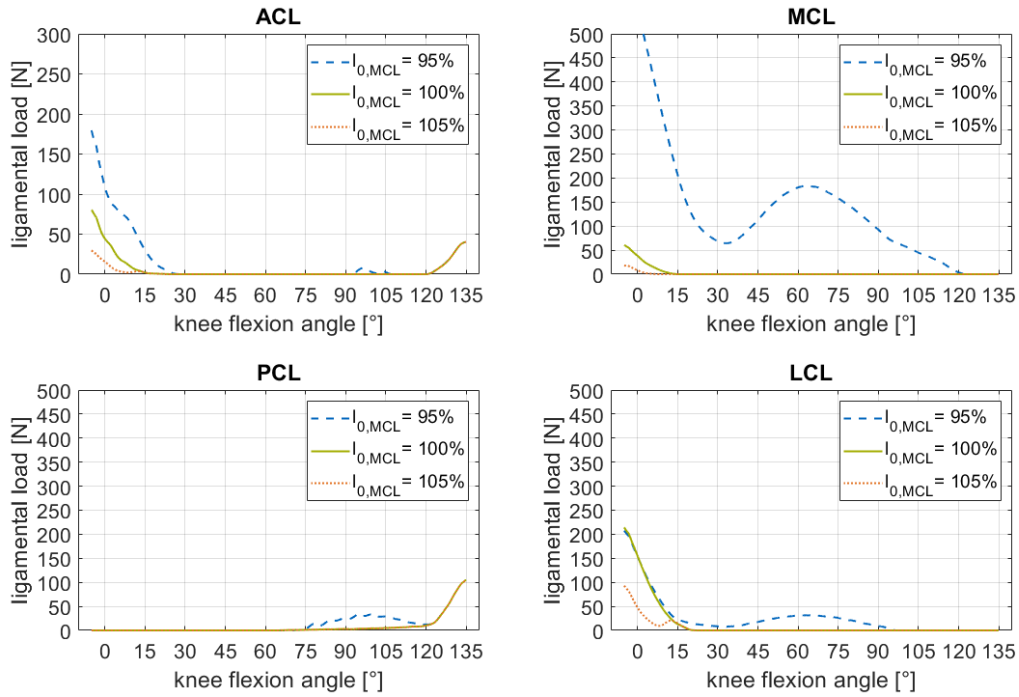


Figure 7-28 Effect of a variation of the initial length of the MCL on the ACL, PCL, and LCL.

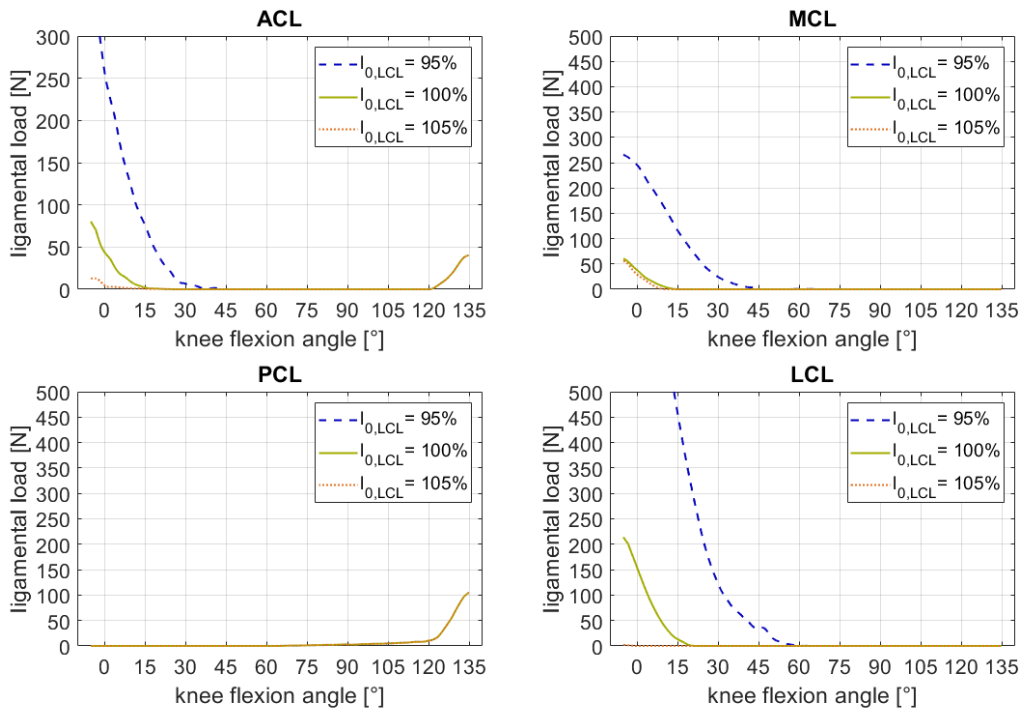


Figure 7-29 Effect of a variation of the initial length of the LCL on the MCL, PCL, and ACL.

Effect of a variation of the initial length of the cruciate and collateral ligaments on the ACL

It is observable that a shortening of the initial length of all four ligaments has a more significant effect on the resulting ACL loads (Table 7-13). This is not surprising, as a shortening of a ligament corresponds with an increase of tensile stress in the ligament, which consequently must be counteracted by the other structures of the knee.

Table 7-13 Influence of the initial lengths of the ACL, PCL, MCL, LCL on ACL loads

Varied ligament	$I_0 = 95$ NRMSE [%]	$I_0 = 105\%$ NRMSE [%]
ACL	28.7	11.1
PCL	71.7	8.6
MCL	30.3	12.2
LCL	86.9	15.7

Variation of the spring characteristics

The results shown in Figure 7-30 clearly show that it is not simply possible to use the spring characteristic of the LARS ligaments for the digital model, even though the model represents the surrogate with LARS ligaments implemented. Using these spring characteristics would lead to unrealistic high ligamental loads. On the other hand, it is also not expedient to use spring characteristics reported in the literature, as, in this case, this would result in unrealistic small ligamental loads.

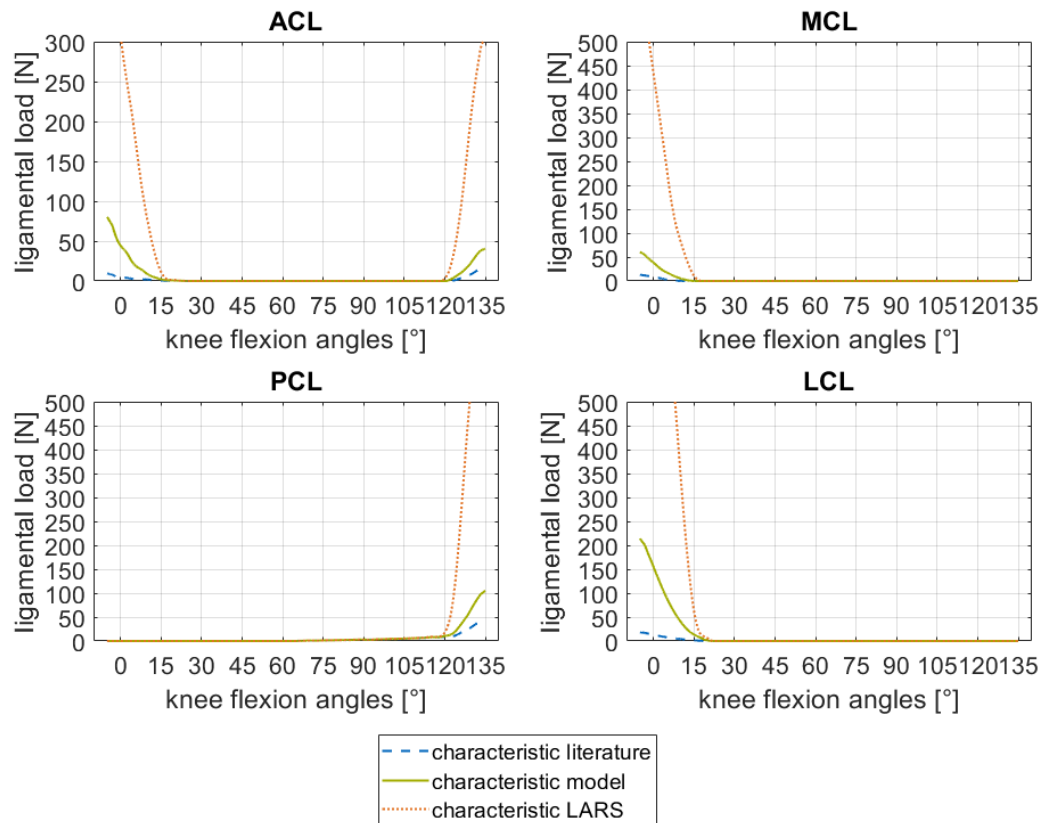


Figure 7-30 Effect of using different spring characteristics of the ligaments. Blue: characteristics reported by Blankevoort and Huiskes (1991); green: characteristics used in the digital model presented in this work; orange: characteristics of the LARS ligaments used in the surrogate presented in chapter 3.1.

7.6.4.3 Discussion

Variation of the initial length of the ligaments

The initial length of the ligaments strongly affects the ligament loads. As the initial length corresponds to a pre-loading of the ligaments, this was expected. Moreover, the results show that ACL, MCL, and LCL are strongly interacting in small knee flexions, and ACL and PCL are interacting in larger knee flexions. These results need to be considered when doing further tests with the surrogate (see chapter 3.1), as the surrogates LCL and PCL do not have implemented force sensors to control the pre-tension.

The initial length of the ligaments does affect the joint's kinematics (Bloemker et al. 2012). For example, the relative position, and thus, the resulting kinematics, of the tibia and femur in the sagittal plane is influenced by the length of the ACL and PCL (Jagodzinski et al. 2016). The initial ligament length in this study was determined by

measuring the distance between the insertion sites for defined tibia-femur-alignments (see appendix 7.6.3). The optimised initial length of a modelled patient or specimen can be determined by elaborate methods (Bloemker et al. 2012; Bertozzi et al. 2008), which would be valid for the individual but may not be transferable to other individuals.

Variation of the spring characteristics of the ligaments

The results show that using literature-based characteristics leads to large deviations from the results when using the model-based characteristics. The latter is a result of an optimization to resemble the behaviour of the surrogate presented in chapter 3.1. Naghibi Beidokhti et al. (2017) also came to the conclusion that using literature-based parameters lead to large errors compared to individualized parameters. As each model is developed with different goals, assumptions, and simplifications, this is to be expected. The simulations using LARS-characteristics result in extremely higher loads than measured in the surrogate studies. This indicates that the mechanical properties of the surrogate (e.g., bone contact areas, fibre structure of the ligaments, friction coefficient) differ or are more complex than implemented in the digital model. Therefore, a model-specific spring characteristic aims to compensate for these differences.

7.7 Basics of Pressure Sensors and Pressure Sensor Measurements

This chapter provides an overview of various physical principles for pressure measurement.

Pressure as a physical quantity is defined as the ratio of a force to the area on which it acts. Various principles are available for measuring pressure: piezoelectric, resistive, and capacitive measuring systems as well as pneumatic and hydraulic pressure measuring methods.

In biomechanical applications, thin, flexible sensors, so-called thin-film sensors, are often used to measure pressure, as these can adapt to the natural curvature and, due to their small thickness, do not press into the softer object (e.g. the subject's body), which would locally increase the pressure (Ashruf 2002). Pneumatic and hydraulic sensors, however, require a complicated structure, which in turn is associated with a thickness of several millimetres (Gyi et al. 1998) and can therefore not be implemented as thin-film sensors (Ashruf 2002).

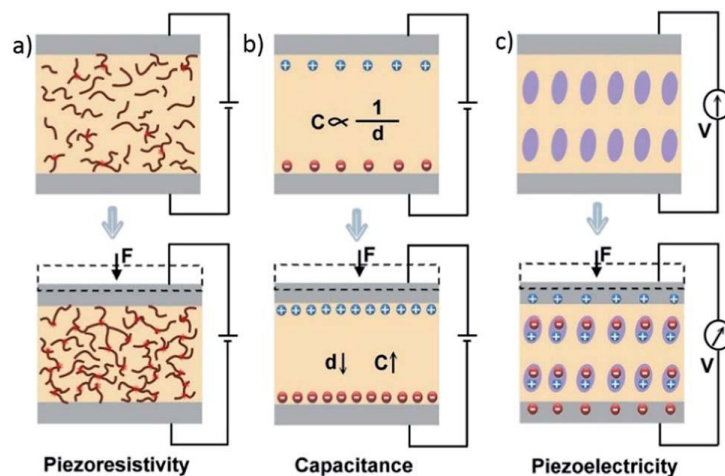


Figure 7-31 Commonly used principles for pressure measurement in thin film sensors. Image taken from (Zang et al. 2015) © Royal Society of Chemistry, reprinted with permission.

The three other principles of pressure measurement (resistive, capacitive, and piezoelectric) and their characteristics are described in detail by Zang et al. (2015) and are shown schematically in Figure 7-31. The methods are based on the conversion of compressive forces into electrical signals.

- Piezoresistive sensors measure changes in electrical resistance as a result of the applied pressure (Figure 7-31 a)).
- Capacitive pressure measurement is based on the principle of changing the capacitance between two capacitor plates, caused by a change in the distance between the plates (Figure 7-31 b)).
- Piezoelectric sensors determine the change in the electrical charge of certain materials as a result of mechanical deformation (Figure 7-31 c)).

The piezoelectric measuring principle is not suitable for static measurements due to a leakage current (Ashruf 2002) which results in a decrease in the measured value of the sensor which would finally become zero. Therefore, the most widely used measuring principles are capacitive and resistive pressure measurement.

Capacitive pressure measurement

Capacity is the ability to absorb and store electrical charge. The capacitance C of a plate capacitor with area A is inversely proportional to the distance d between the plates (electrodes):

$$C = \varepsilon_0 \varepsilon_r \frac{A}{d}$$

with the material constant ε_r as the relative static permittivity of the material between the plates and ε_0 as the electric field constant. As observable in Figure 7-31 b), external forces change the distance d between the plates, which results in a change in the capacitance C (Zang et al. 2015). Various methods are available to measure this change in capacity, including frequency measurement, impedance measurement, or the measurement of charging and discharging times (Meyer 2008).

A capacitive sensor is made up of two capacitor plates made of conductive material with a dielectric, elastic layer in between (Morère et al. 2016). An example of a textile capacitive sensor by Meyer (2008) is shown in Figure 7-32 consisting of two layers of conductive textile lying perpendicular to one another, which represents the capacitor plates at the overlapping points, with a compressible intermediate layer and non-conductive yarn as a spacer in between.

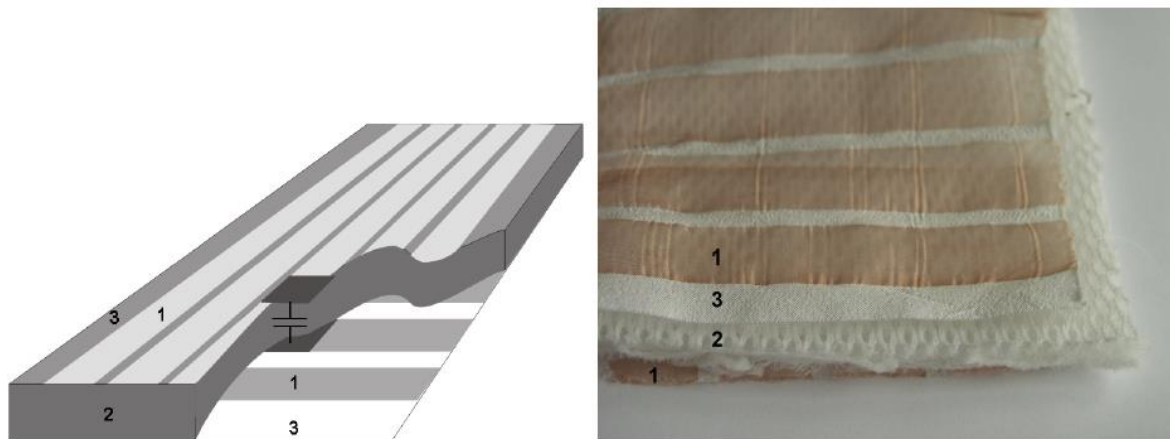


Figure 7-32 Principle of a capacitive textile sensor (left) and prototype (right) presented by Meyer (2008). The conductive textiles are arranged in perpendicular stripes (1) forming the capacitor and are separated by a compressible spacer (2). The stripes are separated by non-conductive yarn (3).

The main advantage of capacitive measurement technology lies in its moisture and temperature resistance (Ashruf 2002). The drawback is the need for a complicated evaluation unit. The changes in capacity are mostly in the range of pF or less, which requires a highly sensitive and precise readout module (Ashruf 2002; Zang et al. 2015). Due to the structure of the various layers, the sensor also requires a certain thickness (Morère et al. 2016).

The output of capacitive sensors is the mean of the acting pressure on the sensor surface.

Examples of commercial capacitive pressure sensors are the emed®-system as well as the pedar® pressure measurement insole, both from Novel (Munich, Germany, <http://www.novelelectronics.de/>) for measuring the plantar pressure distribution.

Resistive pressure measurement

The principle of resistive pressure measurement is based on the decrease in the specific resistance of a piezoelectric layer with increasing pressure. This is caused by the formation of percolation networks (Figure 7-33) with increasing pressure (Ashruf 2002; Razak et al. 2012).

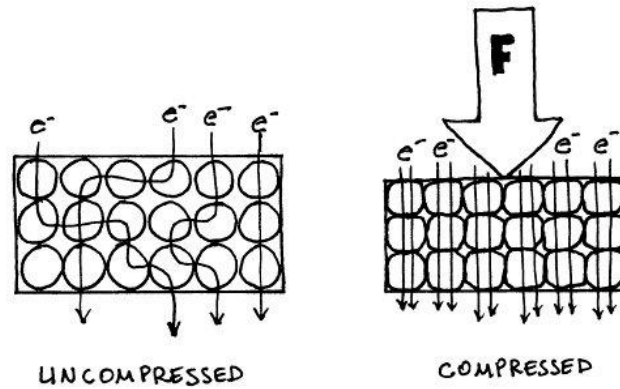


Figure 7-33 Pressure dependant resistance by the formation of percolation networks. Image source: www.openmusiclabs.com/learning/sensors/fsr/, visited on 2021, Jan 10.

The most widespread structure of a resistive pressure sensor consists of two thin, flexible polymer foils fitted with electrically conductive structures. Either pressure-sensitive semiconducting ink is applied to the conductive connection pattern or a piezoresistive semiconducting foil is used as a pressure-sensitive material layer between the two conductive layers (Ashruf 2002).

Examples of commercial sensors based on this principle are the pressure sensors from Tekscan Inc. (Boston, USA, <https://www.tekscan.com/products-solutions/sensors>). These are available on the one hand as a platform system (Tekscan MatScan®), as a pressure measurement sole for use in the shoe (Tekscan F-Scan®), or as individual thin-film pressure sensors (FlexiForce™). The manufacturing process of these thin film sensors is described in Hunston (2002).

An example of a logging unit for six resistive pressure sensors is described by Shu et al. (2010) and is shown in Figure 7-34. The signals from the sensors enter the circuit via a connector and are connected in series with a reference resistor (R_{ref}). The sensors are connected to the input voltage V_{cc} and the earth (GND) via this series connection.

The voltage between the reference resistor and the sensors is read out via a channel of the analog-digital converter (ADC) of the microprocessor (MCU).

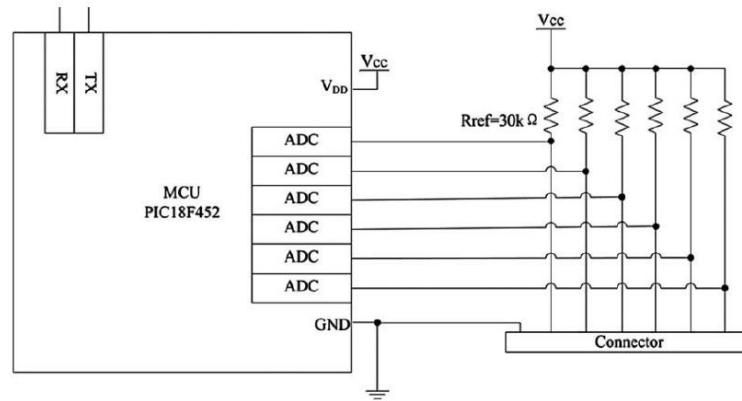


Figure 7-34 Schema of a data acquisition unit for recording six textile pressure sensors (Shu et al. 2010) © 2010 IEEE, reprinted and altered with permission.

The digitalized values D_{out} are then recalculated into the respective resistive values of the sensors R_{Sensor} via the formula:

$$D_{out} = 2^m \frac{R_{ref}}{R_{ref} + R_{Sensor}}$$

with m being the bit-number of the A/D-converter and R_{ref} the reference resistor (Shu et al. 2010).

The advantages of resistive pressure technology are the simple evaluation module as well as the simple structure and the fast response time. In addition, resistive sensors are well suited for the measurement of a wide range of pressure (Zang et al. 2015). Limitations of resistive pressure sensors are non-linearities and sensitivity to temperature and humidity.

The output of resistive sensors is the maximum of the acting pressure on the sensor surface. Therefore, small wrinkles in textiles pressing on the sensor can result in a significant distortion of the measured pressure distribution.

Limitations of thin-film sensors

Thin-film sensors, regardless of which type, have limitations that must be considered. These can include hysteresis and non-linear behaviour (Ashruf 2002). A sensor maps the relationship between the measured variable pressure (input) and the electrical signal of the sensor (output). If the output signal of the sensor is plotted against the pressure acting on the sensor (input signal), a characteristic curve for each individual

sensor can be acquired (see Figure 7-35). If this line is linear, there is a proportional relationship between the two quantities. If the characteristic curve is not linear an evaluation becomes significantly more complicated, since the input and output variables are not proportional to one another or are only proportional to one another over part of the measuring range. For this reason, a sensor with linear behaviour is to be preferred (Razak et al. 2012).

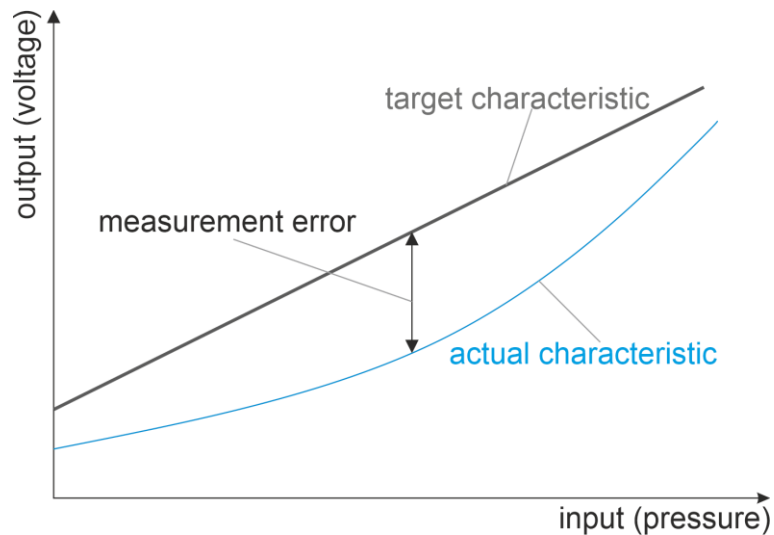


Figure 7-35 Schematic visualisation of an ideal and true sensor characteristic

The problem of hysteresis is illustrated in Figure 7-36. For a sensor showing hysteresis, the output signal of the sensor behaves differently when the pressure is increased than when the pressure is decreased. This problem can be attributed to effects at the molecular level, such as molecular friction, through which energy is lost (Beeby 2004).

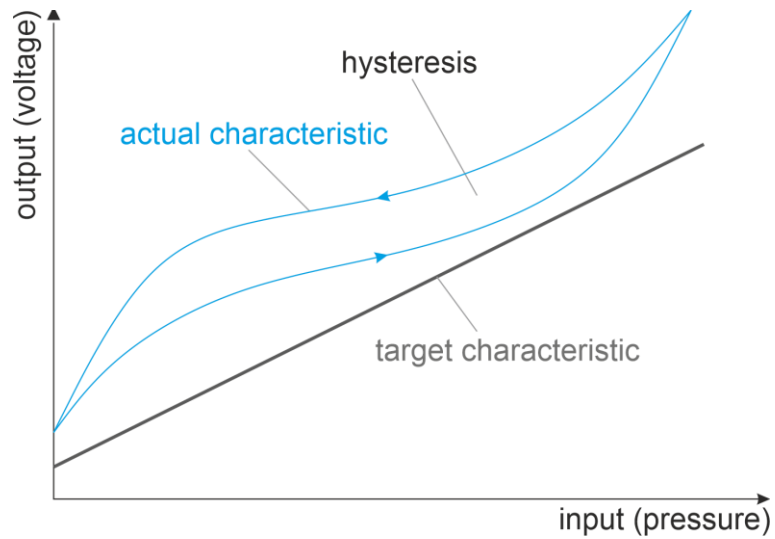


Figure 7-36 Schematic visualisation of sensor hysteresis

More detail on the problems of hysteresis and drift of pressure measurement sensors can be found in Meyer (2008). In his work, the author developed models to quantify these problems, by which he was able to reduce measurement errors of a pressure sensor caused by hysteresis from 60% to below 10%.

7.8 Pressure Sensors Measuring Loads on the Feet

In Chapter 4.2.3 three pressure sensing prototypes to measure loads in the ski boot were discussed. The following figure gives the Spearman correlations of each individual pressure sensor of all three systems with the six load components measured with the measurement binding.

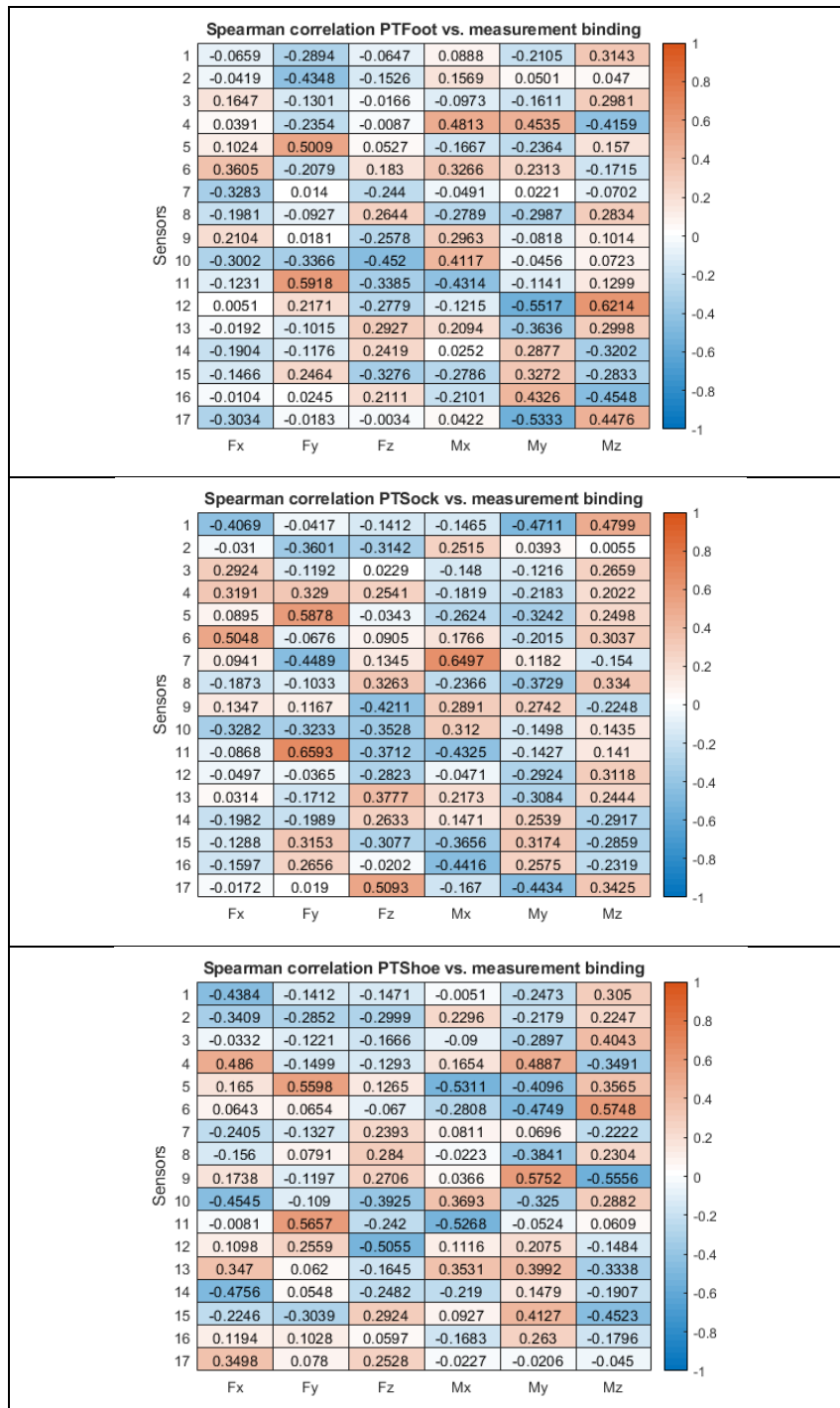


Figure 7-37 Spearman correlations between all sensors of each of the three prototypes and the measurements of the measurement bindings.

7.9 Speed of the Skier

7.9.1 Map Visualisation of Runs – Scenario D

Following Figures are referenced in Table 4-9 and visualize die six runs performed for test scenario D.

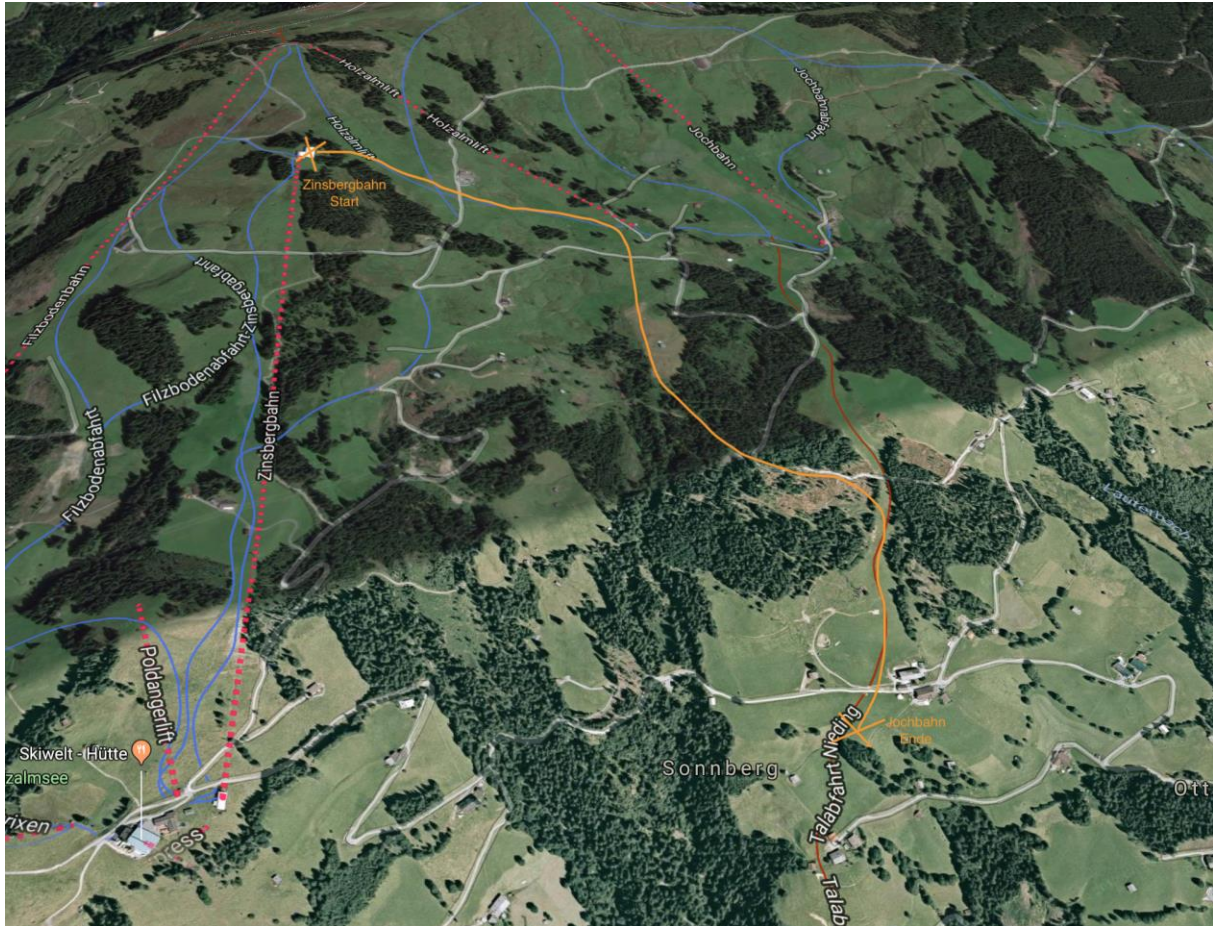


Figure 7-38 Map of run (orange line) "Zinsberg (top) to Jochbahn (bottom)

APPENDIX



Figure 7-39 Map of run (orange line) "Jochbahn (bottom) to Südhangbahn (bottom)"



Figure 7-40 Map of run (orange line) "Südhangabfahrt 2"

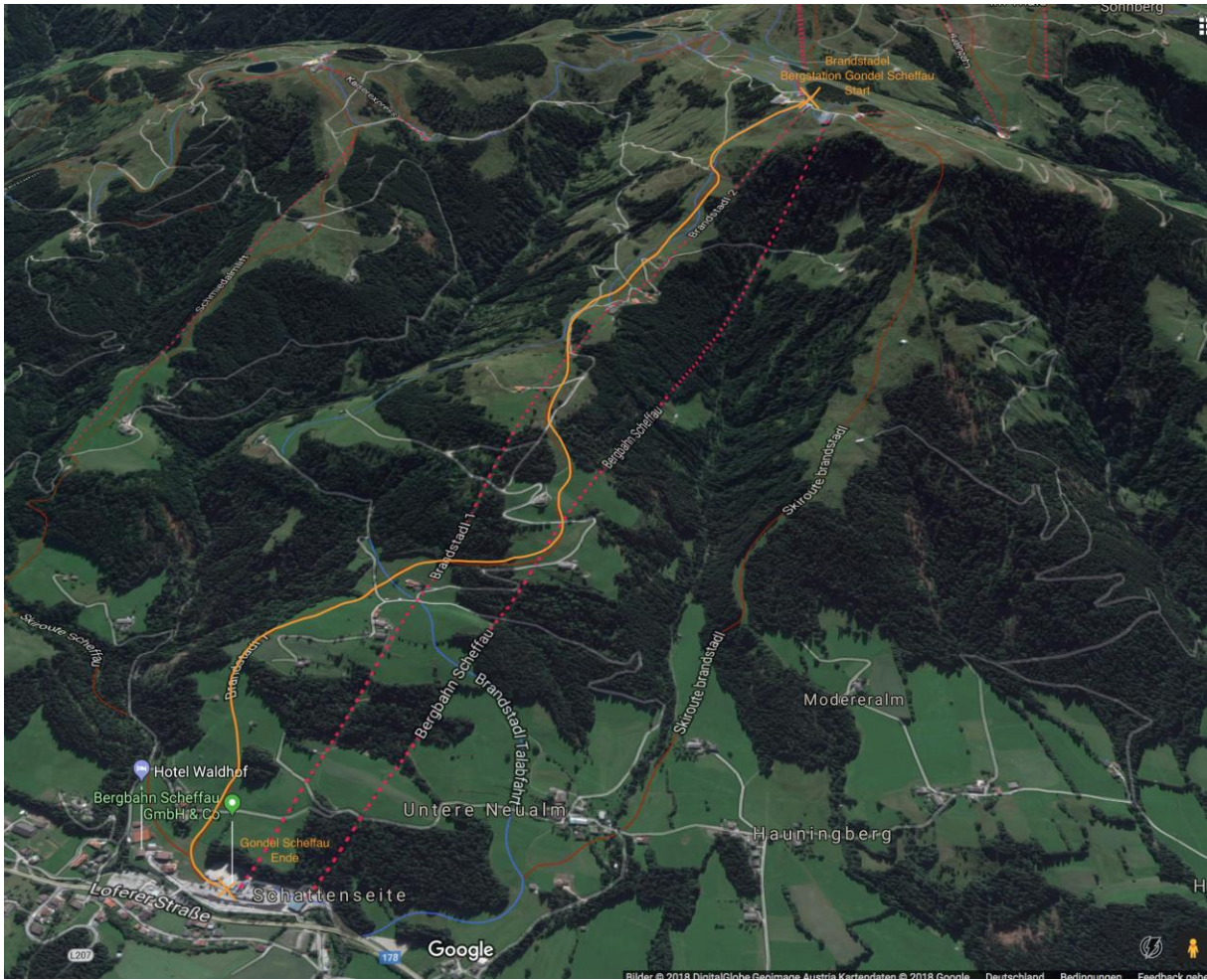


Figure 7-41 Map of run (orange line) “Talabfahrt Scheffau”

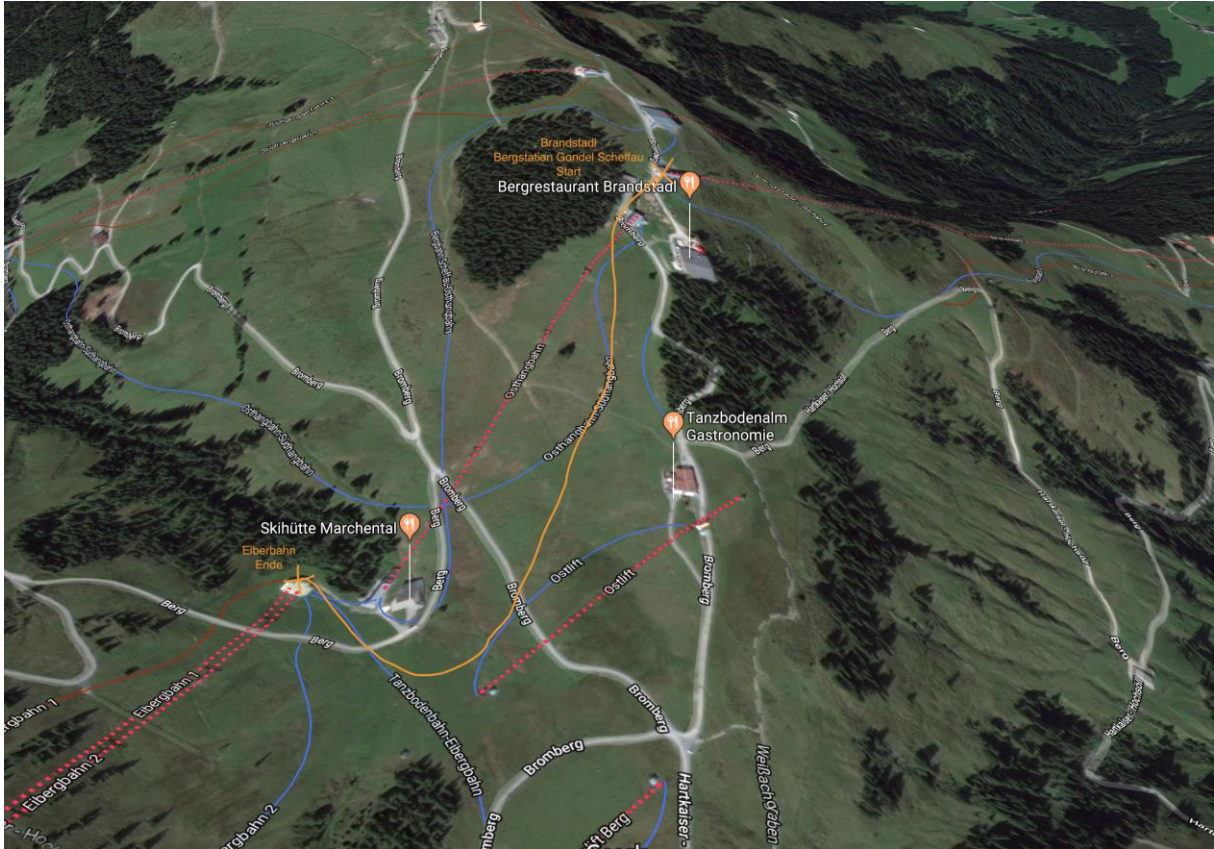


Figure 7-42 Map of run (orange line) "Gondel Scheffau (top) to Eiberbahn"



Figure 7-43 Map of run (orange line) "Aualmbahn (top) to Kälbersalvenbahn"

7.9.2 Kalman Filter

Since it is very difficult to determine the accuracy of the various measurements due to the high level of noise, this also leaves a certain amount of freedom when defining the covariance in the Kalman filter. The results of the data fusion can therefore be influenced by the different weighting.

If the uncertainty of the GPS measurement is very high, this leads to a drift of the integrated navigation solution with respect to the reference solution. The changes in speed are nevertheless displayed very precisely. With a low uncertainty of the GPS measurement, the noise of the filter navigation solution (integration of GPS in IMU data) increases, and the inertial solution is hardly taken into account (see Figure 7-44).

The filtered navigation solution (integrated navigation solution) from INS and GPS behaves better than the individual systems. Above all, the noise of the GPS measurement is greatly reduced by data fusion. If the GPS measurement deviates from the reference solution over a short period of time, this can in most cases be corrected by the integrated navigation solution. However, if the GPS measurement is subject to a major error for a longer period of time, the INS / GPS navigation solution will also drift. However, the merged solution adapts itself again relatively quickly to GPS measurements with minor deviations. Figure 7-45 and Figure 7-46 illustrate this behaviour using the example of a descent in long turns.

A consideration of the speed in the three coordinate axes of the earth-based system provides even better information about the course of the error. Any errors that cancel each other out due to the calculation of the absolute speed are also visible here. The behaviour in the different axes is shown in Figure 7-47.

Without assistance, the pure inertial navigation solution drifts after a few seconds and becomes unusable. Figure 7-48 illustrates the strong drift over a large time interval. Nevertheless, the recording of the dynamics of the system can be seen especially in the representation in the three spatial directions. Significant changes in speed in the reference solution are also detected by the inertial navigation solution.

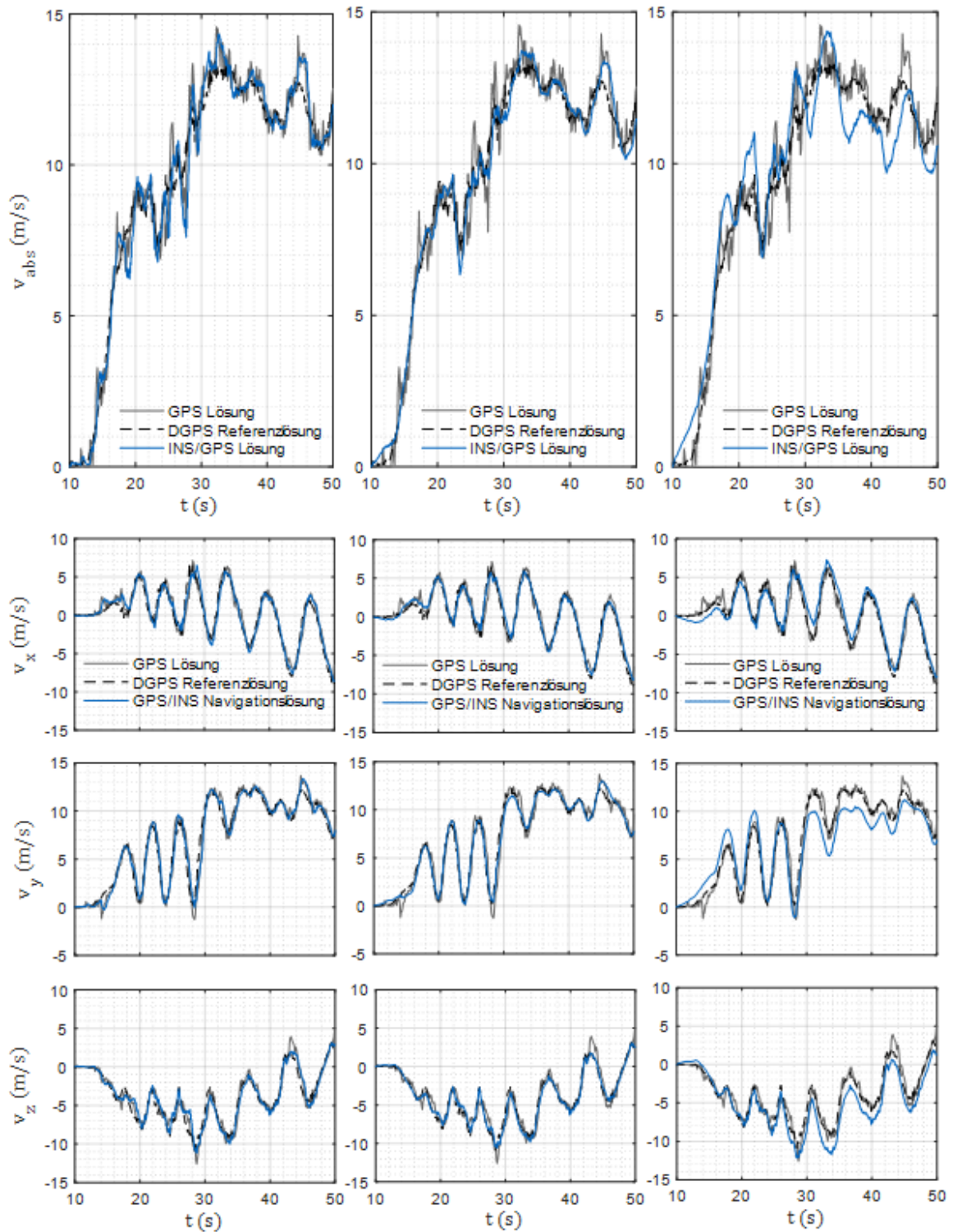


Figure 7-44 Speed absolute and in the axes of the earth-frame assuming a low (left), medium (middle) and high (right) uncertainty of the GPS measurement.

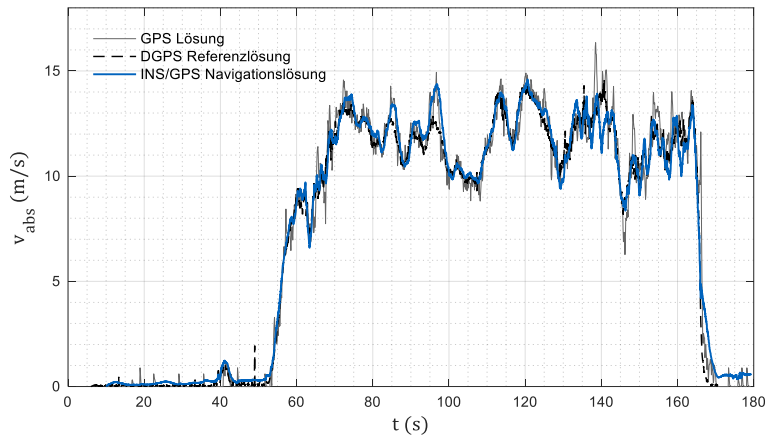


Figure 7-45 Behaviour of the absolute speed of the integrated navigation solution compared to the pure GPS measurement and the reference solution when skiing "long turns".

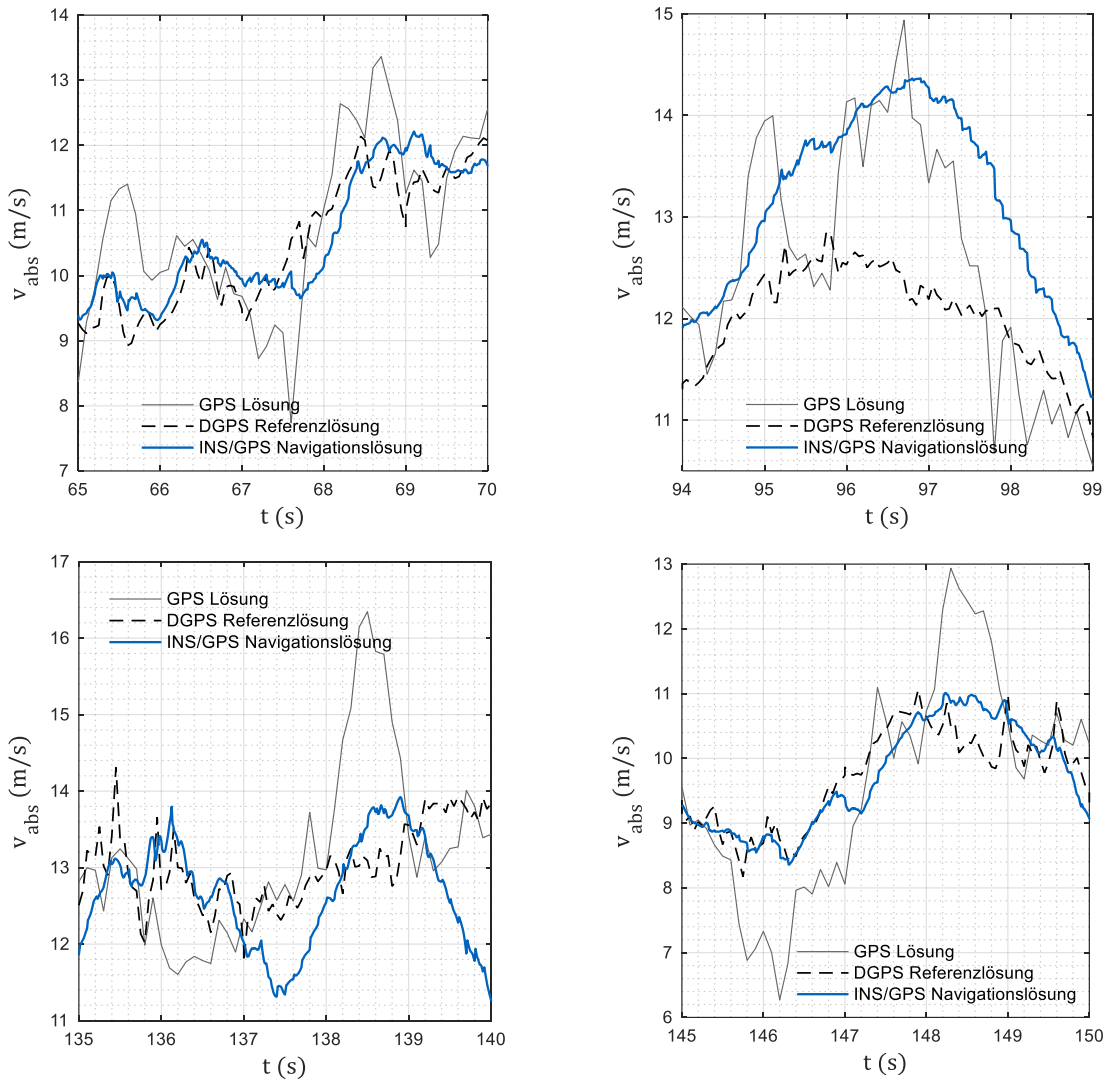


Figure 7-46 Examples of the behaviour of the absolute speed of the integrated navigation solution in the event of strong deviations of the GPS measurement from the reference solution when skiing "long turns".

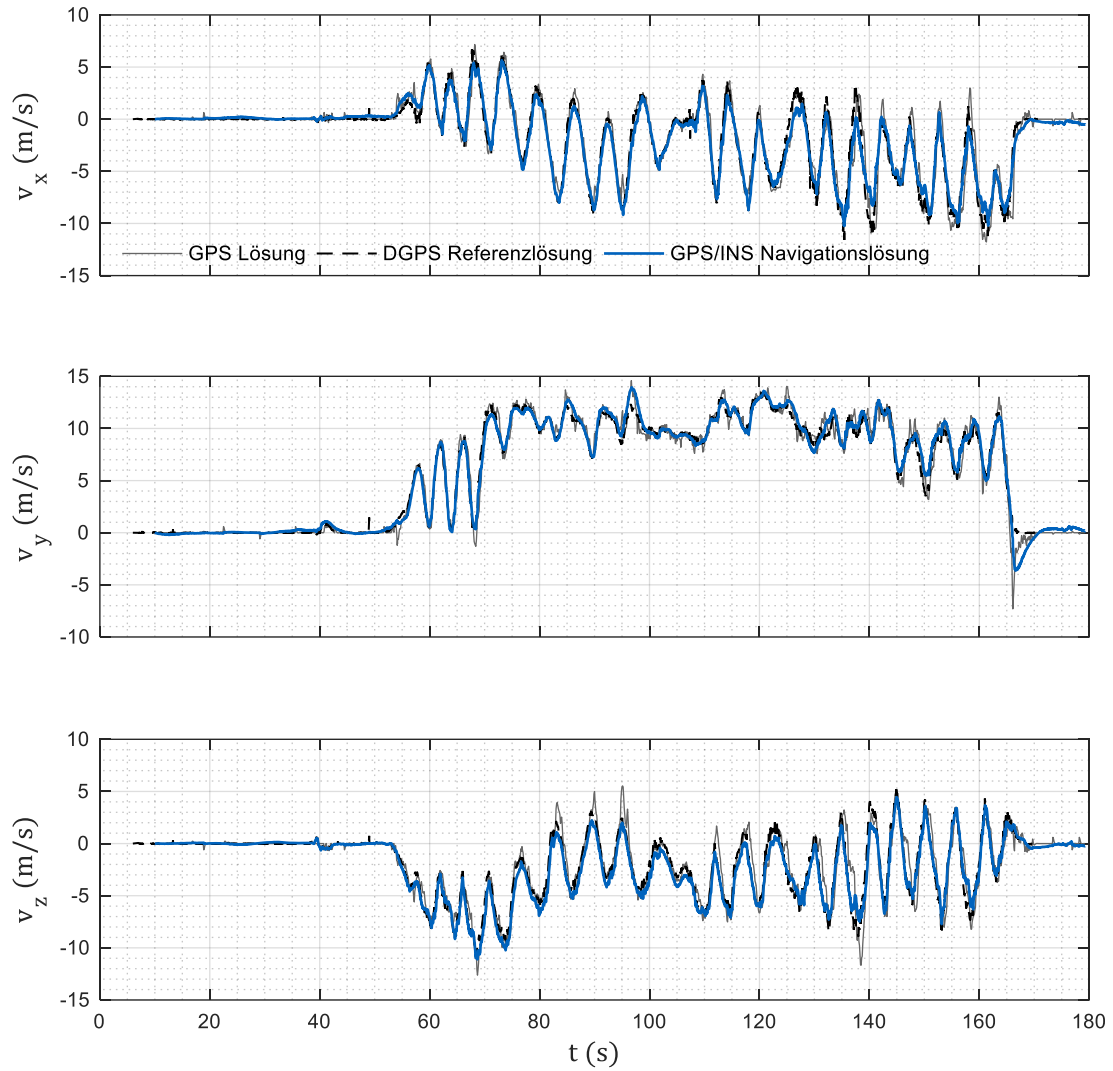


Figure 7-47 Behaviour of the speed of the integrated navigation solution in comparison to the pure GPS measurement and the reference solution when skiing "long turns" shown in the three coordinate axes of the earth-fixed coordinate system.

APPENDIX

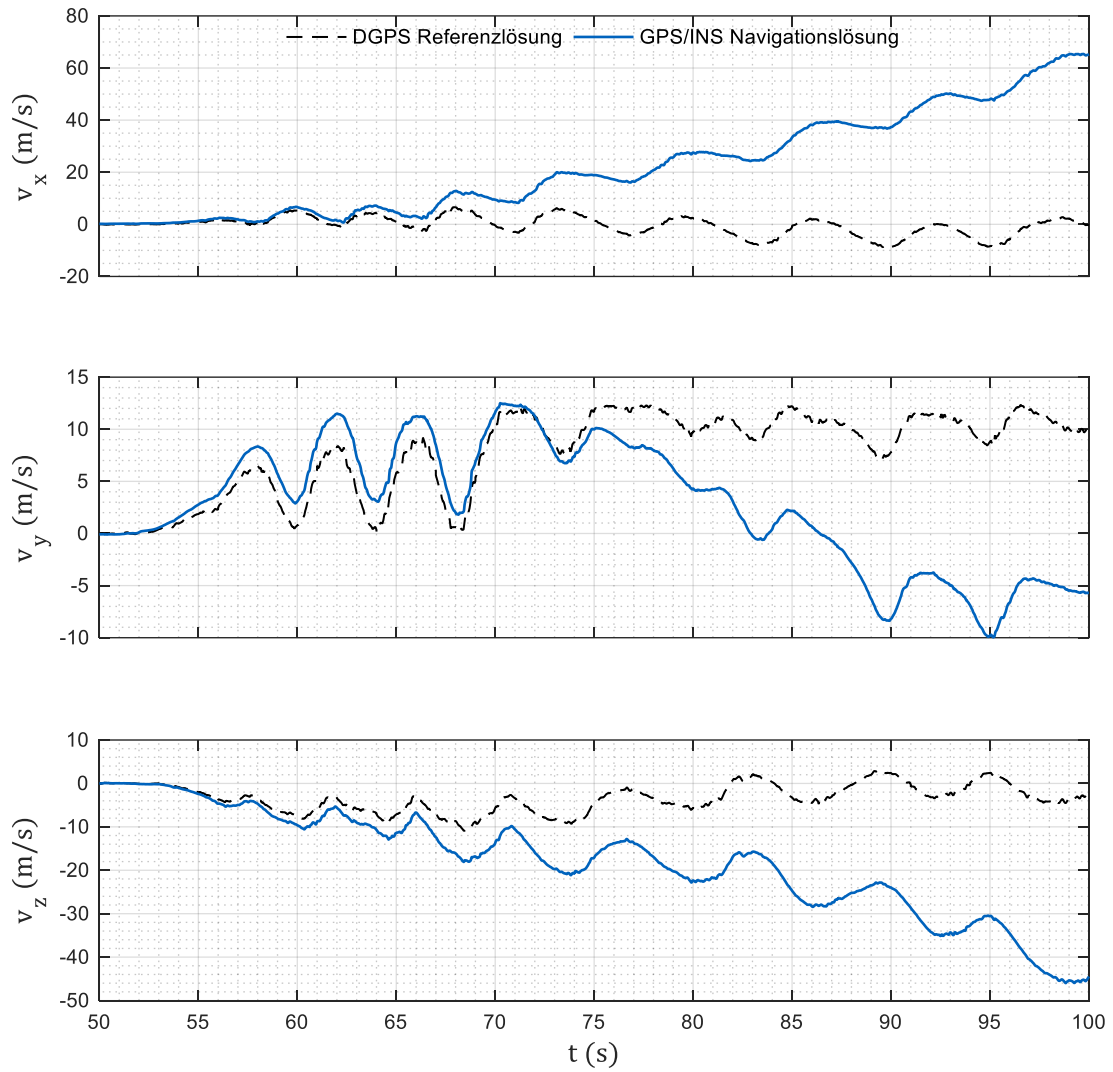


Figure 7-48 Behaviour of the speed of the integrated navigation solution compared to the reference solution when skiing "long turns" shown in the three coordinate axes of the earth-based coordinate system.

7.10 Algorithm of the Mechatronic Ski Binding

7.10.1 Definition of Risk Values

The following risk values are generated by manually defining a probability of injury for the ACL and are therefore subjective and should not be used in a real system without extensive validation and reassessment by other experts. For some load cases, the available information is not sufficient to allow a solely based definition of a risk value.

The risk values are used to define the membership functions for the output set of the fuzzy controller 1 (see Figure 4-53, Proposed Structure of the Algorithm).

The determination of the probability of injury to the ACL is mainly based on publications of Markolf's research group, as many different load conditions are investigated in the publications of this research group, and often a large flexion range of the knee joint is taken into account.

For this purpose, the diagrams from the publications were digitised using the software Get-Data GraphDigitizer 2.26 (<http://getdata-graph-digitizer.com/>; retrieved on 02.07.2018) by manually clicking on the measurement points in the software. Due to inaccuracies, it is possible that the exact values are not recorded. A random comparison of values measured with the software with the corresponding values stated exactly (in the body text of the publication) reveals an inaccuracy of up to 0.3 N. The values measured with the software are not exact. With a value range of 0 N to 300 N of the corresponding diagram, this inaccuracy seems acceptable.

In order to quantify, which load condition is present in the ACL, the mean values of the "force values" of the ACL of each test setup are divided on a scale from 1 (least force) to 10 (most force) to determine a "relative risk value". The difference between individual values varies depending on the range between the smallest and largest mean value and is calculated according to equation 7-16.

$$Difference = \frac{Mean_{most\ force} - Mean_{least\ force}}{10} \quad 7-16$$

Subsequently, the allocation to one of the seven knee positions (see appendix 7.10.2 Definition Membership Functions for the Knee Flexion Angle) takes place. For this

purpose, the values for the hyperextension and extension positions are taken directly from the studies if direct measured values are also available for the respective angle (-5° or 0°). If not (for example, Wascher et al. (1993) give measured values for the -1° and +1° positions, but not for the 0° position), the larger of the neighbouring measured values is used. For the other knee positions (near extension, small flexion, 90° flexion, and full flexion), the measured data in the range ±10° of the corresponding angle are also considered and the most frequently occurring risk value is taken. If several test results are available for the same load case (also by other authors), the most critical risk value is always taken for the respective knee angle.

This means that a relative risk value is assigned for each knee angle, depending on the other parameters (thigh muscle tension, rotation moment, varus/valgus moment). This relative risk value must then be compared to the other conditions and evaluated. Therefore, k adjustment values are added to the relative risk value depending on the load case, so that the absolute risk value for each load case i results according to equation 7-17:

$$\text{risk value} = \text{relative risk value} + \sum_{k=1}^i \text{adjustment}_k \quad 7-17$$

Results from the studies with the multi-body-model reported in chapter 3.2 are not included in the definition of the risk values because not all results of these investigations are validated satisfactorily as some simulation cases were far outside the boundaries of the validated range of the model. Similar load cases must first be investigated using the surrogate (chapter 3.1) or by other laboratories.

The resulting risk values for a total of 30 load cases are given in Table 7-14 to Table 7-17.

Risk values above 10 are assigned as “critical” and the retention torques My and Mz are adjusted by reducing them by 15 %. There is no gradual adaption at this stage of the proposed algorithm (for example a reduction of 5% would be conceivable for risk values between 11 and 15, a reduction of 10% for risk values between 15 and 20, etc.). An implementation of a gradual adaption may be thinkable, as more experience is

available with respect to the relationship of the critical loads and the defined (or redefined) risk values.

Table 7-14 List of the risk values for the respective load cases: without external loads and pure individual loads. These single-load cases are not expected to occur in real-life skiing. Nevertheless, the values are the basis for comparison between loading scenarios. The reference for the derivation of the risk values is given in the last column.

Load case Knee angle	Risk Value	Reference
No External Loads		
Hyperextension (-5°)	10	Hame et al. (2002), Markolf et al. (1990), Wascher et al. (1993), Markolf et al. (2004)
Extension (0°)	6	
NearExtension (25°)	1	
SmallFlexion (55°)	1	
90degFlexion (90°)	3	
FullFlexion (120°)	3	
Hyperflexion (130°)	15	
Internal Torque on Tibia		
Hyperextension (-5°)	18	Hame et al. (2002), Markolf et al. (1995), Wascher et al. (1993), Markolf et al. (2004), Markolf et al. (1990), Lehner (2007)
Extension (0°)	19	
NearExtension (25°)	13	
SmallFlexion (55°)	7	
90degFlexion (90°)	7	
FullFlexion (120°)	9	
Hyperflexion (130°)	17	
External Torque on Tibia		
Hyperextension (-5°)	14	Hame et al. (2002), Markolf et al. (1995), Wascher et al. (1993), Markolf et al. (2004), Markolf et al. (1990), Lehner (2007)
Extension (0°)	13	
NearExtension (25°)	9	
SmallFlexion (55°)	6	
90degFlexion (90°)	5	
FullFlexion (120°)	5	
Hyperflexion (130°)	14	
Varus Moment		
Hyperextension (-5°)	16	Markolf et al. (1990), Markolf et al. (1995), Wascher et al. (1993), Lehner (2007)
Extension (0°)	13	
NearExtension (25°)	6	
SmallFlexion (55°)	4	
90degFlexion (90°)	4	
FullFlexion (120°)	4	
Hyperflexion (130°)	15	
Valgus Moment		
Hyperextension (-5°)	13	Markolf et al. (1990), Markolf et al. (1995), Wascher et al. (1993), Lehner (2007)
Extension (0°)	7	
NearExtension (25°)	8	
SmallFlexion (55°)	8	
90degFlexion (90°)	6	
FullFlexion (120°)	6	
Hyperflexion (130°)	17	

APPENDIX

Continued
Table 7-14

Quadriceps Contraction		
Hyperextension (-5°)	11	Markolf et al. (2004), Markolf et al. (1990), Lehner (2007)
Extension (0°)	7	
NearExtension (25°)	4	
SmallFlexion (55°)	3	
90degFlexion (90°)	2	
FullFlexion (120°)	2	
Hyperflexion (130°)	16	
Hamstring Contraction		
Hyperextension (-5°)	9	Markolf et al. (2004)
Extension (0°)	4	
NearExtension (25°)	1	
SmallFlexion (55°)	4	
90degFlexion (90°)	5	
FullFlexion (120°)	1	
Hyperflexion (130°)	15	

Table 7-15 List of the risk values for the respective load cases: combination of two loads.

Load case Knee angle	Risk Value	Reference
Internal Torque and Varus Moment		
Hyperextension (-5°)	24	Combination of load cases pure internal torque and pure varus moment. Lehner (2007)
Extension (0°)	25	
NearExtension (25°)	17	
SmallFlexion (55°)	10	
90degFlexion (90°)	10	
FullFlexion (120°)	12	
Hyperflexion (130°)	16	
Internal Torque and Valgus Moment		
Hyperextension (-5°)	18	Markolf et al. (1995)
Extension (0°)	19	
NearExtension (25°)	18	
SmallFlexion (55°)	12	
90degFlexion (90°)	7	
FullFlexion (120°)	8	
Hyperflexion (130°)	17	
External Torque and Varus Moment		
Hyperextension (-5°)	16	Combination of load cases pure external torque and pure varus moment. Lehner (2007)
Extension (0°)	13	
NearExtension (25°)	9	
SmallFlexion (55°)	6	
90degFlexion (90°)	5	
FullFlexion (120°)	5	
Hyperflexion (130°)	16	
External Torque and Valgus Moment		
Hyperextension (-5°)	14	Markolf et al. (1995)
Extension (0°)	15	
NearExtension (25°)	11	
SmallFlexion (55°)	6	
90degFlexion (90°)	6	
FullFlexion (120°)	6	
Hyperflexion (130°)	15	
Internal Torque and Quadriceps Contraction		
Hyperextension (-5°)	18	Markolf et al. (2004), Lehner (2007)
Extension (0°)	19	
NearExtension (25°)	13	
SmallFlexion (55°)	7	
90degFlexion (90°)	5	
FullFlexion (120°)	7	
Hyperflexion (130°)	17	
Internal Torque and Hamstring Contraction		
Hyperextension (-5°)	16	Markolf et al. (2004), Lehner (2007)
Extension (0°)	17	
NearExtension (25°)	9	
SmallFlexion (55°)	7	
90degFlexion (90°)	11	
FullFlexion (120°)	9	
Hyperflexion (130°)	17	

Continued Table 7-15

External Torque and Quadriceps Contraction		
Hyperextension (-5°)	14	Markolf et al. (2004), Lehner (2007)
Extension (0°)	14	
NearExtension (25°)	11	
SmallFlexion (55°)	9	
90degFlexion (90°)	8	
FullFlexion (120°)	7	
Hyperflexion (130°)	16	
External Torque and Hamstring Contraction		
Hyperextension (-5°)	14	Markolf et al. (2004), Lehner (2007)
Extension (0°)	12	
NearExtension (25°)	8	
SmallFlexion (55°)	7	
90degFlexion (90°)	8	
FullFlexion (120°)	5	
Hyperflexion (130°)	14	
Varus Moment and Quadriceps Contraction		
Hyperextension (-5°)	17	Combination of load case pure varus and load case
Extension (0°)	14	pure quadriceps contraction.
NearExtension (25°)	8	Lehner (2007)
SmallFlexion (55°)	6	
90degFlexion (90°)	5	
FullFlexion (120°)	5	
Hyperflexion (130°)	13	
Varus Moment and Hamstring Contraction		
Hyperextension (-5°)	15	Combination of load case pure varus and load case
Extension (0°)	12	pure hamstring contraction
NearExtension (25°)	6	
SmallFlexion (55°)	6	
90degFlexion (90°)	6	
FullFlexion (120°)	1	
Hyperflexion (130°)	15	
Valgus Moment and Quadriceps Contraction		
Hyperextension (-5°)	13	Combination of load case pure valgus and load case
Extension (0°)	7	pure quadriceps contraction
NearExtension (25°)	9	
SmallFlexion (55°)	9	
90degFlexion (90°)	6	
FullFlexion (120°)	6	
Hyperflexion (130°)	20	
Valgus Moment and Hamstring Contraction		
Hyperextension (-5°)	12	Combination of load case pure valgus and load case
Extension (0°)	6	pure hamstring contraction
NearExtension (25°)	8	
SmallFlexion (55°)	10	
90degFlexion (90°)	8	
FullFlexion (120°)	6	
Hyperflexion (130°)	17	

Table 7-16 List of the risk values for the respective load cases: combination of three loads.

Load case Knee angle	Risk Value	comment
Internal Torque and Varus Moment and Quadriceps Contraction		
Hyperextension (-5°)	24	Combination of the load case “internal torque and varus” and pure quadriceps contraction
Extension (0°)	25	
NearExtension (25°)	17	
SmallFlexion (55°)	10	
90degFlexion (90°)	10	
FullFlexion (120°)	10	
Hyperflexion (130°)	14	
Internal Torque and Varus Moment and Hamstring Contraction		
Hyperextension (-5°)	22	Combination of the load case “internal torque and varus” and pure hamstring contraction
Extension (0°)	23	
NearExtension (25°)	15	
SmallFlexion (55°)	10	
90degFlexion (90°)	12	
FullFlexion (120°)	12	
Hyperflexion (130°)	16	
Internal Torque and Valgus Moment and Quadriceps Contraction		
Hyperextension (-5°)	18	Combination of the load case “internal torque and valgus” and pure quadriceps contraction
Extension (0°)	19	
NearExtension (25°)	18	
SmallFlexion (55°)	12	
90degFlexion (90°)	7	
FullFlexion (120°)	6	
Hyperflexion (130°)	19	
Internal Torque and Valgus Moment and Hamstring Contraction		
Hyperextension (-5°)	16	Combination of the load case “internal torque and valgus” and pure hamstring contraction
Extension (0°)	17	
NearExtension (25°)	16	
SmallFlexion (55°)	12	
90degFlexion (90°)	9	
FullFlexion (120°)	8	
Hyperflexion (130°)	17	
External Torque and Varus Moment and Quadriceps Contraction		
Hyperextension (-5°)	16	Combination of the load case “external torque and varus” and pure quadriceps contraction
Extension (0°)	13	
NearExtension (25°)	11	
SmallFlexion (55°)	8	
90degFlexion (90°)	7	
FullFlexion (120°)	7	
Hyperflexion (130°)	18	
External Torque and Varus Moment and Hamstring Contraction		
Hyperextension (-5°)	16	Combination of the load case “external torque and varus” and pure hamstring contraction
Extension (0°)	13	
NearExtension (25°)	9	
SmallFlexion (55°)	6	
90degFlexion (90°)	7	
FullFlexion (120°)	5	
Hyperflexion (130°)	16	

Continued Table 7-16

External Torque and Valgus Moment and Quadriceps Contraction		
Hyperextension (-5°)	14	Combination of the load case “external torque and valgus” and pure quadriceps contraction
Extension (0°)	15	
NearExtension (25°)	13	
SmallFlexion (55°)	8	
90degFlexion (90°)	8	
FullFlexion (120°)	8	
Hyperflexion (130°)	19	
External Torque and Valgus Moment and Hamstring Contraction		
Hyperextension (-5°)	14	Combination of the load case “external torque and valgus” and pure hamstring contraction
Extension (0°)	15	
NearExtension (25°)	11	
SmallFlexion (55°)	6	
90degFlexion (90°)	8	
FullFlexion (120°)	6	
Hyperflexion (130°)	15	

Table 7-17 List of the risk values for the respective load cases: anterior tibial translation and combination of anterior tibial translation with muscle activation.

Load case Knee angle	Risk Value	Reference
Anterior Tibial Translation		
Hyperextension (-5°)	20	Markolf et al. (2004)
Extension (0°)	19	
NearExtension (25°)	16	
SmallFlexion (55°)	11	
90degFlexion (90°)	11	
FullFlexion (120°)	11	
Hyperflexion (130°)	25	
Anterior Tibial Translation and Quadriceps Contraction		
Hyperextension (-5°)	20	Markolf et al. (2004)
Extension (0°)	20	
NearExtension (25°)	19	
SmallFlexion (55°)	13	
90degFlexion (90°)	9	
FullFlexion (120°)	9	
Hyperflexion (130°)	23	
Anterior Tibial Translation and Hamstring Contraction		
Hyperextension (-5°)	20	Markolf et al. (2004)
Extension (0°)	20	
NearExtension (25°)	12	
SmallFlexion (55°)	7	
90degFlexion (90°)	7	
FullFlexion (120°)	7	
Hyperflexion (130°)	21	

7.10.2 **Definition Membership Functions for the Knee Flexion Angle**

Table 7-18 Definition of ranges for the membership functions for the knee flexion angles.

Label	Knee Flexion Angle	Rationale
Hyperextension	-5°	Schünke (2014); Markolf et al. (1995); Markolf et al. (2004)
Extension	0°	In the range from extension to hyperextension, a large change in the force in the ACL occurs in most loading situations. Therefore, a small distance is chosen between hyperextension and extension. Markolf et al. (2004); Markolf et al. (1995); own results chapter 3.
NearExtension	25°	The range between 0° and 90° is divided into two similarly sized knee angle ranges.
SmallFlexion	55°	
90degFlexion	90°	Availability of data is higher from 0 to 90° knee flexion, as some investigations are carried out up to a flexion angle of 90° (Markolf et al. 1995)
fullFlexion	120°	According to Schünke (2014) the range of maximum possible active flexion starts at 120°. Data availability, as some studies are carried out up to a flexion angle of 120° (Markolf et al. 2004).
Hyperflexion	130°	The range of possible hyperflexion varies from person to person. Since the tension in the ACL is more critical in hyperflexion than in flexion, a small angle is chosen for hyperflexion. In this way, people who cannot bend the knee joint as much are also taken into account for the increased risk of an ACL injury; own results chapter 3.

7.10.3 Definition Membership Function High Internal/External Torque

It is assumed that a sensor system measuring loads on the foot gives the moment M_z accurately. Moreover, it is assumed that this moment is equivalent to the moment about the longitudinal axis of the tibia.

Shoemaker et al. (1988) determined the rotational torque around the tibia provoked through muscle contraction in 18 male subjects. Depending on the test conditions (different knee angles, different shoes, etc.), the mean values were between 30 Nm and 71 Nm. The authors found no great correlation between maximum torque and body size or weight. The release values according to *Skibindungen für den alpinen Skilauf - Auswahl von Auslösedrehmomentwerten mittels Tibia-Verfahren 2018* for the moment around the z-axis range from 5 Nm to 137 Nm depending on the skier. Although no great correlation was found between weight or height and possible rotational moment, it is assumed that approximately a release moment can be muscularly applied to trigger the binding (a more precise examination of the individual test subjects would be necessary).

The algorithm calculates release torques up to 15 % below those recommended by the standard. It is therefore assumed that a "high moment" is present at this very moment M_z .

7.10.4 **Definition Membership Function High Varus/Valgus Moment**

Woo et al. (1991) determined the tensile strength of ACLs. For the age group of 60 to 97 years, they determined an average tear strength of 658 N with a standard deviation of 129 N. Since 95.45 % of all measured values can be expected with a normal distribution in the interval of two standard deviations, the value $F_{critical}$ is calculated using equation 7-18 is set as the critical value for the tearing of the ACL.

$$F_{critical} = 658 N - (2 * 129 N) = 400 N \quad 7-18$$

In the next step, the force data from Markolf et al. (1990), in which the Varus bending moment was continuously increased from 0 Nm to 15 Nm, are linearly extrapolated to determine at which moment the critical load of the ACL of 400 N is reached. The values determined by Markolf et al. (1990) also include a double standard deviation. Considering the double standard deviation should ensure that a critical classification is already made for people with low ACL tear strength.

Using values from Markolf et al., the resulting critical value M_{VV_crit} is calculated as the critical varus/valgus load according to equation 7-19:

$$M_{VV_krit} = 3 Nm + \frac{15 Nm - 3 Nm}{156 N - 60,8 N} * (400 N - 156 N) = 33,8 Nm \quad 7-19$$

Not only the moment M_x has an influence on the varus and valgus load at the knee joint, but also the force at the ski edges in y-direction (F_y). This force must be multiplied by the lever arm. The body height of the skier and the height of the ski is used to calculate the lever arm and consequently the acting varus or valgus moment using equation 7-20. As a proportion of the skier's height, the distance from the sole of the foot to the distal femur is assumed 28.5 % (Drillis et al. 1966). The height of the ski is added to the lever arm and is assumed to be 20 mm.

$$Valgus_Varus\ Moment = M_x + F_y (ski\ hight + 0.285 * body\ hight) \quad 7-20$$